Politecnico di Milano

Ph.D. programme in
Structural, Seismic and Geotechnical Engineering
XXVIII Cycle

Department of Civil and Environmental Engineering (DICA)

February 2016

VIBRATION-BASED STRUCTURAL HEALTH MONITORING FOR HISTORIC MASONRY TOWERS

Ing. Marco Guidobaldi

Supervisor: Prof. Ing. Carmelo Gentile

Coordinator of the Ph.D. programme: Prof. Ing. Roberto Paolucci

-Page intentionally left blank-

Acknowledgments

I would like to thank all the people who have believed in me and supported my work during the past three years.

In particular, my sincere gratitude goes to my supervisor Prof. Carmelo Gentile, who throughout my whole Ph.D. career has been a patient mentor, a steady motivator and an invaluable advisor.

Marco Antico and Marco Cucchi are also acknowledged for all the practical advice they have provided during many dynamic tests.

Thanks to all of my Ph.D. colleagues who added a lot of fun to our everyday research.

Thanks also to my running team, because many times the solution to a complex problem came while running together.

Finally, none of this would have been possible without my amazing family. Your endless love and support is the fuel that powers my work day after day. Thank you.

-Page intentionally left blank-

Index

-Page intentionally left blank-

Introduction

Structural Health Monitoring (SHM) typically indicates the process of assessing the health condition of a structure. Originally developed in the field of aeronautical and mechanical engineering, SHM has significantly grown in importance in civil engineering applications too, due to the increasing need of controlling a large number of ageing and more complex structures.

Within the wide group of SHM methodologies, SHM based on Operational Modal Analysis (OMA) represents a sub-category that has progressively asserted itself over the recent years, and is based on the identification of the modal parameters of a structure (i.e. frequencies, damping ratios and mode shapes) subjected to ambient vibrations. Indeed, the possibility of assessing the structural health condition under operational loads and with no need for artificial inputs represents an advantage that, in many applications, is hard to overlook. Moreover, many civil structures and infrastructures often represent strategic assets whose interruption, even if temporary, cannot be considered an option.

Because of its non-destructive and sustainable way of testing, OMA-based SHM represents an investigation technique particularly suitable to Cultural Heritage. Within the framework of Cultural Heritage structures, ancient masonry towers represent a very common typology, whose characteristics and functions have continuously changed over the centuries: bell towers (particularly relevant in Italy as part of the numerous religious complexes), lookout or defensive towers, chimneys, minarets, etc. Such structural typology is not only characterized by the common issues of historic buildings (i.e. ageing of materials, presence of cracks and damage, effects of successive construction phases or modifications), but is usually also particularly vulnerable to dynamic

actions (e.g. traffic-induced micro-tremors, swinging of bells, wind and earthquakes, etc.) due to the slenderness of the geometry and the typical presence of significant dead loads.

Therefore, the preservation and preventive conservation of historic towers represents a major challenge in the SHM of Cultural Heritage. Nevertheless, the usual high sensitivity of historic towers to ambient excitation allows to bypass the abovementioned issues, suggesting the use of ambient vibration tests (AVT) to assess the current global behavior of the structure. This is also confirmed by the growing number of applications where AVTs have been successfully adopted in the diagnostic process of historic towers [see e.g. Ivorra & Pallares 2006, Gentile & Saisi 2007, Ramos et al. 2010, Gentile et al. 2015]. As a further advantage, the cantilever-like structural scheme of towers allows an effective dynamic monitoring with just few accelerometers installed in the upper part of the building, resulting in a non-expensive and easy to maintain system that can be used for preventive conservation and/or SHM purposes [Ramos et al. 2010].

In the present Dissertation, a vibration-based SHM strategy has been proposed and adopted within the diagnostic and preservation process of two historic masonry towers in Northern Italy: the *Gabbia* tower in Mantua [Zuccoli 1984, Saisi & Gentile 2015] and the bell tower of the *Chiesa Collegiata di San Vittore* in Arcisate [Cazzani 1964, Gentile & Saisi 2013].

The present work is organized in 5 different chapters, whose content is outlined in the following.

Chapter 1 focuses on the techniques commonly adopted for the SHM monitoring of civil structures and infrastructures using OMA, with particular regards to the techniques applied in this Dissertation. The first part of the chapter provides the theoretical background of the most common OMA procedures, categorized as working in the frequency domain (Peak Picking [Bendat & Piersol 1993], Frequency Domain Decomposition [Brincker et al.

2000]) or in the time domain (Stochastic Subspace Identification [Van Overschee & De Moor 1996]). Subsequently, an overview of the state of the art of automated OMA is provided. The last part of the chapter deals with the removal of environmental and operational effects from the dynamic response of the structure. This fundamental phase is aimed at obtaining features insensitive to the external factors, which can therefore be used as indicators of the structural condition. The models most commonly adopted for this purpose are outlined and grouped as input-output (e.g. multiple regression analysis, ARX) and output-only (e.g. PCA). Additionally, brief descriptions of the most relevant practical SHM applications where the previous methods have been successfully adopted are provided. Finally, different damage detection approaches, based on control charts and on the analyses of the environment-independent features, are addressed and outlined.

In Chapter 2, an overview is provided of the main case studies where OMA has been applied for the structural assessment of historic structures. In particular, this chapter is organized in three sub-sections:

1. Ambient Vibration Test of towers and minarets. This section is in turn divided into three groups, depending on the main objective of the performed dynamic investigation: evaluation of the effects induced by the bells, structural assessment, seismic assessment;

2. Continuous dynamic monitoring of masonry towers, where the effects of the environmental factors on the natural frequencies are highlighted;

3. Ambient Vibration Tests and monitoring of monuments, which collects the main applications of OMA to historic buildings.

Furthermore, the case studies related to minarets and towers (which represent the central element of interest of the present Dissertation) are collected in two tables. In both tables, the main characteristics of the considered structure and of the performed investigation are provided: location, year of

construction, existence of a FE model, OMA technique, dimensions and first vibration frequency.

The third Chapter has the purpose of outlining the main characteristics of the SHM methodology applied to the investigated masonry towers. In particular, the section starts with a description of the preparatory data collection stage and moves on to the operational phases of the adopted strategy: preliminary AVTs, continuous dynamic monitoring and automated OMA, evaluation and removal of the environmental effects on the natural frequencies and, finally, the damage detection process.

In Chapter 4 and Chapter 5 the results of the vibration-based SHM of the two considered historic masonry towers are presented. For both case studies, the continuous dynamic monitoring has been performed by installing just three piezoelectric accelerometers (oriented along orthogonal directions) on a single cross section. Furthermore, the monitoring was completed by continuously recording the temperature of the masonry walls. For the *Gabbia* tower, the temperature acquisition was carried out by a single temperature sensor installed on the outside of the structure. On the other hand, for the bell tower of the *Chiesa Colleggiata di San Vittore* it was possible to take advantage of the temperature measurements recorded by an existing static monitoring system [Binda et al. 2012], which included 8 temperature sensors measuring internal and external wall temperature.

Chapter 4 focuses on the *Gabbia* tower in Mantua. This chapter is divided into four main parts:

1. description of the structure and historical background;

2. results of the structural assessment performed after the seismic events of May 2012. In particular, this section presents the results of the experimental survey carried out between July and November 2012;

3. general results of the subsequent continuous dynamic monitoring. Dedicated subsections have been defined to describe the different behavior of the global modes and of a local mode involving the upper part of the tower. Furthermore, large emphasis has been put to the correlation between temperature and frequencies and to the dynamic behavior of the structure under seismic excitation. Indeed, some far field earthquakes have been recorded during the monitoring, with significant effects observed on the dynamic characteristics of the tower;

4. effects of temperature and damage on the natural frequencies of the tower. This section presents the results obtained by removing the effects of temperature with input-output models (i.e. Dynamic Regression and ARX models) and output-only models (PCA) in order to successfully identify the occurrence of possible structural modifications.

The fifth Chapter presents the results obtained by applying the proposed SHM methodology to the bell tower of the *Chiesa Colleggiata di San Vittore*, Arcisate. The chapter is organized according to the same four sections previously defined for Chapter 4. As previously mentioned, the main difference with respect to the *Gabbia* tower case study was the availability of indoor and outdoor temperature measurements coming from 8 different sensors, installed as part of an existing static monitoring system. This allowed to remove the environmental effects by considering multiple inputs in the implement models. Nonetheless, in order to reproduce the same conditions characterizing the *Gabbia* tower, the correction of the natural frequencies has at first been performed by using only measurements coming from one external temperature sensor. The main goal in this phase was to determine the accuracy level achievable for masonry towers when only one external temperature sensor is available. Subsequently, input-output models characterized by measurements of both indoor and outdoor temperature have been implemented, in order to

highlight the improvements of the results when multiple inputs can be taken into account.

1 Structural Health Monitoring of civil structures using Operational Modal Analysis

1.1 Introduction

The process of assessing the health condition of a structure is typically referred to as *Structural Health Monitoring* (SHM). Even though SHM represents a large field including different methodologies, all SHM procedures are characterized by the following common tasks: i) the collection of measurements over time; ii) the extraction of features sensitive to damage from the recorded measurements; iii) the subsequent analysis of the obtained features to assess the current structural health condition.

In recent years, the amount of SHM applications to civil structures and infrastructures has significantly increased. Among the many motivations for this mounting scientific interest, the most relevant are the need of controlling a large number of ageing structures, the necessity of assessing the performance of new structures characterized by a growing level of complexity and, of course, the technological progress that has made SHM systems cheaper, easier to install and more reliable.

Within this framework, SHM using Operational Modal Analysis (OMA) represents a sub-group of SHM methodologies that has considerably grown in importance in the last decade. The main reason is related to the possibility of assessing the health condition of a structure from the analysis of its dynamic response in operational conditions, with no need for artificial inputs. Since civil structures and infrastructures are often characterized by strategic uses whose temporary interruption is considered difficult or even impossible, the opportunity of performing tests that do not interfere with the normal operational tasks and do not induce additional overloads represents a significant advantage.

The goal of OMA-based SHM is to identify the modal parameters (i.e. frequencies, damping ratios and mode shapes) of the structure under investigation from the collected dynamic responses, and to use those quantities to assess the current structural health condition. To this aim, a large number of output-only modal analysis techniques can be adopted (e.g. Frequency Domain Decomposition [Brincker et al. 2000], Stochastic Subspace Identification [Van Overschee & De Moor 1996], etc.). Subsequently, the occurrence of structural anomalies referable to damage is detected by exploring the time evolution of the identified modal parameters, as modal parameters change with changed structural characteristics (i.e. mass and/or stiffness distribution). Therefore, irreversible changes in the dynamic characteristics of the structure arise as damage happens, leading to abnormal variations of the modal parameters that can be detected from their evolution in time. Such important task necessarily requires the automation of the modal identification techniques in order to minimize the need for human interaction in continuous dynamic monitoring (where a large amount of data needs to be processed in short time). Therefore, several automated techniques based on classic output-only algorithms have been presented in recent years [Peeters & De Roeck 2001, Brincker et al. 2007, Magalhães et al. 2008, Reynders et al. 2012, Ubertini et al. 2013].

It is worth noting that the stiffness reductions commonly associated with damage usually correspond to anomalous decreases of the natural frequencies. Therefore, in practical applications, these are the features most widely adopted to detect the occurrence of damage. Nonetheless, natural frequencies are also affected by factors other than damage, such as environmental and operational effects (e.g. temperature, wind, amplitude of the excitation, etc.). The influence of external factors may lead to relevant fluctuations that can mask modifications due to damage. Therefore, for SHM purposes, the influence of any extra-structural feature must be accounted for and removed, so that any residual

variation in the monitored modal parameters can only be related to changes of the structure itself. To achieve this goal, two classes of models are usually adopted:

1. *input-output models*: within the OMA-based SHM framework, input-output models are used to reproduce the relationship between natural frequencies and measured external variables;

2. *output-only models*: to overcome the need to determine and measure the features with the most relevant influence on the frequencies, output-only methods can be used to remove the effect of unmeasured external factors.

In the first part of this chapter, the theoretical background of the OMA techniques applied in the present Dissertation is described and a concise overview of the automated OMA methods is provided. Subsequently, the main input-output and output-only models are outlined, along with brief summaries of some relevant SHM applications where those methods have been adopted to remove the influence of external factors. Finally, the damage detection process is addressed and the statistical tools known as Control Charts are described.

1.2 Operational Modal Analysis: theoretical background

1.2.1 Basic assumptions

In Operational Modal Analysis (OMA), structures are typically excited by ambient and operational sources: wind, micro tremors, human-induced excitations, traffic, etc. All these kinds of excitation combine for an unknown input, typically represented by a stochastic process. Therefore, all the techniques employed to extract the modal parameters of a structure in operational conditions are defined as *output-only* (or stochastic) identification methods.

A stochastic process is a set of n ($n \rightarrow \infty$) time dependent random functions,

designated by realizations, associated with the characterization of one or several variables (as for instance a set of excitation forces). In practical applications, the stochastic processes exciting the structure are assumed to be stationary, ergodic and zero-mean:

1. stationary process means that its statistical properties do not change in time;

2. a stationary process is called ergodic when any sample of the process represents the average statistical properties of the entire process. Therefore, for an ergodic process, the statistical properties can be extracted from a sufficiently long realization, as it will be representative of the whole process and not just of that sample;

3. the zero mean assumption is usually fulfilled by de-trending the recorded signals.

For stochastic and ergodic processes $p(t)$ and $q(t)$, sampled at time t and $t + \tau$, define:

$$\Sigma_{pp}(\tau) = \mathrm{E}[p(t)p(t + \tau)]$$
$$\Sigma_{qq}(\tau) = \mathrm{E}[q(t)q(t + \tau)]$$
$$\Sigma_{pq}(\tau) = \mathrm{E}[p(t)q(t + \tau)]$$

(1.1)

The quantities $\Sigma_{pp}(\tau)$ and $\Sigma_{qq}(\tau)$ are called the *autocorrelations functions* of $p(t)$ and $q(t)$, respectively, whereas $\Sigma_{pq}(\tau)$ is the so-called *cross-correlation function* between $p(t)$ and $q(t)$ [Bendat & Piersol 1986]. The autocorrelation function provides the correlation of a time signal with its own values after the time separation τ. Similarly, the cross-correlation function allows to estimate the degree to which the two processes $p(t)$ and $q(t)$ are correlated.

Once autocorrelation and cross-correlation functions have been computed, the *correlation matrix* can be defined: the diagonal terms of the matrix correspond to the autocorrelations functions, whereas the cross-correlations functions represent the off-diagonal terms.

The correlation matrix characterizes stochastic processes in the time domain.

14

In the frequency domain, stochastic processes are described by their s*pectral density matrix* **G***(ω)*, collecting the (auto- and cross-) *spectral density functions*. A possible way to define the spectral density functions is to take a Fourier transform of a previously calculated correlation function. In particular, assume that the autocorrelation and cross-correlation functions $\Sigma_{pp}(\tau)$, $\Sigma_{qq}(\tau)$ and $\Sigma_{pq}(\tau)$ exist and that the integrals of their absolute values are finite:

$$\int_{-\infty}^{\infty} |\Sigma(\tau)| d\tau < \infty \qquad \textbf{(1.2)}$$

Hence, the Fourier transforms of $\Sigma(\tau)$ will exist as defined by:

$$G_{pp}(\omega) = \int_{-\infty}^{\infty} \Sigma_{pp}(\tau) e^{-j\omega\tau} d\tau$$

$$G_{qq}(\omega) = \int_{-\infty}^{\infty} \Sigma_{qq}(\tau) e^{-j\omega\tau} d\tau \qquad \textbf{(1.3)}$$

$$G_{pq}(\omega) = \int_{-\infty}^{\infty} \Sigma_{pq}(\tau) e^{-j\omega\tau} d\tau$$

$G_{pp}(\omega)$ and $G_{qq}(\omega)$ are called *autospectral density functions* of *p(t)* and *q(t)*, respectively, whereas $G_{pq}(\omega)$ is the *cross-spectral density function* between the two processes [Bendat & Piersol 1986].

Finally, it is to be noticed that all output-only identification methods are based on the assumption of the stochastic input be a white noise process. A white noise process is characterized by constant energy content over a large frequency band, meaning that the corresponding spectrum is flat independently on the frequency. As a consequence, the spectrum of the output can be used to extract all the useful information about the structure.

1.2.2   Frequency domain OMA techniques

Classic spectral techniques: Peak Picking

The simplest technique to estimate the modal parameters of a structure excited by ambient vibrations is the so called *Peak Picking* (PP) method [Bendat &

Piersol 1993]. The name originates from the identification methodology of the procedure: selecting the natural frequencies of the system from the peaks of the (auto- and cross-) spectral density plots. The approach is based on the assumption that, in the proximity of resonance, only one mode is dominant and the contribution of all other modes can be neglected.

The PP method is based on the estimation of the spectral matrix $\mathbf{G}_{yy}(\omega)$, formed by auto-spectral (ASD) and cross-spectral density (CSD) functions (1.3) of the signals recorded in every instrumented position [Bendat & Piersol 1993]. The spectral matrix $\mathbf{G}_{yy}(\omega)$ of the output can be defined at a certain frequency ω as:

$$\mathbf{G}_{yy}(\omega) = \begin{bmatrix} G_{11}(\omega) & G_{12}(\omega) & \cdots & G_{1N}(\omega) \\ G_{21}(\omega) & G_{22}(\omega) & \cdots & G_{2N}(\omega) \\ \vdots & \vdots & & \vdots \\ G_{N1}(\omega) & G_{N2}(\omega) & \cdots & G_{NN}(\omega) \end{bmatrix} \tag{1.4}$$

The relationship between an unknown input $x(t)$ and a measured output $y(t)$ can be expressed as

$$\mathbf{G}_{yy}(\omega) = \mathbf{H}(\omega)\mathbf{G}_{xx}(\omega)\mathbf{H}^{\mathrm{H}}(\omega) \tag{1.5}$$

where:

- $\mathbf{G}_{xx}(\omega)$ is the spectral matrix of the input;
- $\mathbf{G}_{yy}(\omega)$ is the spectral matrix of the output;
- $\mathbf{H}(\omega)$ is the *Frequency Response Function* (FRF);
- $^{\mathrm{H}}$ indicates the Hermitian operator.

The FRF $\mathbf{H}(\omega)$ can be written by using the classic pole/residue form [Harris 1995] as:

$$\mathbf{H}(\omega) = \sum_{k=1}^{n} \frac{\mathbf{R}_k}{j\omega - \lambda_k} + \frac{\mathbf{R}_k^*}{j\omega - \lambda_k^*} \tag{1.6}$$

where n is the number of modes, λ_k is the k-th pole and $\mathbf{R}_k$ is the k-th residue, expressed as:

16

$$\mathbf{R}_k = \boldsymbol{\phi}_k \boldsymbol{\gamma}_k^{\mathrm{T}} \tag{1.7}$$

being $\boldsymbol{\phi}_k$ the k-th mode shape vector and $\boldsymbol{\gamma}_k^{\mathrm{T}}$ the modal participation vector of mode k.

If the considered input is a white noise process, its spectral matrix $\mathbf{G}_{xx}$ will be a constant $\mathbf{C}$ and, therefore, equation (1.5) can be re-written as:

$$\mathbf{G}_{yy}(\omega) = \sum_{k=1}^{n} \sum_{s=1}^{n} \left[\frac{\mathbf{R}_k}{j\omega - \lambda_k} + \frac{\mathbf{R}_k^*}{j\omega - \lambda_k^*} \right] \mathbf{C} \left[\frac{\mathbf{R}_s}{j\omega - \lambda_s} + \frac{\mathbf{R}_s^*}{j\omega - \lambda_s^*} \right]^{\mathrm{H}} \tag{1.8}$$

Additionally, if the assumptions are made of light damping and vibration modes characterized by well-spaced frequencies, in the neighborhood of resonant frequencies (Figure 1.1) it is possible to write:

$$\mathbf{G}_{yy}(\omega) = \left[\frac{\mathbf{R}_i}{j\omega - \lambda_i} + \frac{\mathbf{R}_i^*}{j\omega - \lambda_i^*} \right] \mathbf{C} \left[\frac{\mathbf{R}_i}{j\omega - \lambda_i} + \frac{\mathbf{R}_i^*}{j\omega - \lambda_i^*} \right]^{\mathrm{H}} \tag{1.9}$$

where the spectral matrix has been expressed by considering the contribution of just one dominating mode (e.g. the i-th mode).

The previous equations (1.7)-(1.9) highlights that, at a resonant frequency, each column (or row) of the spectral matrix can be considered as an estimate of the corresponding mode shape.
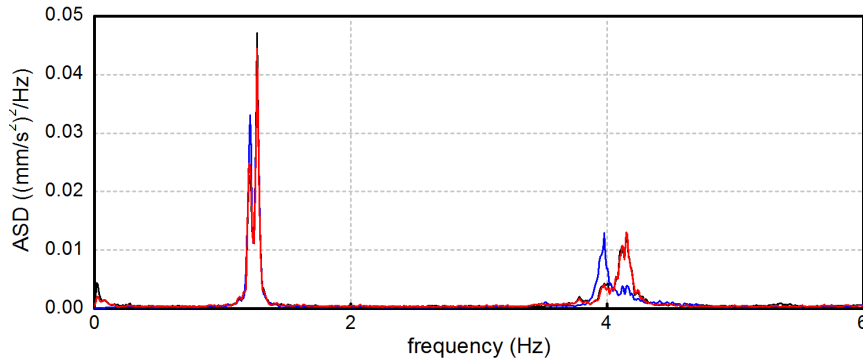

Figure 1.1 PP: auto-spectral density functions (ASD) obtained from signals recorded on the *San Vittore* bell-tower

The PP approach only provides estimates of natural frequencies and mode shapes. The corresponding values of damping ratios can be determined by using the so-called *half-power bandwidth* method, as suggested in [Bendat & Piersol 1993].

The classical PP technique is widely acknowledged to be very simple and not computationally demanding. Nevertheless, such user-friendly features are balanced by some relevant drawbacks. The PP method is based on the assumptions of low damping and well-separated modes. When these conditions are not fulfilled, the obtained results may not be accurate nor reliable. Indeed, the procedure does not allow to identify the actual mode shapes; instead, it provides estimates of the so-called *operational deflection shapes*. As defined in [Peeters 2000], an operational deflection shape is a deformation of the structure when this is excited by a pure harmonic. From a theoretical standpoint, an operational deflection shape is a combination of all mode shapes; however, in real applications only the contribution of those modes characterized by an eigenfrequency close to the excitation frequency becomes relevant. This feature turns into a limitation when modes are closely spaced, for the identified operational deflection shape will appear as the superposition of the actual mode shapes of multiple modes. Another significant drawback is related to the manual selection of the spectrum peaks: if the spectrum is not clear and well defined, the identification of the eigenfrequencies may turn into a very subjective task and depend on the user's skills as an analyst. Finally, the selected frequency resolution may highly influence the quality of the results, as fine enough values are required in order to obtain good estimates.

Finally, it should be mentioned that the results of the PP method can be further improved by inspecting the *coherence function* [Bendat & Piersol 1986], defined as:

$$C_{pq} = \frac{|G_{pq}(\omega)|^2}{G_{pp}(\omega)G_{qq}(\omega)} \qquad \textbf{(1.10)}$$

The coherence function assumes values in the range between 0 and 1, and provides information on how two different spectral density functions are correlated at a specific frequency. At a resonant frequency, values will be close to 1, since the signal-to-noise ratio tends to be high. Moreover, the coherence function can be useful in defining the nature of a mode: if real modes are expected, the phase angles at the resonance frequency should be either 0° or 180°.

Frequency Domain Decomposition (FDD)

The *Frequency Domain Decomposition* (FDD) technique was proposed in [Brincker et al. 2000] with the main purpose of removing the described limits of the PP technique related to the presence of closely spaced modes. Indeed, the basic concepts of the method had already been adopted in the analysis of structures excited by ambient vibrations [Prevosto 1982] and for the extraction of modal parameters from the FRF in the form of *Complex Mode Indication Function* (CMIF) [Shih et al. 1988].

The FDD method is based on the *Singular Value Decomposition* (SVD) of the spectral matrix of the output $\mathbf{G}_{yy}$. The results provided by this procedure can be considered highly reliable if the following basic assumptions are fulfilled:
1. the excitation is a white noise;
2. the mode shapes are orthogonal;
3. the investigated structure is lightly damped.

If such hypothesis are not satisfied, the SVD has to be considered approximate. Nevertheless, the obtained results are still more accurate than those provided by traditional techniques.

In order to intuitively grasp the basic concepts at the base of the FDD

19

method, let us consider the classic structural vibration model. The theory of modal analysis allows to write the response *y(t)* of a vibrating structure as the superposition of *n* vibration modes (each one characterized by its mode shape ϕ_i), combined by means of the modal coordinates η_i:

$$y(t) = \phi_1\eta_1(t) + \phi_2\eta_2(t) + \cdots + \phi_n\eta_n(t) = \Phi\eta(t) \qquad (1.11)$$

Hence, the correlation matrix of the response can be expressed as:

$$\Sigma_{yy}(t) = \mathrm{E}[y(t+\tau)y(t)^{\mathrm{T}}] = \mathrm{E}[\Phi\eta(t+\tau)\eta(t)^{\mathrm{T}}\Phi^{\mathrm{T}}]$$
$$= \Phi\Sigma_{\eta\eta}(t)\Phi^{\mathrm{T}} \qquad (1.12)$$

where $\Sigma_{\eta\eta}(t)$ indicates the correlation matrix of the modal coordinates. By applying the the Fourier Transform, to eq. (1.13), the spectral matrix $G_{yy}(\omega)$ is obtained:

$$G_{yy}(\omega) = \Phi G_{\eta\eta}(\omega)\Phi^{\mathrm{T}} \qquad (1.13)$$

It is worth mentioning that equations (1.8) and (1.13) are two equivalent ways of expressing the spectral matrix of the output $G_{yy}(\omega)$. By recalling the initial assumptions of orthogonal mode shapes Φ and white noise input, the modal coordinates can be considered uncorrelated. Therefore, the correspondent spectral matrix $G_{\eta\eta}(\omega)$ is diagonal.

The SVD of a generic matrix **A** with dimensions $m{\times}l$, can be written in the form:

$$A = U\begin{bmatrix} \sigma & 0 \\ 0 & 0 \end{bmatrix}V^{\mathrm{H}} \qquad (1.14)$$

where $\sigma = diag[\sigma_1, \sigma_2,\ldots, \sigma_p]$, $\sigma_1 \geq \sigma_2 \geq \ldots \geq \sigma_p \geq 0$ and $p = min\ (m,\ l)$.

Elements σ_i ($i = 1,\ 2,\ldots,p$) forming the diagonal matrix σ are the singular values of **A**, whereas **U** and **V** are unitary matrices containing the right and left singular vectors of matrix **A**. Hence, considering the characteristics of the terms forming equation (1.13) and the initial assumptions of the procedure, the spectral matrix of the output can be formally re-written for the generic

20

frequency ω according to the SVD formulation:

$$\mathbf{G}_{yy}(\omega) = \mathbf{U}(\omega)\boldsymbol{\sigma}(\omega)\mathbf{V}^{\mathrm{H}}(\omega) \tag{1.15}$$

The first (and largest) singular value represents the magnitude of the dominant vibration mode at that frequency, whereas the corresponding singular vector is an estimate of the associated mode shape:

$$\widehat{\boldsymbol{\phi}} = \boldsymbol{u}_1 \tag{1.16}$$

The higher singular values contain either the effects of noise (electric or environmental) or the effects of normal modes close to the dominant one.

A typical plot of the singular values of matrix $\mathbf{G}_{yy}(\omega)$ is shown in Figure 1.2: the diagram highlights that the first singular value is significantly larger than the following ones. Furthermore, the modal peaks associated to the natural frequencies of the structure are well defined, as expected according to the properties of the functions forming the spectral matrix.

A limitation of the FDD technique is represented by the possibility of estimating only natural frequency and mode shape of each mode, with no information about the correspondent damping ratio. To overcome this drawback, an improved version of the algorithm was proposed by [Brincker et al. 2001], usually referred to as *Enhanced Frequency Domain Decomposition* (EFDD).
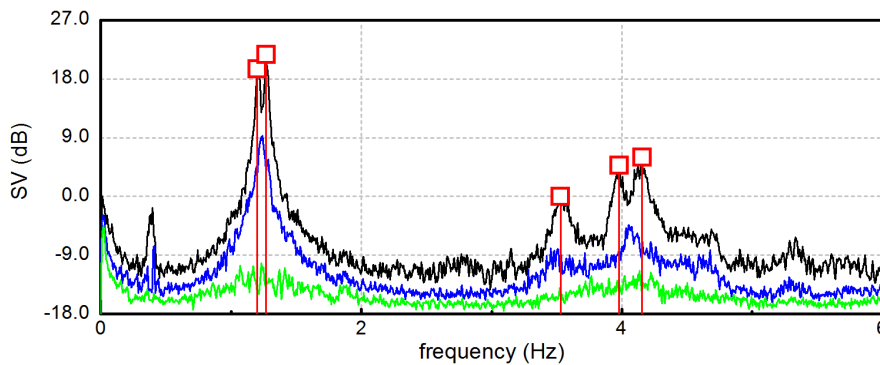

Figure 1.2 FDD: typical plot of the singular values and identification of the natural frequencies (*San Vittore* bell-tower)

Nevertheless, some drawbacks of the method should be pointed out. Firstly, low values of the signal-to-noise ratio may lead to difficulties in the identification process, as the peaks of the SV diagrams may not be very clear. Secondly, the case can happen when the second singular values are close to the first. In this circumstance, it should be recalled that in structural dynamics the orthogonality between mode shapes is related to mass and stiffness matrices, whereas the SVD leads to singular vectors whose orthogonality has a geometrical nature. Therefore, the estimated mode shape might differ from the actual one when first and second singular values are close to each other.

1.2.3   Time domain: Stochastic Subspace Identification (SSI)

The *Stochastic Subspace Identification* (SSI) method [Van Overschee & De Moor 1996, Peeters & De Roeck 1999, Peeters 2000] is a parametric identification technique working in the time domain. The procedure is based on the extraction and identification of a system matrix *A* defined in a discrete-time state-space representation of the equation of motion. Two subspace algorithms are usually adopted in OMA: the *Data-driven SSI* (SSI-Data) [Van Overschee & De Moor 1996] and the *Covariance-driven SSI* (SSI-Cov) [Peeters & De Roeck 1999, Peeters 2000].

The equation of motion of a multi degree of freedom (MDOF) system characterized by N degrees of freedom can be expressed as:

$$\mathbf{M}\ddot{U} + \mathbf{C_N}\dot{U} + \mathbf{K}U(t) = F(t) = \mathbf{B_N}u(t) \qquad (1.17)$$

where **M**, $\mathbf{C_N}$ and **K** are the $N \times N$ mass, damping and stiffness matrices, respectively, *F(t)* is the exciting force vector and *U(t)* is the displacements vector, both at continuous time t. It should be noted that, since usually not all the N degrees of freedom of the system are excited, the *F(t)* vector composed by N elements can be replaced by a vector *u(t)* with dimensions $m<N$ which only takes into account the m applied inputs. This vector *u(t)* is then multiplied by a

$N{\times}m$ matrix $\mathbf{B}_N$, mapping the m inputs with the N degrees of freedom of the system.

Starting from (1.17) and performing some mathematical derivations, it is possible to transform the second order differential equation of motion into a first order differential equation. One of the possible ways is based on the so-called *state-space model*, often used in civil engineering to derive the modal parameters of a structure with general viscous damping.

Starting from the following assumptions:

$$x(t) = \begin{bmatrix} U(t) \\ \dot{U}(t) \end{bmatrix}, \quad \mathbf{A}_c = \begin{bmatrix} 0 & I \\ -\mathbf{M}^{-1}\mathbf{K} & -\mathbf{M}^{-1}\mathbf{C}_N \end{bmatrix}, \quad \mathbf{B}_c = \begin{bmatrix} 0 \\ \mathbf{M}^{-1}\mathbf{B}_N \end{bmatrix} \qquad \text{(1.18)}$$

the continuous equation of motion (1.17) can be re-written in the following form, referred to as *state equation*:

$$\dot{x}(t) = \mathbf{A}_c x(t) + \mathbf{B}_c u(t) \qquad \text{(1.19)}$$

where $\bullet_c$ stands for 'continuous-time' and:

- $\mathbf{A}_c$ is the $n{\times}n$ state matrix ($n{=}2N$);
- $\mathbf{B}_c$ is the $n{\times}m$ input matrix;
- $x(t)$ is the *state vector* with dimensions n.

The number of elements of the state vector is the number of independent variables needed to describe the state of the system.

When defining a state space model, the state equation is combined with the so-called *observation equation*. In practical applications only a limited number of degrees of freedom are monitored and, therefore, the output measurements (accelerations, velocities or displacements) are usually evaluated in $l{<}N$ instrumented positions. The observation equation establishes the relation between the l measured outputs and the N degrees of freedom of the system as:

$$y(t) = \mathbf{C}_a \ddot{U}(t) + \mathbf{C}_v \dot{U}(t) + \mathbf{C}_d U(t) \qquad \text{(1.20)}$$

where $y(t)$ is the measurement vector with dimensions l and $\mathbf{C}_a$, $\mathbf{C}_v$, $\mathbf{C}_d$ are the $l{\times}N$ output location matrices for accelerations, velocities and displacements

respectively. By assuming:

$$\mathbf{C_c} = [\mathbf{C_d} - \mathbf{C_a}\mathbf{M}^{-1}\mathbf{K} \quad \mathbf{C_v} - \mathbf{C_a}\mathbf{M}^{-1}\mathbf{C_N}], \quad \mathbf{D_c} = \mathbf{C_a}\mathbf{M}^{-1}\mathbf{B_N} \qquad (1.21)$$

equation (1.20) can be re-written in the usual form:

$$\boldsymbol{y}(t) = \mathbf{C_c}\boldsymbol{x}(t) + \mathbf{D_c}\boldsymbol{u}(t) \qquad (1.22)$$

where:

- $\mathbf{C_c}$ is the $l \times n$ output matrix;
- $\mathbf{D_c}$ is the $l \times m$ direct transmission matrix.

The state equation (1.19) and the observation equation (1.22) form the following continuous-time deterministic state-space model:

$$\dot{\boldsymbol{x}}(t) = \mathbf{A_c}\boldsymbol{x}(t) + \mathbf{B_c}\boldsymbol{u}(t)$$
$$\boldsymbol{y}(t) = \mathbf{C_c}\boldsymbol{x}(t) + \mathbf{D_c}\boldsymbol{u}(t) \qquad (1.23)$$

In real applications, measurements are always available at discrete time instants $k\Delta t$; therefore the continuous-time state-space model defined by (1.23) has to be re-written in discrete form to fit the experimental data:

$$\boldsymbol{x}_{k+1} = \mathbf{A}\boldsymbol{x}_k + \mathbf{B}\boldsymbol{u}_k$$
$$\boldsymbol{y}_k = \mathbf{C}\boldsymbol{x}_k + \mathbf{D}\boldsymbol{u}_k \qquad (1.24)$$

where $\boldsymbol{x}_k = \boldsymbol{x}(k\Delta t)$. If the time functions are assumed to be constant between two consecutive discrete samples, the matrices of the continuous and discrete models are related by:

$$\mathbf{A} = e^{\mathbf{A_c}\Delta t}$$

$$\mathbf{B} = \int_0^{\Delta t} e^{\mathbf{A_c}\tau}d\tau \, \mathbf{B_c} \qquad (1.25)$$

$$\mathbf{C} = \mathbf{C_c}$$

$$\mathbf{D} = \mathbf{D_c}$$

So far, the system was assumed to be subjected to deterministic inputs $\boldsymbol{u}(t)$. However, deterministic models are not able to exactly describe real measurements, for experimental data are always affected by noise. Therefore, noise has to be considered in the discrete-time state-space model (1.24) by adding two stochastic components. The obtained model is referred to as

24

discrete-time stochastic state-space model:

$$\begin{aligned} x_{k+1} &= \mathbf{A}x_k + \mathbf{B}u_k + w_k \\ y_k &= \mathbf{C}x_k + \mathbf{D}u_k + v_k \end{aligned}$$ (1.26)

where vector w_k represents the process noise due to disturbance and modeling inaccuracies and vector v_k is the measurement noise due to sensor inaccuracy. It should be noted that both these immeasurable vector signals are assumed to be white noise processes, with zero-mean and the following covariance matrices:

$$E\left(\begin{bmatrix} w_p \\ v_p \end{bmatrix} \begin{bmatrix} w_p^{\mathrm{T}} & v_p^{\mathrm{T}} \end{bmatrix}\right) = \begin{bmatrix} \mathbf{Q} & \mathbf{S} \\ \mathbf{R} & \mathbf{S}^{\mathrm{T}} \end{bmatrix}$$

$$E\left(\begin{bmatrix} w_p \\ v_p \end{bmatrix} \begin{bmatrix} w_q^{\mathrm{T}} & v_q^{\mathrm{T}} \end{bmatrix}\right) = 0 \ \ p \neq q$$ (1.27)

where p and q are two arbitrary time instants. In case of ambient vibration testing the input vector u_k is unknown and can be modeled together with the noise terms w_k and v_k. Therefore, the stochastic state-space model (1.26) assumes the form:

$$\begin{aligned} x_{k+1} &= \mathbf{A}x_k + w_k \\ y_k &= \mathbf{C}x_k + v_k \end{aligned}$$ (1.28)

where the new terms w_k and v_k are slightly different than the quantities introduced in (1.26) and representing just the effect of noise. However, even for these new terms the white noise assumption has to be valid: if this assumption is not fulfilled and the input contains some dominant frequency components, it will not be possible to distinguish those components from the eigen-frequencies of the system, since both will result as poles of the state matrix $\mathbf{A}$.

Covariance-driven SSI (SSI-Cov)

The SSI-Cov method [Peeters & De Roeck 1999, Peeters 2000] addresses the problem of identifying the stochastic state-space model (matrices $\mathbf{A}$ and $\mathbf{C}$) described by equation (1.28) starting from output-only data.

The first phase of the algorithms consists of defining the covariance matrix of the output. In discrete time, the output covariance matrix can be written as:

$$\Sigma_{yy_i} = \mathrm{E}[\boldsymbol{y}_{k+i}\boldsymbol{y}_k^{\mathrm{T}}] \tag{1.29}$$

where $i=1,\ldots,p+q$ is an arbitrary value of the time-lags, with in general $p+1=q$.

By considering equations (1.27), (1.28) and (1.29), Σ_{yy0} can be obtained as:

$$\begin{aligned}
\Sigma_{yy_0} = \mathrm{E}[\boldsymbol{y}_k\boldsymbol{y}_k^{\mathrm{T}}] &= \mathrm{E}[(\mathbf{C}\boldsymbol{x}_k + \boldsymbol{v}_k)(\mathbf{C}\boldsymbol{x}_k + \boldsymbol{v}_k)^{\mathrm{T}}] \\
&= \mathbf{C}E[\boldsymbol{x}_k(\boldsymbol{x}_k)^{\mathrm{T}}]\mathbf{C}^{\mathrm{T}} + \mathrm{E}[\boldsymbol{v}_k(\boldsymbol{v}_k)^{\mathrm{T}}] = \mathbf{C}\Sigma_{xx}\mathbf{C}^{\mathrm{T}} + \mathbf{R}
\end{aligned} \tag{1.30}$$

In the same way, the use of equations (1.27) and (1.28) allows to write the covariance matrix Σ_{xy} between the next state and the reference output as:

$$\begin{aligned}
\Sigma_{xy} = \mathrm{E}[\boldsymbol{x}_{k+1}\boldsymbol{y}_k^{\mathrm{T}}] &= \mathrm{E}[(\mathbf{A}\boldsymbol{x}_k + \boldsymbol{w}_k)(\mathbf{C}\boldsymbol{x}_k + \boldsymbol{v}_k)^{\mathrm{T}}] \\
&= \mathbf{A}\mathrm{E}[\boldsymbol{x}_k(\boldsymbol{x}_k)^{\mathrm{T}}]\mathbf{C}^{\mathrm{T}} + \mathrm{E}[\boldsymbol{w}_k(\boldsymbol{v}_k)^{\mathrm{T}}] = \mathbf{A}\Sigma_{xx}\mathbf{C}^{\mathrm{T}} + \mathbf{S}
\end{aligned} \tag{1.31}$$

By substituting equations (1.28) in (1.29) and considering the statistic properties of the noise components and of their covariance matrices (1.27), it is possible after some manipulations to re-write the covariance matrix of the output in the form:

$$\Sigma_{yy_i} = \mathbf{C}\mathbf{A}^{i-1}\Sigma_{xy} \tag{1.32}$$

Once the correlation matrices (estimated from the measurement data) have been computed for all the i time lags, the next step of the identification algorithm consists of gathering them together in a Hankel matrix:

$$\mathbf{H} = \begin{bmatrix}
\Sigma_{yy_1} & \Sigma_{yy_2} & \cdots & \Sigma_{yy_q} \\
\Sigma_{yy_2} & \Sigma_{yy_3} & \cdots & \Sigma_{yy_{q+1}} \\
\vdots & \vdots & \ddots & \\
\Sigma_{yy_{p+1}} & \Sigma_{yy_{p+2}} & \Sigma_{yy_{p+q}} &
\end{bmatrix} \tag{1.33}$$

By using the factorization property (1.32), the Hankel matrix $\mathbf{H}$ can later be factorized into the observability matrix $\mathbf{O}$ and the stochastic controllability matrix $\boldsymbol{\Gamma}$ as $\mathbf{H}=\mathbf{O}\boldsymbol{\Gamma}$. The observability matrix $\mathbf{O}$ can be obtained from $\mathbf{H}$ by performing the following singular value decomposition:

$$\mathbf{H} = \boldsymbol{U}\Delta\boldsymbol{V}^T = (\boldsymbol{U}_1 \quad \boldsymbol{U}_0)\begin{pmatrix} \Delta_1 & \\ & \Delta_0 \end{pmatrix}\mathbf{V}^T \tag{1.34}$$

26

$$\mathbf{O} = \boldsymbol{U\Delta}^{1/2} = \begin{pmatrix} \mathbf{C} \\ \mathbf{CA} \\ \vdots \\ \mathbf{CA}^p \end{pmatrix} \tag{1.35}$$

with matrix **O** having dimensions $(p+1)l \times n$. Matrix **C** is obtained from the first block row whereas the system matrix **A** is extracted from a least squares solution of:

$$\overline{\mathbf{O}}\mathbf{A} = \underline{\mathbf{O}} \; with \; \overline{\mathbf{O}} = \begin{pmatrix} \mathbf{C} \\ \mathbf{CA} \\ \vdots \\ \mathbf{CA}^{p-1} \end{pmatrix}, \underline{\mathbf{O}} = \begin{pmatrix} \mathbf{CA} \\ \mathbf{CA}^2 \\ \vdots \\ \mathbf{CA}^p \end{pmatrix} \tag{1.36}$$

It should be noted that, due to noise effects (modeling inaccuracies, measurement noise and computational noise) the order n of the model is unknown in Operational Modal Analysis.

Therefore, defined a range of variation for parameter n, the previous operations have to be performed for each possible model order. Subsequently, frequencies f_k and damping ratios ξ_k are extracted for each value of n by performing the eigenvalue decomposition of the system matrix **A**, first transforming the eigenvalues μ_k into the poles of the continuous time model and then using the poles with a positive imaginary component. In this way, $n/2$ poles are provided and plotted versus the frequency

values in the so-called *stabilization diagram*:

$$\lambda_k = \frac{\ln(\mu_k)}{\Delta t} \Rightarrow f_k = \frac{|\lambda_k|}{2\pi} \; ; \quad \xi_k = -\frac{\mathrm{Re}(\lambda_k)}{|\lambda_k|} \tag{1.37}$$

An example of stabilization diagram, referred to the same dataset adopted to exemplify the ASD and SV plots showed in Figures 1.1 and 1.2, is reported in Figure 1.3.

Finally, the mode shapes $\boldsymbol{\phi}_k$ are evaluated by multiplying the output matrix **C** and the corresponding eigenvectors $\boldsymbol{\psi}_k$ of **A**:

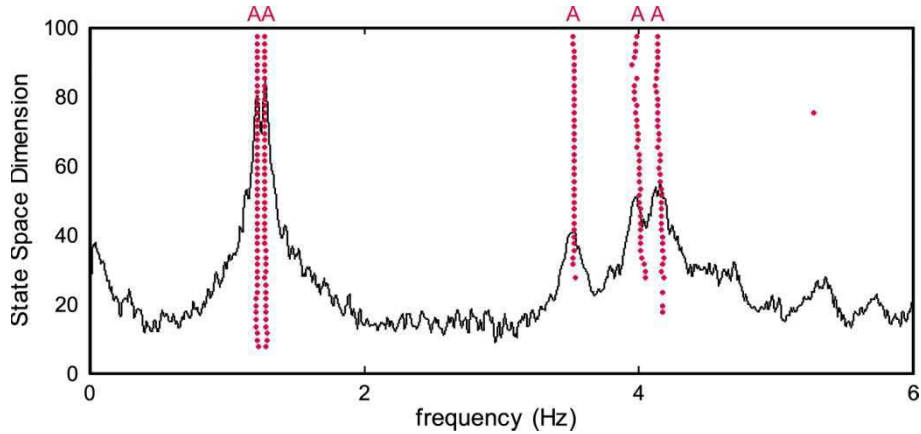$$\boldsymbol{\phi}_k = \mathbf{C}\boldsymbol{\psi}_k \tag{1.38}$$

Figure 1.3 SSI: Stabilization diagram and identification of the natural frequencies of the *San Vittore* bell-tower

Data-driven SSI (SSI-Data)

Unlike the SSI-Cov, the *Data-driven Stochastic Subspace Identification* method (SSI-Data) [Van Overschee & De Moor 1996] avoids the computation of covariance between the outputs. This step is replaced by projecting the row space of future outputs into the row space of past outputs. Indeed, the concepts of covariance and projection are closely related as they both aim at cutting out the (uncorrelated) noise.

The *Kalman filter* state [Ljung 1987, Juang 1994, Van Overschee & De Moor 1996] plays a crucial role in the SSI-Data technique, therefore its meaning is shortly described.

The main goal of the Kalman filter is to make optimal predictions $\hat{x}_{k+1}$ of the state vector x_{k+1} starting from the observations of the output at previous time instants (up to time $k\Delta t$), the available system matrices and the known noise covariances. The Kalman filter state estimates $\hat{x}_{k+1}$ are defined by recursive formulas obtained from the initial estimate $\hat{x}_0$, the initial covariance of the state estimate (Σ_{yy0}=E[$\hat{x}_0$ $\hat{x}_0^{\mathrm{T}}$]=0) and the output measurements at the previous time instants ($y_0,...,y_k$):

$$\dot{x}_{k+1} = \mathbf{A}\dot{x}_k + \mathbf{K}_k(\mathbf{y}_k - \mathbf{C}\dot{x}_k)$$

$$\mathbf{K}_k = \left(\mathbf{\Sigma}_{xx} - \mathbf{AP}_k\mathbf{C}^{\mathrm{T}}\right)\left(\mathbf{\Sigma}_{yy_0} - \mathbf{CP}_k\mathbf{C}^{\mathrm{T}}\right)^{-1}$$

$$\mathbf{P}_{k+1} = \mathbf{AP}_k\mathbf{A}^{\mathrm{T}} + \left(\mathbf{\Sigma}_{xx} - \mathbf{AP}_k\mathbf{C}^{\mathrm{T}}\right)\left(\mathbf{\Sigma}_{yy_0}\right.$$
$$\left. - \mathbf{CP}_k\mathbf{C}^{\mathrm{T}}\right)^{-1}\left(\mathbf{\Sigma}_{xx} - \mathbf{AP}_k\mathbf{C}^{\mathrm{T}}\right)^{\mathrm{T}}$$

$$(1.39)$$

The estimates $\dot{x}_{k+1}$ are subsequently gathered to form the Kalman filter state sequence, used in the SSI-Data algorithm:

$$\dot{\mathbf{X}}_i = (\dot{x}_i \ \dot{x}_{i+1} \ldots \ \dot{x}_{i+j+1}) \in \mathbb{R}^{n \times j} \tag{1.40}$$

A fundamental preliminary task in the SSI-Data technique consists of collecting the output measurements in a block Hankel matrix (a matrix being constant along its anti-diagonal) with $2i$ block rows and N columns. For statistical reasons it is assumed $N \to \infty$. The Hankel matrix can be subdivided into a past and a future part:

$$\mathbf{H} = \frac{1}{\sqrt{N}} \begin{pmatrix} y_0 & y_1 & \cdots & y_{N-1} \\ y_1 & y_2 & \cdots & y_N \\ \vdots & \vdots & \ddots & \vdots \\ y_{i-1} & y_i & \cdots & y_{i+N-2} \\ y_i & y_{i+1} & \cdots & y_{i+N-1} \\ y_{i+1} & y_{i+2} & \cdots & y_{i+N} \\ \vdots & \vdots & \ddots & \vdots \\ y_{2i-1} & y_{2i} & \cdots & y_{2i+N-2} \end{pmatrix} = \begin{pmatrix} \mathbf{Y}_{0|i-1} \\ \mathbf{Y}_{i|2i-1} \end{pmatrix} = \begin{pmatrix} \mathbf{Y}_p \\ \mathbf{Y}_f \end{pmatrix} \tag{1.41}$$

The output is scaled by a factor $1/\sqrt{N}$. The subscripts of $\mathbf{Y}_{(0|i-1)}$ are the subscripts of the first and last element in the first column of the Hankel matrix. The subscripts p and f indicate *past* and *future* and the two matrices are obtained by splitting the $\mathbf{H}$ matrix in two sub-matrices of i block rows each.

The first step of SSI-Data procedure is the projection of the row space of the future outputs into the row space of the past outputs:

$$\mathcal{P}_i \equiv \frac{\mathbf{Y}_f}{\mathbf{Y}_p} \equiv \mathbf{Y}_f \mathbf{Y}_p^{\mathrm{T}} \left(\mathbf{Y}_p \mathbf{Y}_p^{\mathrm{T}}\right)^* \mathbf{Y}_p \tag{1.42}$$

The main motivation behind this projection is that it retains all the information in the past that is useful to predict the future. From equation (1.42) it

is clear how projections and covariances are closely related: the products $\mathbf{Y}_f\mathbf{Y}_p^{\mathrm{T}}$ and $\mathbf{Y}_p\mathbf{Y}_p^{\mathrm{T}}$ are block Toeplitz matrices containing covariances between outputs. The projections defined by equation (1.41) are numerically computed by using the *QR-factorization* of the Hankel matrix [Peeters & De Roeck 1999].

The main theorem of the stochastic subspace identification [Van Overschee & De Moor 1996] states that the projection $\mathcal{P}_i$ can be factorized as the product of the previously defined extended observability matrix (1.35) and the Kalman filter state sequence (1.40):

$$\mathcal{P}_i \equiv \mathbf{O}_i\dot{\mathbf{X}}_i = \begin{pmatrix} \mathbf{C} \\ \mathbf{CA} \\ \vdots \\ \mathbf{CA}^p \end{pmatrix} (\dot{x}_i \;\; \dot{x}_{i+1} \; \dots \; \dot{x}_{i+j+1}) \tag{1.43}$$

In order to identify the system matrices $\mathbf{A}$ and $\mathbf{C}$, another projection can be defined, obtained by shifting one block row down the separation between past and future outputs of the Hankel matrix:

$$\mathcal{P}_{i-1} \equiv \frac{\mathbf{Y}_f^{\,-}}{\mathbf{Y}_p^{\,+}} \equiv \mathbf{O}_{i-1}\dot{\mathbf{X}}_{i+1} \tag{1.44}$$

The Kalman state sequences $\dot{\mathbf{X}}_i$, $\dot{\mathbf{X}}_{i+1}$ are computed from output data only. The system matrices can be determined from the following over-determined set of linear equations, obtained by stacking the state space models for time instants i to $i+N-1$:

$$\begin{pmatrix} \dot{\mathbf{X}}_{i+1} \\ \mathbf{Y}_{i|i} \end{pmatrix} = \begin{pmatrix} \mathbf{A} \\ \mathbf{C} \end{pmatrix} \dot{\mathbf{X}}_i + \begin{pmatrix} \mathbf{W}_i \\ \mathbf{V}_i \end{pmatrix} \tag{1.45}$$

where $\mathbf{Y}_{(i|i)}$ is a Hankel matrix with only one block row and $\mathbf{W}_i$, $\mathbf{V}_i$ are the residuals. Since the Kalman state sequences and the outputs are known and the residuals are uncorrelated with $\dot{\mathbf{X}}_i$, the set of equations can be solved for $\mathbf{A}$ and $\mathbf{C}$ in a least square sense:

$$\begin{pmatrix} \mathbf{A} \\ \mathbf{C} \end{pmatrix} = \begin{pmatrix} \dot{\mathbf{X}}_{i+1} \\ \mathbf{Y}_{i|i} \end{pmatrix} \dot{\mathbf{X}}_i^{\,*} \tag{1.46}$$

The noise covariances $\mathbf{Q}$, $\mathbf{R}$ and $\mathbf{S}$ are recovered as the covariances of the

least-squares residuals:

$$\begin{pmatrix} \mathbf{Q} & \mathbf{S} \\ \mathbf{S}^{\mathrm{T}} & \mathbf{R} \end{pmatrix} = \begin{pmatrix} \mathbf{W}_i \\ \mathbf{V}_i \end{pmatrix} \begin{pmatrix} \mathbf{W}_i^{\mathrm{T}} & \mathbf{V}_i^{\mathrm{T}} \end{pmatrix} \qquad (1.47)$$

Considering the properties of stochastic systems, it can be shown that matrices $\mathbf{A}$, $\mathbf{C}$, $\mathbf{Q}$, $\mathbf{R}$, $\mathbf{S}$ can be transformed to $\mathbf{A}$, $\mathbf{\Sigma}_{xx}$, $\mathbf{C}$, $\mathbf{\Sigma}_{yy0}$. Matrices $\mathbf{\Sigma}_{yy0}$ and $\mathbf{\Sigma}_{xx}$ can be computed according to equations (1.30)-(1.31).

The identification problem is now theoretically solved: based on the outputs, the system order n and the system matrices $\mathbf{A}$ and $\mathbf{C}$ are identified. Natural frequencies f_k and mode shapes ϕ_k can be obtained following the same procedure previously described for the SSI-Cov technique.

The remark about model order n is valid for the SSI-Data, too. Due to noise effects (modeling inaccuracies, measurement noise, computational noise) the order n of the model is unknown in Operational Modal Analysis. Therefore, as previously described, the problem of model order determination is better solved by building a stabilization diagram.

1.3 Automated OMA procedures

The identification of modal parameters from recorded structural vibrations usually requires the skills and knowledge of an expert user and, therefore, is a task characterized by significant human interaction. Such features make traditional (manual) OMA techniques not suitable for applications where a large amount of data needs to be processed in a short time. Therefore, in the field of continuous dynamic monitoring of civil engineering structures, the need for tools that can automatically process the recorded response has arisen in the last years.

In order to minimize the need for human interaction, research has recently focused on algorithms that can automatically extract accurate estimates of the modal parameters from continuously recorded dynamic response signals. Such

goal is usually achieved by automating two main steps: i) the modal parameters estimation (MPE) process, meaning the extraction of modal parameters from a single set of data; ii) the modal tracking, consisting in tracking the evolution in time of the modal characteristics of a structure. In the following, a brief overview of the existing approaches for the automation of the MPE phase is presented.

A possible classification of existing automatic OMA techniques can be based on the parametric or non-parametric nature of the automated algorithm.

Considering the case of non-parametric techniques working in the frequency domain, [Brincker et al. 2007] proposed an automated version of the FDD algorithm in order to remove any user interaction in the peak selection process. The procedure is based on the definition of a modal domain for each of the identified peaks of the first SV line by setting limit values for the modal coherence function and the modal domain function. The technique essentially consists of the repeated application of the following steps:

- identification of the maximum of the spectra in a defined search domain;
- application of the modal coherence function and harmonic indicator to check the physical nature of the identified peak;
- definition of a modal domain if the peak is physical, of a noise domain otherwise;
- redefinition of the search domain by removing the previously defined modal or noise domains;
- repetition of the previous steps in the reduced search domain until a defined number of natural frequencies has been identified, the search domain is empty or the maximum spectrum amplitude is lower than a predefined noise level.

An alternative approach based on the same methodology is proposed in [Magalhães et al. 2008] and applied to the response data continuously collected

by the permanent dynamic monitoring system installed on the *Infante D. Henrique bridge* in Portugal. The technique is essentially based on the same passages described in [Brincker et al. 2007]. In this case, a group of points associated to the same mode shape is detected around the identified peak of the first SV line by using the MAC coefficient as similitude value. If points are detected at both sides of the peak and their number is larger than a predefined value, then the peak is elected as physical and the corresponding group of points is defined as modal domain. Subsequently, the modal or noise domains are removed from the search set and the steps are repeated.

The main drawback of the described FDD-based techniques is represented by the high sensitivity of the proposed peak detection technique to noise and spurious harmonics, which can sometimes result in the need for a time consuming calibration process. The LEONIDA algorithm, presented in [Ranieri & Fabbrocino 2010], attempts to overcome this drawback by avoiding the preliminary threshold-based peak detection. The algorithm is still based on the FDD technique but the logical process is reversed with respect to the described automated methods. The first step of the procedure consists of obtaining the first SV line for a number of subsequent records. Afterwards, considering a pair of different records, the MAC coefficient between the two singular vectors at the same frequency line is obtained. The next passages consist of computing the averaged MAC vs. frequency diagram and identifying the bandwidth of each mode by considering mean and standard deviation of the MAC value sequence at each frequency line. Finally, the modal parameters are estimated within each bandwidth.

A common drawback of all the described non-parametric algorithms is the significant dependence on the use of the MAC coefficient. Therefore, the identification of closely spaced modes may be difficult and a sufficient frequency resolution is needed. In order to overcome these drawbacks and

obtain more accurate estimates of the modal parameters, research has focused on the automation of parametric procedures working both in the time domain (e.g. SSI) and frequency domain (e.g. PolyMAX [Peeters et al. 2004]). It is worth mentioning that among these techniques, the SSI algorithm appears particularly suited to be automated due to its algebraic nature and several SSI-based automated procedures have been developed in recent years [Peeters & De Roeck 2001, Andersen et al. 2007, Deraemaker et al. 2008, Magalhães et al. 2010, Ubertini et al. 2013, Reynders et al. 2012].

Considering that parametric modal identification essentially consists of analyzing a stabilization diagram with the aim of detecting alignments of stable poles, several approaches have been presented for the automatic interpretation of such plots. [Reynders et al. 2012] propose the following classification, based on the fact that a large part of these strategies use clustering techniques (i.e. the process of grouping points with analogous characteristics) to identify modes with similar properties:

- *Hierarchical clustering*. This approach consists of gathering all the stable modes of the stabilization diagram in separate clusters. The closest clusters are subsequently grouped together in a single cluster until the distance between the remaining groups is larger than a user-defined threshold value. The physical modes are finally extracted from the cluster with the smallest number of elements, corresponding to the minimum number of modes on a stable alignment in a stabilization diagram. The first application of this procedure to automatic modal identification was presented in [Peppa et al. 1997] who assumed eigenfrequency difference and MAC coefficient as indicators of the distance among clusters. The authors successfully applied the approach to develop an automatic version of the *Eigensystem Realization Algorithm* (ERA) [Pappa et al. 1992] which was later used to perform the *Experimental Modal Analysis* (EMA) of the Space Shuttle's tail rudder. A

34

decade later, the procedure proposed in [Peppa et al. 1997] was further improved by [Chauhan & Tcherniak 2009] who used genetic algorithms to automatically estimate the ERA parameters. An alternative approach is presented in [Goethals et al. 2004]. In this work, the authors propose to incorporate eigenfrequency and damping ratio differences as indicators of the distance. The problem of closely-spaced modes identification is solved by detecting the presence, in the same cluster, of modes with the same model order, which are later extracted and separated using the MAC coefficient. An even different distance measure criterion is proposed in [Allemang et al. 2010], where the MAC coefficient between extended, pole-weighted mode shape vectors identified for each mode shape is used. It is worth mentioning the quite different approach presented by [Verboven et al. 2004], where the number of modes in every cluster is assumed to be a-priori known. Finally, a successful application of the hierarchical clustering procedure is described in [Maghalães et al. 2009]. In this work, the authors implemented an automated version of the SSI-Cov technique by using the hierarchical clustering algorithm for the automatic interpretation of the stabilization diagram. The automated OMA procedure was successfully applied to investigate the evolution in time of the modal parameters of the mentioned *Infante D. Henrique bridge*, by analyzing more than 2500 continuously-recorded acceleration data sets;

- *Partitioning methods* divide the total set of modes into a given number of clusters. Possible approaches are the *K-means* clustering, where the clusters are mutually exclusive, and the *fuzzy C-means* clustering, where the predefined clusters overlap. These algorithms are essentially based on two passages, repeated in sequence until convergence is reached. At first, an initial number of clusters and their respective central values are defined. The data point corresponding to each cluster are or are not included in the group

35

depending on the Euclidean distance from the central point. Subsequently, the central values are iteratively replaced by the mean values of the points gathered in the clusters. In [Ramos et al. 2013] the K-means approach is used to develop an automated version of the SSI-Data technique in order to analyze the data collected by the dynamic monitoring system installed on the *St. Torcato church* in Portugal. In [Verboven et al. 2002] and [Vanlanduit et al. 2003], the fuzzy C-means approach is used to classify as physical or spurious the modes identified in the frequency domain, by defining two categories of clusters (C=2). The fuzzy C-means algorithm can also be used to gather the modes present in a stabilization diagram into a user-defined amount C of clusters, as proposed in [Scionti & Lanslots 2004]. In this case, the clustering is performed in a eigenfrequency-damping ratio plane. As pointed out in [Carden & Brownjohn 2008], damping ratios and eigenfrequencies are characterized by significantly different coefficients of variation, with that of the damping ratios being substantially larger. Therefore, the clustering analysis is better performed on the eigenvalues in the complex plane rather than on the eigenvalues in the eigenfrequency-damping ratio place. This leads to the definition of clusters with a more spherical nature. The main drawbacks in the application of the described non-hierarchical clustering algorithms is the significant sensitivity to the initial selection of clusters, which is a user-defined quantity. To overcome this shortcoming, [Ubertini et al. 2013] proposed an automated modal identification procedure based on the SSI-Data technique. The presented approach uses both frequencies and mode shapes to construct the clusters, whose initial value is not a user-defined quantity as new clusters are automatically created, where needed, during the clustering process. The procedure was applied to some data sets collected during ambient vibration tests performed on two Italian structures: the iron arch *San Michele bridge* in

Paderno d'Adda [Gentile & Saisi 2011] and a long-span steel footbridge near Bologna. The obtained results were subsequently compared to those provided by classical manual OMA techniques (PP, FDD, SSI). The automated procedure showed an excellent agreement with the manual approaches in terms of both natural frequencies and mode shapes, also allowing to identify weak or closely spaced modes that could not easily be detected using classical OMA techniques;

- *Histogram analysis* requires a partition of the frequency axis of the stabilization diagram into narrow bins. The number of stable modes is subsequently counted out of each bin. An application of the histogram analysis approach to automate the modal parameter estimation process is presented in [Scionti et al. 2003], even if the proposed procedure is characterized by quite a few user-defined parameters, including the bin's width. The performance of this approach was evaluated by comparing the obtained results with those provided by manual modal identification techniques. A good agreement was achieved for the PolyMAX procedure, working in the frequency domain and widely known for its clear stabilization diagrams.

Finally, it is worth mentioning the procedure presented by [Reynders et al. 2012] for a fully automated interpretation of the stabilization diagrams which does not require any user-defined parameter or threshold value. The procedure is based on the consecutive application of all the three clustering approaches previously described: first, all modes in the stabilization diagram are classified as physical or spurious by using the partitioning method; subsequently, the hierarchical clustering is applied to group together similar modes and obtain a clearer stabilization diagram; finally, a single mode is chosen from each cluster containing only physical modes by using criteria such as the number of modes in a cluster.

As previously explained, since automated OMA procedures can be successfully used to process data continuously acquired by permanent dynamic monitoring systems, they also allow to highlight possible variations in the time-evolution of the dynamic properties of the monitored structure. This feature represents a key aspect for all the OMA-based damage identification techniques which aim to detect structural anomalies by highlighting changes in the modal properties.

1.4 Effects of environmental and operational factors on modal parameters

One of the main aims of SHM is to detect, locate and assess the possible presence of damage on the investigated structure. A loss of stiffness, consequent to the occurrence of damage, corresponds to irreversible modifications of the structural dynamic behavior. Therefore, when damage detection is performed starting from the global vibrations of a structure, the methodology usually adopted consists of extracting meaningful features from the measured data and subsequently monitoring those features in order to detect variations caused by damage. This approach is in principle rather simple and straightforward. Nevertheless, practical applications are often characterized by several issues (e.g. the "output-only" nature of the data, the large amount of information to manage, etc.) that can significantly complicate the damage detection process. Among these, the most relevant is conceivably the effect of external factors (environmental and operational) on the monitored features, which can lead to such relevant variations of the modal parameters that changes due to damage are masked.

Several practical examples describing the misleading effect of external factors have been reported in literature. Robert & Pearson (1998) described a

monitoring program on a 9 span, 840 m long bridge. The results highlighted that environmental factors could lead to variations of the eigenfrequencies up to 3-4%. During the monitoring of the *Alamosa Canyon bridge* [Farrar et al. 1997], daily fluctuations of the first natural frequency of the structure of about 5% were observed. Approximately the same variation was detected for the first two natural frequencies of the *Z24-bridge* in Switzerland [Peeters & De Roeck 2001] whereas the change in mass due to traffic loading on the *Tamar bridge* in Southwest England led to reductions of the modal frequencies of 1.5-3% [Cross et al. 2013]. Effects of the external factors on the dynamic characteristics of civil structures have also been analyzed in [Sohn 2007; Ramos et al. 2010; Moser & Moaveni 2011; Magalhães et al. 2012].

In light of the above, it may be clear that when the dynamic response of a structure is used for structural condition assessment, all variations due to anything other than changes in the structure itself must be understood and accounted for [Cross et al. 2013]. If the effect of all external factors on the modal parameters can successfully be minimized or removed, any variation in the monitored features will be ascribed to structural changes.

In order to remove the effects of environmental and operational factors, a detailed analysis of the physics driving the variations of the controlled feature should be performed. However, finding a quantitative description of all the involved physical phenomena can result in a very complex and time consuming task. An alternative could be the implementation of black box models that reproduce the relationship between the controlled dynamic features and the external variables measured on the structure. This class of models are referred to as *input-output*. The major drawback of these methods is the need to determine what factors are to be measured because of their relevant influence on the variation of the controlled feature. This selection is not always straightforward and sometimes the measurement of the chosen external factors

is not even possible. To bypass this issue, methods have been developed that allow to remove the external effects without the need to measure any input. This class of models is referred to as *output-only*. The output-only techniques described in this work rely on a decomposition of the covariance matrix of the controlled features, monitored over a long time with changing (but unmeasured) external conditions [Kullaa 2004; Yan et al. 2005a; Deraemaeker et al. 2008]. Other output-only methods, not considered in this context, are based on the direct decomposition of time series with the extracted features or on the use of neural networks. Such methodologies are described and applied for instance in [Vanlanduit et al. 2005; Sohn et al. 2003].

1.4.1 *Input-Output methods*

The input-output methods considered in this Dissertation are essentially based on the development of a regression relationship between estimated features and external factors (environmental and operational) measured on the structure. Such models can be divided in two categories, depending on whether the effects of input variables at previous time instants are accounted for or not. When the relationship is defined only between simultaneously measured data the relationships are defined *static*. However, this characteristic can turn into a limitation when trying to model dynamic processes, such as the heating up/cooling down cycles of structures. In this context, the static relationship can be enhanced by taking into account also the influence of external factors measured at previous time instants. Models with the described characteristics are referred to as *dynamic*.

For both categories of input-output methods, several data sets need to be used to define the relation between inputs and outputs, understand the influence of each factor on the controlled feature and properly calibrate the parameters governing the method. The established model can subsequently be used to

predict future values of the controlled features when only measured external factors and outputs at previous time instants are known. In this way, it is in principle possible to detect variations of the considered feature due to causes other than external factors (e.g. the occurrence of damage).

It is worth mentioning that, in the context of input-output methods, a particular attention should be devoted to the selection of the factors that can significantly contribute to explain the observed variations of the dependent variable. It is important to check how the input candidates interrelate, in order to avoid highly correlated variables that could lead to a problem of multicollinearity and, therefore, to misleading results. Within this framework, it is worth reminding that the correlation r_{xy} between two variables x and y is defined as:

$$r_{xy} = \frac{\sum_{k=1}^{N}(x_k - \bar{x})(y_k - \bar{y})}{\sqrt{\sum_{k=1}^{N}(x_k - \bar{x})^2}\sqrt{\sum_{k=1}^{N}(y_k - \bar{y})^2}} \qquad \textbf{(1.48)}$$

where $\bar{x} = \frac{1}{N}\sum_{k=1}^{N}x_k$ and $\bar{y} = \frac{1}{N}\sum_{k=1}^{N}y_k$ are the average values of the considered variables, k is a discrete time instant and N is the number of data points.

Multiple Regression Analysis: Theoretical background and applications

Multiple Regression Analysis is a statistical technique that can be used to analyze the relation between a single dependent variable and one or more independent variables (predictors) [Hair et al. 1998]. The objective of multiple regression analysis is to use the independent variables whose values are known to predict the single dependent value selected by the researcher. Each independent variable is weighted by the regression analysis procedure to ensure maximum prediction from the set of independent variables. The weights denote

the relative contribution of the independent variables to the overall prediction.

When a regression relationship is established between the dependent variable and a single predictor, the so-called *simple regression* is obtained:

$$y = \theta_0 + \theta_1 x + \varepsilon \qquad (1.49)$$

where y is the dependent variable, x is the predictor, θ_0 and θ_1 are the parameters of the regression relationship, respectively referred to as *intercept* and *regression coefficient*, and ε is the difference between actual and predicted values of the dependent variable, termed *prediction error* or *residual*.

When two or more independent variables are used to predict the value of the dependent variable, the regression problem is referred to as *multiple regression*:

$$y = \theta_0 + \theta_1 x_1 + \theta_2 x_2 + \cdots + \theta_n x_n + \varepsilon \qquad (1.50)$$

The regression relationships (1.49) and (1.50) have been established to reproduce a linear dependence between predictors and dependent variable. Nonetheless, the need to model curvilinear effects can arise in some applications. In such cases, it is possible to adopt power transformations of an independent variable that add a nonlinear component for each additional power of the independent variable. Such relationships are known as *polynomials*:

$$y = \theta_0 + \theta_1 x + \theta_2 x^2 + \varepsilon \qquad (1.51)$$

If two or more independent variables are involved, *multivariate polynomials* are created. In this case, the procedure is the same applied to establish relationship (1.51).

In matrix form, previous equations (1.49) - (1.51) can all be expressed as:

$$\mathbf{y} = \mathbf{X}\boldsymbol{\theta} + \boldsymbol{\varepsilon} \qquad (1.52)$$

where $\mathbf{y}$ is a column vector containing the n measures y_k of the dependent variable y, $\mathbf{X}$ is a $n \times p$ matrix gathering the corresponding n values of the p selected predictors, $\boldsymbol{\theta}$ is a column vector formed by the p parameters weighting the contribution of each independent variable, $\boldsymbol{\varepsilon}$ is the vector of the prediction errors ε_k.

In order to accurately reproduce the experimental estimates of the dependent variable and simulate their future values, it is of utmost importance to select the inputs that lead to the best fit between measured output features and values $\hat{y}_k$ provided by the model. The criterion to be followed in the selection process of the independent variables has already been described in the previous section of this paragraph. Subsequently, the parameters $\boldsymbol{\theta}$ characterizing the model have to be determined. Their estimation can be achieved by using the *Least Squares* (LS) method. The LS approach minimizes the sum of the squared errors and leads to estimates ^ of the model parameters $\boldsymbol{\theta}$ in the form:

$$\widehat{\boldsymbol{\theta}} = (\mathbf{X}^{\mathrm{T}}\mathbf{X})^{-1}\mathbf{X}^{\mathrm{T}}\boldsymbol{y} \tag{1.53}$$

It should also be noted that, in system identification, it is usual to normalize input and output data so that the origin of the x and y axes lies at the "center of gravity" of the data points and the slope of the line of regression corresponds to the correlation coefficient [Newland 1993]. This is achieved by removing the mean value from each measurement x_k and y_k and dividing the results by the variable's standard deviation as follows:

$$\tilde{x}_k = \frac{x_k - \bar{x}}{\sigma_x} \qquad\qquad \tilde{y}_k = \frac{y_k - \bar{y}}{\sigma_y} \tag{1.54}$$

where the mean value $\bar{z}$ and standard deviation σ_z of the generic variable z are defined as:

$$\bar{z} = \frac{1}{N}\sum_{k=1}^{N} z_k \;, \qquad\qquad \sigma_z = \sqrt{\frac{1}{N-1}\sum_{k=1}^{N}(z_k - \bar{z})^2} \tag{1.55}$$

It should be noted that, when different quantities are available as input candidates, multiple relationships between inputs and outputs can be defined. This leads to the possibility of establishing several regression models and, therefore, to the need of assessing and comparing their ability to fit the experimental estimates of the dependent variables. A general discussion on this

issue can be found in [Ljung 1999], whereas in this context only some criteria used to assess and compare the quality of different models will be considered.

As the LS method minimizes the sum of the squares of the equation errors, a first quality criterion is the value of the *Loss Function* (LF):

$$V = \frac{1}{N} \sum_{k=1}^{N} \varepsilon_k^2 \tag{1.56}$$

where N is the total number of samples and the prediction errors are obtained as the difference between experimental and estimated values of the output variable:

$$\boldsymbol{\varepsilon} = \boldsymbol{y} - \boldsymbol{\hat{y}} \tag{1.57}$$

The main drawback of this quality criterion is that the value of the loss function continuously decreases as the model order increases. Another largely used quality criterion is the *Aikake's Final Predictio Error* (FPE) [Ljung 1999], defined as:

$$FPE = V \frac{1 + d/N}{1 - d/N} \tag{1.58}$$

with d being the number of estimated parameters. Alternatively, a widely known indicator of the model quality can be adopted, referred to as *coefficient of determination R^2* and defined as [e.g. Johnson & Wichern 1992]:

$$R^2 = 1 - \frac{\sum_{k=1}^{N} \hat{\varepsilon}_k^2}{\sum_{k=1}^{N}(y_k - \bar{y})^2} = \frac{\sum_{k=1}^{N}(\hat{y}_k - \bar{y})^2}{\sum_{k=1}^{N}(y_k - \bar{y})^2} \tag{1.59}$$

The second equality proves the coefficient of determination correspondent to the ratio between two variances. Therefore, it can be stated that R^2 provides the percentage of the total variation in the experimental outputs y_k explained by the predictors. If the coefficient of determination is equal to zero, then the selected independent variables have no influence on the output, whereas when R^2 is equal to one the variation of y_k is completely explained by the predictors.

In the context of SHM, regression analysis is most likely the simplest

available technique to correlate the observed external factors (predictors) and the identified natural frequencies (dependent variables). Temperatures measured on the structure and amplitude of excitation (e.g. traffic loading) are the environmental and operational factors typically selected as predictors because of their significant influence on the fluctuations of the natural frequencies. It is worth mentioning that, in practical applications, regression models are used in both static and dynamic form. By definition, a dynamic regression relationship is established between the dependent variable at time k and values of a single predictor at current time k as well as at *(p-1)* previous time instants. Therefore, for dynamic regression models, equation (1.49) can be specified as:

$$y_k = \theta_0 + \theta_1 x_k + \theta_2 x_{k-1} + \cdots + \theta_p x_{k-(p-1)} + \varepsilon_k \qquad \textbf{(1.60)}$$

whereas matrix **X** of equation (1.52) assumes the form:

$$\mathbf{X} = \begin{bmatrix} x_1 & \cdots & x_{1-(p-1)} \\ x_2 & \cdots & x_{2-(p-1)} \\ \vdots & \ddots & \vdots \\ x_n & \cdots & x_{n-(p-1)} \end{bmatrix} \qquad \textbf{(1.61)}$$

Due to the simplicity of the established input-output relationship, multiple regression models have been widely adopted in SHM of civil structures and infrastructures, both in their static and dynamic form.

In [Farrar et al. 1997], a static regression model was adopted to quantify the variability of modal parameters measured on the *Alamosa Canyon bridge* due to environmental and operational factors. As previously pointed out, the obtained results suggested that temperature differentials across the bridge deck were the driving forces for the frequency variations, which exhibited daily fluctuations up to 5%.

In [Magalhães et al. 2012] static and dynamic regression models were used to remove the effects of (measured) environmental and operational factors from the natural frequencies automatically identified from the acceleration data collected in *Infante D. Henrique bridge* in Porto, Portugal (Figure 1.4).

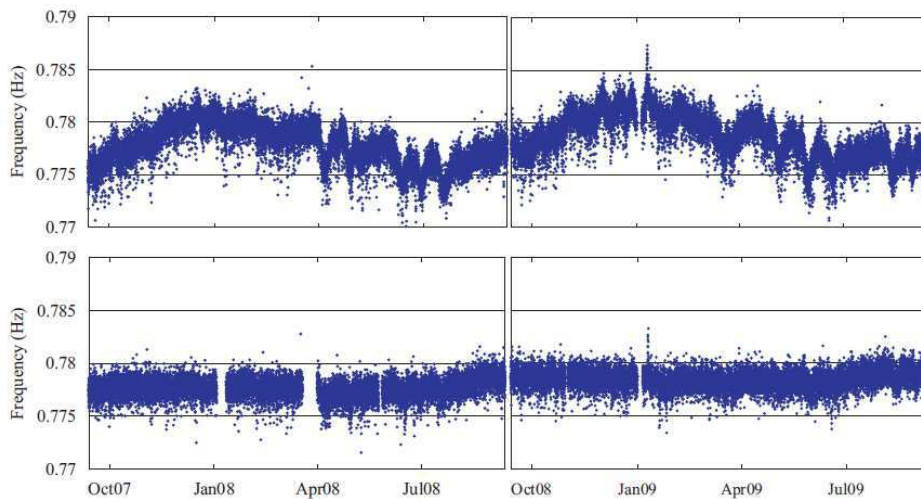**Figure 1.4** The *Infante D. Henrique bridge* in Porto [Magalhães et al. 2012]

Figure 1.5 Time evolution of the first natural frequency before and after the application of the dynamic regression model [Magalhães et al. 2012]

The results obtained for the first frequency (considering as predictors the temperatures referred to 6, 12, 18 and 24 hours time delay) are exemplified in Figure 1.5.

Another application of regression models to the SHM of bridges is presented in [Hu et al. 2015]. The paper describes the continuous dynamic monitoring of the *Westend bridge* in Berlin, Germany, between 2000 and 2013. The structure is a curved pre-stressed concrete box girder bridge built in 1963 (Figure 1.6).

(a) Bridge elevation   (b) Cross section

(c) Plan view and its position
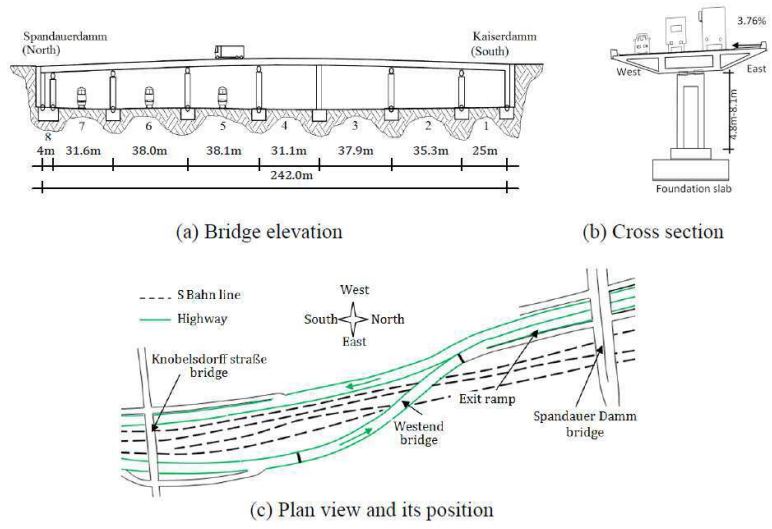
Figure 1.6 The *Westend bridge* in the A100 highway in Berlin [Hu et al. 2015]

(a) Plane view of Span 1-3 and locations of the velocity sensors V1-V20

(b) Section A-A and position of temperature sensors T1-T5
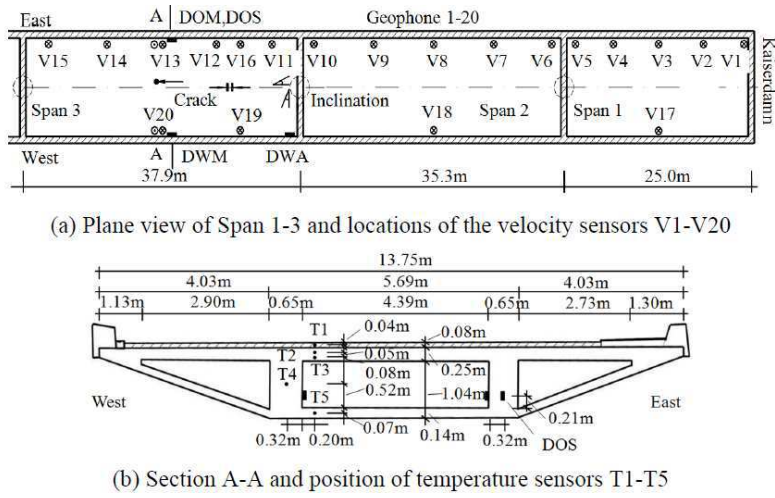
Figure 1.7 Deployment of velocity and temperature sensors on the *Westend bridge* [Hu et al. 2015]

47

(a) Temperature measured in different positions

(b) Estimated frequencies in different modes
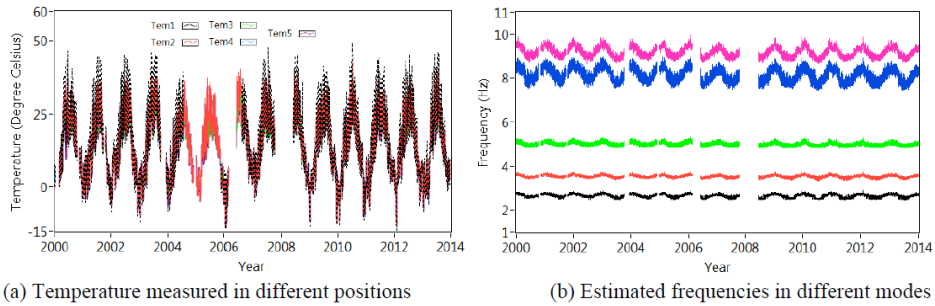
Figure 1.8 Variation of temperature records and estimated frequencies from 01/01/2000 to 31/12/2013 [Hu et al. 2015]

(a) Effect of temperature recorded by T1 on the identified frequencies in 2013

(b) Effect of temperature recorded by T4 on the identified frequencies in 2013
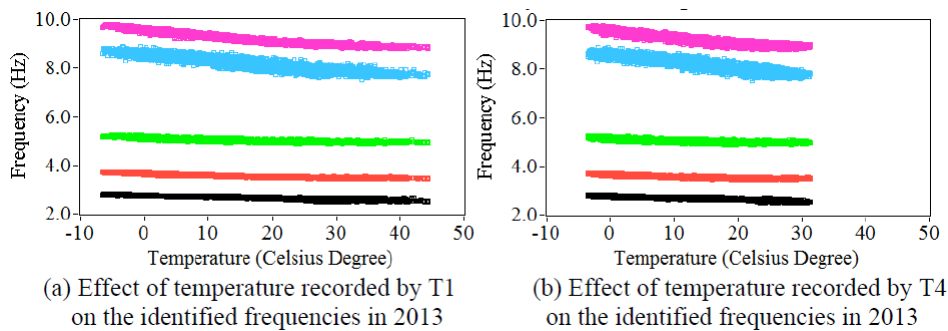
Figure 1.9 Effect of temperatures on the estimated frequencies [Hu et al. 2015]

The bridge consists of eight spans varying from 5.0 m to 38.0 m, with a whole length of 242.0 m. An integrated health monitoring system was implemented in 1994 with the main purposes of continuously recording the structural global dynamic responses, variation of strains, cracks and inclination in the critical sections as well as changes of the ambient factors under normal operational conditions. The system was modified and updated several times and currently consists of 32 sensors including vertical velocity sensors, accelerometers, temperature sensors, strain gauges, inclination sensors and position sensitive devices. In Figure 1.7 the position of velocity sensors, temperature sensors and one strain gauge is shown. The system has continuously recorded data since March 2000, with a sampling frequency of 128 Hz. The obtained results revealed a clear dependency of the frequency on

temperature, as proved by the obvious annual fluctuations of the time evolution reported in Figure 1.8 and by the correlation charts shown in Figure 1.9. In particular, a slight non linear influence of the temperature recorded by all 5 sensors on the identified modal frequencies was observed. The implementation of a polynomial regression relationship established between natural frequencies and measured temperature allowed to successfully remove the environmental effects and carry on the damage detection process on environment-independent features.

ARX models: Theoretical background and applications

As previously stated, static models establish a relationship only between simultaneously measured data and may not be able to accurately reproduce the effects of common dynamic processes. In this kind of applications, the use of dynamic regression models, accounting for the influence of inputs measured at previous time instants, seems to be more feasible.

Among the dynamic methods described in the system identification literature [Ljung 1999], ARX models are probably the most widely used. ARX models consist of an *Auto-Regressive* output and an *eXogeneous* input part. Considering a general time instant k, an output and an input variable designated y_k and x_k, respectively, and an error term ε_k taking into account the effects of non-modeled inputs and measurement noise, ARX models can be expressed in the following form:

$$y_k + a_1 y_{k-1} + \ldots + a_{n_a} y_{k-n_a} = b_1 x_{k-n_k} + b_2 x_{k-n_k-1} + \ldots + b_{n_b} x_{k-n_k-n_b+1} + \varepsilon_k \quad \textbf{(1.62)}$$

It should be noted that in (1.62) only one input (e.g. temperature) and one output (e.g. natural frequency) were considered. Equation (1.62) can be easily generalized to the case of multiple inputs by replacing b_k and x_k with corresponding row and column vectors, respectively.

ARX models are characterized by three model orders: the auto-regressive

order n_a (corresponding to the number of the considered past measures of the dependent variable), the exogenous order n_b (corresponding to the number of previous model inputs taken into account) and the pure time delay between input and output n_k. Orders n_a and n_b determine the number of model parameters: a_i $(i = 1,...,n_a)$, b_j $(j = 1,...,n_b)$. It should be noted that classic static regression models represent a particular class of ARX models, obtained with the specific selection of parameters: $n_a=0$, $n_b=1$, $n_k=0$ (ARX010):

$$y_k = b_1 x_k + \varepsilon_k \tag{1.63}$$

The ARX model (1.62) can also be written in the form:

$$a(q)y_k = b(q)x_k + \varepsilon_k \tag{1.64}$$

where the shift operator $q^{-1}y_k=y_{k-1}$ is introduced and where $a(q)$ and $b(q)$ are two polynomials defined as:

$$a(q) = 1 + a_1 q^{-1}+...+a_{n_a} q^{-n_a}$$
$$b(q) = b_1 q^{-n_k} + b_2 q^{-n_k-1}+...+b_{n_b} q^{-n_k-n_b \mp 1} \tag{1.65}$$

Equation (1.64) can be associated to the general expression typically used to define linear input-output models [Ljung 1999]:

$$y_k = H(q,\boldsymbol{\theta})x_k + W(q,\boldsymbol{\theta})\varepsilon_k \tag{1.66}$$

where $\boldsymbol{\theta}$ is the vector grouping the modal parameters, H is the transfer function and W is the noise model. Comparing (1.64) and (1.66), it is straightforward to obtain:

$$\boldsymbol{\theta}^{\mathrm{T}} = (a_1 ... a_{n_a} b_1 ... b_{n_b})$$
$$H(q,\boldsymbol{\theta}) = \frac{b(q)}{a(q)}, \quad W(q,\boldsymbol{\theta}) = \frac{1}{a(q)} \tag{1.67}$$

As previously described for the case of multiple regression analysis, the parameters of ARX models can be easily estimated by simply applying a LS method. The methodology can be conveniently shown by re-writing equation (1.62) in the form:

$$y_k = \boldsymbol{\varphi}^{\mathrm{T}}\boldsymbol{\theta} + \varepsilon_k \tag{1.68}$$

50

where $\boldsymbol{\varphi}^{\mathrm{T}} = \left[-y_{k-1} \ \dots \ -y_{k-n_a} \ x_{k-n_k} \ \dots \ x_{k-n_k-n_b+1} \right]$ is a row vector grouping the past measures of dependent variables and predictors. Considering N measured values of output and input variables, it is possible to write equation (1.68) for each of the N samples. By doing this, the ARX problem can be described by the same matrix equation (1.52) obtained for the multiple regression analysis. In particular, for the specific case of ARX models:

$$\boldsymbol{y} = \begin{pmatrix} y_1 \\ y_2 \\ \vdots \\ y_N \end{pmatrix} \in \mathbb{R}^N \ , \qquad \mathbf{X} = \begin{pmatrix} \boldsymbol{\varphi}_1^{\mathrm{T}} \\ \boldsymbol{\varphi}_2^{\mathrm{T}} \\ \vdots \\ \boldsymbol{\varphi}_N^{\mathrm{T}} \end{pmatrix} \in \mathbb{R}^{N \times (n_a + n_b)} \ , \qquad \boldsymbol{\varepsilon} = \begin{pmatrix} \varepsilon_1 \\ \varepsilon_2 \\ \vdots \\ \varepsilon_N \end{pmatrix} \in \mathbb{R}^N$$

whereas the estimates $\widehat{\boldsymbol{\theta}}$ of the model parameters are still obtained by solving the considered system of equations using the LS method, according to (1.53).

It should be noted that when multiple input candidates and choices of the model orders n_a, n_b, n_k are available, several different ARX models can be identified from the data. Therefore, the same quality criteria described in the previous paragraph can be adopted to compare the fitting skills of the models.

ARX models were successfully used to remove the effects of environmental and operational factors in different practical applications on civil structures [Peeters & De Roeck 2001; Ramos et al. 2010; Moser & Moaveni 2011; etc.].

The results presented by Peeters & De Roeck (2001) are particularly significant in the context of damage detection, as the investigated structure was intentionally damaged at the end of the monitoring period. This provided the possibility of training the ARX model over a healthy reference period and subsequently using it to detect real damage. The object of the investigation was the *Z24-bridge* in Switzerland (Figure 1.10), a classical post-tensioned concrete box girder bridge with a main span of 30.0 m and two side spans of 14.0 m. The bridge was monitored for 10 months (November 1997-Semptember 1998) using both accelerometers and sensors capturing environmental parameters.
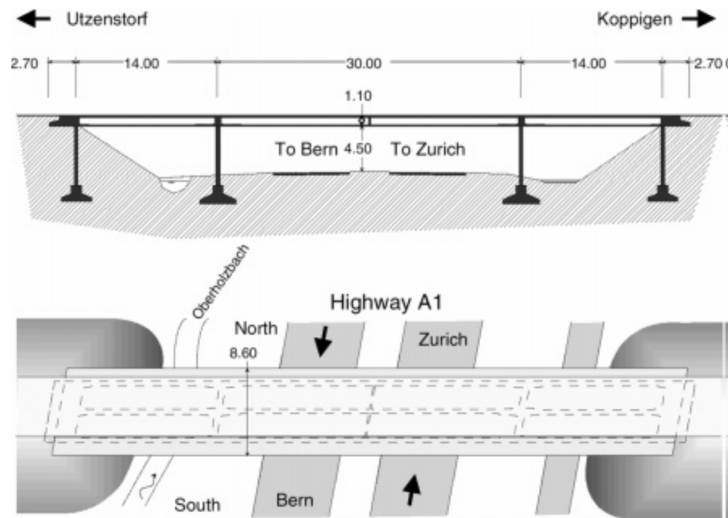
Figure 1.10 The *Z24-bridge*: longitudinal section and aerial view [Peeters & De Roeck 2001]
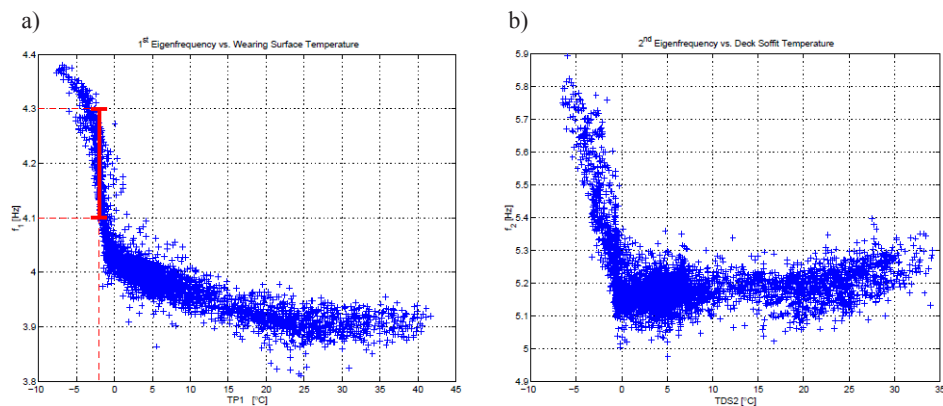

Figure 1.11 a) 1st eigenfrequency vs. wearing surface temperature; b) 2nd eigenfrequency vs. deck soffit temperature [Peeters & De Roeck 2001]

The correlation between the automatically identified four natural frequencies and the recorded temperature showed a bilinear behavior for almost all the frequency-temperature combinations (Figure 1.11). This non-linearity is explained by considering the different behavior of asphalt during warm periods, when it does not significantly contribute to the stiffness of the structure, and
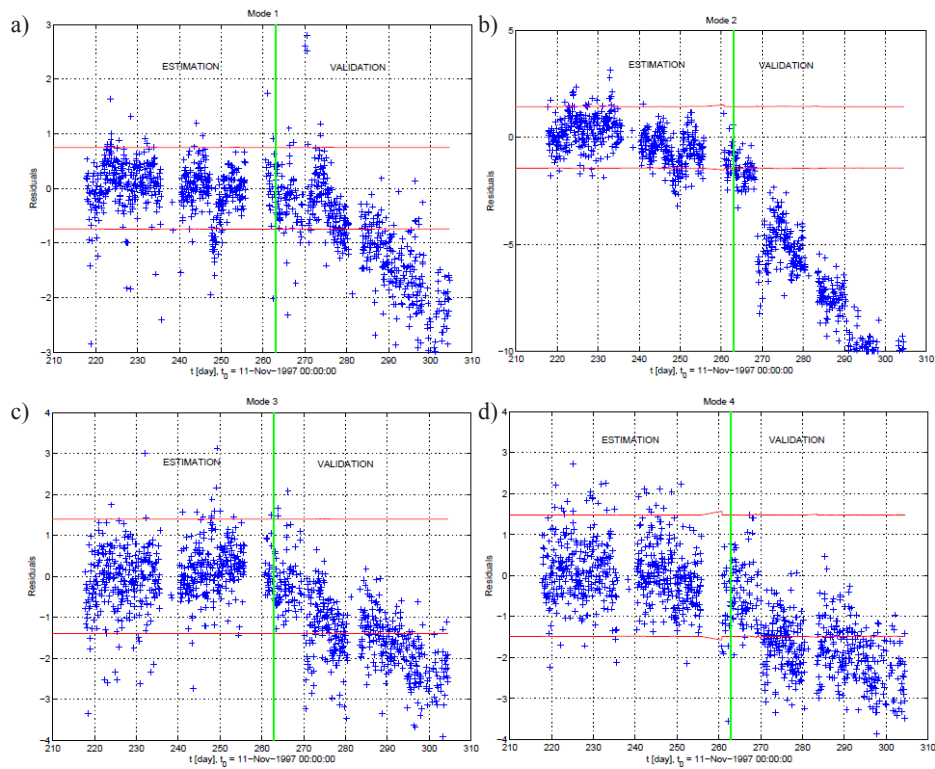
Figure 1.12 Residuals of the ARX-model and 95% confidence intervals for: a) 1st mode; b) 2nd mode; c) 3rd mode; d) 4th mode [Peeters & De Roeck 2001]

cold periods, when its effect becomes relevant. Since the ARX model is defined as a linear technique, the method was applied only to data collected during warm periods.

During the process of selection of the input variable, only temperature variables were retained as possible inputs, because the monitored wind characteristics, rainfall and humidity did not show any relation with the natural frequencies of the structure.

Static regression models and dynamic ARX models were implemented by considering a single input and a single output (SISO), and subsequently by selecting multiple inputs (MISO). Notwithstanding the improved performances

of the static relationship when transitioning from single to multiple inputs, the results were still less accurate than those obtained by the SISO ARX methods.

Finally, the SISO ARX model was adopted to simulate future values of the natural frequencies and detect the damage scenarios actually produced on the bridge. The method was successful and the effects of damage were highlighted by decrease of the eigenfrequencies and values of the simulation error exceeding the set confidence intervals (Figure 1.12).

1.4.2 Output only methods

As anticipated, the correct selection of the factors with the most relevant influence on the controlled modal parameter can be a difficult task. Furthermore, the continuous measurement of such factors is not always available or achievable. To bypass this major drawback, environmental and operational effects can be removed by adopting output-only models, where the measurement of external factors is not required. The only output-only method covered in this context will be the *Principal Component Analysis* (PCA), based on a decomposition of the covariance matrix of the controlled feature [Kullaa 2004; Yan et al. 2005a; Deraemaeker et al. 2008]. Other output-only methods based on the same principle, such as the *Factor Analysis* (FA), are detailed in [Johnson & Wichern 1992].

Principal Component Analysis: Theoretical background and applications

Principal component analysis (PCA) is a multivariate statistical tool performing a linear transformation of data to a new coordinate system. PCA is typically used to reduce the dimensions of a data set by replacing a group of correlated variables with a new set of independent variables, designated principal components (PC), that still take into account those characteristics of the data set significantly contributing to its variance [Deraemaeker et al. 2008].

54

Let us consider a set of n variables collected in a vector $\boldsymbol{y}$. The goal of PCA is to find a $n \times n$ matrix $\mathbf{P}$ that is orthonormal ($\mathbf{PP}^T = \mathbf{P}^T\mathbf{P} = \mathbf{I}$) and that allows the coordinate transformation:

$$\boldsymbol{x} = \mathbf{P}\boldsymbol{y} \qquad (1.69)$$

so that the obtained n principal components $\boldsymbol{x}$ are independent on each other (meaning the covariance matrix of $\boldsymbol{x}$ is diagonal) and their variance decreases from x_1 to x_n. Therefore, the first PC will be the one contributing the most to the variability of the initial data set, whereas some of the last components of $\boldsymbol{x}$ could be ignored as not relevant to explain the variance of the original variables $\boldsymbol{y}$.

Given (1.69) and the properties of matrix $\mathbf{P}$, it is possible to re-write the relation between $\boldsymbol{y}$ and $\boldsymbol{x}$ as:

$$\boldsymbol{y} = \mathbf{P}^T\boldsymbol{x} \qquad (1.70)$$

Therefore, the covariance matrix $\boldsymbol{\Sigma}_{yy}$ of $\boldsymbol{y}$ can be related to the diagonal covariance matrix $\boldsymbol{\Sigma}_{xx}$ of $\boldsymbol{x}$ as follows:

$$\boldsymbol{\Sigma}_{yy} = \mathrm{E}[\boldsymbol{yy}^T] = \mathrm{E}[\mathbf{P}^T\boldsymbol{xx}^T\mathbf{P}] = \mathbf{P}^T\boldsymbol{\Sigma}_{xx}\mathbf{P} \qquad (1.71)$$

The singular value decomposition (SVD) of $\boldsymbol{\Sigma}_{yy}$ gives:

$$\boldsymbol{\Sigma}_{yy} = \mathbf{U\Lambda U}^T \qquad (1.72)$$

where $\mathbf{\Lambda}$ is a diagonal matrix whose elements λ_j are the eigenvalues of the covariance matrix $\boldsymbol{\Sigma}_{yy}$, provided in a descending order, and $\mathbf{U}$ is an orthonormal matrix whose j-th column is the eigenvector corresponding to the j-th eigenvalue. From the comparison of (1.71) and (1.72) it is straightforward to obtain the transformation matrix $\mathbf{P} = \mathbf{U}^T$ and the principal components x_j, correspondent to the eigenvalues λ_j.

To reduce the dimensions of the problem, it is possible to consider only the first m eigenvalues, out of the n collected in $\mathbf{\Lambda}$, that are relevant to explain the variability of the original dataset $\boldsymbol{y}$. Theoretically, the value of m should be selected by looking for a gap in the diagram of the eigenvalues. However, since

a gap is seldom detected in practical applications, the choice of m is usually based on the definition of ratio I:

$$I = \frac{\sum_{i=1}^{m} \lambda_i}{\sum_{i=1}^{n} \lambda_i} \tag{1.73}$$

Ratio I defines the percentage of the variability of the original variables y that is explained by the first m components of x. Therefore, once a threshold value of I has been chosen (e.g. 0.95), the value of m will descend accordingly.

After the decomposition of matrix $\mathbf{\Sigma}_{yy}$ and the following selection of m, the set of m principal components $\hat{x}$ can be obtained from the coordinate transformation (1.69) by using a matrix $\hat{\mathbf{P}}$ obtained from the first m columns of $\mathbf{U}$ (recall that $\mathbf{P} = \mathbf{U}^{\mathrm{T}}$).

The dimension reduction obtained with the selection of the principal components $\hat{x}$ allows to eliminate those features with a non-significant contribution on the variability of the original dataset (e.g. random errors in the identification of natural frequencies) while keeping into account the effects due to relevant factors. The following step consists of transforming the selected $\dot{x}$ PC back to the original coordinate system using the reduced matrix $\hat{\mathbf{P}}$:

$$\hat{y} = \hat{\mathbf{P}}^{\mathrm{T}}\hat{x} = \hat{\mathbf{P}}^{\mathrm{T}}\hat{\mathbf{P}}y \tag{1.74}$$

If the re-mapped values are removed from the original variables as:

$$\varepsilon = y - \hat{y} \tag{1.75}$$

the obtained features ε (residual errors) will not be affected by the factors modeled by the PC. Therefore, computing $\hat{\mathbf{P}}$ from a reference dataset and applying transformation (1.74) to a new group of variables will lead to features subject to the effects of new factors that were not observed in the reference dataset [Magalhães et al. 2012].

PCA has been proved to be efficient in different practical applications, using data obtained both from numerical simulations and permanent dynamic monitoring of real structures.

An interesting application, where multiple linear regression and PCA were adopted in sequence in order to remove the effects of environmental and operational factors, is described in [Magalhães et al. 2012]. In this application, data were provided by the continuous dynamic monitoring system installed on the already mentioned *Infante D. Henrique bridge* over the Douro River in Porto, Portugal (Figure 1.4). The structure, whose dynamic behavior has been continuously monitored since September 2007, consists of a rigid pre-stressed concrete box girder supported by a thin reinforced concrete arch that spans 280 m between abutments.

In this application, the PCA was used after the application of dynamic regression methods in order to minimize the effect of non-monitored factors that that could not be taken into account by the previous models (e.g. humidity, wind, etc.). The obtained results proved the effectiveness of the adopted statistical tools, allowing to detect the effects of simulated damage scenarios which produced frequency variations smaller than 0.4%.

In [Yan et al. 2005a; Deraemaeker et al. 2008] PCA was successful in detecting damage from data produced by the numerical model of a bridge, made of different materials (namely steel and concrete) exhibiting different variations with the temperature. Damage scenarios were introduced as stiffness reductions and during the monitoring process the structure was subject to temperature variations as well as temperature gradients. In both applications it was possible to remove the effect of environmental factors on the dynamic behavior of the structure, therefore detecting the occurrence of damage. In [Yan et al. 2005a] the methodology was also successfully applied to data collected from a physical model of a wooden bridge. The bridge model was randomly excited using an electro-dynamic shaker and damage was simulated by adding different lumped masses to the structure.

1.5   Detection of structural anomalies: Control Charts

The application of the models described in the previous paragraph allows to obtain modal parameters no longer affected by the effect of external factors. Therefore, any variation of the obtained features can be related to structural reasons. In order to detect the presence of anomalous occurrences, the time evolution of the obtained environment-independent features has to be investigated.

One possibility consists of exploring the trend of the modal parameters after the removal of the environmental effects, in terms of:

1. prediction error ε_k between experimental and predicted values of the modal frequencies;

2. depurated experimental frequencies, computed as:

$$\hat{f}_i(T_k) = \bar{f}_i + \varepsilon_{ik} \tag{1.76}$$

where $\bar{f}_i$ is the mean value of the original i-th frequency during the reference period, where the process is known to be in control.

An alternative approach consists of using statistical tools defined *control charts*. A control chart typically consists of a plot where the variation in time of data is represented along with user-defined variation limits. The variation of the monitored variables due to ordinary causes is checked by means of horizontal lines designated *control limits* and computed from the experimental samples only when the process is assumed to be in control. In this way, any observation laying outside the control limits has to be considered the result of unusual sources of variability (e.g. the occurrence of damage). In practical applications control charts can be used according to two different approaches. In one case, the stability of a sample observations can be monitored. This means that several observations are available and the goal is to check if all the samples respect the control limits. In the second case, control charts can be used to define a safe control region to check the quality of future observations. This requires to

identify a reference period (*training period*) where the process is assumed to be in control and to take into account the properties of data collected during this time interval. This second approach is the more adequate to be implemented in a permanent monitoring system, where one of the main goals is to check if each new observation lies within a previously defined "safety" region.

One of the most frequently used control charts is the $\bar{X}$-*chart* (or *X-bar chart*). This particular chart allows to control just one feature and the amount of variation in time of the individual observations (or the mean of groups of observations) is checked by drawing three horizontal line: the center line (CL), the upper control limit (UCL) and the lower control limit (LCL). CL is positioned at the mean of the sample with all observations, indicated with $\bar{\bar{x}}$, whereas the values of UCL and LCL are respectively given by adding and subtracting three times the sample standard deviation σ to the mean value $\bar{\bar{x}}$:

$$\text{CL} = \bar{\bar{x}}$$
$$\text{UCL} = \bar{\bar{x}} + 3\sigma \qquad \textbf{(1.77)}$$
$$\text{LCL} = \bar{\bar{x}} - 3\sigma$$

If the total sample is divided into subsamples of size r, σ can be computed as the sample standard deviation divided by $\sqrt{r}$. Furthermore, the multiplication of σ by 3, together with the assumption of a normal distribution for the feature that is being controlled, corresponds to a confidence interval of 99.7%.

For the specific case of dynamic monitoring systems, x_k is referred to the generic observation at time t_k of a one-dimensional feature independent on operational and environmental effects. Such feature can be referred to as *Novelty Index* (NI) [Worden & Manson 2000] and is defined starting from the prediction error (ε) and using either the Euclidian norm:

$$NI_k^E = \|\boldsymbol{\varepsilon}_k\| \qquad \textbf{(1.78)}$$

or the Mahalanobis norm:

$$NI_k^M = \sqrt{\boldsymbol{\varepsilon}_k^{\mathrm{T}} \boldsymbol{\Sigma}_{yy}^{-1} \boldsymbol{\varepsilon}_k} \qquad (1.79)$$

where $\boldsymbol{\Sigma}_{yy}$ is the covariance matrix of the measured feature y and both the Euclidian and Mahalanobis indices are assumed to be normally distributed.

It should be noted that when more than one feature is to be controlled, multivariate control charts can be applied. In this work, only the multivariate control chart designated *Shewhart T* is covered [Montgomery 1997]. Alternatives approaches are described and detailed in [Johnson & Wichern 1992; Kullaa 2003].

After the definition of a safety region based on the results of the training period, future observations can be checked by following two methodologies: each new observation can be verified or the check can be performed only when a set of new observations is available.

The characteristic plotted in the *Shewhart T* control chart is the so-called T^2-*statistic*. When each future observation $\boldsymbol{x}$ (a vector with p components) is verified, the T^2-*statistic* is obtained as:

$$T^2 = \frac{n}{n+1} (\boldsymbol{x} - \overline{\overline{\boldsymbol{x}}})^{\mathrm{T}} \mathbf{S}^{-1} (\boldsymbol{x} - \overline{\overline{\boldsymbol{x}}}) \qquad (1.80)$$

where n is the number of observations collected during the reference period, $\overline{\overline{\boldsymbol{x}}}$ is the process average and $\mathbf{S}$ is the covariance matrix (both calculated from the observations available during the reference period). The LCL is set equal to zero, whereas the UCL is defined as:

$$\mathrm{UCL} = \frac{(n-1)p}{n-p} F(\gamma) \qquad (1.81)$$

where $F(\gamma)$ denotes the γ percentage point of the F distribution with p and $(n-p)$ degrees of freedom.

When future observations are checked by using subgroups with r observations of $\boldsymbol{x}$, the T^2-*statistic* is calculated as:

$$T^2 = r (\overline{\boldsymbol{x}} - \overline{\overline{\boldsymbol{x}}})^{\mathrm{T}} \mathbf{S}^{-1} (\overline{\boldsymbol{x}} - \overline{\overline{\boldsymbol{x}}}) \qquad (1.82)$$
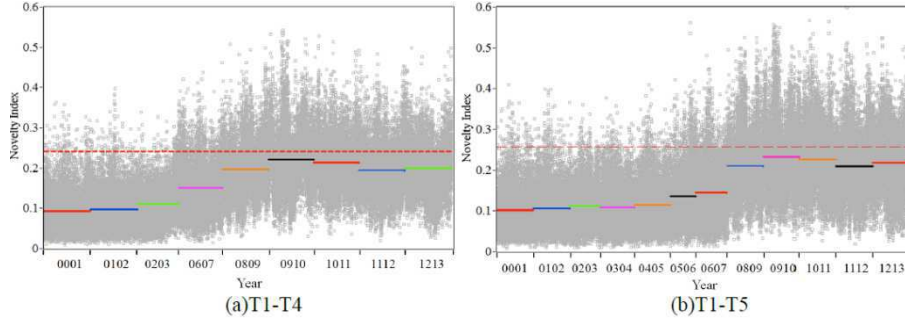
Figure 1.13 Variation of NI considering four and five temperature sensors [Hu et al. 2015].

where $\bar{x}$ is the subgroup average, $\bar{\bar{x}}$ and **S** are the process average and the covariance matrix, respectively, computed during the reference period. The LCL is set equal to zero whereas the UCL is defined as:

$$\text{UCL} = \frac{p(m+1)(r-1)}{mr - m - p + 1} F(\gamma) \qquad \textbf{(1.83)}$$

where p is the dimension of the variable (components of each individual observation of x), m is the number of subgroups collected during the reference period and $F(\gamma)$ denotes the γ percentage point of the F distribution with p and mr-m-p+1 degrees of freedom.

Control charts have been successfully used for damage detection in several SHM practical applications. In the previously described case of the *Westend bridge* in Berlin [Hu et al. 2015], control charts have been used for the detection of progressive damage over 13 years of continuous dynamic monitoring. After the application of a polynomial regression model that allowed to remove the effects of temperature from the identified natural frequencies, the *X-bar* control chart was used to detect possible structural modifications. From the results reported in Figure 1.13 it can be observed that the ratio of mean of the plotted *Novelty Index*, represented by the solid colorful lines, gradually increases and more and more points scatter out of the upper limit. Such outcomes suggest that

the bridge experienced some structural modifications between 2000 and 2013.

A possible motivation may lie in the variation of strain measured in the main prestressed cable on the east web, gradually decreasing from 2000 to the end of 2013. This progressive strain decrease may partially account for the detected slight drop of the frequencies and the increase of the ratio of mean of NI.

2 Dynamic testing and monitoring of historic structures using OMA

2.1 Introduction

In the last decades, preservation of Cultural Heritage has become one of the main issues for modern societies to face. Historic structures are progressively deteriorating so that restoration and strengthening interventions are becoming more and more common. A key role in the preservation and structural assessment of cultural heritage is played by the diagnostic process. Indeed, it is nowadays agreed that effective diagnostic survey (i.e. the assessment of the current health condition) provides a sound basis for any further evaluation of the safety level as well as for the definition of appropriate intervention measures.

A well-planned diagnostic process of historic structures should not neglect the following key passages: (a) data collection of the structure, including historic and documentary research; (b) visual inspection and on-site survey of the crack pattern; (c) on site testing and characterization of the materials.

Once the structural condition has been understood, health monitoring (static and/or dynamic), with data collected continuously or periodically and automatically analyzed, should be performed to detect the occurrence of structural performance anomalies.

Indeed, the preservation of historic buildings makes invasive techniques not totally suitable to collect information on structure and materials. Therefore, a major role in the diagnostic process of Cultural Heritage is played by non-destructive (ND) testing methodologies. Focusing on the dynamic characterization phase, ambient vibration testing (AVT) and continuous

monitoring of the structural response under ambient excitation are well-known ND techniques. Such procedures allow identifying the dynamic characteristics of a structure from output-only records, typically analyzed by using operational modal analysis (OMA) techniques.

AVT and SHM using OMA are especially suitable to historic structures. This is due to the fully non-destructive and sustainable way of testing, performed by just measuring the dynamic response under ambient excitation and not involving additional loads rather than those associated to normal operational conditions.

Ambient vibration testing has already become the primary modal investigation method of civil engineering structures. Nevertheless, notwithstanding the abovementioned advantages, its application to historic structures is still quite limited. It is indeed true that the response of historic buildings to ambient excitation is generally low (because the historical urban centers are often closed to traffic), but this issue can be easily overcome considering the highly sensitive and relatively inexpensive accelerometers currently available in the market.

Among the limited number of applications to historic structures, AVTs have more frequently been adopted in the dynamic investigation of masonry structures with a predominant vertical dimension: towers, bell towers, chimneys, minarets, etc. This structural typology is indeed very common in the European context and particularly relevant in Italy, whose large national Cultural Heritage mainly consists of ancient churches and defensive buildings (usually characterized by bell towers and defensive towers, respectively). Due to their typical structural configuration (relevant slenderness and significant dead loads), historic towers are typically highly sensitive to dynamic actions, such as traffic-induced micro-tremors, swinging of bells, wind and earthquakes.

Furthermore, the cantilever-like behavior of these buildings also suggests the use of simple dynamic monitoring systems, consisting of few sensors installed in the upper part of the structure, with preventive conservation and/or SHM purposes.

By collecting and comparing the existing literature on the subject, it has been possible to identify two dominant structural typologies: i) towers (bell towers and defensive towers), typical of western Europe; ii) minarets, probably the most common historic structure in middle-eastern countries. The analysis of the considered research works also allowed defining some common features in the adopted diagnostic processes. Therefore, the different applications have been classified on the base of the following characteristics:

1. procedure(s) used for modal identification;
2. existence of a FE model and whether the calibration approach adopted to evidence the accordance with the experimental results has been based on manual tuning (*) or structural identification procedures (**);
3. geometric characteristics (dimensions);
4. first natural frequency.

The results of this comparative research are reported in two different tables, according to the two considered structural typologies: Table 2- for towers and Table 2-2 for minarets.

In the present chapter, the considered case studies are organized in three different sections and grouped based on the presented structural typology and nature of the dynamic investigation (single test or continuous monitoring):

1. in the first part of the chapter, case studies where AVTs have been performed on towers and minarets are reported. These applications are in turn categorized based on the purpose of the investigation. Three main general goals have been identified: study of the effects induced by bells, assessment of the structural health, evaluation of the seismic performances;

2. the second section presents the applications available in the literature where continuous dynamic monitoring has been performed on historic masonry towers;

3. finally, the third and last part of the chapter describes the case studies referred to AVTs and continuous dynamic monitoring of historic buildings.

Table 2-1 Towers

Case study	Location	Year	OMA Technique	FEM	Dimensions (m)	f_1 (Hz)
San Luzi bell tower [Cantieni 2014]	Zuoz (Switzerland)	1139	PP	-	Height =60.0 Plan = 5.0×5.0	1.420
Tower of *Matilde* [Bennati et al. 2005b]	Pisa (Italy)	XII Cent.	PP	*	Height =35.0 Plan ≈ 10.0×7.0	1.196
Nuestra Sra. de la Misericordia bell tower [Ivorra & Pallarés 2006]	Valencia (Spain)	1740	PP	*	Height =41.0 Plan = 5.6×5.6	1.294
Santa Justa y Rufina bell tower [Ivorra et al. 2008]	Orihuela (Spain)	XV Cent.	PP	*	Height = 33.9 Plan = 8.8×8.8	2.150
Tower of the *University of Coimbra* [Júlio et al. 2008]	Coimbra (Portugal)	1728-1733	PP - FDD	*	Height ≈ 34.0 Plan ≈ 7.0×8.5	2.133
Hagia Sophia bell tower [Bayraktar et al. 2009]	Trabzon (Turkey)	1250-60	EFDD - SSI	-	Height =23.0 Plan = 5.0×5.5	2.557
Cathedral of Monza bell tower [Gentile & Saisi 2007]	Monza (Italy)	1592-1605	PP - FDD	**	Height = 74.0 Square plan	0.586
San Vittore bell tower [Gentile et al. 2012]	Arcisate (Italy)	≈XVI Cent.	FDD - SSI	**	Height = 37.0 Plan = 5.8×5.7	1.211
Civic tower of *Soncino* [D'Ambrisi et al. 2012]	Cremona (Italy)	X-XII Cent.	PP	**	Height =41.8 Plan = 6.0×6.0	1.080
St. Giorgio bell tower [Bongiovanni et al. 2000]	Trignano (Italy)	1302	PP	*	Height =18.5 Plan = 3.4×3.0	2.700
SS. Annunziata bell tower [Bonato et al. 2000]	Roccaverano (Italy)	XVI Cent.	PP	**	Height =25.3 Plan = 5.0×4.0	1.660
Mogadouro clock tower [Ramos 2010]	Mogadouro (Portugal)	1559	SSI	*	Height =20.4 Plan = 4.7×4.5	2.560

Table 2-2 Minarets

Case study	Location	Year	OMA Technique	FEM	Dimensions (m)	f_1 (Hz)
Qutb Minar [Ramos et al. 2006, Peña et al. 2010]	Delhi (India)	1368	SSI	**	Height =72.5 Diameter =14.1 to 3.1	0.793
Hagia Sofia minaret #1-2 [Oliveira et al. 2012]	Instanbul (Turkey)	-	FDD - EFDD - SSI	*	Height = 66.6 Diameter = 4.7	1.240
Hagia Sofia minaret #3 [Oliveira et al. 2012]	Instanbul (Turkey)	-	FDD - EFDD - SSI	*	Height = 63.2 Diameter = 3.1	1.180
Hagia Sofia minaret #4 [Oliveira et al. 2012]	Instanbul (Turkey)	-	FDD - EFDD - SSI	*	Height = 44.9 Diameter = 3.3	1.030
Süleymaniye minaret #1 [Oliveira et al. 2012]	Instanbul (Turkey)	-	FDD - EFDD - SSI	*	Height = 51.7 Diameter = 3.2	1.050
Süleymaniye minaret #3 [Oliveira et al. 2012]	Instanbul (Turkey)	-	FDD - EFDD - SSI	*	Height = 74.4 Diameter = 4.1	0.990
Yeni Cami minaret [Oliveira et al. 2012]	Instanbul (Turkey)	-	FDD - EFDD - SSI	*	Height = 54.9 Diameter = 3.0	0.840
Akbıyık minaret [Oliveira et al. 2012]	Instanbul (Turkey)	-	FDD - EFDD - SSI	*	Height = 23.0 Diameter = 2.3	0.650
Mihrimah minaret [Oliveira et al. 2012]	Instanbul (Turkey)	-	FDD - EFDD - SSI	*	Height = 38.7 Diameter = 2.3	1.680
Rüstem Paşa Minaret [Oliveira et al. 2012]	Instanbul (Turkey)	-	FDD - EFDD - SSI	*	Height = 41.6 Diameter = 2.5	0.810
Şehzade Minaret [Oliveira et al. 2012]	Instanbul (Turkey)	-	FDD - EFDD - SSI	*	Height = 48.7 Diameter = 2.9	1.350

2.2   Ambient Vibration Tests (AVT) of towers and minarets

2.2.1   *Effects induced by bells*
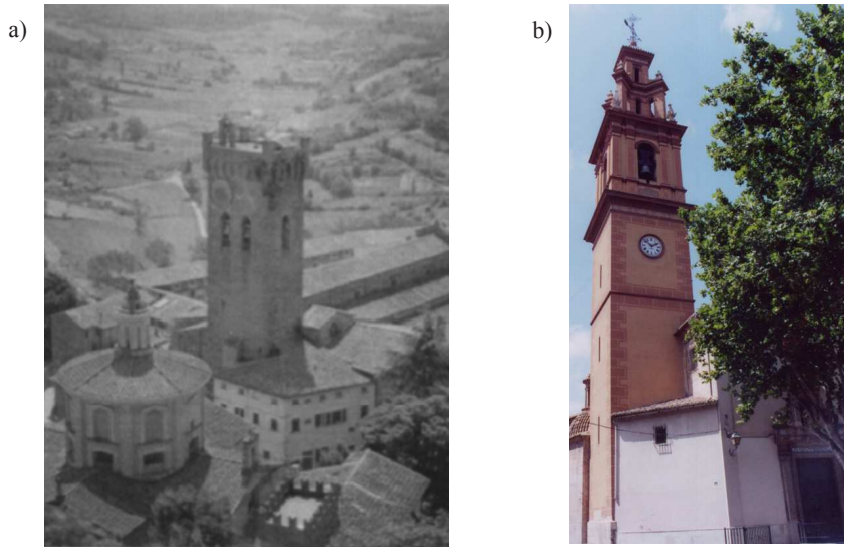
Figure 2.1 General view of a) tower of *Matilde* [Bennati et al. 2005]; b) Bell tower of the *Nuestra S.ra de la Misericordia* church [Ivorra & Pallares 2006]

Many of the towers investigated in the literature are characterized by the presence of bells, either installed at the very beginning of the construction (e.g. bell towers of churches) or during subsequent restoration phases, when a bell house was added. Therefore, it should come as no surprise that a large number of the considered research works are mainly aimed at evaluating the effects of bells on the investigated structure.

In [Bennati et al. 2005], the experimental measurements and analyses performed on the tower of *Matilde* (Figure 2.1a) are described. The study is aimed at determining the effects of the motion of the two largest bells. The investigated structure was originally built as a watchtower. Over the centuries, several consolidation works modified the structural configuration into the

current bell tower, incorporated in the *Cathedral of San Miniato*, Pisa (Italy). The first part of the research was dedicated to the experimental analysis and modeling of the action transmitted by the bells. Subsequently, numerical and analytical models were implemented and manually calibrated to match the experimental results. The analyses performed afterwards revealed that the frequency of oscillation of the largest bell was very close to one of the natural frequencies of the structure.

Several dynamic tests were performed on the bell tower of *Nuestra S.ra de la Misericordia* church [Ivorra & Pallarés 2006] in Valencia, Spain (Figure 2.1b). The research was carried out with the main purposes of defining the global dynamic behavior of the structure as well as the influence of the bells and the overall damping of the system. The tower was built in 1740 and is characterized by a square plan with side of 5.6 m and a total height of 41.0 m. Except for some sections in the lower part, made of stone blocks, the building is realized with solid bricks and mortars. In order to evaluate the modal parameters, two piezoelectric accelerometers were installed at the level of the bell house along the two main directions of the structure. The analysis of the ambient acceleration response allowed to identify six vibration modes in the frequency range 0-5 Hz: four bending and two torsion modes. Additionally, a frequency analysis of the variable forces induced by the bell swinging was performed. After the experimental investigations and geometric survey, cantilever-beam 2D models and more accurate 3D FE models were implemented to assess the structural response of the tower to the bell swinging. All models were later manually calibrated in order to match the results of the dynamic tests. Neither the results obtained by dynamic tests nor those of the validated numerical models highlighted any relevant effect of the bells on the dynamic parameters of the tower.

In [Ivorra et al. 2008], a similar investigation was carried out on the bell tower of the *Santa Justa y Rufina* church (Orihuela, Alicante, XV century).

In [Cantieni 2014], the results of three ambient vibration tests performed in different years to assess the effects of several restoration works on the *San Luzi* bell tower (Zuoz, 1139): none of the interventions turned out to be successful in achieving a definitive reduction of the effects produced by the bells' motion. Therefore, a continuous monitoring of both dynamic structural response and outdoor temperature was performed for more than one year, in order to evaluate the seasonal effects of environmental factors and completely characterize the effects of bells.

2.2.2 Structural assessment
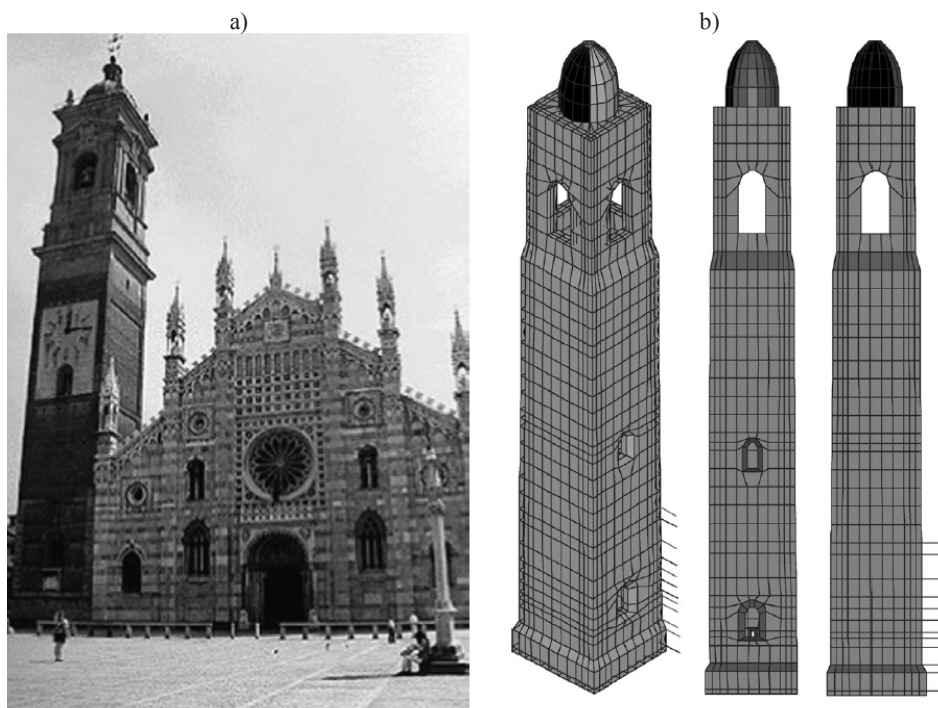
Figure 2.2 a) The *Cathedral of Monza* and the investigated bell tower b) Finite Element model of the bell tower [Gentile & Saisi 2007]

In several occasions, ambient vibration testing of historic masonry towers has been performed to assess the structural condition of the building, in order to obtain a reliable benchmark or to detect the possible presence of damage.

In [Gentile & Saisi 2007] the authors described the methodology adopted to assess the structural condition and the damage scenario of the historic bell tower (1592-1605) adjacent to the *Cathedral of Monza*, Italy (Figure 2.2a). Ambient vibration tests were performed and the acquired acceleration responses were analyzed by using OMA procedures. The results revealed a coupled motion of the dominant bending modes, suggesting either a strong coupling with the adjacent church or a non-symmetric stiffness distribution (due to the damage pattern). Furthermore, since 1995 the tower had been the object of an extensive experimental campaign, including survey of the geometry and of the crack pattern, laboratory tests on samples and double flat-jack tests. Based on this information, a 3D model was implemented (Figure 2.2b), considering a distribution of rigid constraints to reproduce the connection with the Cathedral and assuming a non-homogeneous distribution of the Young's modulus in order to represent the damage scenario. The uncertain parameters of the model were identified in order to match the results of the dynamic survey, and both the elastic modulus and the stiffness of the rigid constraint with the Cathedral were updated by using two system identification techniques: the Inverse Eigen Sensitivity [Collins et al. 1974, Friswell & Mottershead 1995] and the Douglas-Reid [Douglas & Reid 1982] methods. The calibration process provided results in good agreement with the values provided by the double flat-jack and ambient vibration tests, proving the reliability of the model in assessing the structural safety of the tower.

In [Júlio et al. 2008], the bell tower of the *University of Coimbra* (1728-1733) (Figure 2.3a) was the object of ambient vibration testing and numerical modeling in order to evaluate the need of restoration works, after minor
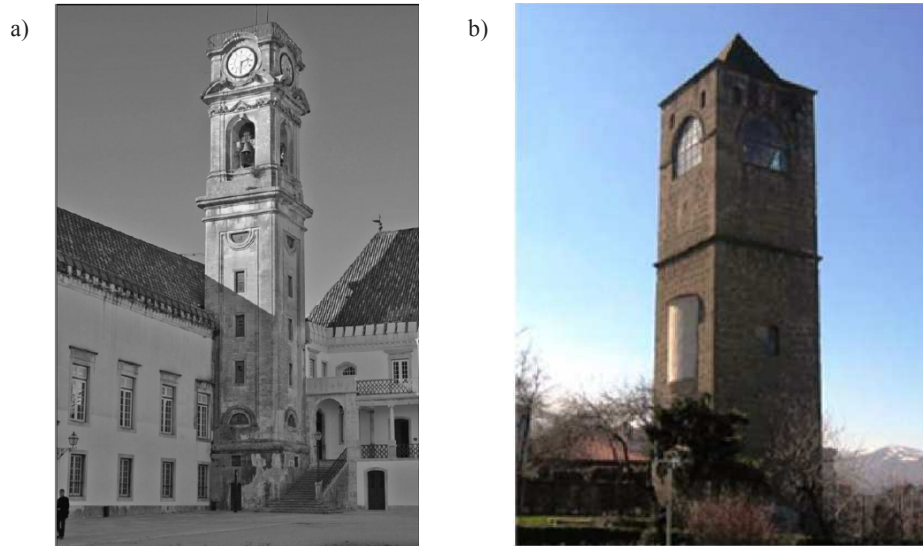
Figure 2.3 General view of a) the bell tower of the *University of Coimbra* [Júlio et al. 2008] b) the bell tower of the *Hagia Sophia* church [Baryraktar et al. 2009]

degradation of the structure was reported. The results obtained from the numerical model, calibrated on the experimental results, highlighted the general good health of the building and did not reveal any evidence of compromised structural integrity. Therefore, it remains unclear why the need to proceed with strengthening intervention works is suggested.

The dynamic characteristics of the bell tower of the *Hagia Sofia* church (XIII century, Figure 2.3b) in Trabzon (Turkey) were determined through ambient vibration tests using two different setups, in order to obtain exhaustive information on natural frequencies and mode shapes and to validate a 3D analytical model [Baryraktar et al. 2009].

2.2.3   *Seismic assessment*

The structural configuration of towers and minarets makes those buildings particularly vulnerable to the actions produced by earthquakes, highlighting the need for seismic assessment. Therefore, several research projects have been

developed during the last years to determine the seismic performances of historic masonry towers (especially in Italy, as a consequence of the significant seismic events of the last decades) and minarets (both in Europe and Asia).

In [Bongiovanni et al. 2000], the authors address the dynamic characterization of the bell tower of the *St. Giorgio* church (Trignano, Italy), damaged by the 1996 Reggio Emilia earthquake. The modal characteristics of the tower were determined by performing both ambient and forced vibration tests. Subsequently, a monitoring system was installed in order to record the aftershocks of seismic episodes. The seismic response was compared to the results of the dynamic characterization, revealing a remarkable variation of the dynamic characteristics of the tower as function of the seismic intensity.

An extensive experimental investigation performed on the historic bell tower of the *SS. Annunziata Roccaverano* church (Asti, Italy) (Figure 2.4a) is described in [Bonato et al. 2000]. The dynamic response of the tower was evaluated by considering the structure subjected to both ambient vibrations and excitation induced by the motion of the bells. The recorded time histories were subsequently analyzed by using the auto-spectral density plots and time-frequency based estimators, which proved to be more efficient especially in the identification of modal frequencies from non-stationary signals (i.e. the response originated by bell tolling). Subsequently, a space truss model, with horizontal members representing the flexural stiffness of the bell-tower and diagonals elements simulating the shear stiffness of the masonry panels, was implemented. The automated calibration of the model allowed accomplishing a more accurate classification of the detected modes and obtaining an estimate of the mechanical properties of masonry.
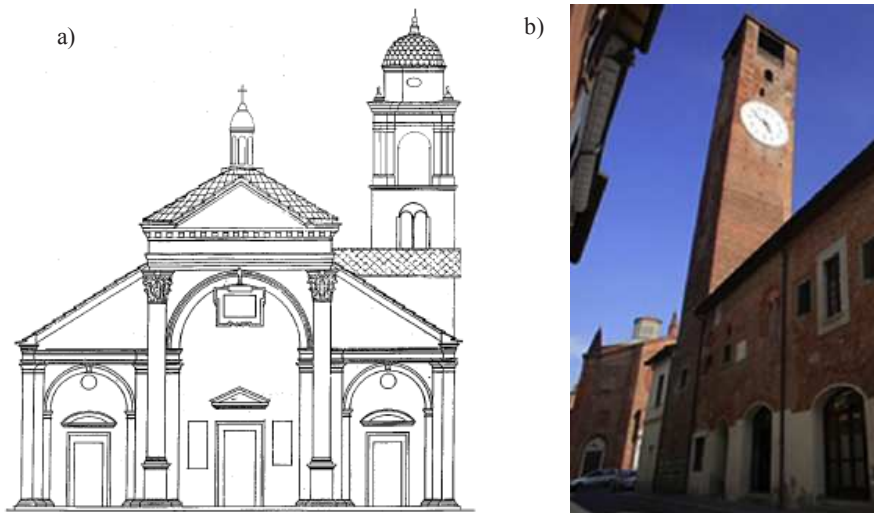
Figure 2.4 a) The bell tower of the *SS.Annunziata Roccaverano* church [Bonato et al. 2000]; b) the civic tower of *Soncino* [D'Ambrisi et al. 2012]

The medieval civic tower of *Soncino* (Figure 2.4b) was subjected to dynamic characterization by measuring the response to ambient excitation [D'Ambrisi et al. 2012]. The experimental results were used to calibrate an analytical model in order to evaluate the elastic modulus *E* of the masonry and the constraint effect given by the adjacent buildings. Based on the obtained value of the Young's modulus and on the geometric survey, a further FE model was implemented. The model was adopted to assess the structure's seismic performance by performing static and dynamic analyses (both linear and non-linear).

The *Qutb Minar* [Ramos et al. 2006, Peña et al. 2010] is one of the tallest stone masonry towers in the world and a typical example of the classical Indo Islamic architecture (Figure 2.5a). The construction began around 1202 and, over the centuries, the building underwent many modifications and restorations. The current configuration is characterized by a total height of 72.5 m and an approximately circular plan with diameter tapering from 14.1 m at the base to

3.0 m at the top. Direct visual inspections [Ramos et al 2006] revealed the presence of severe cracks and material decay, especially in the lower area.

In order to assess the dynamic characteristics of the tower, AVTs were performed by University of Minho [Ramos et al. 2006]. The response accelerations were recorded in twenty points on five levels, using 8 accelerometers installed according to 9 sub-sequential setups.

a)   b)
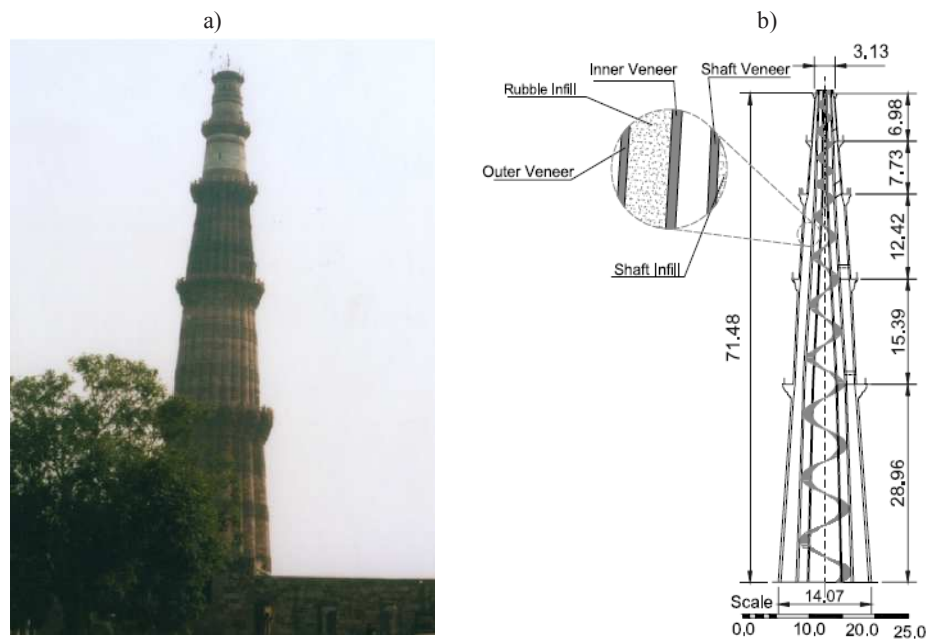
Figure 2.5 The Qutb Minar: a) general view; b) geometric survey: vertical section [Peña et al. 2010]
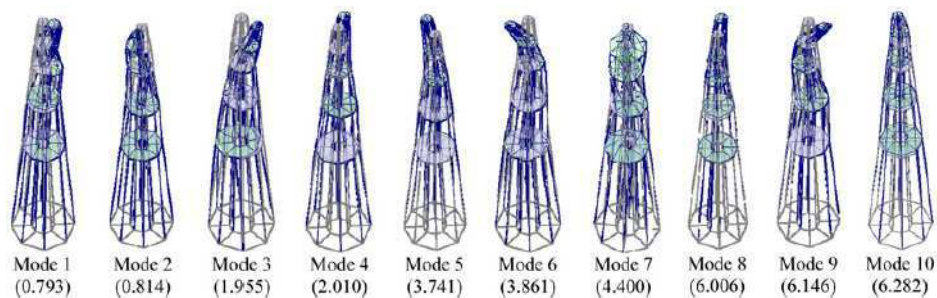
Figure 2.6 Mode shapes of the first seven natural modes (SSI) [Peña et al. 2010]

The following OMA, performed using the SSI technique, allowed the detection of 14 vibration modes within the frequency range 0-10 Hz: ten bending, two torsion, one axial and one non-defined mode shapes. It should be noticed that the structural configuration led to the detection of several pairs of closely spaced frequencies (especially for the lower modes) (Figure 2.6). Further AVTs were performed by the University of Padua by using a different acquisition system. The results of this second tests were obtained using a single FFT on the complete set of points was performed and highlighted a good accordance with the outcomes of the previous survey, revealing a maximum error of 2.7%. The investigation of the minaret was completed by performing sonic pulse velocity tests to qualitatively evaluate the masonry characterizing the structure. Finally, the structural behavior of the minaret was evaluated through 3 numerical models [Peña et al. 2010], validated using the experimentally identified modal parameters: two 3D FE models and one 2D model elements based on the Rigid Element Method.

A systematic study of the seismic performances of minarets is described in [Oliveira et al. 2012]. The authors selected a group of 11 minarets in the historical peninsula of Istanbul, with heights spanning from 27.0 m to 67.0 m.

Ambient vibration testing and geometric survey were performed on all the buildings. The seven structures characterized by the most reliable geometric properties were also modeled by using a FE software (Figure 2.7). These models were subsequently calibrated by varying the elastic modulus E until the experimental results were matched. This, in turn, allowed obtaining an accurate classification of the mode shapes. Finally the structural response of three minarets presenting very dissimilar geometry was evaluated: first a linear response spectrum analysis was performed; subsequently, seven ground motions were used as input for a linear time-history analysis.
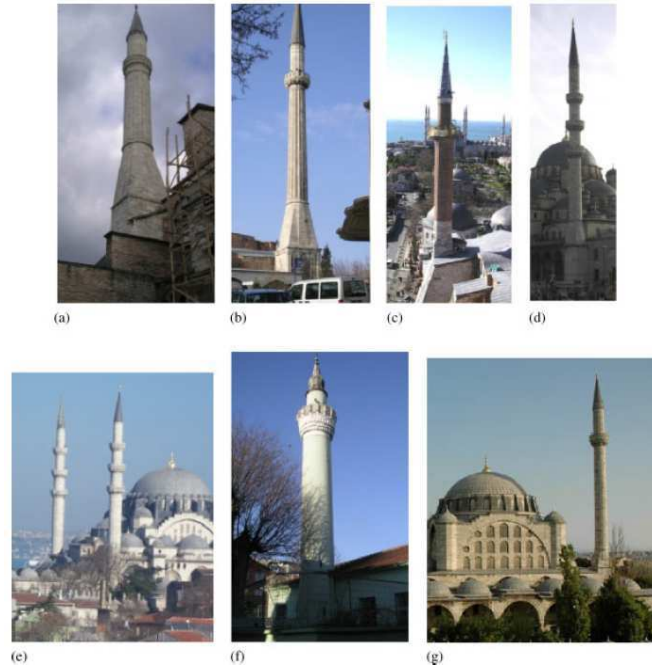
Figure 2.7 The seven modeled minarets: a) Hagia Sophia #2; b) Hagia Sophia #3; c) Hagia Sophia #4; d) Yeni Cami; e) Süleymaniye #3; f) Akbiyik; g) Mihrimah [Oliveira et al. 2012]

2.3 Continuous dynamic monitoring of historic masonry towers

Among the limited number of applications describing ambient dynamic investigation of historic structures present nowadays in the literature, only two cases present the results of continuous dynamic monitoring of masonry towers: the *Mogadouro* clock tower in Portugal [Ramos et al. 2010] and the bell tower of the *San Luzi* church in Switzerland [Cantieni 2014].

2.3.1 Mogadouro Clock Tower, Portugal

The *Mogadouro* clock tower (XVI Cent.) [Ramos et al. 2010] is a stone masonry tower located inside the castle perimeter of Mogadouro, in the Northeast of Portugal (Figure 2.8). The structure is 20.4 m high and characterized by a rectangular cross section, with sides equal to 4.7 m and 4.5 m. In 2004 the tower was severely damaged, with the occurrence of large cracks and loss of material (Figure 2.8a-b). Therefore, rehabilitation works consisting of lime injection, material replacement and installation of steel ties (Figure 2.8c-d) were carried out in the next year. Two ambient vibration tests were performed by the University of Minho before and after the strengthening works, in order to assess the effectiveness of the interventions. As expected, the comparison of the results revealed an increase of natural frequencies and damping ratios, confirming that the rehabilitation works had been successful.

In April 2006, a dynamic monitoring system was installed with the two-fold purpose of checking the actual stabilization of the cracks and evaluating the effects of environmental factors on the identified modal parameters. The system, composed by 3 piezoelectric accelerometers (10 V/g sensitivity) and a combined sensor recording ambient temperature and air humidity, recorded ten

test series between April 2006 and December 2007. During each series, 600 records of ten minutes each were acquired.

The modal analysis was performed by means of a SSI-based automated procedure. The results highlighted the significant effect of environmental factors, revealing the increase of frequency with an increased temperature (Figure 2.9a). As it will be described in Chapter 4, this behavior can be related to a temporary increase of the modal stiffness due to the closure of the minor discontinuities induced by the thermal expansion of masonry. It should be noted that a shift in the linear relation between frequency and temperature could be observed in the correlation diagrams. According to the authors, since no damage was observed, the presence of such transition period was due to water absorption by the walls at the beginning of the raining season, which caused the frequencies to vary of about 4%.

In order to simulate the behavior of the modal frequencies of the structure, a MISO ARX model (i.e. ARX[3,2 2 4, 0 0 0]) was implemented considering temperature, excitation level and air humidity as inputs. The model reproduced the fluctuations of the natural frequencies with good accuracy and the obtained simulation errors did not remark the presence of structural anomalies (Figure 2.9b).
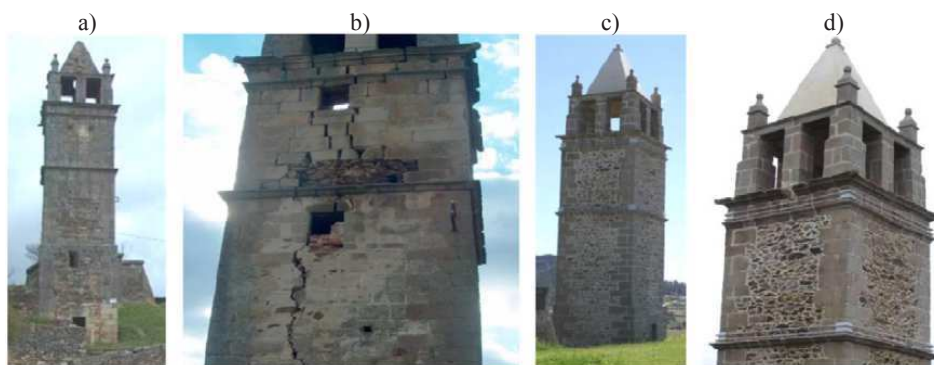
Figure 2.8 The Mogadouro Clock Tower: a-b) before the rehabilitation works; c-d) after the rehabilitation works [Ramos et al. 2010]
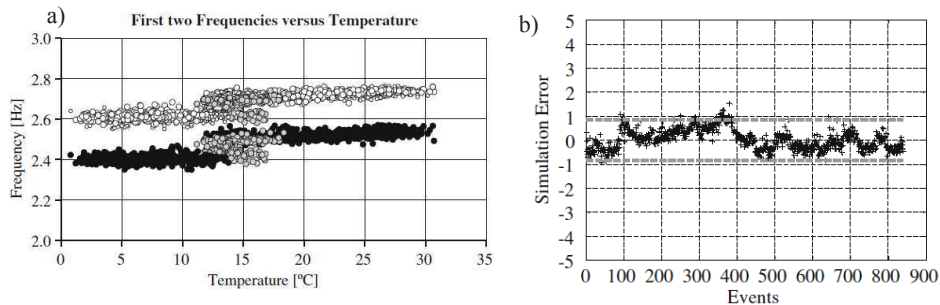
Figure 2.9 a) Temperature vs natural frequency of first (black dots) and second (white dots) vibration modes; b) Simulation error for the ARX[3, 2 2 4, 0 0 0] model [Ramos et al. 2010]

2.3.2   *San Luzi Bell Tower, Switzerland*

In [Cantieni 2014] the author describes the dynamic monitoring of the bell tower of the *San Luzi* church in Zuoz, Switzerland (Figure 2.10). The structure is a 60.0 m high historic masonry bell tower, characterized by a 5.0 m side square plan and connected to the neighboring church on 3 out of 4 walls. After excessive vibrations were reported during the motion of the bells, several ambient and experimental vibration tests were performed through the years to assess the dynamic characteristics of the structure. The tests revealed a highly changing dynamic behavior, with the natural frequency of the tower varying significantly after interventions aimed at reducing the bell-induced vibrations were performed.

The unsteady behavior highlighted by the experimental campaign suggested the installation of a continuous dynamic monitoring system, with the two-fold purpose of keeping track of the first four natural frequencies and recording the tower's vibrations due to the swinging of the bells. To this end, a single IP-68 protected accelerometer was installed to collect accelerations over 20 minutes of bell-free response and each time a vibration trigger level was exceeded. Environmental factors were also monitored by a local weather station.

81

Figure 2.10 The bell tower of the *San Luzi* church [Cantieni 2014]

Data acquired over more than one year (June 2012-October 2013) were analyzed through a Diadem routine which extracted the minimum, maximum and RMS values and calculated the FFT spectrum for the frequency ranges 0.8-2 Hz (including the first two natural frequencies) and 2-4 Hz (including third and fourth natural frequencies). The variation exhibited by the first two vibration frequencies over the monitoring period revealed large modifications of the modal stiffness (i.e. 22-23%), conceivably indicating the presence of significant cracks. According to the author, the frequency variation is associated to the effects of environmental factors, in particular air temperature and wind activity.

The results of the 16 months of monitoring highlighted a tower stiffer in winter than in summer. Nonetheless, considering monthly, weekly or daily variations of temperature, the first natural frequency of the tower increased with

an increased temperature. These behaviors, apparently in contrast with each other, can be related to phenomena already observed in past experiences on masonry structures. The higher stiffness detected in winter is indeed explained by the experienced low temperatures (i.e. -27°C), which caused the structural system (including its foundation) to freeze and therefore induced an increase of the modal stiffness. The second behavior can be associated to the thermal expansion of the materials with an increased temperature, which led to the closure of minor cracks and a temporary increase of the modal stiffness.

2.4 Ambient Vibration Tests and continuous dynamic monitoring of historic masonry buildings

2.4.1 Multi-tiered temples, Nepal

Historical temples represent a significant part of the Nepalese architectural heritage, whose preservation has become of utmost priority in the last decades. Within this context, ten of these structures have been investigated for seismic assessment purposes in [Jaishi et al. 2003].

a) b)
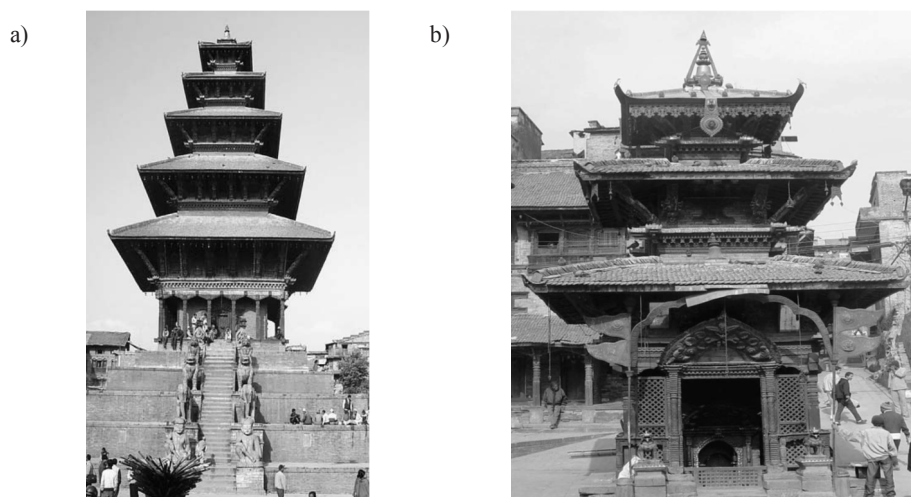
Figure 2.11 a) The Nyatopol temple; b) the Salan Ganesh temple [Jaishi et al. 2003]

The dynamic properties and seismic performance of the investigated temples were analytically estimated from 3D FE models. In order to validate the implemented FE models, AVTs were carried out in December 2002 on three typical temples (Figure 2.11). The structural response to environmental excitation (wind and micro-tremors) was recorded along two orthogonal directions by installing 11, 13 and 14 accelerometers, respectively: one instrument was held fixed as reference whereas the others were moved to the different measurement positions. The acceleration time histories were recorded for about 43 minutes and the modal identification was performed by means of PP and SSI techniques. The obtained dynamic characteristics revealed fundamental periods shorter than 0.6 s, consistently with the values reported in the literature.

The calibration of the 3D models based on the experimental results allowed the authors to perform the dynamic analysis of all of the ten investigated structures and to propose an empirical relation to estimate the fundamental period of multi-tiered Nepalese temples. Finally, the analysis of the seismic performance highlighted the masonry piers between the openings to be the most vulnerable region of the building.

2.4.2   Coliseum, Italy

The Flavian Amphitheater, better known as Coliseum, is undoubtedly the most famous monument of the classical Rome. Built between 70 and 76 AD by the emperor Vespasian and finally completed in 80 AD by the emperor Titus, the amphitheater is elliptical in shape, with external major and minor axes equal to 188.0 m and 156.0 m, respectively (Figure 2.12). The external wall is about 50 m high and is made of travertine blocks originally connected by iron pins and cramps without mortar joints.
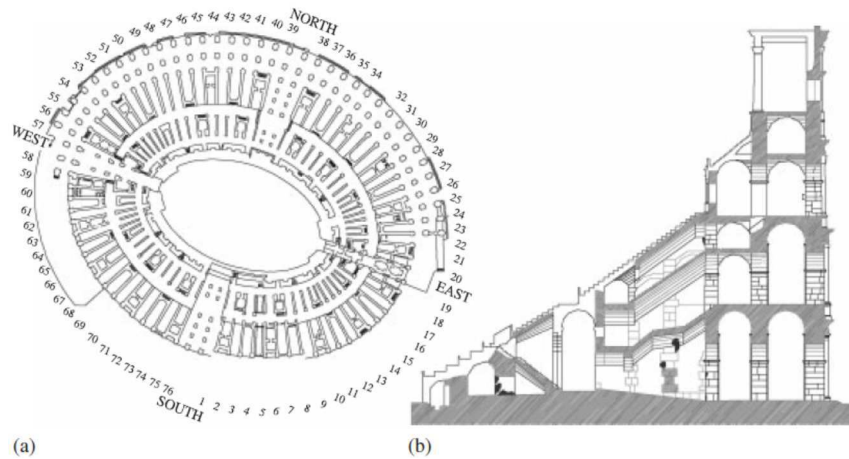
Figure 2.12 a) Plan and b) radial section of the Coliseum [Pau & Vestroni 2008]
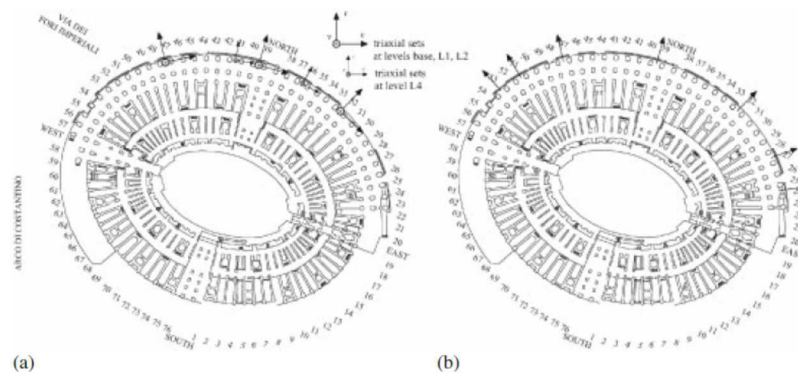
Figure 2.13 a) Location of the triaxial sets; b) location of the radial accelerometers
[Pau & Vestroni 2008]

The structure has been the object of a series of experimental dynamic tests described in [Pau & Vestroni 2008], aimed at identifying the modal parameters (i.e. natural frequencies and mode shapes) and assessing the risk of damage due to traffic-induced vibrations.

A global FE model, implemented by reproducing the geometrical characteristics of the building and taking into account the different materials, was at first used to evaluate the modal properties of the monument. The results of the FE analysis, which indicated the frequency range where the most

significant modes were expected, were used as reference to plan the configuration of the AVTs.

Two groups of ambient vibration recordings were performed. The first group included triaxial recordings, which acquired vibrations at four different levels (Figure 2.13a). The second group of measurements included radial recordings with six instruments simultaneously measuring accelerations along a vertical line (Figure 2.13b). Impact vibration tests were also carried out on the columns, using an instrumented hammer to excite the structure. The modal analysis of the response, recorded over at least 20 minutes, was performed both in the frequency and time domain and revealed the presence of dominant frequencies between 50-100 Hz at the base and within 1-20 Hz at the upper levels. In accordance with the results of the finite element analysis, the identified mode shapes were bending modes involving the external wall, whereas the maximum displacements were always observed at the free end of the wall.

The comparison between experimental results and FE model revealed the experimentally identified frequencies to be smaller of about 50% with respect to the numerically predicted ones. This outcome, along with the results of the impact tests, which provided velocities of the pressure waves smaller than expected, suggested that the real structure is characterized by a lower stiffness than the analytical model.

Finally, since the maximum amplitude of the measured traffic-induced vibrations was found to be below the levels indicated by the ISO guidelines, they are unlikely to be the cause of direct damage.

2.4.3   *Beyelerbeyi palace, Turkey*

The *Bayelerbeyi* palace [Aras et al. 2010], realized between 1861 and 1865 and located on the Asian shore of the Bosporus channel in Istanbul, represents a

masterpiece of the Turkish architectural heritage (Figure 2.14). The palace is characterized by an almost rectangular plan, about 72 m long and 48 m wide.

The structure was the object of AVTs aimed at assessing it seismic performance. Three seismometers were used to acquire the structural response on 24 measurement points: 2 instruments were installed along two orthogonal directions in a reference position at the top floor, whereas the third seismometer was used as a rover to instrument the remaining points. The modal identification, performed by means of PP and FDD techniques, led to the detection of eight vibration modes within 2 and 20 Hz. Notwithstanding the regular and symmetric shape of the building, the detected mode shapes highlighted an articulated behavior, with all modes but the second exhibiting displacements of just a part of the structure. These results are associated by the authors to the non-uniform properties of the materials and to the absence of rigid-floor diaphragms.

Based on the results of the geometric survey, a numerical model of the palace was also implemented. The model was updated using an iterative procedure in order to match the results of the dynamic survey.
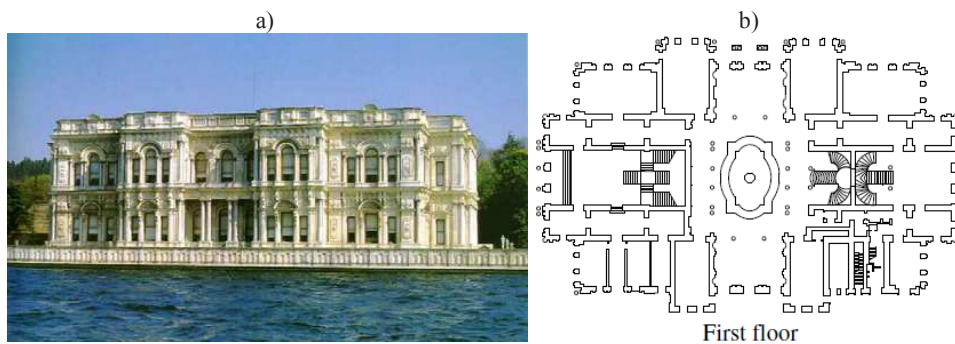
Figure 2.14 a) General view of the *Beyelerbeyi* palace; b) plan of the first floor [Aras et al. 2010]

Mode 1 f = 2.697 Hz   Mode 2 f = 3.593 Hz   Mode 3 f = 4.147 Hz

Figure 2.15 Mode shapes and natural frequencies of the first three vibration modes
[Aras et al. 2010]
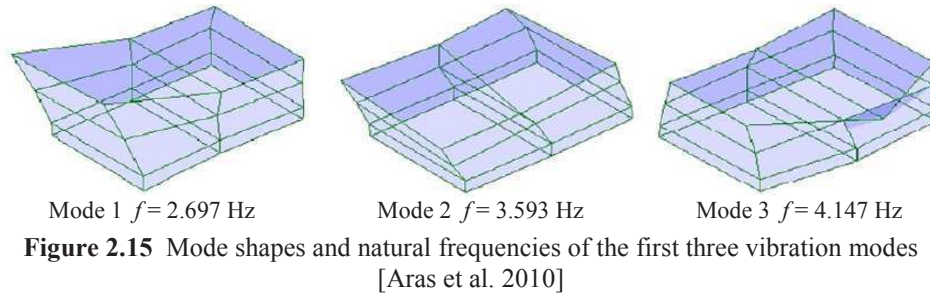
2.4.4   *Santa Maria de Belém church, Portugal*

Figure 2.16 a) Plan of the *Santa Maria de Belém* church; b) view of the three naves
[Ramos et al. 2010]
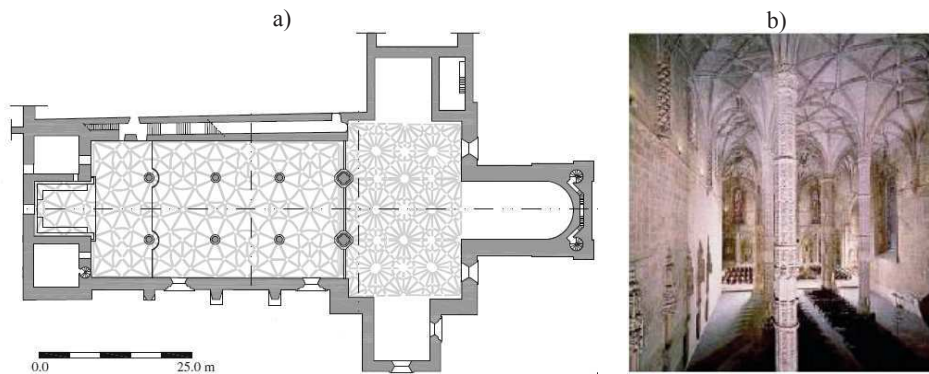
The *Santa Maria de Belém* church [Ramos et al. 2010] is part of the *Monastery of Jerónimos* in Lisbon (Figure 2.16). The building is 24.0 m high and is characterized by a length of 70.0 m and a width of 40.0 m. The modal parameters of the main nave of the church have been monitored by the University of Minho since 2005, with the main goals of evaluating the effects of environmental factors and improving the seismic performances of the structure.

Before installing the monitoring system, a preliminary AVT was performed to assess the dynamic behavior of the main nave. The response was recorded by 30 accelerometers distributed on top of the external walls, columns and vault keys. Both FDD and SSI techniques led to the identification of six natural

modes within the frequency range 3-13 Hz. The inspection of the mode shapes of the first two modes revealed that the dynamic response of the church is influenced by the slenderness of the columns and that the vibration modes mostly exhibit displacements along the North-South and vertical directions.

After the preliminary AVT, two triaxial force balance accelerometers were installed as part of a dynamic monitoring system. One accelerometer was placed at the base of the structure whereas the second one was positioned at the top of the main nave. The monitoring was completed by a static system recording temperature, air humidity, wind velocity and the rotation of the columns. Every month, data are acquired for 10 consecutive minutes and further 10 minutes are seasonally recorded every hour during a full day in order to study the environmental effects. Furthermore, triggered records are occasionally acquired with an average length of 75 seconds. The modal identification, automatically performed by means of a SSI-based technique, led to the detection of three out of the six vibration modes identified during the AVT (first, third and fourth mode). Such difference can be explained by the low level of ambient excitation and the reduced number of sensors.

For all modes, the frequency-temperature correlation diagrams highlighted the existence of a bilinear relationships, revealing a significant influence of the temperature on the dynamic behavior of the church (Figure 2.17 b). The effects of such environmental factor were modeled by means of static regression relationships. In particular, two different models were adopted for data recorded at temperatures lower and higher than 17.5°C, respectively. Nevertheless, the models proved to be ineffective in accurately reproducing the fluctuations of the natural frequencies. According to the authors, considering a larger amount of environmental factors to be used as model inputs could enhance the predictive skills of the model.

a) b)
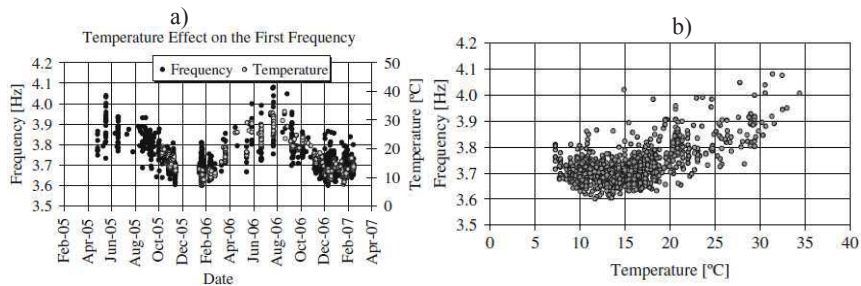
Figure 2.17 a) Variation in time of the first modal frequency; b) frequency-temperature correlation diagram for the first vibration mode [Ramos et al. 2010]

2.4.5   Saint Torcato church, Portugal

a) b) c)
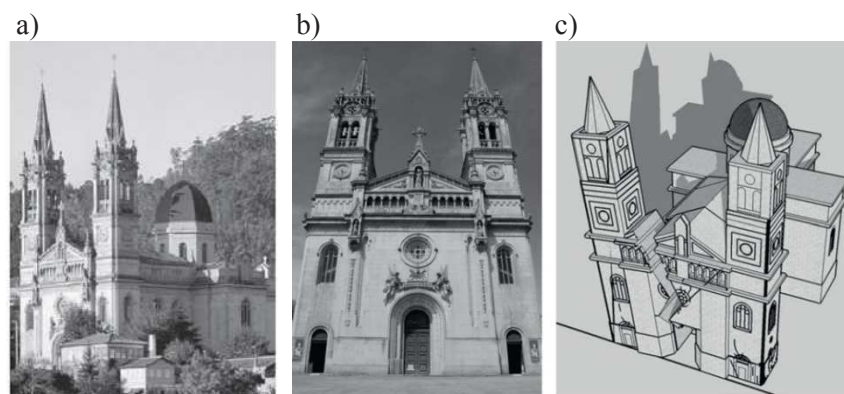
Figure 2.18 a-b) The Saint Torcato church; c) main existing crack and possible collapse mechanism [Ramos et al. 2013]
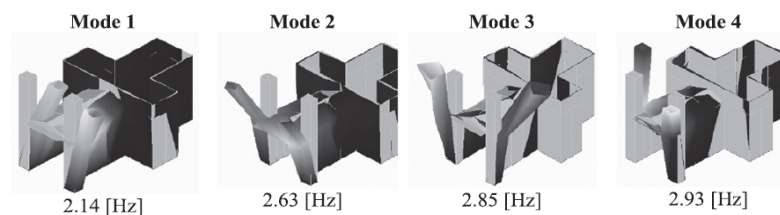
Figure 2.19 Mode shapes obtained from the preliminary AVTs [Ramos et al. 2013]

The *Saint Torcato church* (Figure 2.18) is located in the northern part of Portugal and its construction, carried out over more than 130 years, was

90

completed only in 2008. The structure is characterized by a classical Latin cross plan, with the main nave being 57.5 m long and 17.5 m high. The facade is completed with two gothic towers, 50.0 m high and with a 7.5×6.5 m plan.

The church has been the object of extensive research by the University of Minho for several years, with the main aim of monitoring its structural health condition [Ramos et al. 2013]. Initial crack mapping highlighted the presence of a large crack in the main facade, crossing the wall from side to side (Figure 2.18c). Furthermore, both towers were found to lean outwards. These results suggested a settlement of the front part of the building due to high stress level at the base - conceivably related to the weight of the towers - and possible soil problems.

In order to carry out strengthening interventions on the building, preliminary AVTs were performed in May 2009. Using ten piezoelectric accelerometers (10V/g sensitivity) and nine different test setups, 35 different measurement positions were instrumented. Classical OMA techniques (i.e. FDD, EFDD, SSI) led to the identification of four vibration modes between 2-3 Hz. The corresponding mode shapes revealed such modes to be related to the motion of the towers (Figure 2.19), whereas the low level of excitation and the high stiffness of nave and transept prevented the identification of the higher modes.

In November 2009, a permanent dynamic monitoring system was installed in the church. The system configuration was based on the results of the preliminary AVTs and included 4 piezoelectric accelerometers (10V/g sensitivity) installed on top of the towers. During five monitoring campaigns performed before August 2010, a sample time of 10 minutes was recorded every hour with a sampling frequency of 50 Hz, resulting in 3495 collected events. The modal identification was automatically performed by means of a SSI-Data based procedure. The identified frequencies exhibited small variations over the

monitoring time interval, conceivably related to changes in the environmental conditions (Figure 2.20).
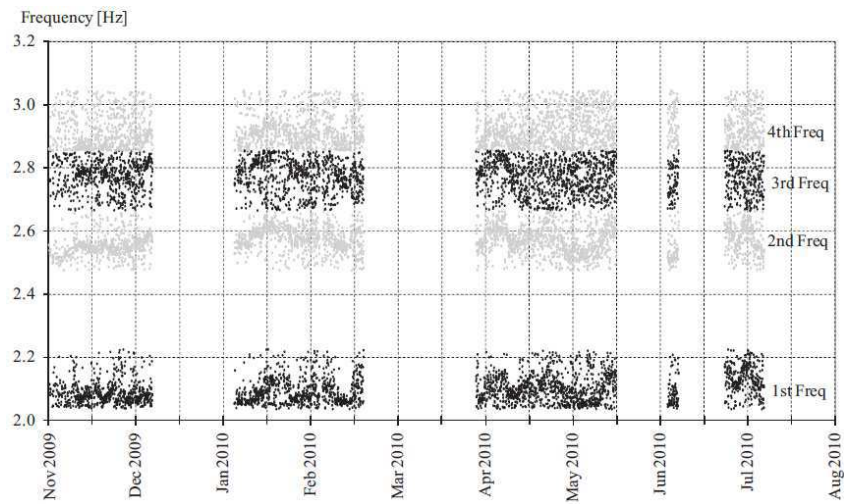
Figure 2.20 Time evolution of the natural frequencies [Ramos et al. 2013]

2.4.6   The Roman Arena of Verona, Italy

Figure 2.21 The Roman Arena of Verona [Casarin et al. 2012]
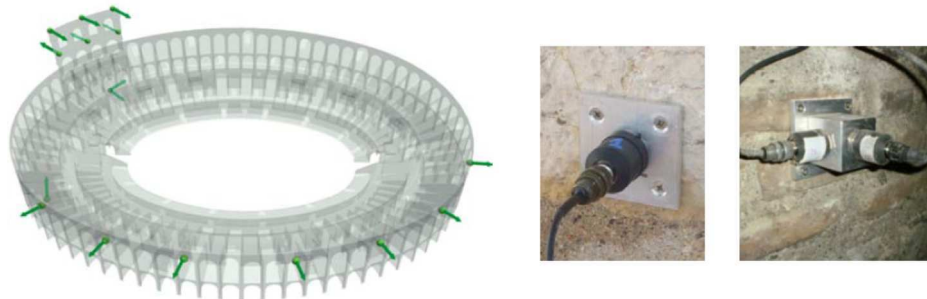
Figure 2.22 Layout of the dynamic system: accelerometers installed on the wing and at the base of the structure [Casarin et al. 2012]

The Roman Amphiteatre or "Arena" (Figure 2.21) represents the symbol and main landmark of Verona, a city in the northern part of Italy. The monument was erected in the I century AD, with an elliptic plan of 138.0×109.0 meters on the outside and about 44.0×73.0 meters for the inner pit.

As a consequence of the growing public interests for the structural health condition of the Arena, also due to its relevant use (the building is still used for concerts and operas), a broad Structural Health Monitoring system was installed in 2011 [Casarin et al. 2012]. The monitoring activity has been performed with the final aim of evaluating the dynamic characteristics of the monument by means of acceleration transducers, as well as assessing the evolution of the crack pattern. The system is composed by sixteen single-axial accelerometers (acceleration transducers) (Figure 2.22), twenty linear potentiometers (displacement transducer) and four integrated sensors of temperature and relative humidity. Two strategies have been adopted to collect the dynamic measurements: acquisitions over "long" time windows on regular intervals, in order to allow the identification of the modal parameters under different environmental conditions; "short" records, automatically collected when the vibration level exceeds a set trigger.

The SHM of the building takes into account three main aspects: (i) control of variations of the static measurements, (ii) daily extraction of the fundamental

modal parameters; (iii) registration and analysis of possible seismic events. With regards to the dynamic characteristics, the modal analysis is automatically performed by an algorithm that implements the poly-reference Least Square Complex Frequency Domain method (pLSCF). The results obtained in terms of frequency evolution over the first few months of monitoring (December 2011 - April 2012) reveal the existence of a strong correlation with the environmental parameters (Figure 2.23).

It should be noted that at the end of January 2012 a series of low/moderate seismic events hit the northern part of Italy. The response of the structure during such events was recorded by the monitoring system, which allowed the evaluation of possible induced damages. In particular, a modal analysis of the collected records was performed by using the FDD technique, with the main aim of evaluating the variation of modal parameters during the seismic excitation. A clear decrement of the frequency values of the first modes was observed during the earthquake. Nonetheless, the modal identification performed on the following days provided results similar to those recorded before the seismic event, indicating that no permanent and significant structural damage of the building had occurred.
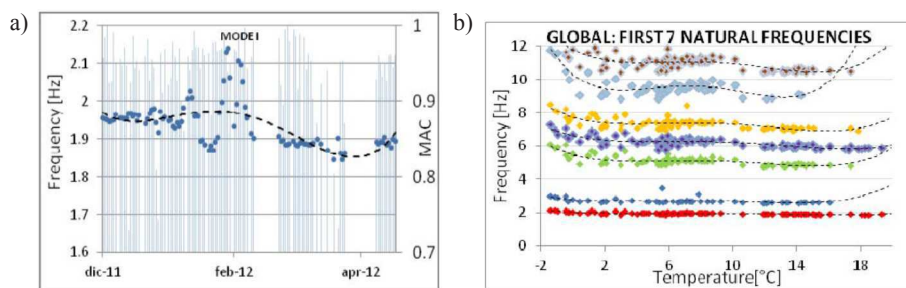
Figure 2.23 a) Time evolution of the first natural frequency (December 2011-April 2012); b) correlation between natural frequencies and temperature [Casarin et al. 2012]

94

3 SHM of ancient masonry towers using OMA: Methodology

3.1 Introduction

Within the framework of Cultural Heritage buildings, ancient masonry towers represent a very common typology of structures, erected over the centuries with different characteristics and functions: bell towers (especially meaningful in Italy, considering the large number of historic churches), lookout or defensive towers, chimneys, minarets, etc. In addition to the general issues characterizing the preservation of historic buildings (i.e. ageing of materials, presence of cracks and damage, effects of successive construction phases or modifications), masonry towers are usually slender and subjected to significant dead loads. Such characteristics, along with the non-uncommon presence of adjacent buildings and large openings at the belfries, may often lead to high sensitivity or vulnerability to dynamic actions, such as swinging of bells, wind and earthquakes. Hence, the preservation and preventive conservation of historic towers represents a major challenge in the SHM of Cultural Heritage.

Since masonry towers are also sensitive to the ambient excitation, dynamic tests in operational conditions or ambient vibration tests (AVT) have been more frequently adopted in recent studies as assessment tools (as it was discussed in Chapter 2). Furthermore, considering the cantilever-like structural behavior of towers, it has to be expected (see e.g. Ramos et al. 2010, Cabboi 2014, Cantieni 2014) that few accelerometers installed in the upper part of the building allow a successful dynamic monitoring of the structure, with preventive conservation and/or SHM purposes.
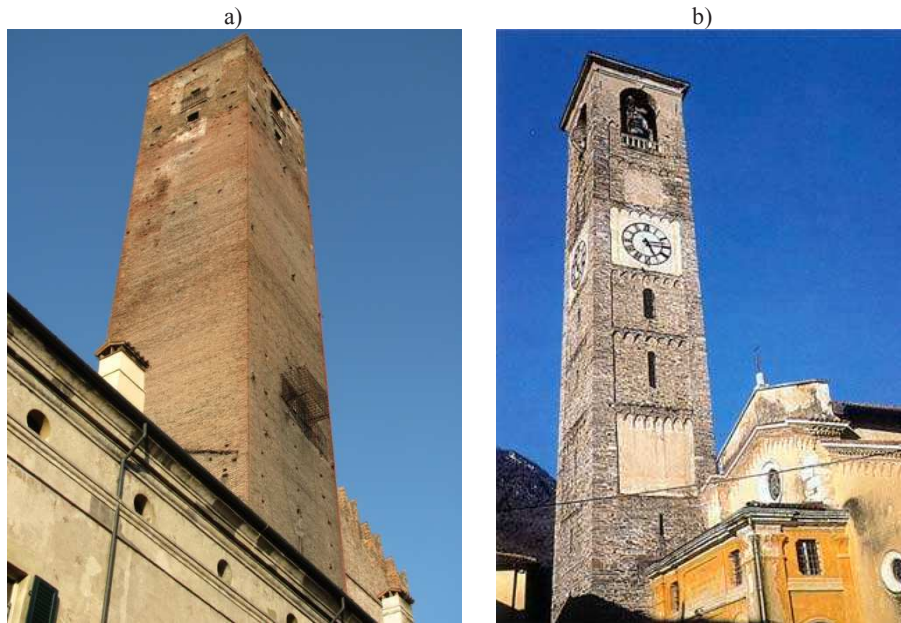
Figure 3.1 a) The *Gabbia* tower in Mantua, Italy; b) The *San Vittore* bell tower.

In the present Dissertation, a SHM strategy based on OMA has been developed and applied within the preservation process of two historic masonry towers in Northern Italy:

1. the *Gabbia* tower in Mantua (Figure 3.1 a) [Zuccoli 1984, Saisi & Gentile 2015], built in the XIII century in solid brick masonry with defensive purposes and named after the external hanged cage, originally used as an open-air jail;

2. the *San Vittore* bell tower (i.e. the bell-tower of the church *Chiesa Collegiata di San Vittore,* Figure 3.1 b) in Arcisate, Varese [Cazzani 1964, Gentile & Saisi 2013], about 37.0 m high and built in irregular stonework masonry.

The SHM methodology applied to the investigated towers is detailed in the following: preliminary AVTs, continuous dynamic monitoring and automated modal identification, evaluation of the environmental effects on the natural

frequencies, removal (or minimization) of environmental effects from frequency tracking and possible detection of abnormal structural changes or damage.

3.2 SHM methodology

Before applying any preservation or SHM strategy, the actual condition of a historic building has to be deeply investigated and understood. Traditionally, the structural condition assessment of Cultural Heritage buildings involves historic and documentary research, on-site and topographic survey, visual inspection, non-destructive (ND) and minor-destructive (MD) tests of materials on site.

Starting from the results of the data collection step, the vibration-based SHM strategy herein adopted consists of the following phases:

a) *Preliminary ambient vibration tests*: preliminary dynamic tests have to be carefully planned with the aim of providing useful indications for the subsequent long-term monitoring. In particular, the number of sensors (i.e. accelerometers and temperature sensors) and the duration of the tests have been properly fixed in order to: (i) obtain complete and accurate estimates of the dynamic characteristics of the structure (i.e. natural frequencies, damping ratio, mode shapes), to be assumed as reference results for the subsequent continuous monitoring; ii) reveal the presence of peculiar behavior (e.g. local modes); (iii) highlight the most appropriate positions to be permanently instrumented; iv) point out the relevant influence of the environmental factors;

b) *Continuous dynamic monitoring and automated modal identification*: as previously mentioned, the cantilever-like behavior of historic towers is expected to allow an effective modal identification by installing a limited number of sensors in the upper region of the structure. In particular, three accelerometers have been installed in each of the investigated towers,

corresponding to the minimum number of sensors needed to correctly capture the dynamic characteristics of the structure in the instrumented level. Considering the large amount of data continuously collected by the monitoring systems, the manual analysis of each recorded dataset would make long-term monitoring excessively time consuming to be considered a convenient approach. For this reason, the automated OMA procedure proposed in [Cabboi 2013] and based on the SSI-Cov technique (see Chapter 1) has been herein applied to continuously identify the modal parameters from the recorded acceleration data (Figure 3.2). A concise theoretical background of the adopted technique will be given in section 3.2.1.

An important aspect in OMA, whose impact is often under-estimated in the scientific literature, is related to the appropriate time window required to obtain reliable and accurate estimation of the modal parameters from ambient vibration data. In fact, all the output-only identification techniques assume the (un-measured) excitation input to be a zero-mean Gaussian white noise and this assumption is as closely verified as the length of the time window acquired is longer. Although a general rule, that can be applied to all types of structures, is very difficult to define, it is generally agreed that in output-only modal identification a minimum duration of the measurement, ranging between 1000 and 2000 times the fundamental period of the structure (see e.g. [Cantieni 2005]), is needed to provide accurate estimates of the modal parameters. Hence, the modal identification of the towers at study has been performed by considering time windows of 3600 s long, corresponding to more than 3000 times the structures' fundamental period.

c) *Evaluation and removal of the environmental effects on the natural frequencies*. When the dynamic monitoring is performed by permanently installing on the structure only a limited number of acceleration transducers, natural frequencies are the parameters typically used as indicators of the

structural condition (Figure 3.2b). Nonetheless, as discussed in Chapters 1 and 2, natural frequencies are also affected by external factors, both environmental (e.g. temperature, wind, etc.) and operational (e.g. amplitude of the excitation, etc.), whose induced fluctuations may jeopardize the detection of abnormal structural occurrences. Therefore, within the SHM framework, the need arises to evaluate and remove/minimize the influence of any extra-structural factor on the natural frequencies (Figure 3.2c).

Since a low level of ambient excitation was expected during the continuous dynamic monitoring of the investigated towers (and this is generally the case in historical urban nuclei), the temperature is conceivably a dominant driver of the variation of natural frequencies. In the case of the *Gabbia* tower, the results of the preliminary AVTs revealed the wall temperature measurements acquired on the outside of the S-W front to be the most reliable and best correlated with the identified natural frequencies: hence, the continuous monitoring system included a temperature sensor in that position. For the *San Vittore* bell tower, the presence of a static monitoring system previously installed by Politecnico di Milano [Binda et al. 2012], and including eight temperature sensors, allowed to select two wall temperatures as most representative of the tower's thermal condition: on the outside of the North front and on the inside of the East front.

As the time evolution of temperature (representing the most relevant environmental factor for the two case studies) was available, both input-output and output-only models (see Chapter 1) have been adopted to correct the natural frequencies of the investigated structures. It is worth recalling that: i) *input-output* models reproduce the relationship between the identified natural frequencies and the external factors, and are characterized by the need to select and measure the features with the most significant influence on the experimental frequencies; ii) *output-only* methods allow to skip the

selection of the external factors, that can sometimes represent a problematic process, as they only rely on the estimated values of the natural frequencies. More specifically, dynamic regression and ARX models (input-output methods) as well as PCA-based tools (output-only methods) have been implemented and applied to the results of the automated OMA.

As usual, the parameters of the input-output model (as well as the PCA) were calibrated considering a significant period of time, denoted as training or reference period and including a statistically representative sample of temperature conditions. It is worth mentioning that the classic quality criteria (already defined in Chapter 1) of *Loss Function* (LF) and *Aikake's Final Prediction Error* (FPE) [Ljung 1999]) as well the *coefficient of determination R^2* (see e.g. [Johnson & Wichern 1992]) have been used to evaluate the skills of dynamic regression and ARX models to fit the experimental estimates of the natural frequencies in the reference period.

As an alternative to input-output models, the output-only method known as PCA (and based on the Principal Component Analysis of the frequency data) has been implemented and applied. The algorithm (already described in Chapter 1) is a multivariate statistical tool performing a linear transformation of data to a new coordinate system. The selection of the most relevant principal components has been carried out over the same reference periods considered for the input-output models, so to take into account statistically significant ranges of variation of the natural frequencies. One of the drawbacks of PCA is the need to define a data set containing (at every hour) the frequency of each selected mode. This necessarily implies some loss of information. Therefore, in order to avoid a excessive loss of data, only the modes with a high identification rate have been considered for the two investigated towers.

a) CONTINUOUS DYNAMIC MONITORING
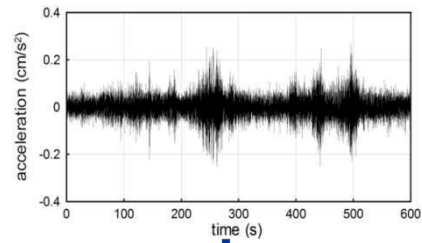
b) AUTOMATED OMA AND FREQUENCY TRACKING
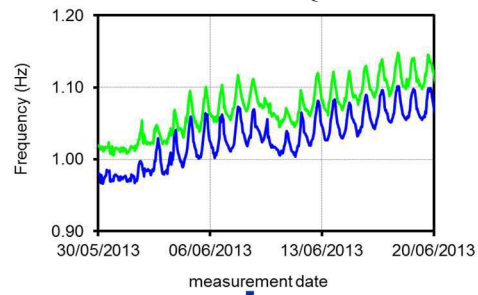
c) REMOVAL OF TEMPERATURE EFFECTS
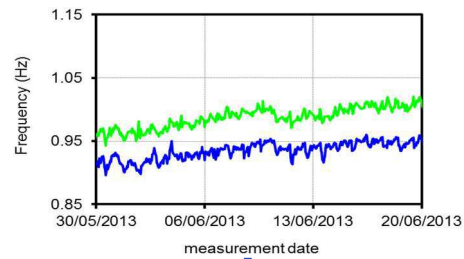
d) CONTROL CHARTS
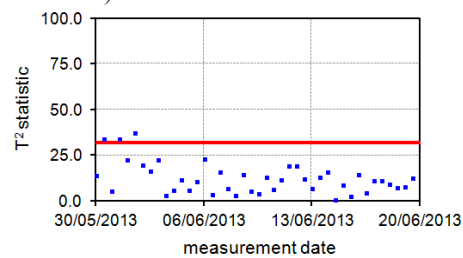
Figure 3.2 Flow chart of the adopted vibration-based SHM methodology

d) *Detection of abnormal structural change and damage*: the final step of the adopted SHM strategy consists of detecting the occurrence of structural changes lying outside of the "control region" defined within the reference period.

Firstly, the possible occurrence of anomalies has been investigated by examining the time evolution of environment-independent features such as the residual errors or the cleaned observations (natural frequencies). Alternatively, the occurrence of abnormal structural changes has been checked by using the statistical tools referred to as *control charts* (see Chapter 1). Control charts are essentially plots where the evolution in time of data is represented along with user-defined variation limits. The control limits are computed from the experimental samples collected during the reference period. This allows to associate any observation laying outside the defined limits to the presence of unusual sources of variability (e.g. the occurrence of damage). In the present Dissertation, the control chart designated *Shewhart T* (Figure 3.2d) has been applied to both case studies, where the plotted characteristic is the so-called T^2 *statistic* (see Chapter 1). In particular, future occurrences have been checked by using subgroups with r observations, where the value of r has been selected from case to case in order to better highlight the effects of possible structural variations.

3.2.1 *Automated Modal Identification*

As previously pointed out, the OMA of the investigated masonry towers has been performed by applying the automated procedure developed in [Cabboi 2013] and based on the SSI-Cov technique. The procedure [Cabboi 2013] consists of two main phases: i) the automatic analysis of the stabilization diagrams obtained from the application of the SSI-Cov algorithm; ii) the subsequent tracking of the most significant structural modes.

102

Focusing on the first step, the automatic interpretation of the SSI-Cov stabilization plots is in turn divided in two phases. At first, poles associated to spurious modes are removed. This allows to obtain cleaner diagrams, making the following automated mode-selection process easier and faster. The automated elimination of noise modes is achieved by using three modal validation criteria: i) firstly, all the identified poles characterized by a damping ratio out of the range 0-10% are rejected; ii) subsequently, the level of complexity of the detected poles is evaluated by applying the *Mean Phase Deviation* (MPD) [Reynders et al. 2012] and the *Modal Phase Collinearity* (MPC) [Pappa et al. 1993] validation criteria. Both indices are based on the investigation of the estimated mode shapes. In particular, the MPD method provides the phase scatter of each identified modal vector (with values close to 0 for well identified structural mode shapes). On the other hand, the MPC allows to evaluate the linear relation between real and imaginary part of each detected mode shape: values close to 0 indicate that the two parts are uncorrelated, whereas a MPC index close to 1 is associated with a mono-phase behavior. Both indices are combined together in the *Modal Complexity Factor* (MCF), defined as:

$$MCF = \frac{1 - MPC + \left(\frac{MPD}{90°}\right)}{2} \qquad \textbf{(3.1)}$$

The MCF assumes values between 0 and 1, with 0 indicating a mono-phase behavior of the structural mode. As detailed in [Cabboi 2013], the selection of a threshold value for the MCF index is not a trivial task and deserves some considerations on the various factors that influence the mode complexity (e.g. measurement errors, non-linear behavior of the structure, identification issues, etc.). Therefore, the characteristics of the investigated structure have to be assessed. Subsequently, assuming good test conditions, low threshold values can be selected if the structure is not likely to exhibit complex modes (e.g. 0.2),

whereas a higher tolerance will be necessary if the presence of non-linearity (even weak) is expected.

After the elimination of the most obvious spurious poles, the following phase consists of grouping together the structural modes sharing the same modal properties. The adopted procedure automatically follows the decision-making process of an experienced-human analyst, thus leading to results similar to those provided by a manual technique. The clustering process is based on the repetition of six steps:

a. select the first available identified mode, corresponding to the lowest model order $n=n_{min}$, and collect the associated modal frequency, damping ratio and mode shape in the first column of corresponding vectors (F_k for frequencies and D_k for damping ratios) and matrix (M_k for mode shapes). The number of columns corresponds to the number of considered model orders (n_{max}-n_{min}) whereas the amount of vectors-matrix sets will be determined by the final number of clustered structural modes;

b. considering the non-zero elements of frequency vector F_k and mode shape matrix M_k, compute the corresponding average values (f_{av} and ϕ_{av}, respectively) and the distance, in terms of frequency and MAC variation, with all frequencies and modal vectors belonging to the next model order $n=n+1$;

c. consider only the poles leading to values of the distance smaller than a predefined threshold value and collect the corresponding estimates of the modal parameters into the vectors and matrix defined in the first step. If more than one pole is selected, the pole characterized by the smallest distance is to be considered, whereas zeros must be put in the vectors-matrix set if no pole is detected;

d. repeat the previous two steps for increasing model orders;

e. once the range of model orders (from n_{min} to n_{max}) has been completely scanned, consider the frequency vector $\boldsymbol{F}_k$. If the number of collected frequencies is larger than a third of the number of columns (i.e. n_{max}-n_{min}), a structural mode is identified. Otherwise, the vector is discarded as spurious;

f. the final passage consists of moving back to the first step and selecting the next identified pole (not included in the previous defined cluster), then whole procedure is repeated.

The iteration of the six steps goes on until all the available poles have been scanned. Subsequently, the most representative estimates of frequency, mode shape, MPC and MPD are obtained from each defined group of consistent structural modes by averaging the corresponding values. Conversely, since the damping estimates are usually more scattered, the most representative value is obtained by computing the median, where the weight of the outliers is less relevant with respect to the average.

After the automatic analysis of the stabilization diagrams, the procedure is completed by a fundamental step for SHM applications: the tracking of the most meaningful modes. The tracking routine is based on the prior selection of a baseline list of modal parameters, that has been obtained from the results of the previously performed preliminary AVTs. After the definition of the baseline list, the evolution in time of the selected structural modes is tracked by computing the variation, between two consecutive data sets, of frequency and MAC index (necessary to distinguish any closely spaced frequencies). At first, for all modes identified in the first data set, the frequency and MAC variations are computed with respect to the reference modes in the baseline list. Only the modes that lead to variations smaller than predefined threshold values are took into account. Afterwards, the mode that exhibits the smallest variation with respect to the corresponding reference mode is gathered in the tracking. The previous two steps are repeated for all data sets, with frequency and MAC

variations always computed with respect to the baseline list, so to avoid error propagation. It should be noted that, since the fixed thresholds also take into account the effects of external factors, the definition of those values have been based on the expected influence of the environmental effects on the natural frequencies, as evaluated from the preliminary AVTs.

4 Structural Health Monitoring of the *Gabbia* tower in Mantua, Italy

4.1 Introduction

The Italian seismic sequence of May-June 2012 [Luzi et al. 2013] highlighted the high vulnerability of the historical architectures especially in the South part of the province of Mantua and in the neighboring Emilia-Romagna region, where several brittle collapses of towers, fortification walls and castles occurred (see e.g. [Sorrentino et al. 2014], [Cattari et al. 2014]) despite the supposed low seismicity of the area.

After the earthquake, an extensive research program was committed to Politecnico di Milano (Polo Territoriale di Mantova) to assess the structural condition of the tallest historic tower in Mantua (Figure 4.1): the *Gabbia* tower [Bertazzolo 1628], [Zuccoli 1988]. The post-earthquake survey [Saisi & Gentile 2015] included: (a) historic and documentary research; (b) on-site survey and visual inspection of the load-bearing walls and structural discontinuities; (c) non-destructive and minor-destructive tests of materials on site; (d) dynamic tests in operational conditions.

Both visual inspection and pulse sonic tests [Saisi & Gentile 2015] of the load-bearing walls highlighted the vulnerability of the upper part of the tower, due to the complex evolution of the structure. In addition, one local mode − involving the top of the building − was clearly detected in the dynamic tests and confirmed the remarkable structural effects of the change in the masonry morphology and quality observed on top of the tower and suggested the need for repair interventions to be carried out.

a)

b)
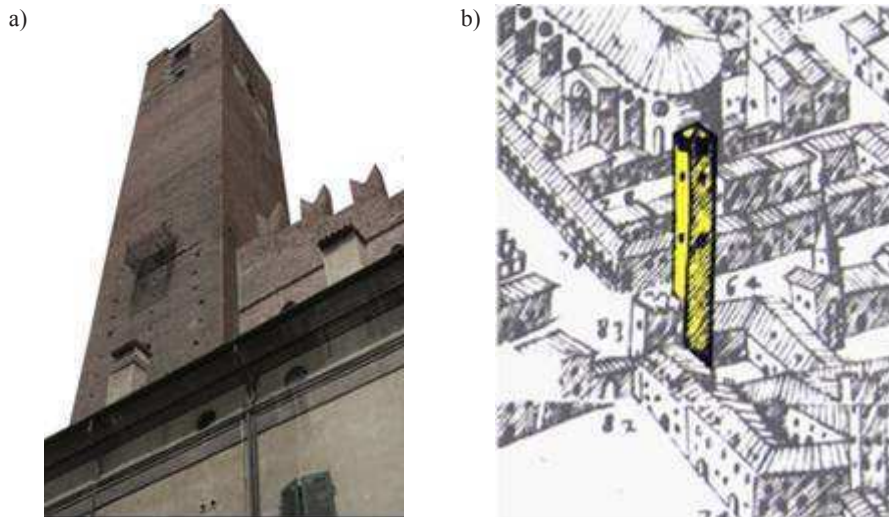
Figure 4.1 The *Gabbia* tower in Mantua, Italy: a) South-West view; b) picture from the XVII Century [Bertazzolo 1628]

While waiting for the retrofit design and funding, a dynamic monitoring system (consisting of three highly sensitive accelerometers and one temperature sensor) was installed in the tower [Saisi et al. 2015] with Structural Health Monitoring (SHM) purposes.

This Chapter, after a brief description of the investigated tower and the post-earthquake survey, focuses on the results of the continuous dynamic monitoring until June 2015 and on the application of the vibration-based SHM methodology outlined in the previous Chapter 3. More specifically, full details are given on the following main tasks: (1) installation of the continuous dynamic monitoring system with remote control and data transmission via Internet; (2) application of efficient tools to process [Busatta 2013] the raw data regularly received and to automatically identify the modal parameters [Cabboi 2014]; (3) tracking of the time variation of natural frequencies and analysis of the temperature effects on those features; (4) identification of structural performance anomalies.

It should be mentioned that, about 6 months after the beginning of the

continuous dynamic monitoring, the tower was subjected to a far-field earthquake with the recorded accelerations exceeding 40-50 times the response generally observed in operational conditions. Hence, this case study represents a challenging opportunity to check the practical feasibility of the methodology proposed in this Dissertation and, more generally, to identify the occurrence of abnormal structural changes or damage under changing environment.

4.2   Description of the tower and historic background

The *Gabbia* tower ([Bertazzolo 1628], [Zuccoli 1988], Figure 4.1-Figure 4.3), about 54.0 m high, is the tallest tower in Mantua and overlooks the historic center, listed within the UNESCO heritage. The name *Gabbia* (literally "jail" in Italian) descends from the hanged dock built in the XVI century on the S-W front and originally used as open-air jail. The tower was privately owned for many years and only in the 1980s it came into possession of the Municipality of Mantua.

Very few historic documents are available about the structure and its evolution, making it hard to learn in detail the history of the tower [Zuccoli 1988]. Nevertheless, some recent research conceivably dates the construction between the late XII century and the year 1227, when the building was probably completed. Since the tower was integrated in the town defensive system claimed by the Bonacolsi family − the Lords governing Mantua in the XIII century − the entrance is located at a higher position with respect to the ground level (Figure 4.3), as usual for historic defensive structures. At present, the access to the tower is positioned at a height of about 17.7 m (Figure 4.3b), with the lower portion and the base of the structure being still inaccessible.

As it can be observed in Figure 4.1 and Figure 4.3a, the tower is nowadays part of an important palace whose architecture has continuously evolved since the XIII century, complicating the geometry of the structure and the mutual

links between the walls. In general, the load bearing walls of the palace seem to be not effectively linked but just drawn to the masonry walls of the tower, whereas the tower itself directly supports several floors and vaults. Precious frescoes, dating back to the XIV and XVI centuries, decorate the tower's fronts embedded in the palace (Figure 4.4), whereas in 1811 also the interior walls of the tower were painted with refined decorations [Zuccoli 1988].
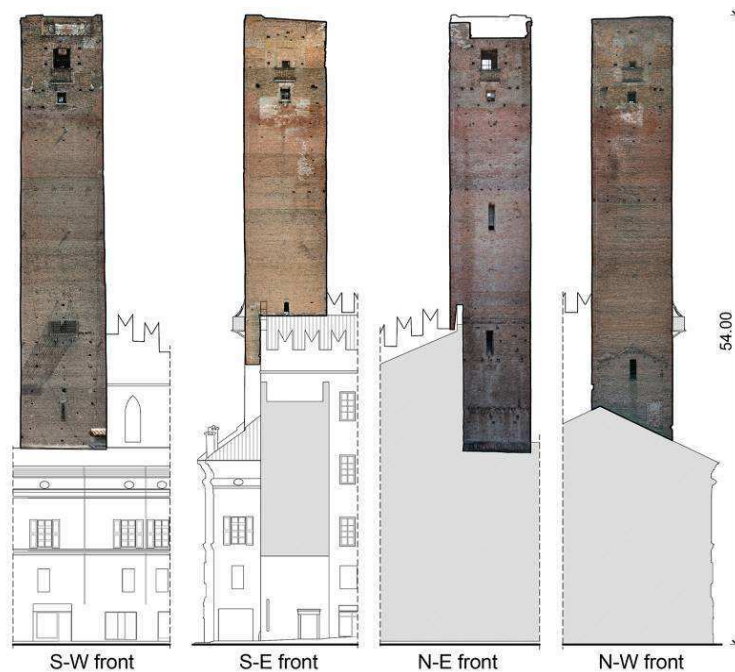
Figure 4.2 Fronts of the Gabbia tower (dimensions in m) [Saisi et al. 2015]

The structure is built in solid brick masonry and is characterized by an almost square plan with approximately 7.0 m long sides. The load-bearing walls are about 2.4 m thick except for the upper levels, where the masonry section decreases to about 0.7 m and a two level lodge is located (Figure 4.3b). During the XIX century and at the beginning of the XX century, the lodge hosted an observation and telegraph post used for military and communication purposes. The wooden staircase that was used to reach the lodge in the past decades has

110

not been practicable since the 1990s due to lack of maintenance. The inner access to the tower was re-established only in October 2012, when provisional scaffoldings (Figure 4.5a) and a light wooden roof (Figure 4.5b) were installed to allow the post-earthquake visual inspection and geometric survey of the inner load-bearing walls.
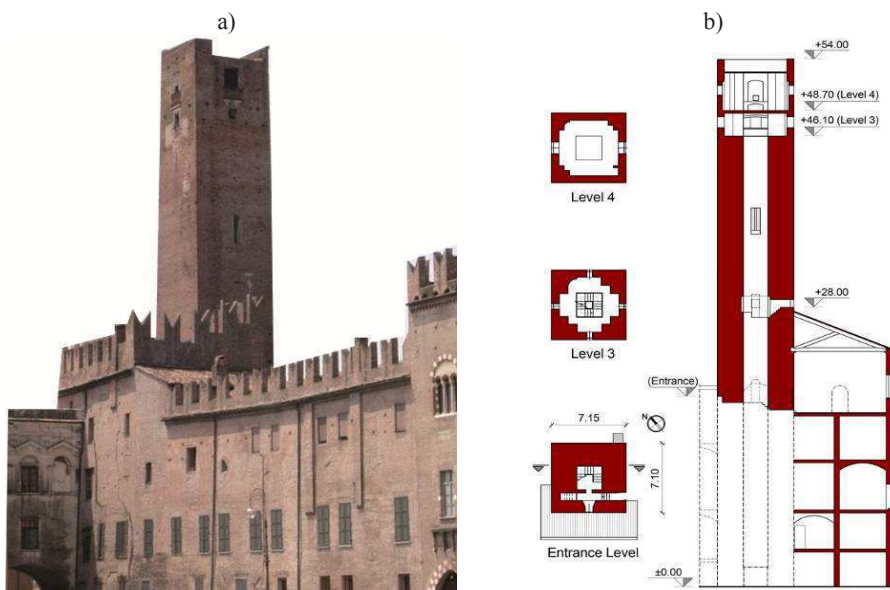
Figure 4.3 General view (a) and sections (b) of the *Gabbia* tower (dimensions in m)

Figure 4.4 Decorations on the tower's fronts embedded in the palace

111
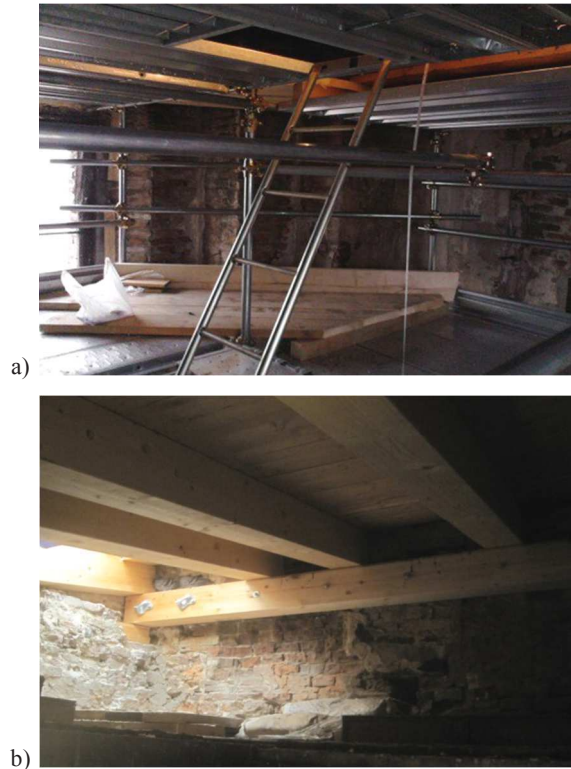
Figure 4.5 Details of the added provisional scaffoldings (a) and wooden roof (b)

Due to its historic relevance, the *Gabbia* tower is an outstanding symbol of Mantua's Cultural Heritage. Therefore, the fall of small masonry pieces from the upper region, reported during the Italian seismic sequence of May 2012, motivated the municipality of Mantua to deeply investigate the state of preservation and the seismic vulnerability of the structure. Consequently, the Politecnico di Milano (Polo Territoriale di Mantova) was committed to carry out an extensive program of on-site survey and non-destructive tests to assess the structural condition of the monument.

The overall investigation, whose results are summarized in sections 4.3 and 4.4, was performed in two phase: in Summer 2012 (visual inspection of the outer load-bearing walls and first series of ambient vibration tests, section 4.3)

and in Autumn 2012 (visual inspection of inner walls, non-destructive tests on the materials and second series of ambient vibration tests, section 4.4).

4.3 First post-earthquake survey: Summer 2012

4.3.1 Visual inspection of the outer load-bearing walls

On-site survey of all outer fronts of the building was performed between 30/07/2012 and 02/08/2012 making use of a movable platform (Figure 4.6). Visual inspections highlighted two different structural conditions [Saisi & Gentile 2015] for the tower:

1. in the main body of the building, until the height of about 46.0 m from the ground level, no evident structural damage was observed and the materials appeared only affected by superficial decay (i.e. mostly erosion of the mortar joints), associated to natural ageing and lack of maintenance;

Figure 4.6 Visual inspection of the tower using a movable platform
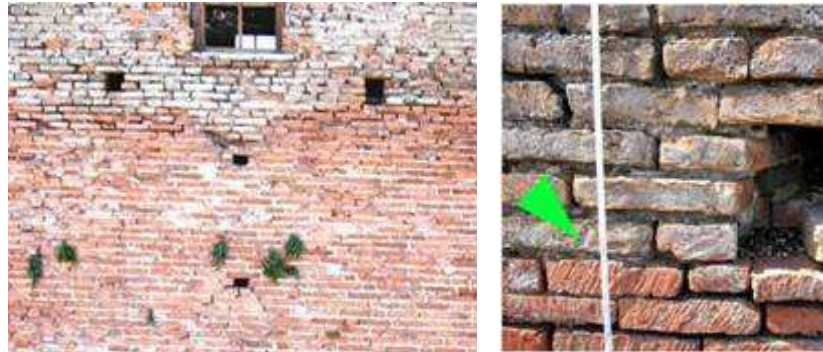
Figure 4.7 Change of the surface workmanship at about 8.0 m from the top
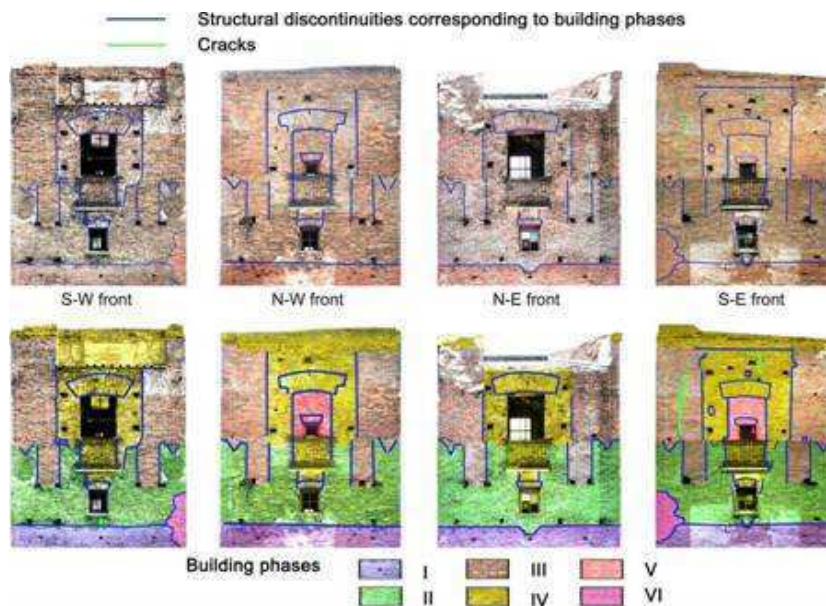
Figure 4.8 Map of the structural discontinuities observed in the upper part of the *Gabbia* tower and supposed building phases

2. at about 8.0 m from the top, the brick surface workmanship is characterized by a clear change, as shown in Figure 4.7, with the upper portion of the tower exhibiting on all fronts extensive masonry decay and passing-through discontinuities (Figure 4.8), that are conceivably related to the tower evolution phases. The stratigraphic survey – revealing traces of past structures and merlon-shaped discontinuities on all fronts (Figure 4.8) – and

114

the available historic pictures (Figure 4.9) allowed to recognize at least six main building phases of the upper region of the tower, as shown in Figure 4.8: i) erection of the main body until about 46.0 m from the ground level; ii) subsequent elevation until the merlons level; iii) addition of 4 corner piers supporting a four side roof; iv-v) closure of the previous openings and realization of new windows, crowning and roof; vi) repair of the South corner.

The poor state of preservation of this region was confirmed by the presence of one local vibration mode involving the upper part of the tower, that was clearly identified from the structural response recorded for more than 24 hours during the ambient vibration tests (AVTs) described in the next sub-section 4.3.2.
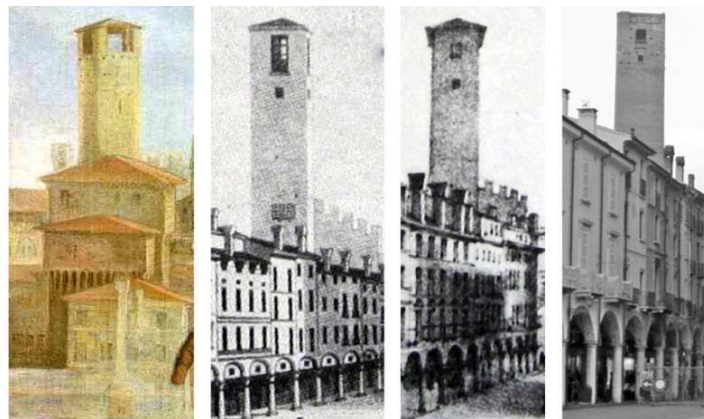
Figure 4.9 Historic evolution of the tower [Saisi et al. 2015]

It is worth mentioning that the local structural issues observed in the upper part of the tower are conceivably worsened by the change in the masonry resisting section (Figure 4.3) detected at about 8.0 m from the top, where the 2.4 m thick walls turn into corner masonry piers and un-toothed infillings. The section decrease at the top level is especially significant for the piers on the North and South corners. In particular, the pier on the South corner turns out to

be partially dismantled and to include merlon-shaped discontinuities as well as an embedded water pipe.

4.3.2   *Ambient vibration tests and dynamic characteristics of the tower*

Within the post-earthquake survey of Summer 2012, the dynamic characteristics of the *Gabbia* tower were investigated by means of an AVT performed between 31/07/2012 and 02/08/2012.

The tower's acceleration time histories were acquired in 12 points using a single set-up. The instrumented positions belonged to 4 different cross-sections selected along the height of the building, according to the sensors' layout shown in Figure 4.10. It should be noticed that one of the purposes of the survey was to check whether the observed change in the masonry texture at about 8.0 m from the top induced some effects on the dynamic characteristics of the tower. Therefore, the positioning of the accelerometers at the upper levels was conveniently planned, identifying two cross sections to be instrumented at the crowning (about 2.0 m from the top and 52.0 m from the ground level) and just below the change in the masonry (around 9.3 m from the top). As at the time of the first survey the access to the inside of tower was not available, all the accelerometers were mounted on the outer walls of the building by using the same movable platform employed meanwhile for the visual inspection. (Figure 4.10 and Figure 4.11).

Assuming the building to be excited by low-level ambient vibrations (because the historic center of Mantua is closed to traffic), the acceleration responses of the tower were measured by using high sensitivity piezoelectric accelerometers (WR model 731A, 10 V/g sensitivity, Figure 4.11). The frequency range for the considered sensors is 0.05-500 Hz, typically far beyond the relevant frequency range of masonry towers. A short cable (1.0 m) connected each sensor to a power unit/amplifier (WR model P31), providing the

constant current needed to power the accelerometer's internal amplifier, signal amplification and selective filtering. Furthermore, two-conductor cables connected the amplifiers to a 24-channel data acquisition system (24-bit resolution, 102 dB dynamic range and equipped with anti-aliasing filters).
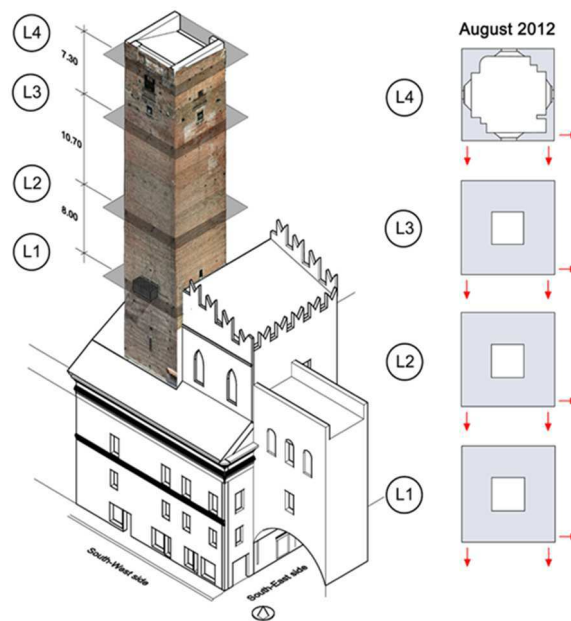
Figure 4.10 Instrumented cross-sections and sensors' layout adopted in the first dynamic test (from 31/07/2012 to 02/08/2012)

Figure 4.11 Typical external mounting of the accelerometers (01/08/2012)
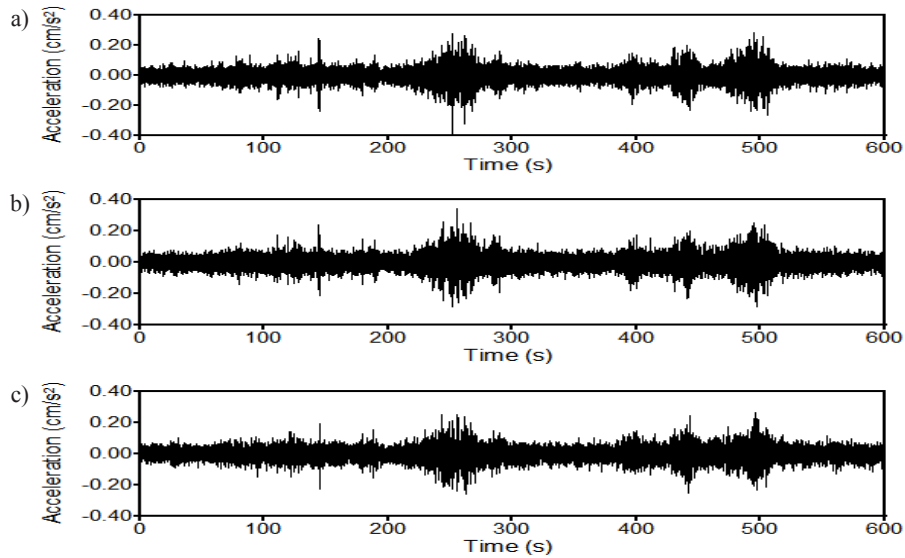
Figure 4.12 Sample of the acceleration recorded on the top level of the tower
between 31/07/2012 and 02/08/2012

As a consequence of the absence of vehicles in the neighboring area, wind and micro-tremors were the only available sources of ambient excitation. Acceleration time histories were acquired for 28 hours: between 16:00 and 23:00 on 31/07/2012 and from 9:00 on 01/08/2012 to 6:00 on 02/08/2012. Figure 4.12 show samples of the acceleration acquired in the upper instrumented cross-section and highlights the very low level of ambient excitation experienced during the test, with the maximum recorded value being lower than 0.4 cm/s^2.

The modal identification was performed using 3600 s long time windows, corresponding to more than 3000 times the fundamental period of the tower. As specified in previous Chapter 3, this choice allowed to largely satisfy the well-known condition regarding the length of the acquired time window (not shorter than 1000-2000 times the fundamental period of the structure [Cantieni 2005]).

The extraction of modal parameters from ambient vibration data was carried out by using the FDD and the data-driven SSI (SSI-Data) algorithms available

in the commercial software ARTeMIS [SVS 2012]. More specifically, the FDD was mainly applied on site to quickly estimate the dynamic characteristics of the structure, whereas the same estimates were later refined by using the SSI-Data method.

Notwithstanding the very low level of ambient excitation (Figure 4.12) experienced during the AVT, the application of the SSI-Data technique to all data sets generally led to the identification of 5 vibration modes within the frequency range 0-10 Hz.

(a) Mode B_1   **(b) Mode B_2**   **(c) Mode B_3**   **(d) Mode T_1**   **(e) Mode L'_1**

$f = 0.976$ Hz $f = 1.023$ Hz $f = 3.886$ Hz $f = 4.745$ Hz $f = 6.930$ Hz
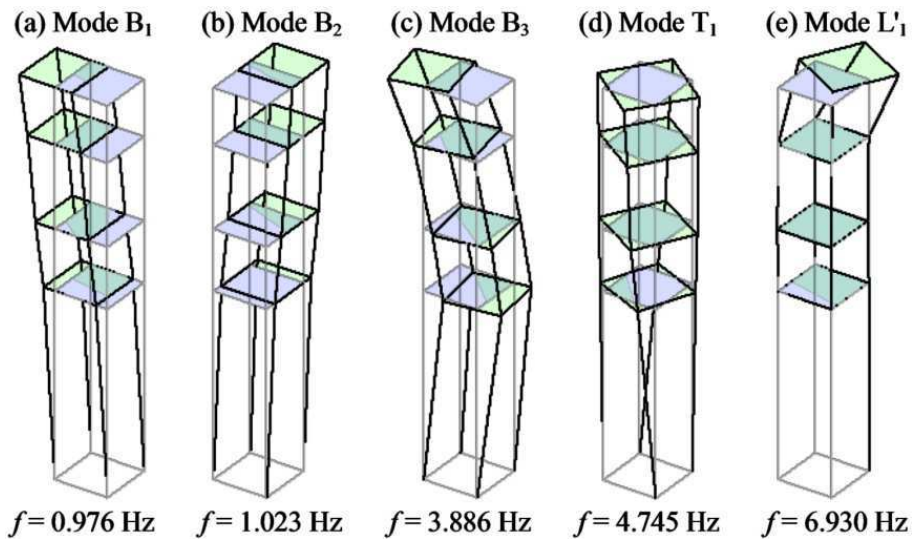
Figure 4.13 Vibration modes generally identified in the post-earthquake AVT (SSI-Data, 31/07/2012 16:00-17:00)

Typical results in terms of natural frequencies and mode shapes are shown in Figure 4.13, and refer to the acceleration data recorded on 31/07/2013 in the time interval 16:00-17:00. Inspection of the mode shapes allows the following comments on the dynamic characteristics of the tower:

1. two closely spaced modes were identified around 1.0 Hz. These modes (Figure 4.13a-b) are dominant bending (B) and involve flexure in the two main planes of the structure, respectively: mode B_1 (Figure 4.13a) is

119

characterized by bending displacements in the N-E/S-W plane, whereas the modal deflections of mode B_2 belong to the orthogonal N-W/S-E plane;

2. the third mode (Figure 4.13c) mainly involves bending in the N-E/S-W plane, with slight components also in the orthogonal N-W/S-E plane;

3. only one torsion mode (T) was identified (Figure 4.13d) at a frequency of 4.77 Hz (in the examined time window);

4. the last identified mode is local (L) and only involves deflections of the upper region (Figure 4.13e). The mode shape looks dominant bending, with significant components along the two main planes of the tower. The presence (and general detection) of a local vibration mode in the higher levels of the building provides further evidence of the structural effect of the change in the masonry quality and morphology (including un-toothed opening infillings and discontinuities) observed in this region during the preliminary visual inspection.

It is worth noting that the fundamental frequencies of about 1.0 Hz fall exactly in the range of dominant frequencies characterizing the earthquakes recorded in May 2012 and, more in general, the seismic events typically expected in the Mantua area. Such a consideration, along with the presence of the local mode involving the top of the tower, would explain the fall of small masonry pieces reported during the seismic sequence of May 2012.

Therefore, the results of post-seismic assessment, both in terms of visual inspection and OMA, confirm the concerns about the vulnerability of the building and highlight the need of preservation actions.

Frequency variation and correlation with outdoor temperature

Other experimental investigations presented in literature [Ramos et al. 2010; Cantieni 2014] report clear effects of temperature on the natural frequencies of masonry towers. To highlight such effects, a second acquisition system was

used during the AVT, measuring the temperature in three different points of the tower. Both indoor and outdoor temperature were measured on the S-W load-bearing wall, whereas only the outdoor temperature was measured on the S-E front. Figure 4.14 shows the evolution in time of the two recorded outdoor temperatures. As it can be observed, both plots reveal significant variations, ranging between 25°C and 55°C. The tracking referred to the S-W sensor exhibits a more regular trend, conceivably due to the fact that this front is directly exposed to sun rays for the larger part of the day. On the other hand, it is worth mentioning that only slight fluctuations were measured by the indoor sensor (29°C-30°C), as a consequence of the high thermal inertia of the masonry walls.

The time evolution of the natural frequencies identified between July 31st and August 2nd, 2012 is reported in Figure 4.15. The corresponding statistics are summarized in Table 4-1 through the mean value (f_{ave}), the standard deviation (σ_f) and the extreme values (f_{min}, f_{max}) of each modal frequency. It should be noticed that the natural frequencies of all modes exhibit slight but clear variation, with the standard deviation ranging between 0.011 Hz (mode B_2) and 0.0037 Hz (mode L_1'). As it can be observed by comparing the diagrams reported in Figure 4.14 and Figure 4.15, the time evolution of the natural frequencies seems to follow the fluctuations of temperature, revealing a possible dependence between the two features. Furthermore, considering the very low level of ambient excitation experienced during the test, the observed variations of the modal frequencies can only be explained by considering the dominant effect of temperature.
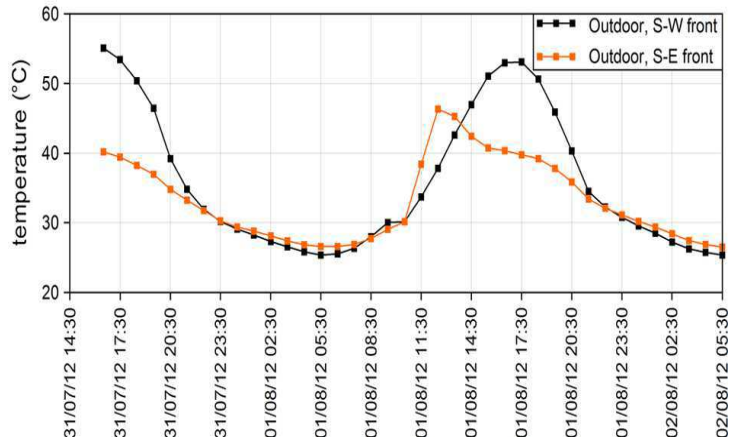
Figure 4.14 Time evolution of the recorded outdoor temperatures recorded during the first AVT (July-August 2012)
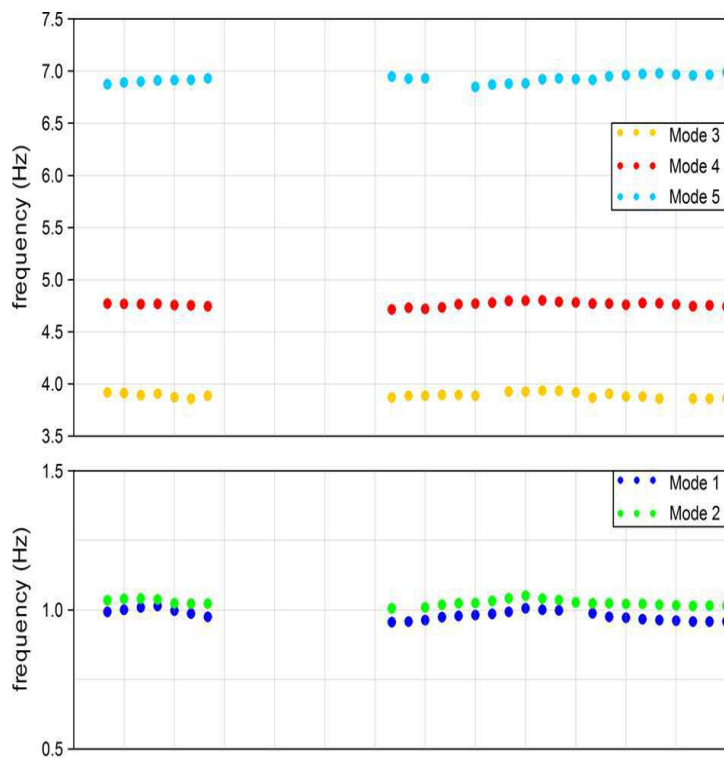
Figure 4.15 Time evolution of the natural frequencies identified during the first AVT (July-August 2012)

Table 4-1 Statistics of the natural frequencies identified (SSI-Data) in the first AVT

Mode	f_{ave} (Hz)	σ_f (Hz)	f_{min} (Hz)	f_{max} (Hz)
B_1	0.981	0.018	0.957	1.014
B_2	1.026	0.011	1.006	1.052
B_3	3.891	0.025	3.857	3.936
T_1	4.763	0.022	4.714	4.802
L_1'	6.925	0.037	6.849	6.987

B = bending mode; T = torsion mode; L = local mode

In order to investigate the possible relationship between modal frequencies and temperature, a very simple approach consists of plotting the estimates of each frequency versus temperature, as reported in Figure 4.16. More specifically, the presented diagrams show the identified natural frequencies plotted with respect to the hourly averaged temperature measured on the outside of the S-W front. Each graph also reports the best fit line and the coefficient of determination R^2 [e.g. Johnson & Wichern 1992].

From the inspection of Figure 4.16, it can be clearly observed that the natural frequencies of bending modes B_1-B_3 increase with increased temperature. Furthermore, the two features exhibit an almost linear correlation, with the coefficient of determination R^2 assuming high values and ranging between 0.64 (mode B_3, Figure 4.16c) and 0.75 (mode B_2, Figure 4.16b). The correlation appears less strong for the torsion mode (mode T, Figure 4.16d), characterized by a lower value of coefficient R^2 (0.37). Nevertheless, the increasing trend of the natural frequency remains clear. This behavior, observed also in other long-term studies of masonry towers [Ramos et al. 2010, Cabboi et al. 2013, Cantieni 2014] can be explained through the closure of superficial cracks, minor masonry discontinuities or mortar gaps induced by the thermal expansion of materials. Hence, the temporary "compacting" of the materials induces a temporary increase of stiffness and modal frequencies, as well.
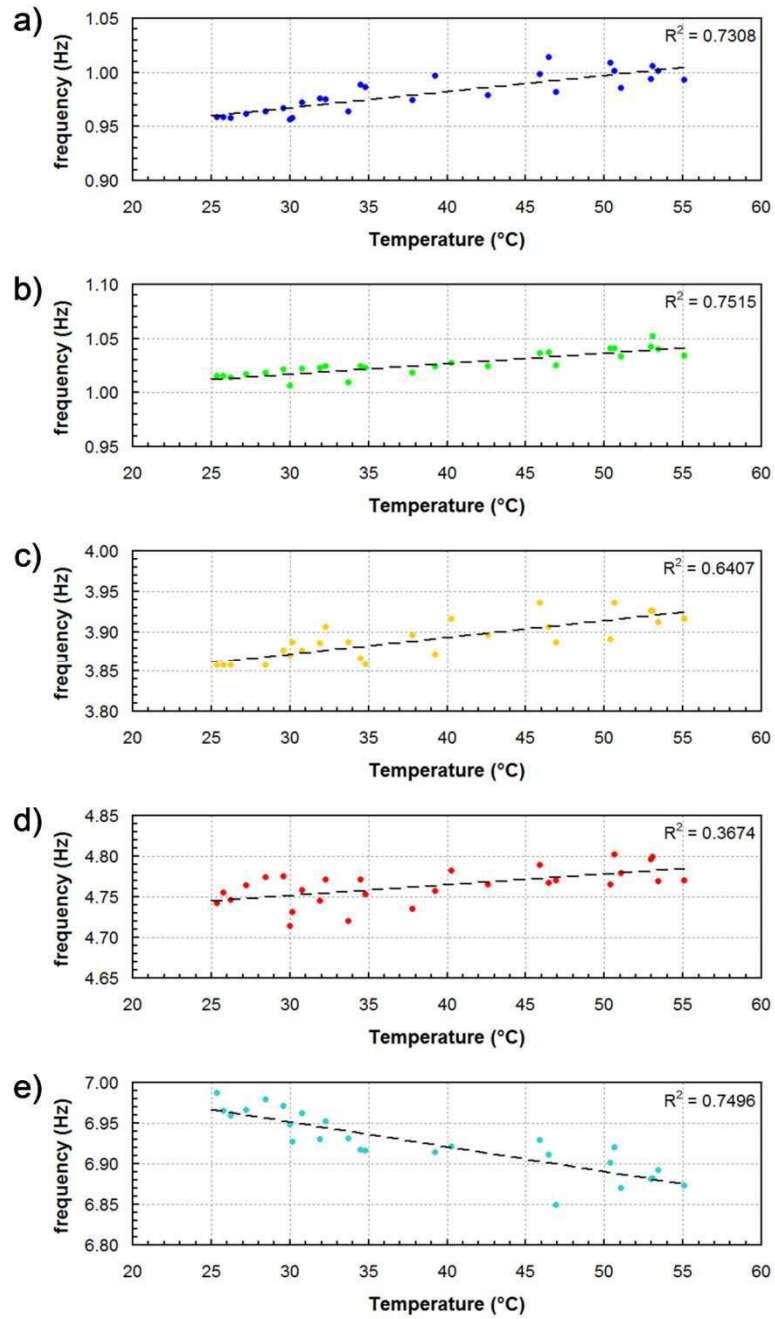
Figure 4.16 Frequency (SSI-Data) variation vs. measured outdoor temperature (S-W front): a) mode B_1, b) mode B_2, c) mode B_3, d) mode T, e) mode L_1'
[Saisi & Gentile 2015]

Unlike the global modes, the natural frequency of local mode L_1' (Figure 4.16e) decreases with an increased temperature, with the coefficient of determination assuming a relevant value ($R^2 \approx 0.75$). This result suggests that the thermal expansion of materials in a very heterogeneous area of the structure causes a general worsening of the connection between the masonry portions. Hence, further evidence is provided of the poor state of preservation of the upper part of the tower (again in agreement with the main results of the visual inspection).

4.4 Second post-earthquake survey: Autumn 2012

4.4.1 Visual inspection of the inner walls and on site tests

As mentioned in the general description of the *Gabbia* tower, the access to the inside of the structure was not possible for many years, after the deterioration of the wooden stairs used to reach the top. This prevented from performing on site tests on materials and visual inspections of the inside of the masonry walls. To overcome such obstacle, a light wooden roof and an internal metallic scaffolding (Figure 4.5) were installed after the first experimental survey.

As shown in Figure 4.5a, the wooden roof, although very light, is slightly inclined (in the N-E/S-W direction) and directly supported by the weakest structural part of the building. The roof slope and the redundant connection with the masonry walls contribute to create a static scheme that, when subjected to thermal expansion, is likely to induce not negligible thrusts on the already vulnerable upper levels. The effects of the wooden roof on the dynamic behavior of the *Gabbia* tower will be discussed in the next sub-section 4.4.2.

The visual inspection of the inner load-bearing walls as well as the tests performed on the materials (i.e. pulse sonic tests and double flat-jack tests) fully confirmed the conclusions drawn after the first post-earthquake survey (section

4.3) on the compactness of the masonry in the main portion of the structure [Saisi & Gentile 2015]. More specifically:

1. the results obtained from the pulse sonic tests provided evidence of solid brick section, with sonic velocity values ranging between 1100 m/s and 1600 m/s.;

2. double flat jack tests were carried out on the outer S-W wall, at the ground level and on the inner S-W wall (taking advantage of the scaffolding), at about 32.8 m from the ground level. The Young's modulus obtained from both tests turned out to be larger than 3.00 GPa;

3. the good quality of the masonry materials also resulted from the laboratory tests on sampled bricks and mortars.

Similarly, the poor state of preservation of the upper 8.0 m of the tower was confirmed by the low average value of the sonic velocity (600 m/s) obtained in this area as well as by the direct survey.

4.4.2   *Ambient vibration tests and effects of the wooden roof on the dynamic characteristics of the tower*

To check possible variations of the modal characteristics of the structure consequent to the new additions, a second dynamic test was performed on 27/11/2012. Such test was also performed in readiness for the installation of a small dynamic monitoring system in the building. In this sense, it was even more important to make sure of the current dynamic behavior of the tower.

The AVT was performed by using the same acquisition chain and sensors' configuration of the previous survey: 12 high sensitivity piezoelectric accelerometers (WR model 731A, 10 V/g sensitivity) powered by power unit/amplifiers (WR model P31), in turn connected to a 24-channel data acquisition system (24-bit resolution, 102 dB dynamic range and equipped with anti-aliasing filters). Considering that, at the time of the second test, the access

126

to the inside of the tower had been re-established, an inner mounting of the sensors on the four cross-sections was preferred (Figure 4.17 and Figure 4.18).
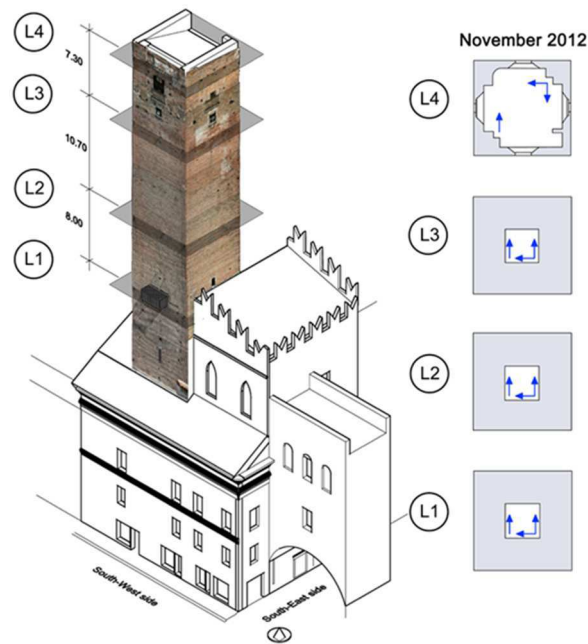
Figure 4.17 Instrumented cross-sections and sensors' layout adopted in the second AVT (27/11/2012)

Figure 4.18 View of the metallic scaffolding installed after Summer 2012 (a) and typical inner mounting of the accelerometers in the second AVT (b)

It is worth mentioning that a single temperature sensor was installed during this second AVT. The sensor recorded the wall temperature on the outside of the S-W front, where the most regular time trend was obtained during the previous survey. In this circumstance, due to the lower daily temperature range typical of Autumn months, the values recorded by the sensor were almost constant (10°C-11°C).Acceleration time histories were acquired for two hours in mid-morning of 27/11/2012. Considering that the main sources of ambient vibrations were again represented by wind and micro-tremors, a level of ambient excitation comparable to the one of the first survey was experienced.

As for the first AVT, the modal identification was performed using 3600 s long time windows, and applying the SSI-Data technique available in ARTeMIS software [SVS 2012]. The low level of ambient excitation did not prevent the SSI-Data procedure from identifying 5 vibration modes between 0 Hz and 10 Hz. The natural frequencies and modes shapes identified from the modal analysis of the recorded acceleration time histories are reported in Figure 4.19.

The obtained results and the comparison with the outcomes of the first AVT (Figure 4.13) allow the following comments:

1. beyond the difference in terms of natural frequency (conceivably related to temperature effects), the mode shapes of modes B_1-B_3 did not exhibit significant changes between the two AVTs (see Figure 4.13a-c and Figure 4.19a-c). Hence, the metallic scaffolding and the wooden roof practically do not affect those modes;

2. The identified frequency of the fourth mode (Figure 4.19d) did not change appreciably with respect to the first dynamic survey. On the other hand, the mode shape looks significantly different, involving dominant torsion of the tower until the height of 46.0 m and coupled torsion-bending of the upper region. The local behavior of the higher levels modifies what would

128

otherwise be classified as a pure torsion mode. Furthermore, a closer inspection of the results of the two AVTs reveals that the identified mode shape of fourth mode (Figure 4.19d) results from the superposition of the previous torsion (Figure 4.13d, mode T_1, lower part of the structure) and local modes (Figure 4.13e, mode L_1', upper part of the structure). This modification can be conceivably referred to the effects produced by the installation of the wooden roof;

3. as a consequence of the shift of mode L_1' to a lower frequency, the previous local mode (Figure 4.13e) has been "replaced" by another local mode, with higher frequency (i.e. 9.89 Hz in the considered time window) and involving torsion of the upper part of the tower (Figure 4.19e). This mode, not identified before, is probably related to the increasing of connection between the masonry walls at the top levels induced by the new covering.

From the results of the previous comparison, it is possible to conclude that the dynamic characteristics of the upper region of the building are significantly affected by the presence of the wooden roof.

(a) Mode B_1	(b) Mode B_2	(c) Mode B_3	(d) Mode T_1	(e) Mode L_1
$f = 0.918$ Hz	$f = 0.986$ Hz	$f = 3.887$ Hz	$f = 4.648$ Hz	$f = 9.893$ Hz
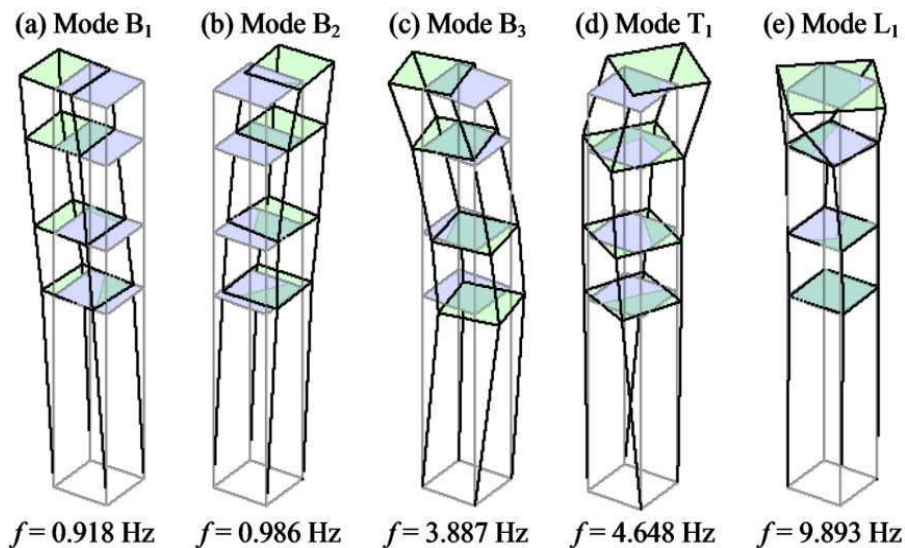
Figure 4.19 Vibration modes identified in the second AVT (SSI-Data,. 27/11/2012)
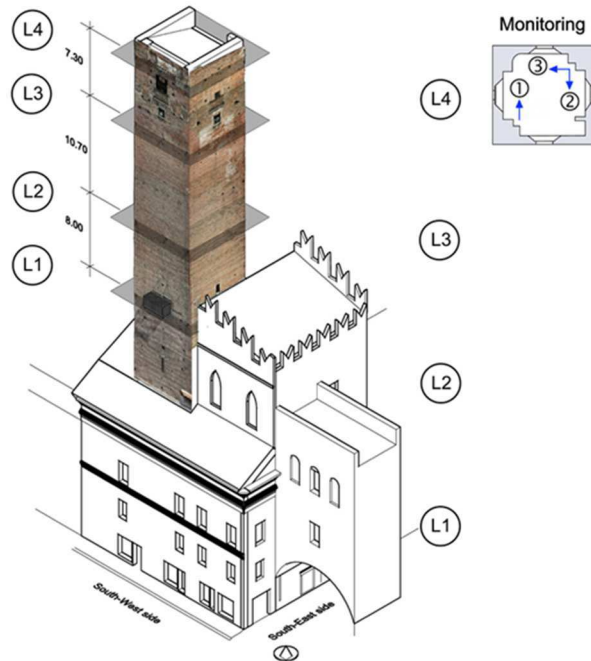
Figure 4.20 Accelerometers permanently installed in the tower

4.5 Description of the continuous dynamic monitoring system and automated OMA

The results obtained from the preliminary AVTs highlighted that, as a consequence of the cantilever-like structural behavior of the *Gabbia* tower (and, in general, of all historic masonry towers), the dynamic behavior of the structure can be monitored with confidence just by instrumenting the upper section (Figure 4.19). Therefore, few weeks after the execution of the second AVT, a simple dynamic monitoring system was installed in the structure. The monitoring system is composed by:

1. one 4-channel data acquisition system (24-bit resolution, 102 dB dynamic range and anti-aliasing filters);

2. 3 piezoelectric accelerometers (10 V/g sensitivity, ±0.50 g peak and 0.05-500 Hz frequency range) mounted on the cross-section corresponding to the

crowning level of the tower (Figure 4.20);

3. one temperature sensor, installed on the S-W front and measuring the outdoor temperature of the wall. This decision was motivated by the very regular trend obtained in the same position during the first AVT;

4. one industrial PC on site, for system management and data storage purposes.

A binary file, containing 3 acceleration time series and the temperature data, is created every hour, stored in the local PC and transmitted to Politecnico di Milano for being processed.

The continuous dynamic monitoring system has been active since late December 2012. As for the preliminary tests, the modal identification is performed using time windows of 3600 s, to comply with the recommendation of using an appropriate duration of the acquired time windows.

The adopted sampling frequency is 200 Hz. This value is significantly higher than the one required for the investigated structure (as the significant frequency content of the recorded signals is below 12 Hz). Hence, data are low pass filtered and decimated before applying the identification tools, thus reducing the sampling frequency from 200 Hz to 40 Hz.

The data files received from the monitoring system are managed by a pre-processing routine developed in LabVIEW, consisting of the automated execution of the following tasks [Busatta 2012]:

1. creation of a database with the original data;

2. preliminary pre-processing (i.e. de-trending, automatic recognition and extraction of possible seismic events, creation of 1 dataset per hour);

3. evaluation of hourly-averaged acceleration amplitudes and temperature;

4. low-pass filtering and decimation of each dataset;

5. creation of a second database, with essential data records, to be used in the modal identification phase.

As already mentioned in Chapter 3, the modal parameters of the tower were

extracted from the measured acceleration data by using the automated procedure developed in [Cabboi 2013] and based on the SSI-Cov algorithm. As it is usual for automated OMA procedures, some general parameters and thresholds are dependent on the specific case study and their calibration is performed through several manual analyses of the collected data-sets. In the case of *Gabbia* tower, the following values have been selected:

1. the SSI-Cov time lag parameter i was set equal to 70, whereas data were fitted using stochastic subspace models with order n ranging between 30 and 120;

2. since the preliminary AVTs did not reveal the presence of complex modes, the automated cleaning and interpretation of the stabilization diagrams has been performed by using a threshold value of the MCF index equal to 0.2;

3. finally, the tracking of the most meaningful modes has been carried out using a baseline list based on the results of the second AVT (i.e., after the installation of the wooden roof). Considering the expected effects of temperature (see e.g. Figure 4.16), threshold values have been set so that identified modes are kept when their variation is lower than 15% for frequency and higher than 0.85 for the MAC.

A typical stabilization diagram after cleaning and selection of physical modes is shown in Figure 1.3. The plot was obtained by applying the automated SSI-Cov algorithm to the dataset recorded on 08/02/2013 between 08:00 and 09:00 and reports the poles alignments along with the first Singular Value (SV) line of the spectral matrix, which is the mode indication function adopted in the FDD method. The inspection of Figure 1.3 highlights that the alignments of the stable poles obtained with the SSI-Cov algorithm provide a clear indication of the tower's modes and correspond to local maxima in the first SV line of the FDD technique.

In order to obtain an extensive validation of the results automatically

computed, the frequency estimates obtained from the automated procedure were compared to those evaluated by manually applying the SSI-Data algorithm of the ARTeMIS software [SVS 2012]. To this purpose, 4321 datasets collected over 6 months of monitoring (i.e. from 17/12/2012 to 14/06/2013) have been manually processed [Xu 2013].
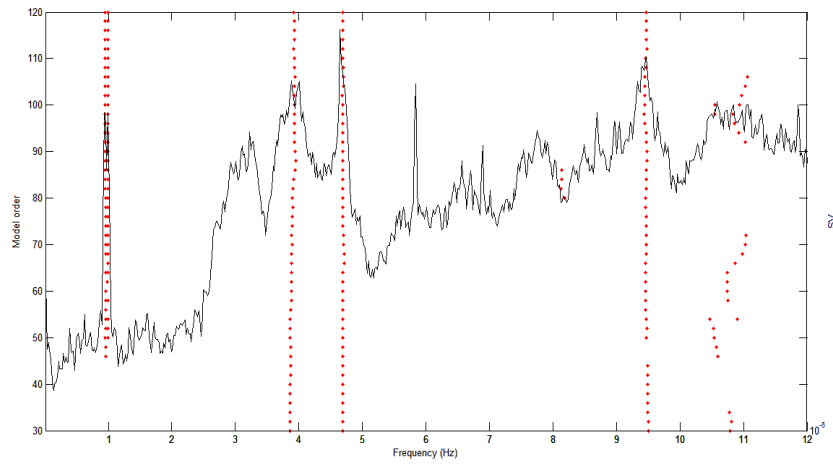
Figure 4.21 Stabilization diagrams obtained from the data set recorded on: 08/02/2012 08:00-09:00

Table 4-2 Statistics of the natural frequencies manually (SSI-Data) and automatically (SSI-Cov) identified from 17/12/2012 to 14/06/2013

Mode	f_{ave} (Hz)		σ_f (Hz)		f_{min} (Hz)		f_{max} (Hz)	
	SSI Data	SSI Cov	SSI Data	SSI Cov	SSI Data	SSI Cov	SSI Data	SSI Cov
B_1	0.983	0.981	0.036	0.034	0.910	0.910	1.085	1.083
B_2	1.024	1.020	0.031	0.027	0.961	0.961	1.129	1.122
B_3	3.918	3.940	0.061	0.074	3.784	3.758	4.208	4.194
T_1	4.759	4.748	0.072	0.069	4.629	4.621	4.991	4.981
L_1	9.236	9.243	0.546	0.552	8.327	8.320	10.290	10.327

B = bending mode; T = torsion mode; L = local mode

133
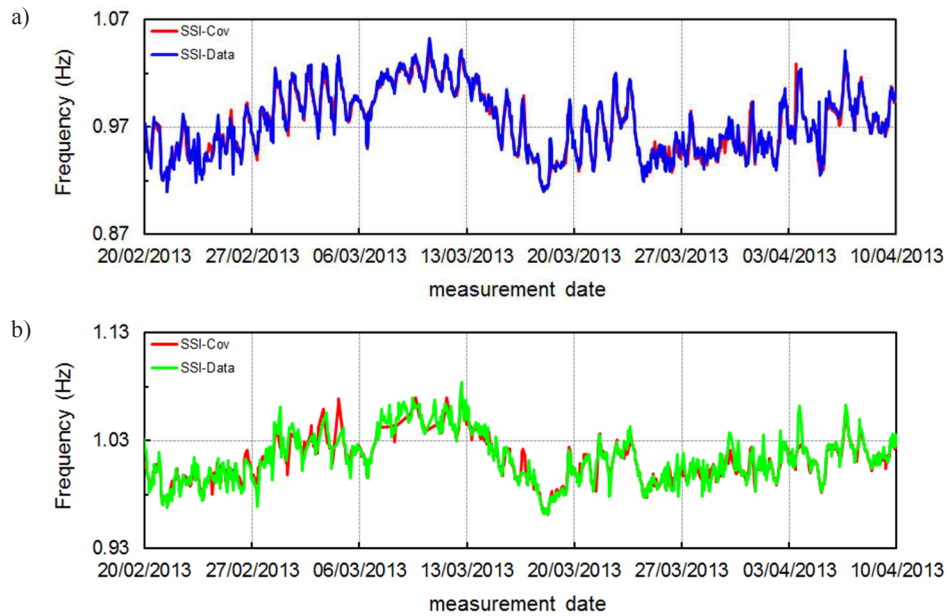
Figure 4.22 Comparison between manually (SSI-Data) and automatically (SSI-Cov) identified frequencies: a) mode B_1; b) mode B_2

Table 4-2 summarizes the statistics (in terms of mean values, standard deviations and extreme values) of the frequencies manually and automatically identified during the investigated time. Furthermore, in Figure 4.22 the time evolution of the estimates of modes B_1 and B_2 (blue and green lines, respectively) obtained from the SSI-Data technique has been plotted along with the results of the automated SSI-Cov procedure (red line). The statistical values reported in Table 4-2 and the comparison presented in Figure 4.22, reveal an excellent agreement between the two techniques. This confirms the accuracy of the estimates obtained by automatically processing the response data through the adopted SSI-Cov procedure [Cabboi 2013].

4.6 Continuous dynamic monitoring: general results

This section summarizes the results of the dynamic monitoring over a period of about 30 months, from 17/12/2012 to 30/06/2015. For the whole period, the modal parameters were automatically identified from more than 16000 1-hour long datasets, using the previously described SSI-Cov technique.

Figure 4.23 presents the time evolution of the outdoor wall temperature recorded on the S-W front. The temperature tracking reveals large fluctuations, between -2°C and 50°C. Furthermore, significant daily variations can be observed during warm months (i.e. from May until September), especially on sunny days. The automated identification of the modal frequencies from the collected datasets allowed to obtain the time evolution diagram reported in Figure 4.24. The corresponding statistics are summarized in Table 4-3 through mean values, standard deviations and extreme values.

It should be noticed that standard deviations are larger than 0.03 Hz for all modes, with a particularly relevant value for the local mode L_1. Indeed, the tracking of mode L_1 looks very different from the others (Figure 4.24), as the natural frequency ranges with relevant fluctuations approximately between 8.14 Hz and 10.33 Hz. The causes of such behaviour cannot be grasped at once and accurate and dedicated evaluations are required.

On the other hand, global modes exhibit a more regular behaviour, characterized by slight oscillations and small dispersion of the estimates. Furthermore, as observed for the AVT performed in Summer 2012, the comparison of Figure 4.23 and Figure 4.24 reveals a certain accordance between frequency and temperature fluctuations. The correlation between the two features will be discussed in the following. It is worth mentioning that, since the analyses carried out for the global modes do not apply to the local mode as well, results obtained for mode L_1 and modes B_1-T_1 are presented in different sections.

135
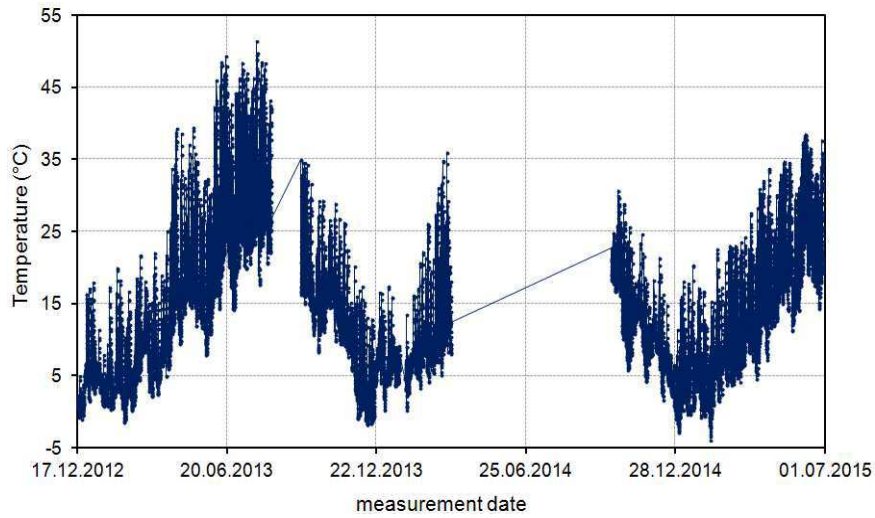
Figure 4.23 Temperature variation between 17/12/2012 and 30/06/2015
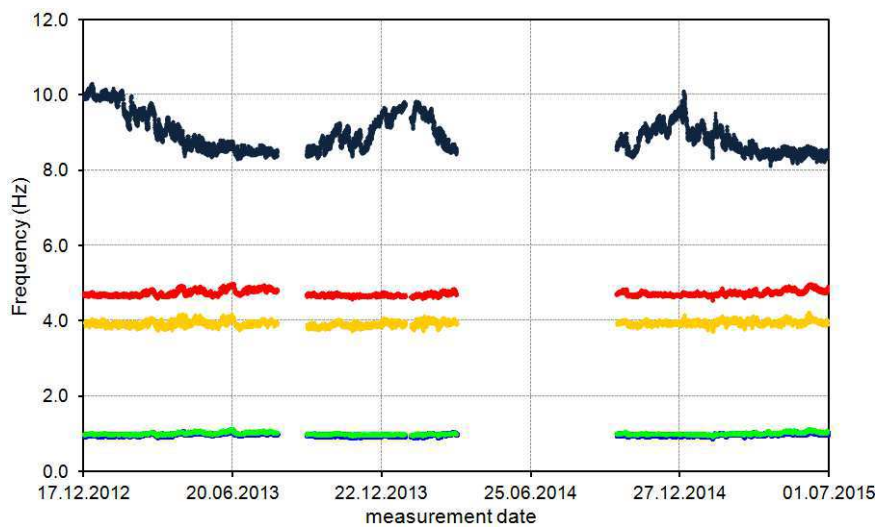
Figure 4.24 Variation of identified natural frequencies between 17/12/2012 and 30/06/2015

It should also be noted that, during the investigated time period, the monitoring activity suffered some interruptions, as revealed by the gaps in the reported time histories (Figure 4.23 and Figure 4.24): the shorter interval was associated to maintenance of the monitoring system, whereas the longer one

136

was motivated by logistic issues related to the temporary non-availability of the room hosting the data acquisition system and local PC.

Table 4-3 Statistics of the natural frequencies identified (SSI-Cov) from 17/12/2012 to 30/06/2015

Mode	f_{ave} (Hz)	σ_f (Hz)	f_{min} (Hz)	f_{max} (Hz)
B_1	0.977	0.036	0.885	1.102
B_2	1.021	0.030	0.929	1.148
B_3	3.943	0.066	3.724	4.232
T_1	4.749	0.070	4.558	5.010
L_1	8.949	0.479	8.136	10.327

B = bending mode; T = torsion mode; L = local mode

4.6.1 *Dynamic behavior under seismic excitation*

Between January and June 2013, the monitoring system installed on the *Gabbia* tower acquired the response to different far-field seismic events occurred in the neighboring regions. In particular, Figure 4.25 shows time histories related to far-field seismic events recorded on 25/01/2013, 04/05/2013 and 21/06/2013.

It can be observed that, generally, the maximum seismic response exceeds several times the highest level of experienced ambient vibrations (0.4-0.5 cm/s^2, Figure 4.12). Considering the seismic event of January 25th, 2013 the maximum amplitude of the earthquake-induced accelerations on the top of the tower was quite low (2.5 cm/s^2), but still 5 times larger than those produced by typical ambient excitation. The strongest of the recorded seismic events (Figure 4.25c) corresponds to an earthquake occurred in the Garfagnana area, Tuscany, on 21/06/2013. This seismic event determined peak accelerations on top of the tower more than 40 times larger than the usual ambient vibration responses and produced significant structural effects on the building.
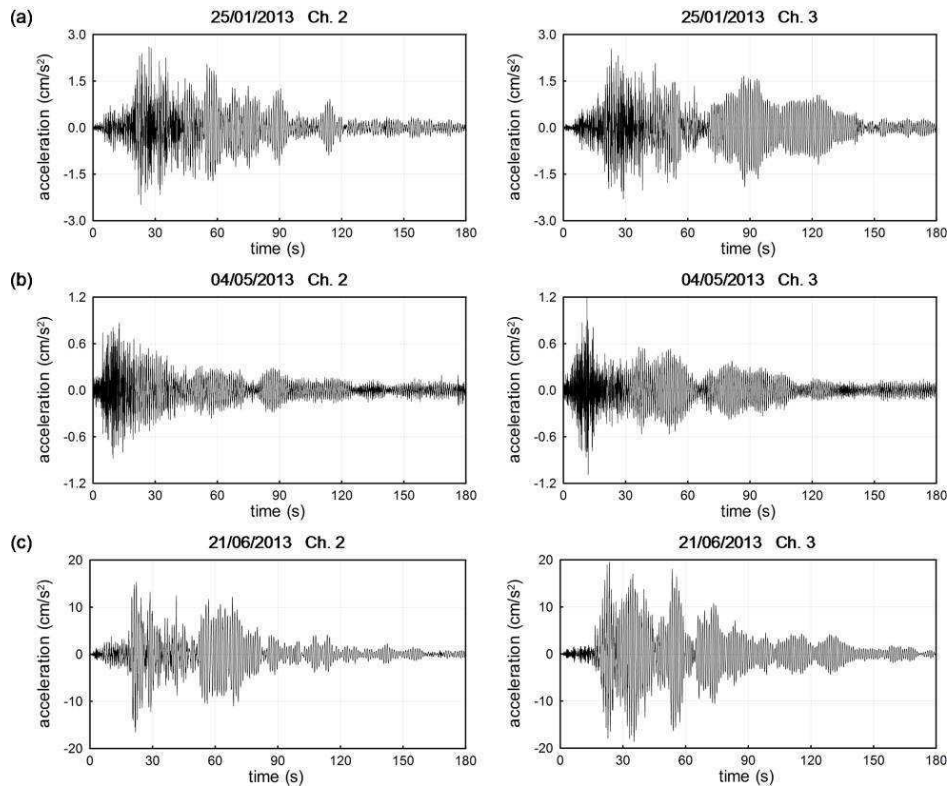
Figure 4.25 Samples of the tower's seismic response [Saisi et al. 2015]

In order to investigate possible variations of the tower's structural behavior induced by the seismic action, a time-frequency analysis − based on the *Choi-William* (CW) distribution − of the recorded signals has been performed, using the Matlab routine developed by Ubertini et al. (2013). The routine allows to estimate the energy distribution of the signals in the time-frequency domain.

Results of the time-frequency analyses are presented for the two most significant recorded earthquake, occurred on 25/01/2013 (Figure 4.25a) and 21/06/2013 (Figure 4.25c). Since the installed accelerometers are oriented along the two main directions of the tower, two different analyses have been carried out for the response time histories recorded by sensor A02 (i.e. N-W/S-E direction) and sensor A03 (i.e. N-E/S-W direction.
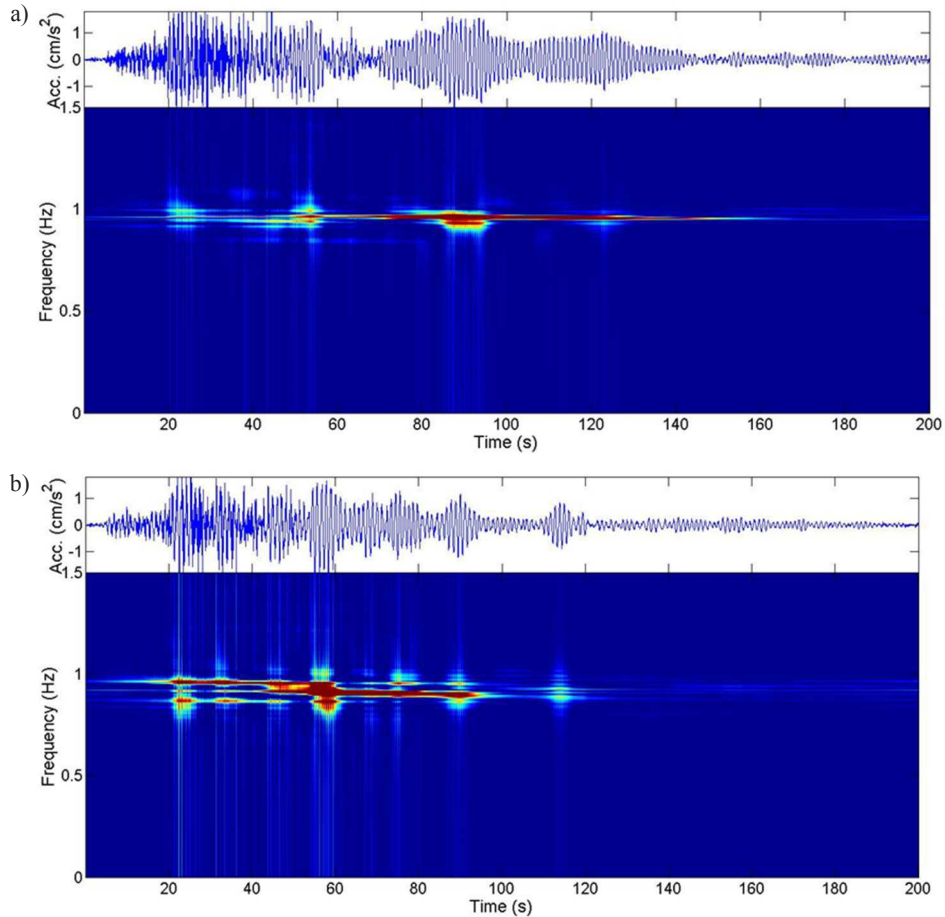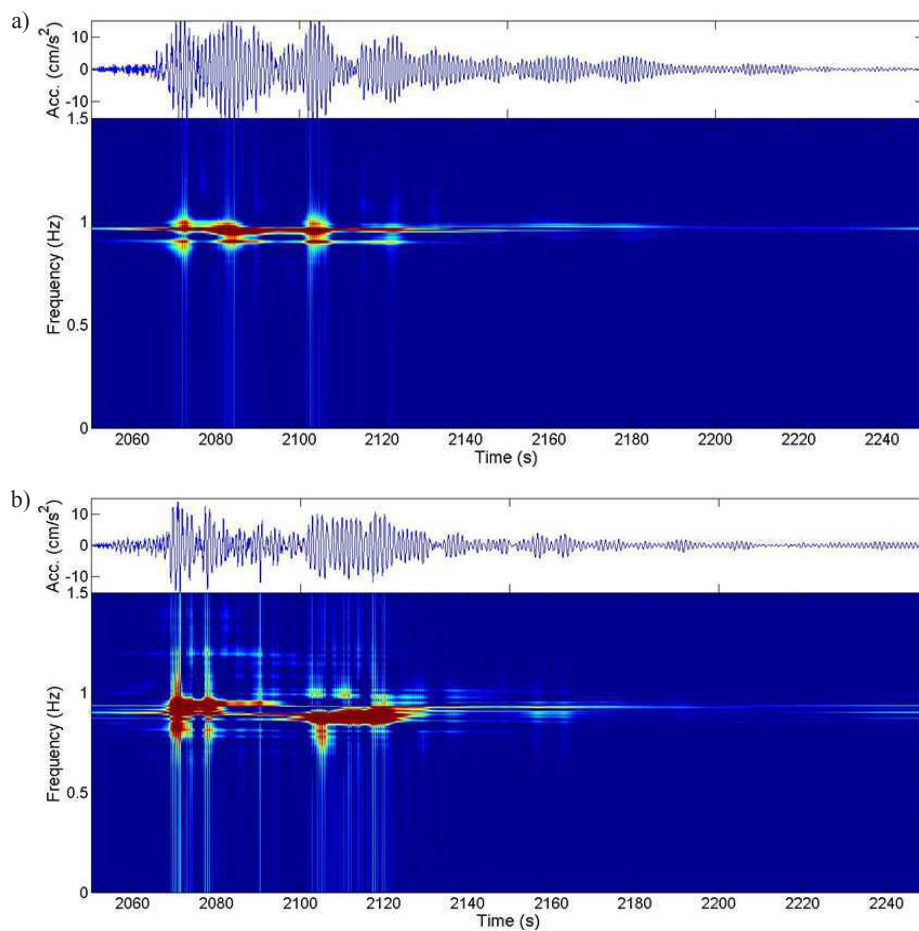
Figure 4.26 Time-frequency analysis of the time-histories recorded on 25/01/2013 on top of the tower: (a) N-W/S-E direction; (b) N-E/S-W direction

Figure 4.26 refers to the seismic event occurred on 25/01/2013 and reports the time-frequency analysis of a 200 s long time history, containing the acceleration responses induced by the earthquake on the top level of the tower. It should be noted that, in order to better highlight the effects of the seismic event, only the frequency range 0-2 Hz, related to the first two modes, is shown.

Figure 4.26a, illustrating the time-frequency analysis of the response along the N-W/S-E direction (i.e. the bending direction of mode B_2, Figure 4.19b), reveals a quite stable situation: the acceleration response looks linear and

dominated by the frequency of mode B_2 (i.e., no variations of the correspondent frequency line are detected for the whole duration of the seismic event).

On the other hand, Figure 4.26b reveals a more complex response in the N-E/S-W direction (i.e. the bending direction of mode B_1, Figure 4.19a). In the first part of the record, the response shows two main frequency components between 0.8 and 1.Hz. After the peak acceleration (60 seconds), some variations of the frequency content can be observed: in particular, just one frequency becomes dominant − conceivably corresponding to the frequency of mode B_1 − and its value slightly decreases. The slight shift of the dominant frequency suggests the occurrence of slight non-linearity and proves the top levels of the tower to be particularly sensitive to the seismic action, especially along the N-E/S-W direction.

In Figure 4.27, results are presented for the strongest recorded seismic event, occurred on 21/06/2013 in the Garfagnana region. Again, the time-frequency analysis was performed on time histories of about 200 seconds and only the frequency range related to the first two modes (0-2 Hz) is shown.

Figure 4.27a refers to the response along the N-W/S-E direction (mode B_2). Unlike the previous case, the stronger accelerations induce slight variations of the frequency content also in this direction. Before the earthquake, the structural response looks dominated by the frequency of mode B_2 (indicated by the continue frequency line). As the recorded acceleration reach its peak (between 2075s and 2120s), the signal frequency content exhibits some slight fluctuations and a second frequency line is detected at a smaller value. After the peak acceleration, the fluctuations tend to disappear and the frequency corresponding to mode B_2 becomes dominant again.

As expected from the results of the previous smaller earthquake, the frequency-time analysis along the N-E/S-W direction (mode B_1) provides more complex results. After the peak acceleration (2070 s), the frequency content of

140

the signal suffers significant fluctuations. In particular, the frequency line of mode B_1 exhibits a shift at about 2090 s and does not return to the original position as the earthquake-induced accelerations decrease.

The described behavior provides further evidence of the high seismic vulnerability of the upper part of the structure. In particular, the results obtained for the two earthquakes prove the N-E/S-W direction to be the most sensitive to the seismic action.

Figure 4.27 Time-frequency analysis of the time-histories recorded on 21/06/2013 on top of the tower: (a) N-W/S-E direction; (b) N-E/S-W direction

4.6.2 Global modes

Correlation with temperature

Consistently with the results of the first AVT (31/07/2012-02/08/2012), the inspection of Figure 4.23 and Figure 4.24 suggests that the natural frequencies of the identified global modes (B_1-B_3 and T_1, Figure 4.19) vary accordingly with the outdoor temperature.

Following the same approach applied to investigate the results of the first dynamic survey, the natural frequencies of the global modes have been plotted versus the outdoor temperature in Figure 4.28, along with the best fit line and the coefficient of determination R^2. The plots in Figure 4.28 refer to the period from 17/12/2012 to 20/06/2013 and reveal that the natural frequencies almost linearly increase with increased temperature, exhibiting high values of R^2 for modes B_1, B_2 (Figure 4.28a-b) and T_1 (Figure 4.28d). The frequency-temperature correlation appears weaker for mode B_3 (Figure 4.28c), as R^2 assumes a lower value (0.36) in comparison with the other modes.

Nevertheless, Figure 4.28 confirms the behavior already observed in the first dynamic survey for the first four modes: the natural frequency of the global modes tends to increase with increased temperature as a consequence of the thermal expansion of the materials. This behavior, inducing the closing of the minor gaps and cracks of the masonry, leads to a transitory "compacting" and therefore to a temporary increasing of modal stiffness and frequency.

The results of the time-frequency analysis reveal that the Garfagnana earthquake of 21/06/2013 produced significant effects on the structural behavior of the tower. Therefore, further checks were performed to investigate such effects. Firstly, the time evolution of the natural frequencies was checked in the neighborhood of the seismic event. Zooming in the time evolution of the natural frequencies of modes B_1, B_2, and T_1 − including data collected in the 3 weeks

142
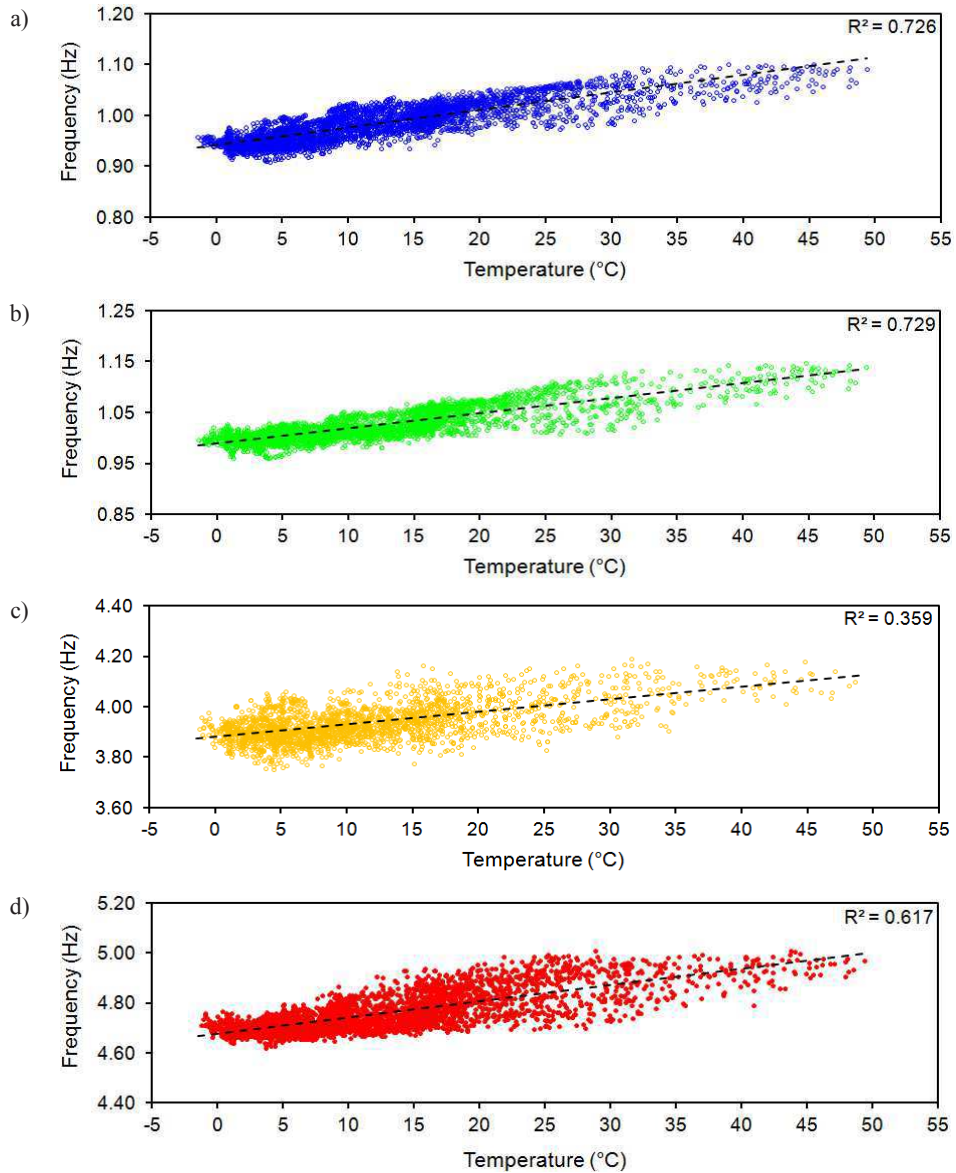
Figure 4.28 Variation of identified natural frequencies (global modes) vs. temperature between 17/12/2012 and 20/06/2013: a) mode B_1; b) mode B_2; c) mode B_3; d) mode T_1

before and after the earthquake − is shown in Figure 4.29 and highlights a clear drop of the modal frequencies corresponding to the occurrence earthquake.
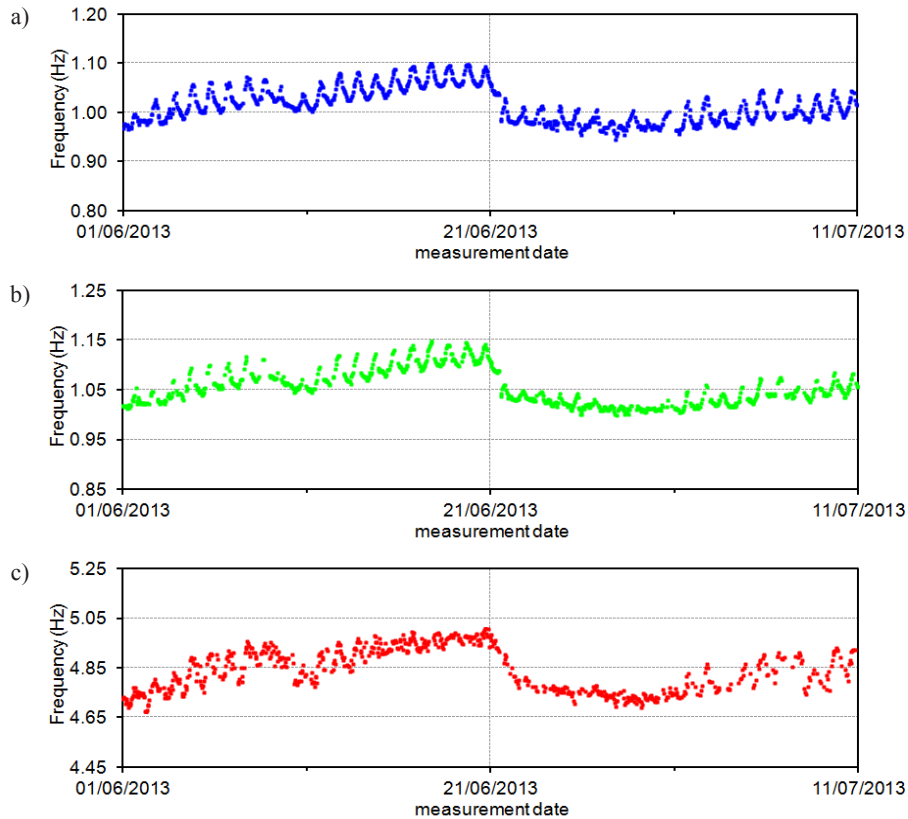
Figure 4.29 Variation of natural frequency between 01/06/2013 and 10/07/2013: (a) mode B_1; (b) mode B_2; (c) mode T_1

The frequency shift is also made clear by comparing the modal peaks (first SV line) of the data recorded in the hour before and after the seismic event: as reported in Figure 4.30, the modal peaks of the two lower modes identified after the earthquake (between 13:00 and 14:00) are characterized by a lower frequency than those detected before (between 11:00 and 12:00). Had this variation been related to temperature effects, the natural frequencies identified after the seismic episode should have been higher than the previous one, in accordance with the frequency-temperature plots presented in Figure 4.28. Therefore, the observed decrease can only be referred to the effects produced by the earthquake occurred on June 21st, 2013 between 12:00 and 13:00.
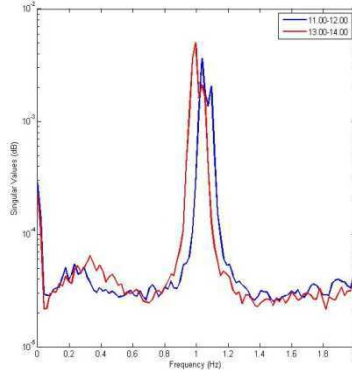
Figure 4.30 Comparison between the modal peaks of modes B_1 and B_2 identified before and after the earthquake of 21/06/2013
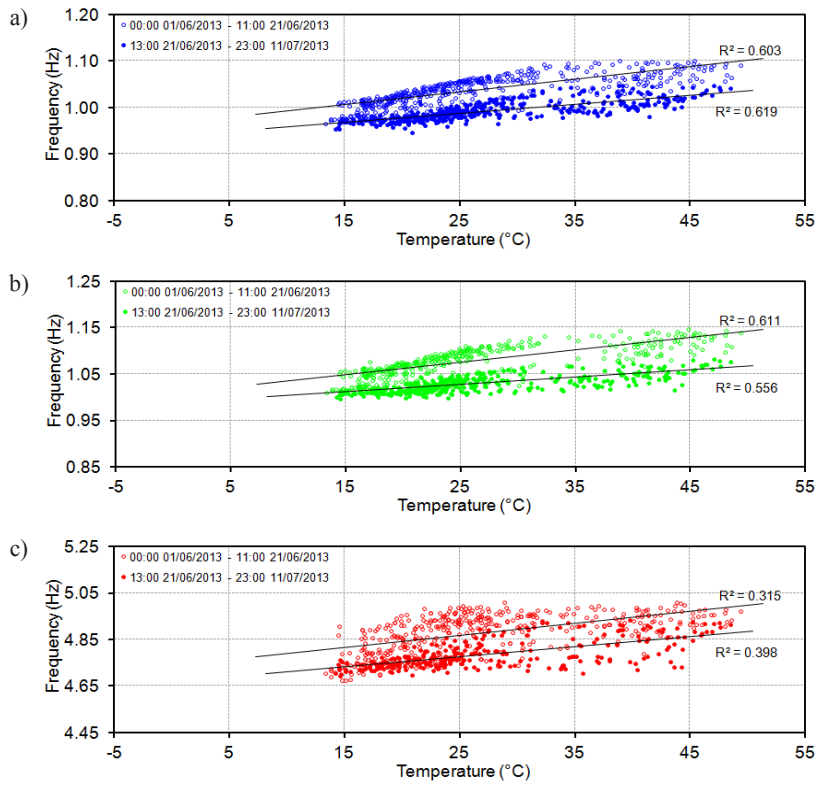
Figure 4.31 Change in the frequency-temperature correlation induced by the seismic event of 21/06/2013: (a) mode B_1; (b) mode B_2; (c) mode T_1

The short-term effects of the seismic event can be further assessed by examining the frequency-temperature correlation in the neighborhood of the earthquake occurrence. The correlation diagrams were evaluated, as in Figure 4.28, by considering just the data collected during the 3 weeks before and after the earthquake. The results obtained for modes B_1, B_2 and T_1 are summarized in Figure 4.31, where best fit lines have been added as a visualization aid: the regression lines exhibit a remarkable variation after the seismic event, with the temperature range being almost unchanged.
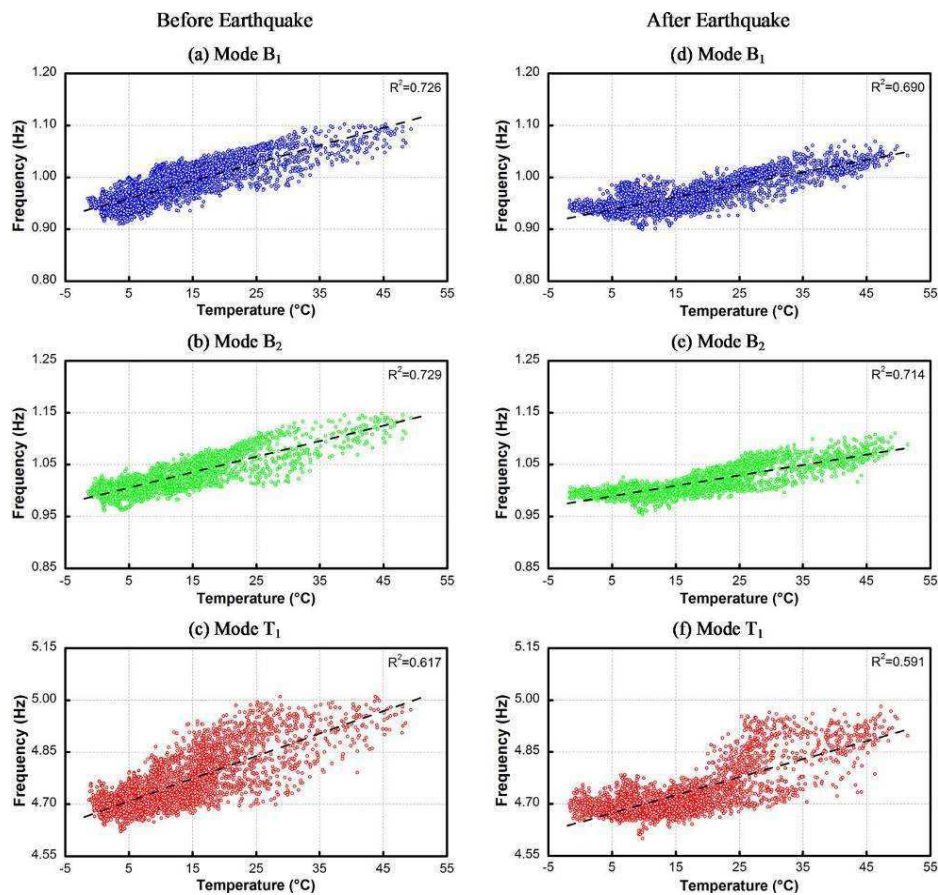
Figure 4.32 Natural frequency of modes B_1, B_2 and T_1 plotted vs. temperature: (a)-(c) from 17/12/2012 to 20/06/2013; (d)-(f) from 21/06/2013 to 17/03/2014

146

The same analysis can be extended to longer time intervals. For example, Figure 4.32 shows the temperature-frequency populations relative to modes B_1, B_2 and T_1 and the regression lines in the two periods: (a) from 17/12/2012 to 20/06/2013 (before earthquake, Figure 4.32a-c); (b) from 21/06/2013 to 17/03/2014 (after earthquake, Figure 4.32d-f). It should be noticed that the two selected time intervals are characterized by the same temperature range and a similar number of collected datasets (i.e., similar population of temperature-frequency points).

The frequency-temperature relationships obtained after the Garfagnana earthquake (21/06/2013) are shown in Figure 4.32d-f. The comparison with the results referred to the first six months of monitoring (Figure 4.32a-c) reveals significant differences: the "clouds" of temperature-frequency points are shifted downward after the earthquake and, consequently, the regression lines of all modes exhibit remarkable variations, with the temperature range being almost unchanged. This trend is also confirmed by the general decrease of the statistics of the natural frequencies (mean value, standard deviation, extreme values) summarized in Table 4-4 and, again, suggests the occurrence of an abnormal and permanent structural change.

Table 4-4 Statistics of the natural frequencies identified before (from 17/12/2012 to 20/06/2013) and after (from 21/06/2013 to 17/03/2014) the seismic event of 21/06/2012

Mode	f_{ave} (Hz)		σ_f (Hz)		f_{min} (Hz)		f_{max} (Hz)	
	Before	*After*	*Before*	*After*	*Before*	*After*	*Before*	*After*
B1	0.985	0.968	0.038	0.031	0.910	0.897	1.102	1.070
B2	1.024	1.012	0.032	0.025	0.961	0.953	1.148	1.110
B3	3.941	3.929	0.075	0.063	3.758	3.742	4.194	4.137
T1	4.754	4.727	0.077	0.066	4.621	4.600	5.010	4.982
L1	9.222	8.937	0.554	0.433	8.385	8.332	10.327	9.862

B = bending mode; T = torsion mode; L = local mode

It is important to remark that the time-frequency analysis (Figure 4.27), the inspection of the frequency tracking (Figure 4.29), the correlation between natural frequencies and temperature both in the short- (Figure 4.31) and in the long-term (Figure 4.32) clearly indicate that the seismic event of 21/06/2013 induced a non-reversible modification of the structural behavior of the *Gabbia* tower. The results provide a clear evidence of the possible key role of simple monitoring systems and state-of-art tools for automated OMA in the preventive conservation of historic towers.

It is marginally noted that few results have been presented on mode B_3. Indeed, the modal identification process for this mode revealed some unexpected issues: by observing the SV plot of the recorded data, it is possible to detect the presence of spurious harmonics close to the investigated natural frequency. The impossibility of eliminating such perturbing elements, conceivably produced by some active machineries present in the building, undermines the quality of the frequency estimates of the third bending mode. Therefore, since the obtained results are not as reliable as those related to the other modes, the decision has been made not to consider mode B_3 in the SHM of the *Gabbia* tower.

4.6.3 *Local mode*

The time evolution of the natural frequency of mode L_1 is presented in Figure 4.33. As previously pointed out, the behavior of the local mode looks very different than the one exhibited by the global modes. The natural frequency is characterized by significant fluctuations over the considered 30 months, with a range of variation spanning between 10.33 Hz and 8.14 Hz. The inspection of Figure 4.33 shows that the identified frequency clearly decreases with increased temperature (as the maximum and minimum values of the natural frequency are attained in the cold and in the hot seasons, respectively). Actually, plotting the

148
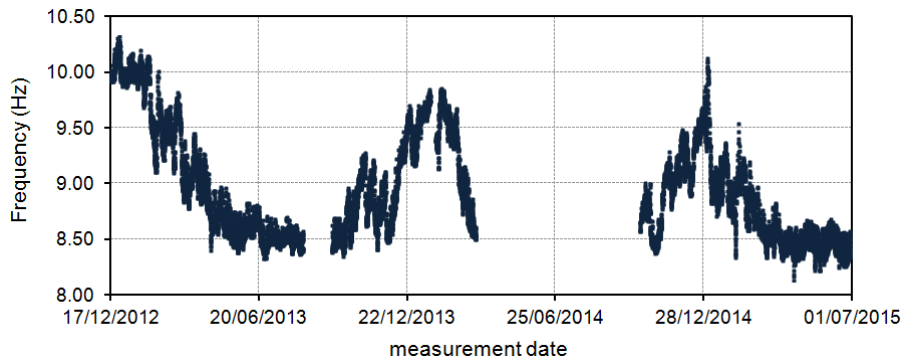
Figure 4.33 Time evolution of the natural frequency of mode L_1 between 17/12/2012 and 30/06/2015
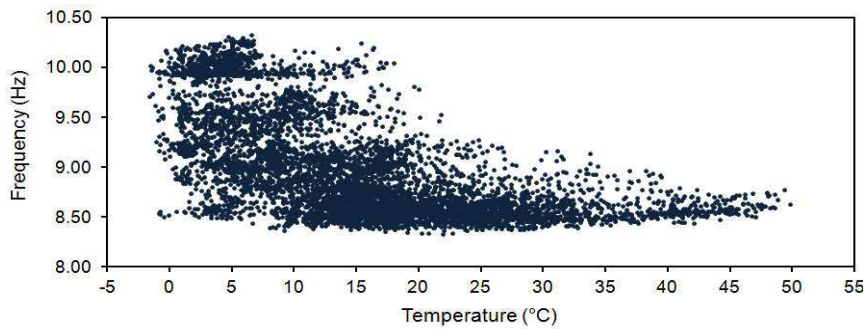
Figure 4.34 Natural frequency of mode L_1 vs. outdoor temperature (between 17/12/2012 and 30/06/2015)

frequency vs. temperature in the whole investigated period (Figure 4.34), it is possible to detect a more cluttered dependence than what at first hinted by the frequency evolution. As it can be observed, the diagram in Figure 4.34 does not reveal any clear correlation between the two considered quantities, as the frequency-temperature points look very dispersed and with no particular trend.

A better understanding of the local mode's behavior can be achieved by exploring the time evolution of the modal frequency. In particular, the first 15 months of monitoring (Figure 4.35). have been considered to exemplify. A close inspection of Figure 4.35 allows to define three time windows, depending on the tendency exhibited by the natural frequency.

149
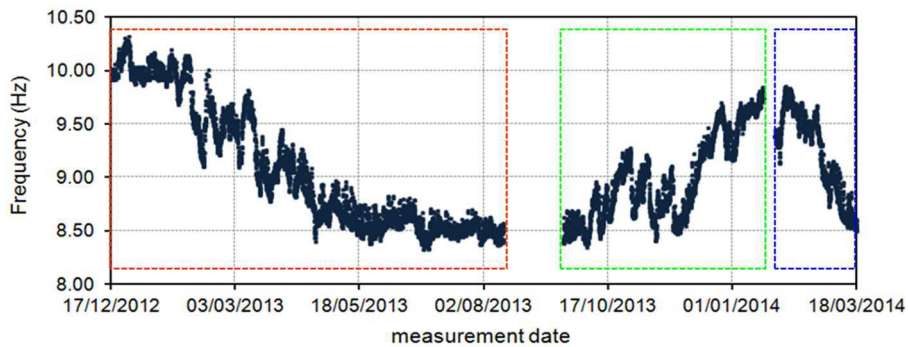
Figure 4.35 Separation of the time evolution of the natural frequency of mode L_1 into different time windows (17/12/2012 – 17/03/2015)

In a first phase (between 17/12/2012 and 13/08/2013) the frequency clearly decreases in time, from an initial value of about 10.0 Hz to a final value of about 8.3 Hz; after the Summer period (from 19/09/2013 to 19/01/2014) the natural frequency increases again, even if the new maximum values do not reach those identified one year before in similar temperature conditions; a further descending phase is observed from 02/02/2014 to 17/03/2014.

More in details, each of the mentioned three intervals is characterized by the presence of some discontinuities (drops or increases), which define the general trend of the frequency tracking:

1. before September 2013, 3 clear drops can be detected between: (a) 03/02/2013 and 04/02/2013; (b) 14/03/2013 and 15/03/2013 and (c) 13/04/2013 and 15/04/2013. These three discontinuities divide the considered time interval in four parts, that can be recognized in the corresponding frequency-temperature plot (Figure 4.36). Best fit lines are reported along with the four groups of frequency-temperature points, indicated by different colors. As it can be observed, the slope of the regression lines does not vary significantly among the four populations of temperature-frequency points, whereas the modal frequency progressively decreases from about 10.3 Hz to around 8.3 Hz, as both the average daily
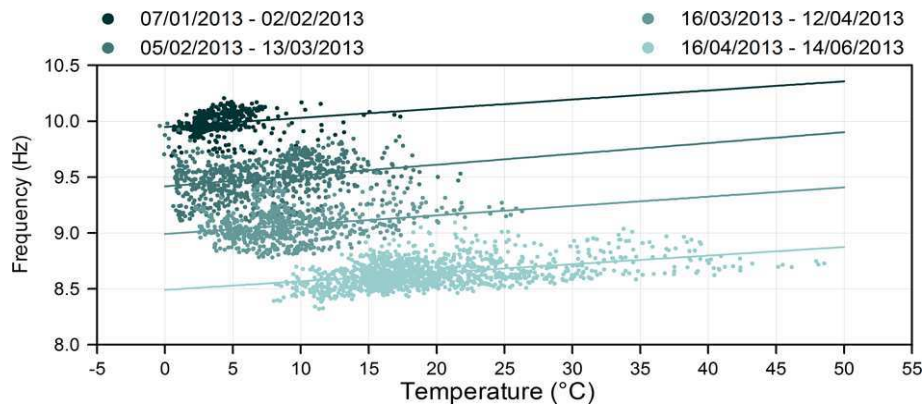
Figure 4.36 Natural frequency of mode L_1 vs. outdoor temperature: first phase
(07/01/2013 - 14/06/2013)

2. temperature and the daily temperature range increase. A possible explanation of such behavior can be related to the effects of the wooden roof, directly supported by the weakest part of the tower. As previously described, the roof is slightly inclined along the N-W/S-E direction and redundantly connected to the surrounding walls. The thermal expansion of the roof covering induces an increased thrust on the structural elements of the upper levels: as the thrust increases, a worsening of the connection between the masonry portions of the most heterogeneous region of the structure is induced, so that the progressive development of damage mechanisms has to be expected;

3. in the second phase, detected between September 2013 and January 2014, one main discontinuity is observed between 05/12/2013 and 06/12/2013. In this time period, the natural frequency increases at each step and follows backwards the course charted during the previous phase. Therefore, two groups of points are detected in the corresponding frequency-temperature plot (Figure 4.37). As for the previous time interval, the two best fit lines exhibit an almost identical slope, whereas the frequency increases with a decreasing average daily temperature.

151
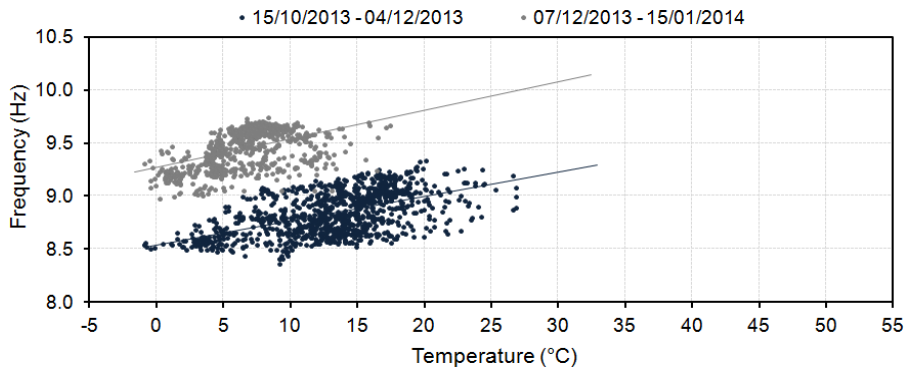
Figure 4.37 Natural frequency of mode L_1 vs. outdoor temperature: second phase (15/10/2013 - 15/01/2014)
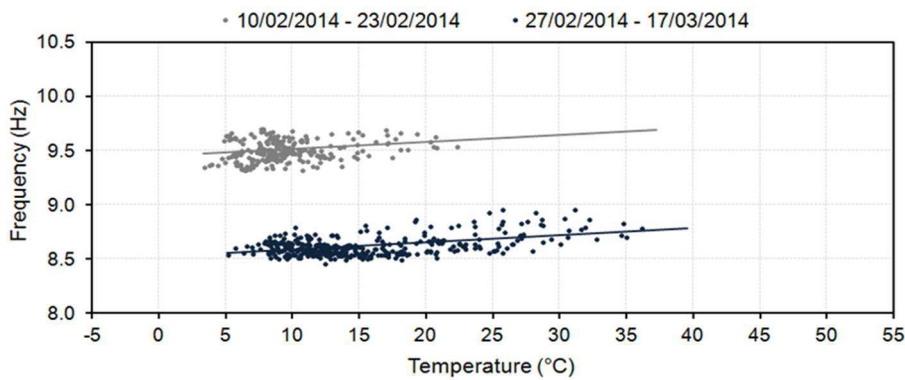
Figure 4.38 Natural frequency of mode L_1 vs. outdoor temperature: third phase (10/02/2014 - 23/03/2014)

From the comparison between Figure 4.36 and Figure 4.37, it can be observed that the maximum values identified in January 2014 do not reach the frequencies identified in the previous year, even if the temperature range is almost unchanged. The detection of such frequency loss is consistent with the assumption of a progressive damage mechanism involving the top levels of the *Gabbia* tower;

4. also for the third time window, a single frequency drop is detected between 24/02/2014 and 26/03/2014. In this case the trend looks similar to the one observed in the first phase: the frequency decreases for an increase

temperature and the frequency-temperature clouds are characterized by a similar slope (Figure 4.38). The comparison between the three plots reported in Figure 4.36-Figure 4.38 shows that the slope of the best fit lines is similar for increasing temperature / decreasing frequency (i.e., first and third time windows, Figure 4.36 and Figure 4.38), but varies when the selected time period is characterized by decreasing temperature / increasing frequency (i.e., second time window, Figure 4.37).

The obtained results allowed to reveal the active role played by the wooden roof and the possible presence of a progressive damage mechanism, conceivably triggered by the thrust exerted by the covering on the surrounding walls. Such assumption seems to be confirmed by the frequency loss of the local mode detected after one year of monitoring, with the natural frequency unable to reach the maximum values identified one year before with almost unchanged temperature range. This provides further evidence of the poor structural condition and the high vulnerability of the upper part of the tower, highlighting the urgent need for preservation actions.

4.7   Temperature and damage effects

The OMA described in the previous sections revealed the presence of one dataset (21/06/2013, 12:00-13:00) from which the occurrence of small damage could be identified. As a natural consequence, it was decided to take advantage of the availability of such records to verify the level of accuracy of SHM procedures aimed at detecting the presence of damage, after removing/minimizing the effects of environmental factors on the natural frequencies.

In Chapter 1, large emphasis was given to the need of removing the effects of environmental factors on natural frequencies, in order to obtain features insensitive to anything different than structural changes that can be used as indicators of the structural condition.

As described in Chapter 3, in the SHM strategy applied to the case study of the *Gabbia* tower, the influence of temperature on the natural frequencies have been minimized by using two classes of models:

1. *Input-output models*

   Input-output models allow to reproduce the relationship between experimental frequencies and measured temperature. With regards to this category, dynamic linear regression [Hair 1998] and ARX [Ljung 1999] models have been implemented in Matlab and applied. It is worth reminding that, in the present application, the only quantity available as input of the model was the outdoor temperature measured on the S-W front;

2. *Output-only methods*

   These models remove the effects of temperature without the need to measure the considered environmental factor. Within the output-only class, a routine performing the Principal Component Analysis (PCA) of the experimental frequencies has been developed in Matlab and applied.

   Once the environmental effects have been removed or minimized, the

occurrence of possible anomalies has been checked by investigating the time evolution of:

3. the residual errors $\varepsilon_{ik} = f_i(T_k) - f_i^*(T_k)$, i.e. the difference between the identified frequencies $f_i(T_k)$ and the model predictions $f_i^*(T_k)$;

4. the cleaned observations, i.e. the identified frequencies depurated from the temperature effects and computed as:

$$\hat{f}_i(T_k) = \bar{f}_i + \varepsilon_{ik} \qquad\qquad \textbf{(4.1)}$$

where $\bar{f}_i$ is the mean value of the original i-th frequency in the reference period;

as these quantities contain data conceivably not affected by the changing environment.

Furthermore, the possibility of detecting the occurrence of structural anomalies from residual errors has been investigated also by using the T^2-*statistic*, plotted in the corresponding *Shewhart T* control chart.

As already mentioned at the end of section 4.6.2, due to some issues in the identification of mode B_3, it was decided to not considering the frequency of that mode in the following analyses and to only take into account the global modes characterized by higher accuracy of the identified natural frequencies (i.e. modes B_1, B_2 and T_1).

4.7.1 Dynamic regression model

In the static regression models, the value of the natural frequency at instant k was correlated with the outdoor temperature measured at the same time instant. The relationship between simultaneously recorded data does not allow to consider the effect of dynamic processes, such as the heating up/cooling down cycles of the structure. Therefore, the prediction ability of the model is expected to significantly improve when the influence of past temperatures is also taken into account.

Therefore, a dynamic linear regression model (referred to, in the following, as DR model) has been implemented, where the value f_k of the natural frequency at time k is assumed to be affected by the outdoor temperature at the same time k as well as by temperatures recorded at previous time instants (see Chapter 1).

Depending on the number of previous time intervals considered for the selected input, many regression relationships can be fitted to the experimental data. Therefore, the performances of the models have been compared by considering three quality criteria [Ljung 1999, Johnson & Wichern 1992]: the *Loss Function* (LF), the *Aikake's Final Prediction Error* (FPE) and the *coefficient of determination R^2* (see Chapter 3). The adopted criteria provided consistent results and led to the selection of a DR characterized by 14 values of the external temperature: one at the current time and 13 referred to previous hourly time intervals.

Training period: 17/12/2012-16/06/2013

For the calibration of the dynamic regression model, a training period of 6 months has been selected (i.e. between 17/12/2012 and 16/06/2013). This allowed to define the parameters of the model by taking into account only frequency changes due to environmental effects, meanwhile leaving out any structural variation triggered by the earthquake of 21/06/2013.

It should be noted that, even if the training period does not characterize the behavior of the *Gabbia* tower during a whole year, it can still be considered statistically representative of the temperature conditions of the structure. In particular, the selected reference interval takes into account the whole temperature range experienced by the tower, as well as the daily and seasonal fluctuations observed during both cold and warm periods.

The implemented DR model has been validated by comparing experimental and numerical results over the reference period. In particular, Figure 4.39 and

Figure 4.40 show the overlapped time evolutions of identified and predicted natural frequencies for modes B_1, B_2 and T_1. As it can be observed, two 12-day time intervals characterized by cold and warm temperatures have been selected for Figure 4.39 and Figure 4.40, respectively. The inspection of the reported diagrams reveals a generally satisfying accordance between the two trends. In particular, a good agreement is observed when the tower is subjected to high temperatures (Figure 4.40), ranging between 15°C and 48°C within the considered time window.
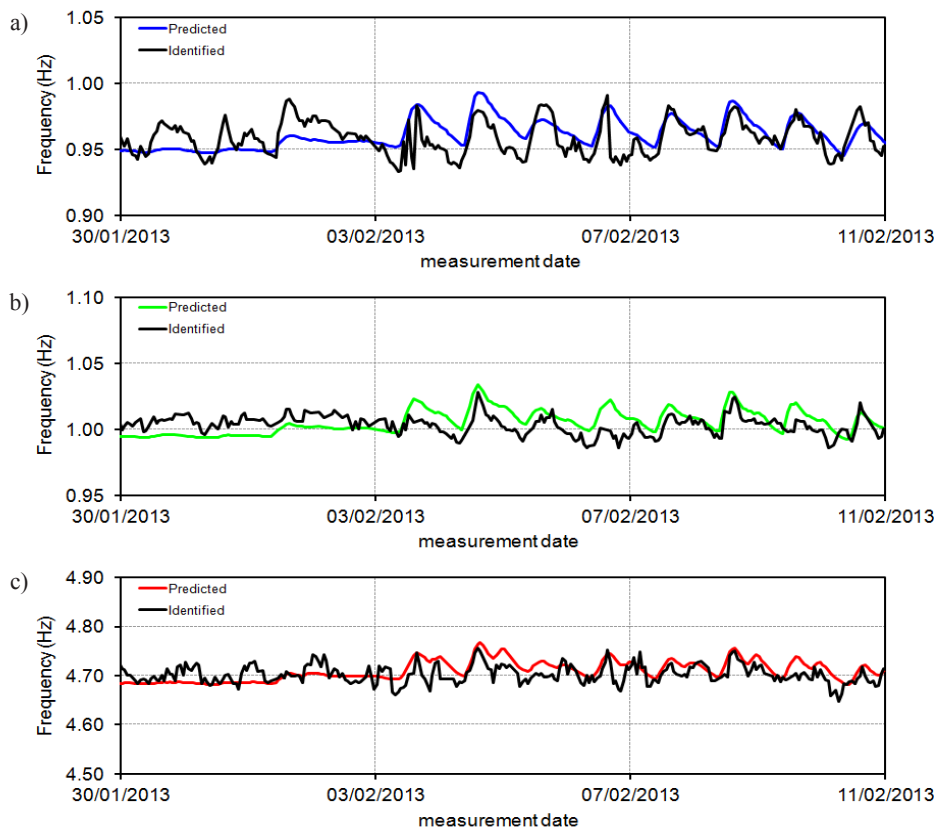
Figure 4.39 Predicted vs. Identified natural frequencies between 30/01/2013-10/02/2013 (DR model): a) Mode B_1; b) Mode B_2; c) Mode T_1

157
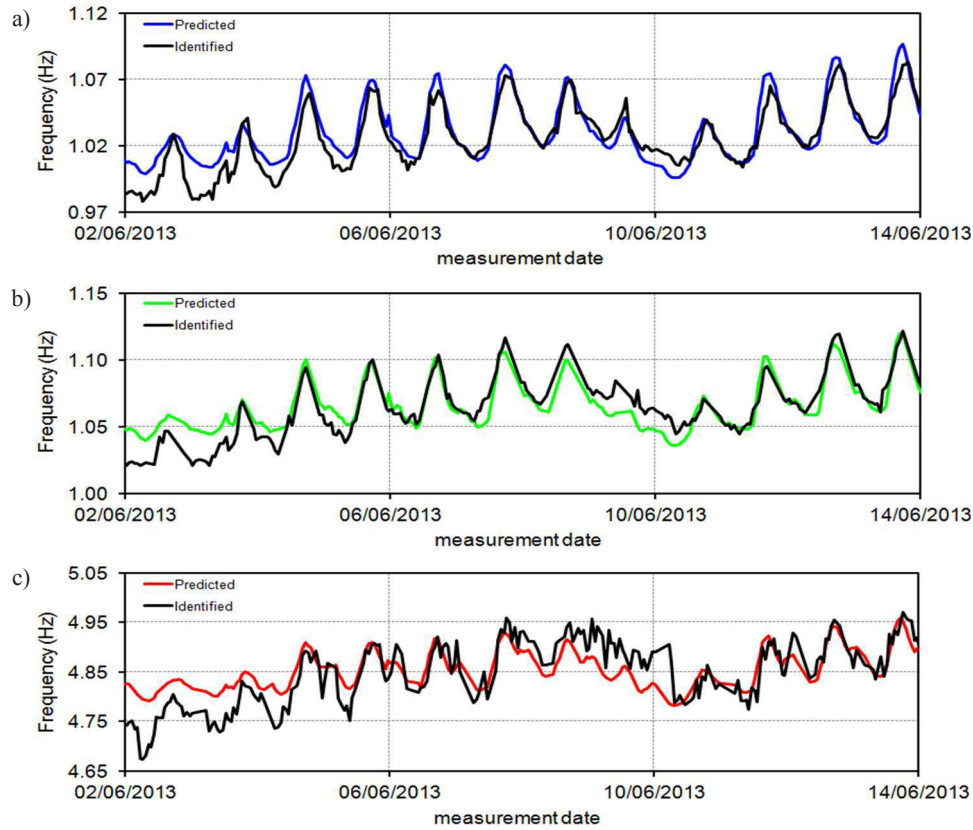
Figure 4.40 Predicted vs. Identified natural frequencies between 02/06/2013-13/06/2013 (DR model): a) Mode B_1; b) Mode B_2; c) Mode T_1

In this case, the predicted frequencies follow with good precision the fluctuations of the experimental estimates: differences in terms of magnitude are generally limited and no delay can be observed between correspondent peaks. On the other hand, the overlapping is less accurate in the considered cold period (Figure 4.39), where the temperature ranges with less significant oscillations between 0° and 20°C. The inspection of Figure 4.39 clearly reveals that the predictions of the DR model only partially reproduce the oscillations of the experimental frequencies.
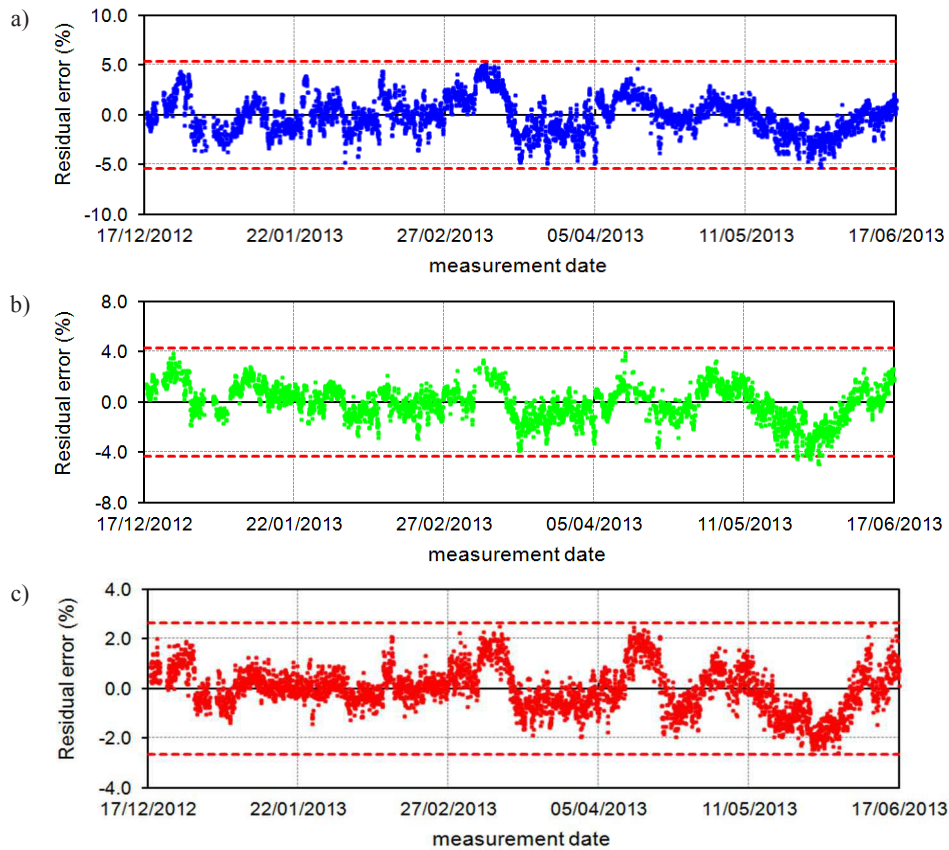
Figure 4.41 Time evolution of the residual error within the training period (DR model): a) Mode B_1; b) Mode B_2; c) Mode T_1

The described results suggest that the influence of temperature on the dynamic behavior of the *Gabbia* tower is not constant over the whole year but changes from cold to warm periods. This, in turn, modifies the skills of the implemented linear dynamic regression model, whose predictions are based on the assumption of linear correlation between input (i.e. outdoor S-W temperature) and output (i.e. frequency).

The evolution, within the training period, of the residual error of the three considered modes is reported in Figure 4.41. It should be noted that the reported values have been normalized with respect to the average natural frequency

computed within the training period. This is the case also for all of the following diagrams presenting the time evolution of the residual error. The red dotted lines define a control interval of ±3σ, where σ indicates the standard deviation of the normalized residuals in the training period. Fluctuations between ±4% are detected for the first two modes (Figure 4.41 a, b), whereas the error ranges between ±2% for mode T_1 (Figure 4.41 c). Even if the range of variation of the residual error (±4%) can still be considered acceptable, the diagrams reported in Figure 4.41 reveal a not negligible dispersion of the values, as well as evident fluctuations. Had the dependence on temperature been completely removed by the DR model, the plotted feature should be characterized by small scattering and very slight variations around the zero line. Therefore, the oscillations exhibited by the residual of all modes suggest that the DR relationship does not entirely model the effects of temperature on the natural frequencies.
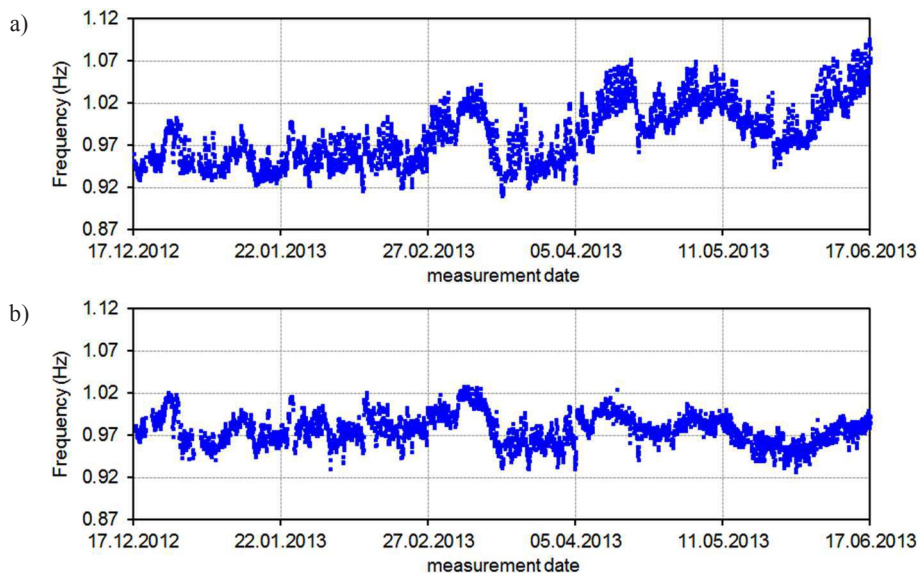
Figure 4.42 Time evolution, during the training period, of the natural frequency of Mode B_1 before (a) and after (b) the removal of the environmental effects (DR model)
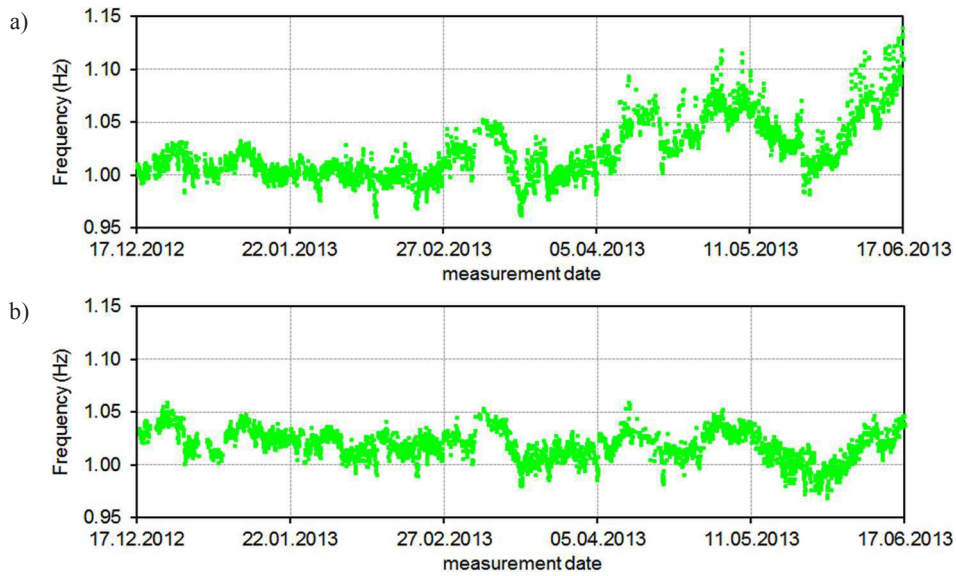
Figure 4.43 Time evolution, during the training period, of the natural frequency of Mode B_2 before (a) and after (b) the removal of the environmental effects (DR model)
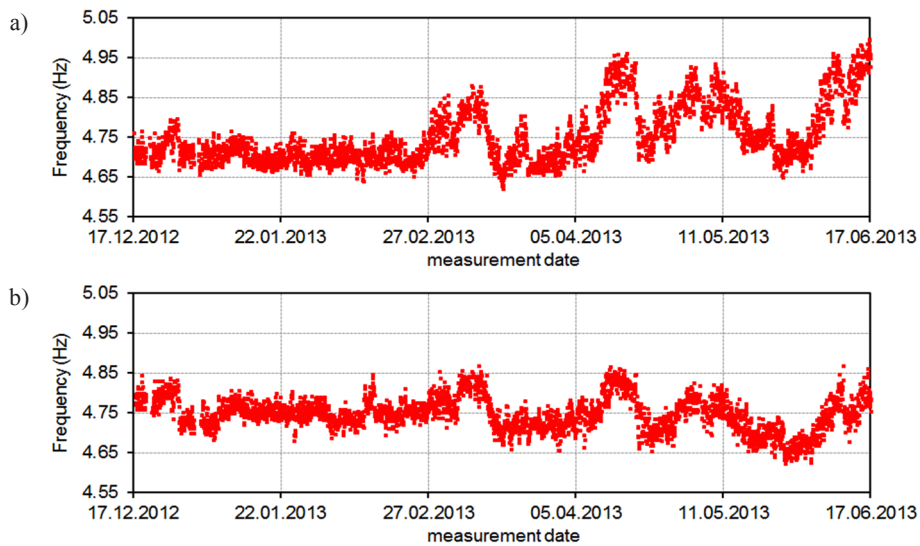
Figure 4.44 Time evolution, during the training period, of the natural frequency of Mode T_1 before (a) and after (b) the removal of the environmental effects (DR model)

The previous consideration is, of course, confirmed by the results obtained in terms of natural frequencies depurated from the environmental effects. In Figure 4.42-Figure 4.44, the time evolution of the experimental estimates before and after the removal of the temperature effects is shown. The inspection of the reported plots reveals that, after the depuration process, the range of variation of the natural frequencies of all modes has been at least halved and the trend looks sensibly straightened. Nevertheless, just like for the residual errors, some non-negligible fluctuations can still be observed.

A possible motivation for such results may conceivably lie in the presence of unobserved factors (e.g. wind, humidity, etc.), not taken into account by the implemented regression models. Furthermore, one should be reminded of the two-fold effect played by the outdoor temperature. Such effect can be observed from the reported time evolution of the experimental estimates (Figure 4.42a-Figure 4.44a): the presence of short-time oscillations highlights the influence of the daily variations of the external temperature on the natural frequencies of the structure. On the other hand, slow fluctuations of the experimental frequencies over long time periods can be detected as well, revealing that also the average temperature plays a significant role.

The application of the DR model, and the resulting mitigation of the temperature effects, allow to achieve a significant reduction of the fluctuations of the frequency tracking (Figure 4.42b-Figure 4.44b). In particular, the decrease is especially relevant for the short term variations. This suggests that the daily effects of temperature can be properly modeled by considering 14 values of temperature (i.e. 1 current value and 13 previous values) as input of the model. Nevertheless, residual fluctuations of the depurated natural frequencies can be detected, revealing that the supposedly environment-free features are still characterized by some residual correlation. Since these fluctuations develop over long time periods, the presence of some remaining

effect of the average temperature (probably combined with the non-modeled influence of unobserved factors) can be assumed.

In order to further investigate the nature of the common factors still affecting the depurated natural frequencies, as well as the reason of the changing performances of the prediction model between colder and warmer periods, the time evolution of temperature has been firstly explored. In Figure 4.45 the tracking of current and average temperature has been reported, referred to the whole monitoring period to allow a more comprehensive understanding of the problem. In particular, average values of temperature have been computed by considering 24, 96 and 168-hour long time intervals (corresponding to one day, four days and one week, respectively).

The inspection of Figure 4.45 allows the following comments:

1. apparently, the change in the frequency-temperature correlation is not triggered by the hourly value of temperature. Indeed, some of the local maxima detected during colder months are comparable to temperature values measured during warmer periods, but a corresponding improvement in the prediction ability of the DR model has not been detected;

2. the time evolution of the average temperatures exhibits a more regular trend: the average daily temperature is still characterized by several short-term fluctuations, whereas the values averaged over 96 and 168 hours show a less uneven trend. In particular, the two average temperatures progressively increase moving from colder to warmer months, revealing a behavior more relatable with the residual fluctuations detected for prediction error and depurated frequencies of the global modes.
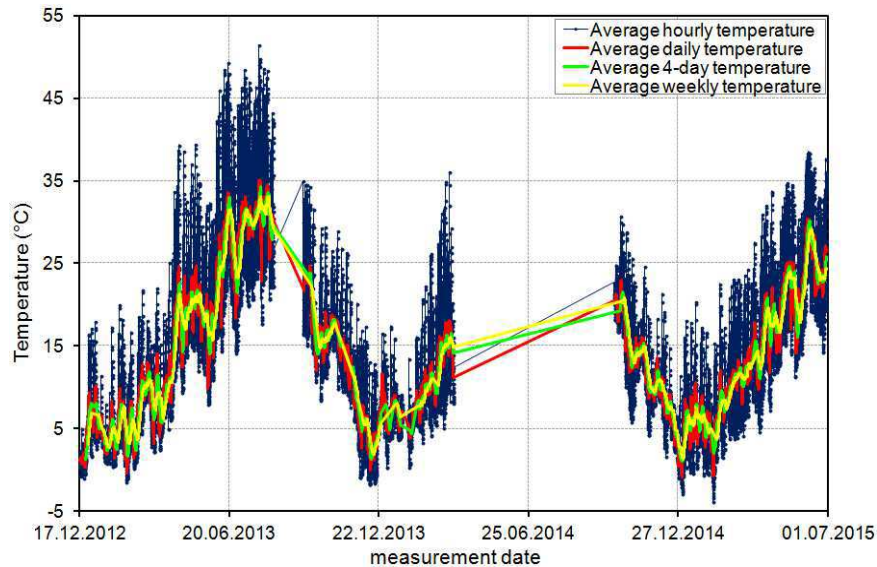
Figure 4.45 Time evolution of current and average temperature over the whole monitoring period

The previous observations suggest the existence of a correlation between natural frequencies and average temperature. To further explore this dependence, the two features have been plotted with respect to each other. The results obtained for the three considered modes are reported in Figure 4.46-Figure 4.48, where temperature values averaged over one day, four days and one week have again been considered. On the base of the presented diagrams, the following considerations can be drawn:

1. the natural frequencies of the three global modes exhibit a certain degree of correlation with the average temperature. Such correlation, still weaker than the one observed for the current temperature (Figure 4.28), appears stronger for the average daily temperature (Figure 4.46-Figure 4.48) and progressively weakens as the average interval increases;

2. the comparison between the diagrams referred to modes B_1, B_2 and T_1 reveals the presence of some common characteristics: moving from shorter to longer average intervals, two distinct groups of points become more

definite; furthermore, for all modes the separation between the two clouds can be detected between 12°C-14°C;

3. the definition of best fit lines for the two clusters allows to detect a variation of the slope from one group to the other. This, in turn, confirms what previously supposed: the correlation between natural frequency and average temperature changes within the investigated monitoring period, according to what could be schematically described as a bi-linear dependence. Furthermore, the difference in the slope of the two best fit lines seems to increase as the average interval gets longer.
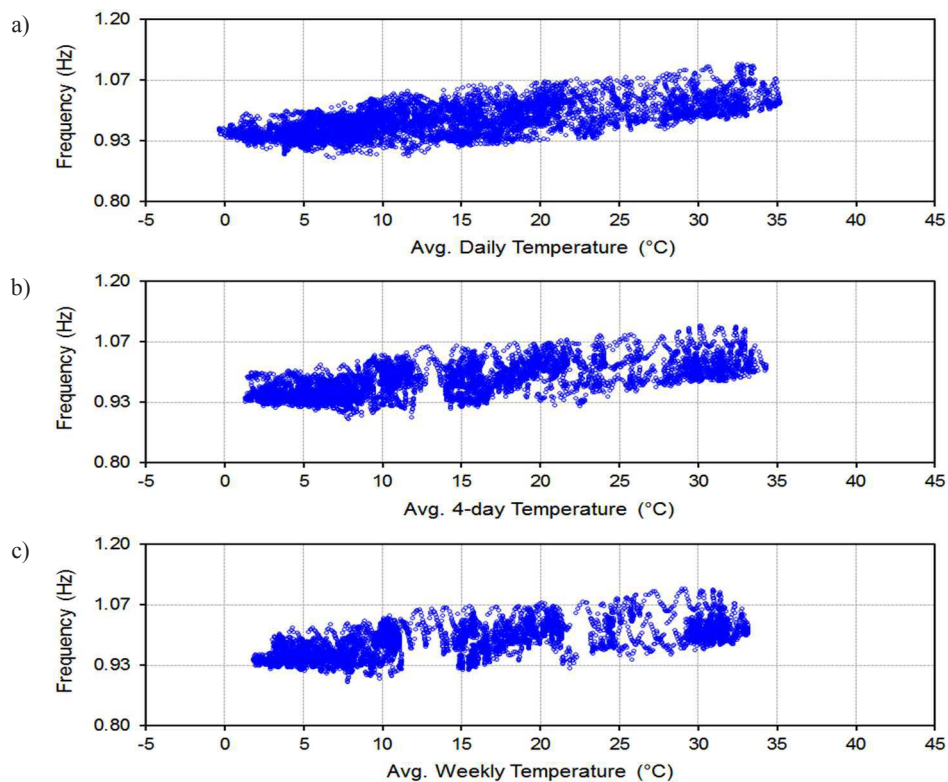
Figure 4.46 Correlation between the natural frequency of mode Mode B_1 and the values of temperature averaged over : a) 1-day; b) 4 days; c) 7-days

The results reported in Figure 4.45-Figure 4.48 provide a reasonable explanation for the residual correlation of the natural frequencies detected after the depuration process. In particular, since the implemented linear DR relationship is based on the assumption of linearity between input and output, the model is more performing in modeling the effects of current temperature, characterized by an almost linear correlation with the frequency (Figure 4.28).
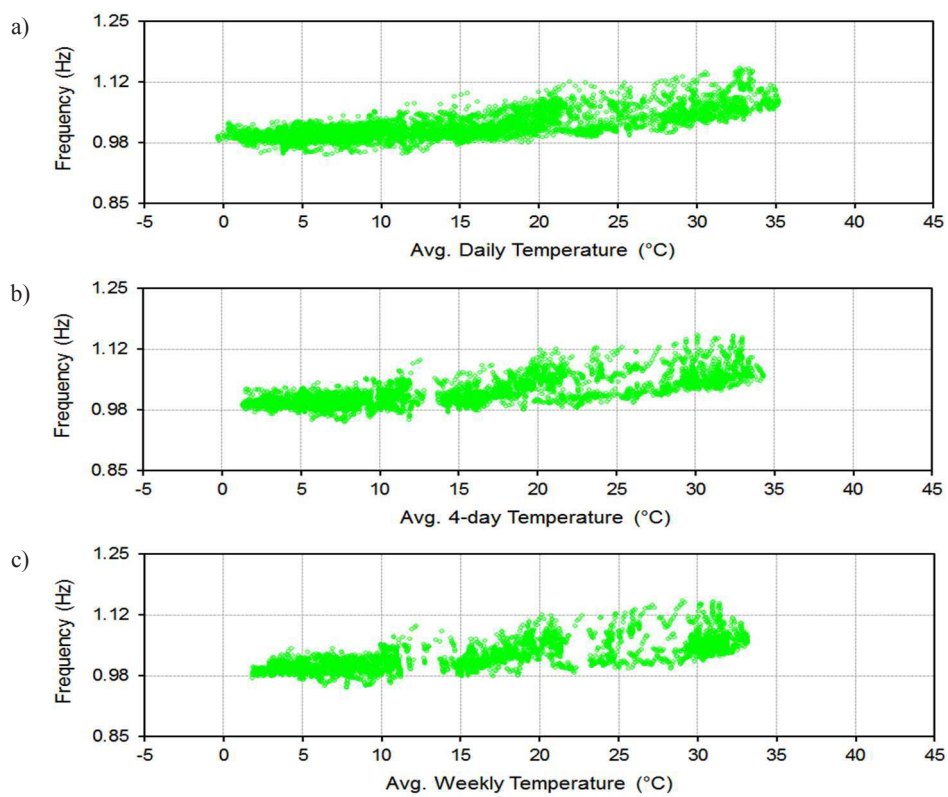
Figure 4.47 Correlation between the natural frequency of mode Mode B_2 and the values of temperature averaged over : a) 1-day; b) 4 days; c) 7-days

166

a)

b)

c)
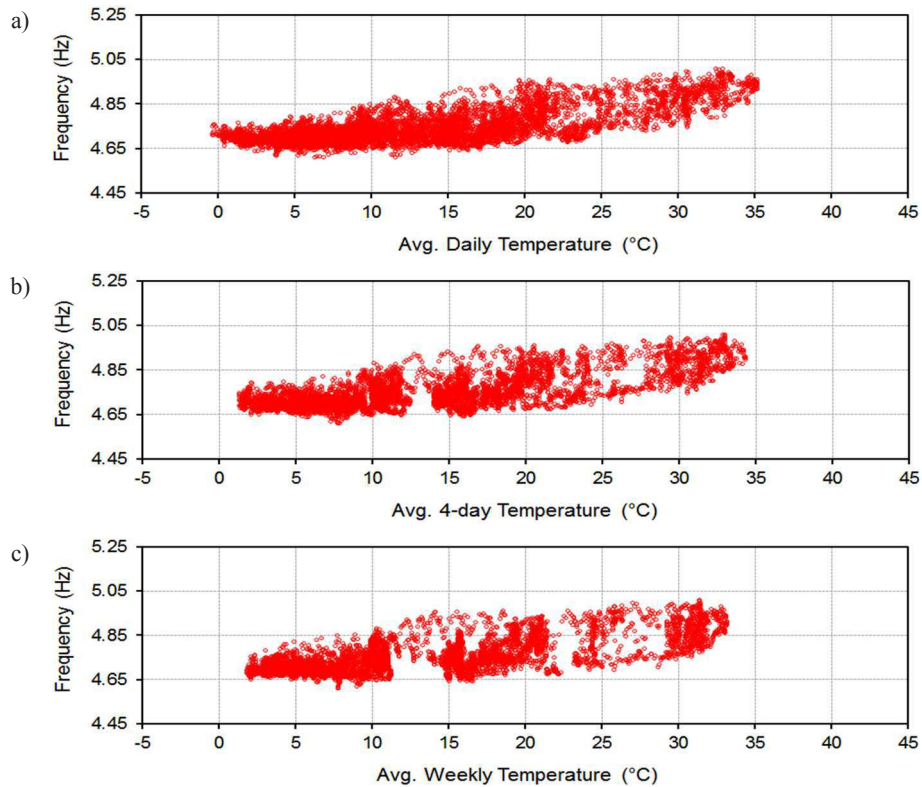
Figure 4.48 Correlation between the natural frequency of mode Mode T_1 and the values of temperature averaged over : a) 1-day; b) 4 days; c) 7-days

This is proved by the achieved significant reduction of the short term fluctuations of all modes. On the other hand, the described non-linear effects of the average temperature can only be partially reproduced by the DR model, leading to residual long term fluctuations of the depurated frequencies. Furthermore, this assumptions would also explain why the prediction skills of the linear dynamic regression model are not constant during the whole monitoring period but improve for warm months, where the correlation between natural frequencies and average temperature is more significant.

With regards to the described slight limitations of the DR model in completely removing the effects of temperature, it is worth reminding that the presented results are obtained by using a single temperature sensor installed on

the outside of the S-W front. The prediction skills of the model, as well as the ability of reproducing both the effects of current and average temperature, are supposed to significantly improve if mote temperature measurements are used as inputs. In the following Chapter 5, proof will be provided in support of the previous statement by presenting the results of the application of the same SHM strategy to a different case study, where the measurements of two temperature sensors (one internal and one external) were available.

The comparison, over the six months of training, between experimental and predicted results provided a satisfactory validation of the dynamic regression model, proved able to predict the experimental frequencies of the tower at study with enough accuracy. As a consequence, the relationships established for the three modes have been subsequently applied to the whole investigated period. The main purpose in this phase was to check whether the dynamic regression model is able to identify the structural anomaly detected on 21/06/2013 and, therefore, if it can be considered as part of a correct SHM methodology.

Entire monitoring period: 17/12/2012-30/06/2015

In Figure 4.49 the residual error of modes B_1, B_2 and T_1 is presented, with respect to the whole monitoring period. The inspection of the reported plots allows the following considerations:

1. in the training period (i.e. from 17/12/2012 to 16/06/2013), the plotted feature oscillates around 0%. Zooming in on the first part of the diagrams (from 17/12/2012 until 13/08/2013, Figure 4.50), it is possible to observe that, during the reference period, the ranges of variation for modes B_1 (Figure 4.50a), B_2 (Figure 4.50b) and T_1 (Figure 4.50c) are approximately equal to ±5%, ±4% and ±2.5%, respectively;
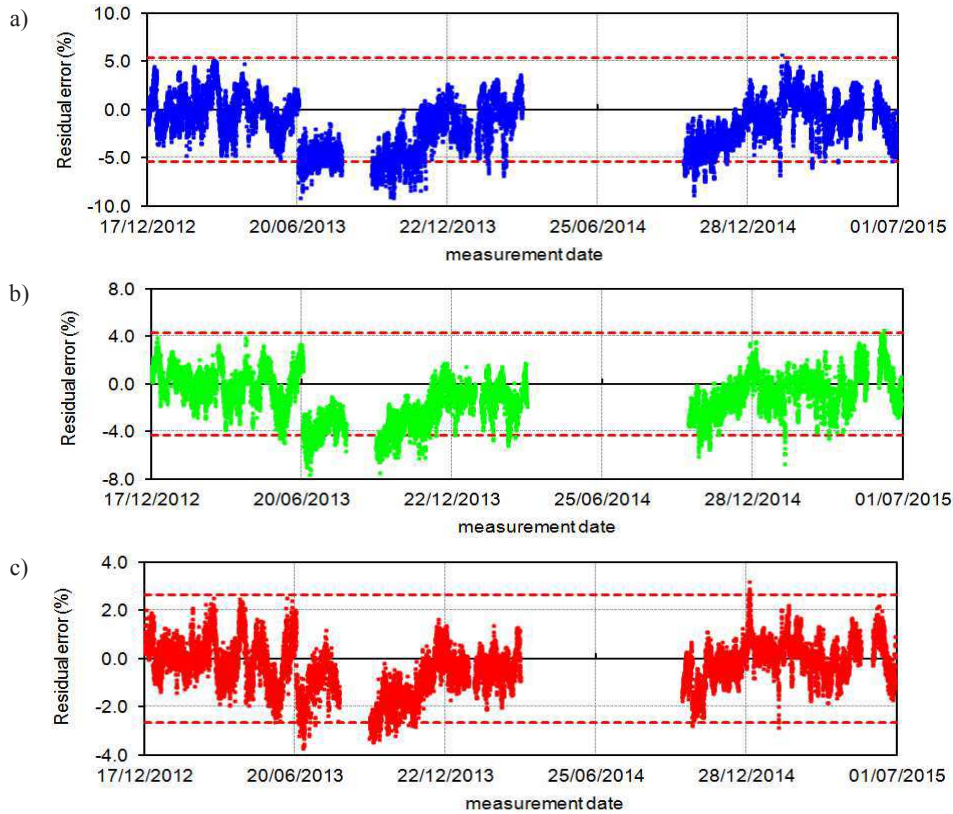
Figure 4.49 Residual errors during the entire monitored time period (DR model): a) Mode B_1; b) Mode B_2; c) Mode T_1

2. corresponding to the seismic event of 21/06/2013, a clear and sudden drop can be detected in the residual error of all modes. Furthermore, the error abruptly departs from the previous trend and starts oscillating in the field of negative values, exhibiting a distinct variation with respect to the training period. The investigation of Figure 4.50 also allows to detect a slight but not negligible increase in the dispersion of the values. Such behavior reveals that the structural change induced by the Garfagnana earthquake can still be detected after the application of a dynamic regression model and the removal of the environmental effects;

3. in the few weeks after the earthquake, until about mid-November 2013, the

169

error neither decreases nor gets back to the previous trend. Instead, it hovers around the new negative offset. This is especially true for the first two bending modes, whereas a slight upward curve is observed for mode T_1. The values of the residual error observed after the earthquake vary between -2.5% ÷ -8% for mode B_1 (Figure 4.50a), -1% ÷ -7% for mode B_2 (Figure 4.50b) and between +1% ÷ -4% for mode T_1 (Figure 4.50c);
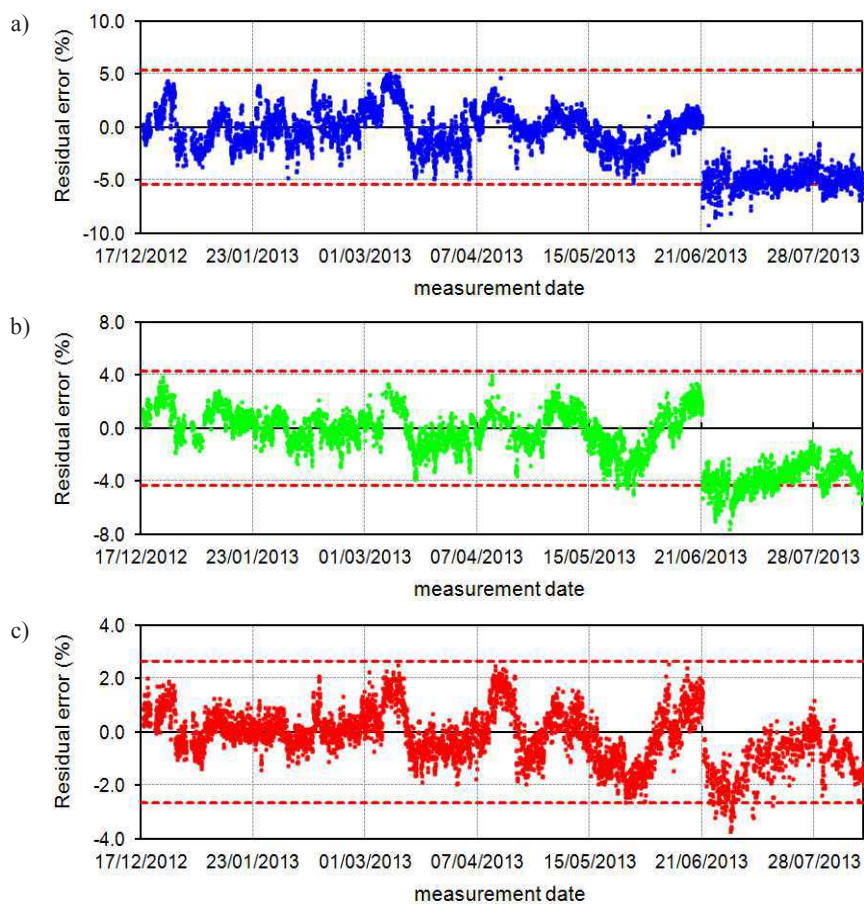
Figure 4.50 Residual error between 17/12/2012 and 13/08/2013 (DR model): a) Mode B_1; b) Mode B_2; c) Mode T_1

170
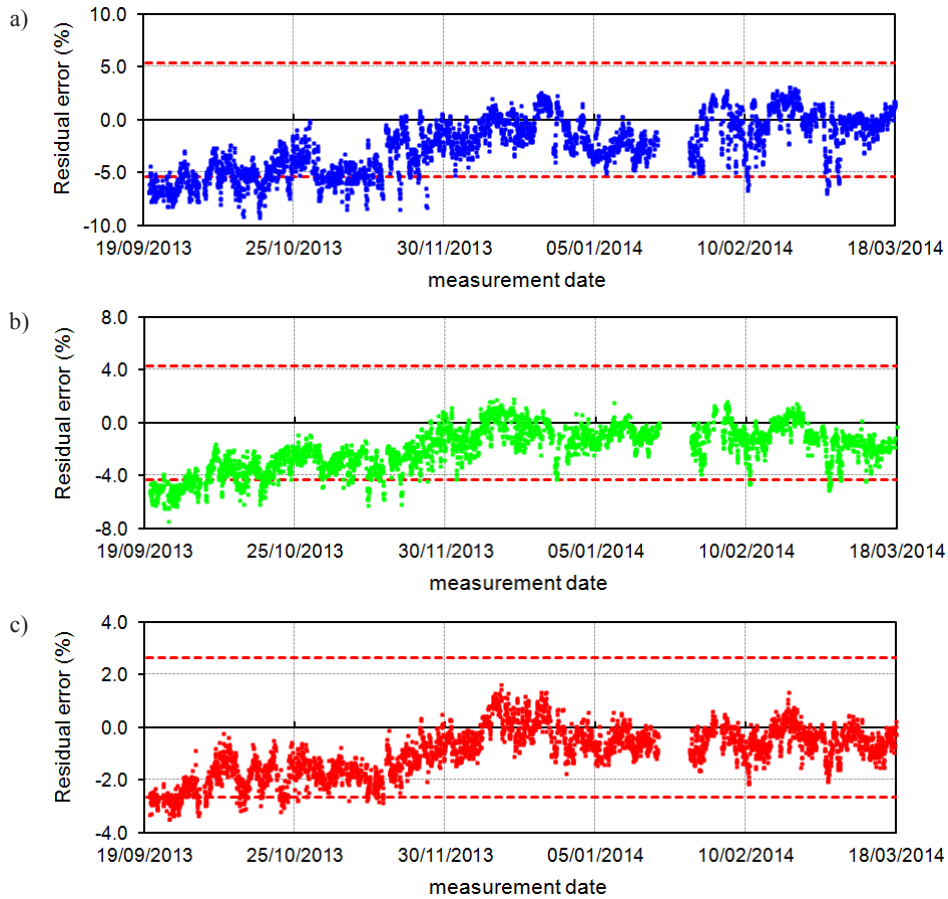
Figure 4.51 Residual error between 19/09/2013 and 17/03/2014 (DR model): a) Mode B_1; b) Mode B_2; c) Mode T_1

4. approaching Winter time, a progressive decrease of the residual error is observed. This behavior can actually be explained by recalling the slightly non-linear correlation between natural frequencies and average temperature described before, that leads to a worsening of the prediction skills of the linear DR model as the average temperature decreases. Notwithstanding the lower prediction ability of the model during cold periods, Figure 4.51 − where the residual has been reported with respect to the interval 19/09/2013-17/03/2014 − shows that some differences in the trend of the residual can

still be observed with respect to the reference period. In particular, after November 2013 the error no longer oscillates around 0%, as for the first six months of monitoring, but maintains a small negative offset;

5. the interruption of the monitoring between March and September 2014 does not allow to observe any increase of the residual error during warmer months, when the performances of the dynamic regression model improve again. Nevertheless, corresponding to the re-start of the monitoring activity (Figure 4.51) in October of the same year, values of the error comparable to the ones obtained in the first weeks after the earthquake are observed, confirming the previous assumptions. Furthermore, the maximum values of the residual error detected in October 2014 are characterized by the same magnitude of those identified right after the seismic event. Hence, no further decreases of the residual errors were detected between 21/06/2013 and 10/10/2014, suggesting that no other irreversible structural anomalies occurred during that period;

6. as for the previous year, when the average temperature decreases, the residual error reduces too. The inspection of Figure 4.52, referred to the time interval between 10/10/2014 and 30/06/2015, allows to detect a slight but not negligible further drop of the prediction error during the decreasing phase. Such discontinuity, identified on 22/10/2014, is observable in all of the three diagrams and particularly significant for modes B_2 (Figure 4.52b) and T_1 (Figure 4.52c). On the first days after the drop, the prediction error hovers around a new larger negative offset and is characterized by a slightly increased scattering. In two weeks' time, on 05/11/2014, the observed prediction error moves back to the previous trend and no residual signs of the suffered decrease can be detected. This behavior suggests that the observed drop is not associated with the occurrence of irreversible structural anomalies. Indeed, the analysis of the recorded response signals and the

weather information collected from a near meteorological station revealed the occurrence of strong winds over the investigated time interval. This confirmed that the detected frequency drop is related to a temporary modification of the tower's response as a consequence of unusual levels of ambient excitation;
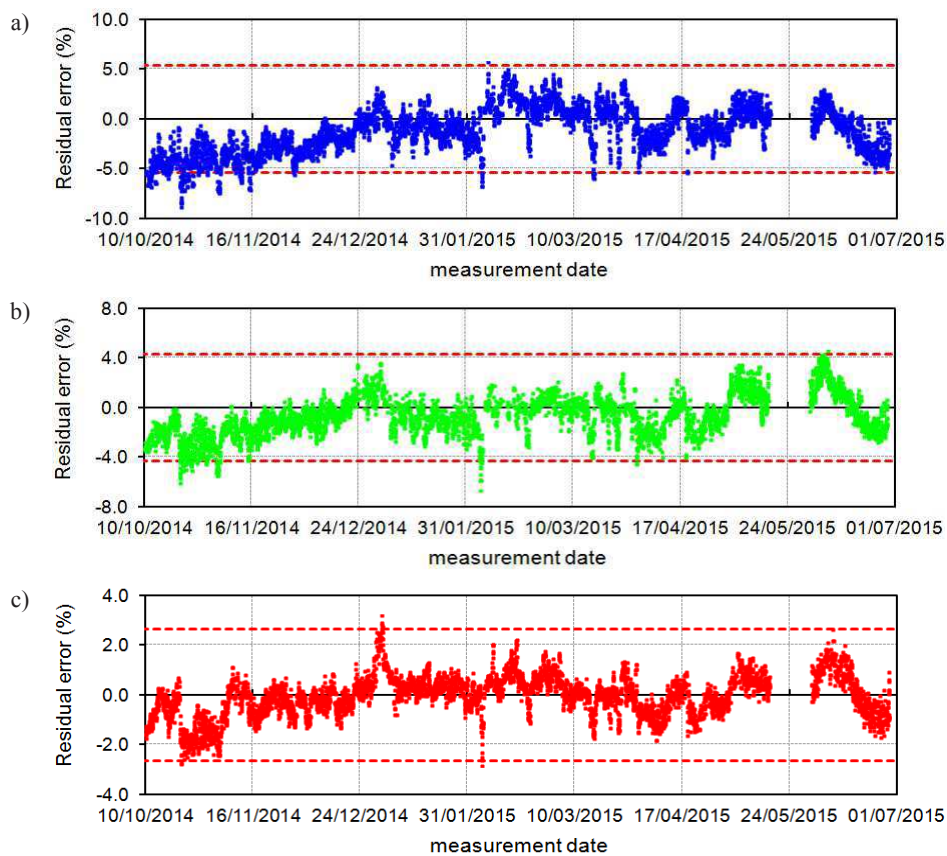
Figure 4.52 Residual error between 10/10/2014 and 30/06/2015 (DR model): a) Mode B1; b) Mode B2; c) Mode T1

7. starting from mid-November 2014, the prediction error begins to hover around a small negative offset. It should be noted that some isolated spikes, referred to time intervals of few days, are detected in Winter 2014/2015. Again, the presence of those anomalous occurrences suggests a temporary

173

variation of the structural response of the tower. As for the previous point, the investigation of the acceleration signals acquired during the corresponding hourly intervals revealed the presence of anomalous wind activity, stronger than the usual level of environmental vibration experienced by the tower.

The inspection of the previous results revealed a very articulated behavior of the *Gabbia* tower, with the residual effects of the average temperature determining significant fluctuations of the prediction error during the investigated 30 months.

Such outcome is consistent with the appearance of the natural frequencies of modes B_1, B_2 and T_1 after the minimization of the temperature effects, reported in Figure 4.53-Figure 4.55. The application of the dynamic regression model allows a significant reduction of the range of variation of the natural frequencies, leading to straightened time evolution diagrams. As observed for the prediction error, the drop related to the occurrence of damage due to the Garfagnana earthquake can be clearly detected for all modes, along with a variation of the trend that shifts towards lower frequency values. This provides further proof of the fact that the frequency loss is not related to the influence of environmental factors, but to the occurrence of structural anomalies.

The inspection of Figure 4.53-Figure 4.55 leads to the following considerations:

1. the time evolution of the experimental frequencies is characterized by large ranges of variation and relevant fluctuations, as a consequence of the effects of temperature (Figure 4.53a-Figure 4.55a);
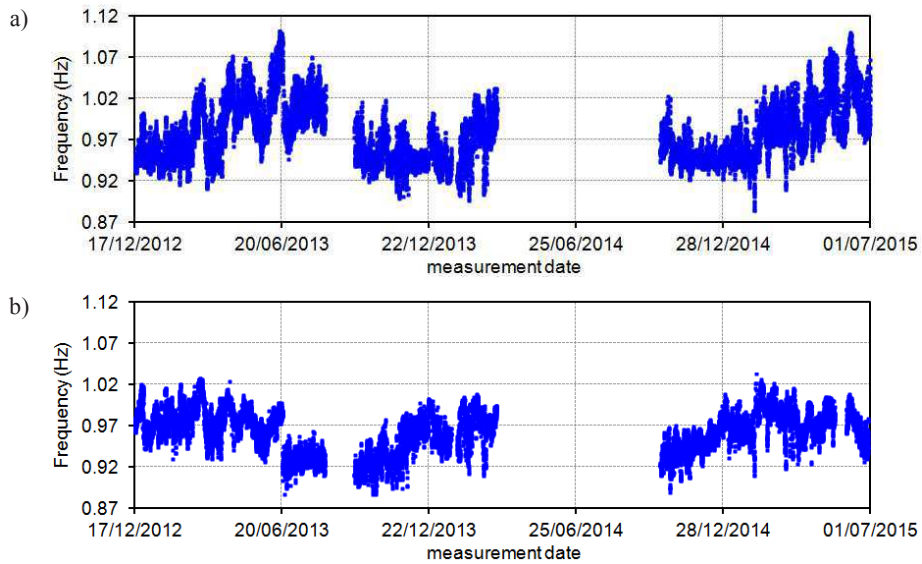
Figure 4.53 Time evolution of the natural frequency of Mode B$_1$: a) before and b) after the removal of the environmental effects (DR model)
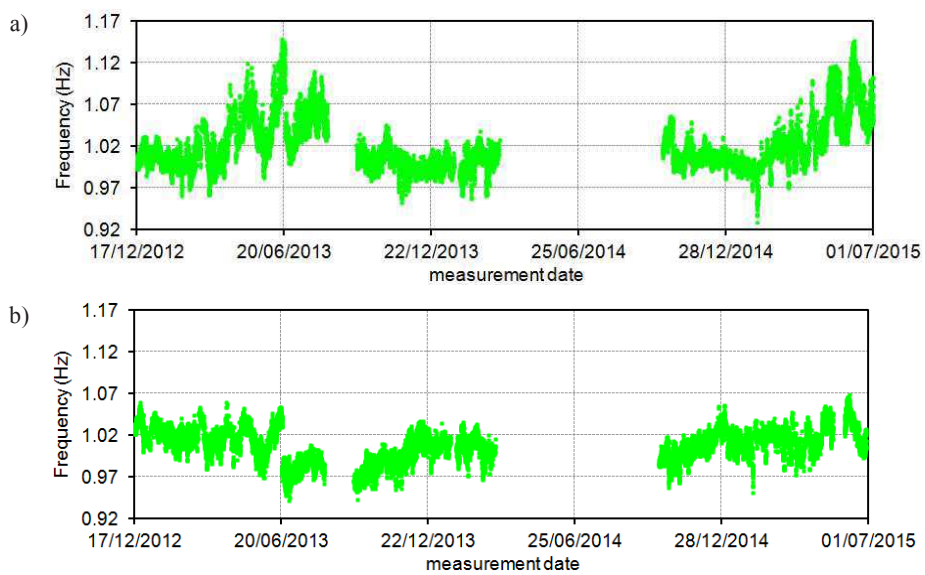

Figure 4.54 Time evolution of the natural frequency of Mode B$_2$: a) before and b) after the removal of the environmental effects (DR model)
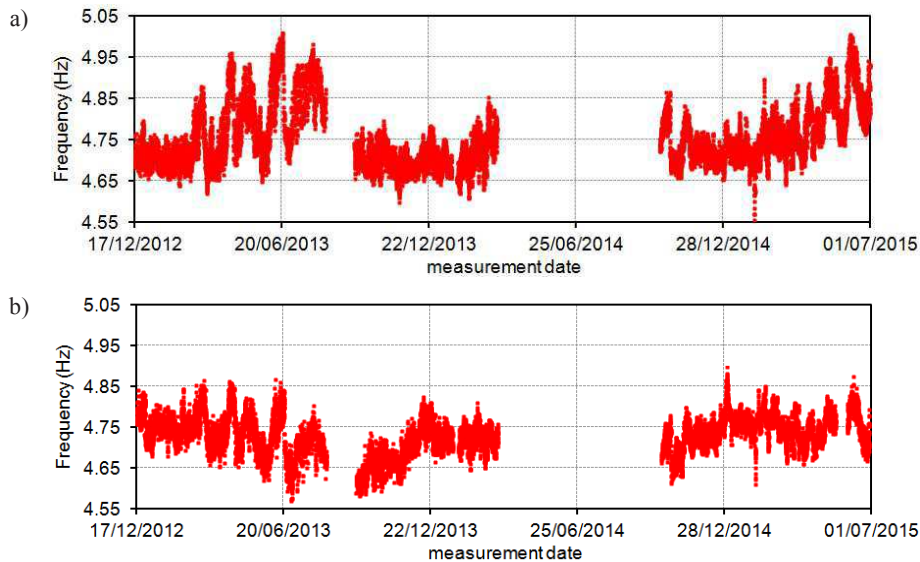
Figure 4.55 Time evolution of the natural frequency of Mode T_1: a) before and b) after the removal of the environmental effects (DR model)

2. after the application the mitigation of the temperature effects, the fluctuations and dispersion of the values are significantly reduced, even if small (but not negligible) residual oscillations around the average frequency can still be observed (Figure 4.53b-Figure 4.55b). This behavior is conceivably related to the influence of unmeasured factors and to the described limitations of the linear DR model in accurately reproducing the non-linear correlation between average temperature and natural frequency;

3. on 21/06/2013, the depurated frequencies exhibit a frequency drop of about 5% for the first two modes (Figure 4.53b and Figure 4.54b) and about 2% for mode T_1 (Figure 4.55b). In the following weeks, the time evolutions hover around the new offsets and reveal a small increase of the scattering with respect to the previous months;

4. as a consequence of the poorer performances of the DR model with low average temperatures, after the Summer period the depurated frequencies gradually slide away from the post-earthquake values and move upward

(Figure 4.53b-Figure 4.55b). Nonetheless, the frequency drop of 21/06/2013 is not entirely recover and the depurated frequencies fluctuate around lower average values. This confirms the presence of irreversible anomalies caused by the seismic event;

5. the lower frequency values identified at the end of Summer 2014 (Figure 4.53b-Figure 4.55b), where the DR model results more performing, are consistent with the corresponding estimates detected in right after the Garfagnana earthquake, confirming that no further irreversible anomalies occurred on the *Gabbia* tower;

6. the decrease on 22/10/2014 and the isolated spikes in Winter 2014/2015 can still be detected from the inspection of (Figure 4.53b-Figure 4.55b). This validates the assumption that those anomalous occurrences are not related to temperature effects, but to unusual levels of ambient excitation.

Control charts

As described in Chapter 3, the occurrence of anomalies not observed during the training period has been also investigated by applying the multivariate *Shewhart T* control chart [Montgomery 1997], where the variation in time of the T^2-*statisti*c feature is represented along with a user-defined Upper Control Limit (UCL), computed from the experimental samples collected during the training period.

In Figure 4.56, the *Shewhart T* control chart referred to the whole monitoring period has been reported, along with the UCL (i.e. the solid horizontal red line). The presented results have been obtained by considering subgroups of data of 12 hours and are consistent with the assumptions previously made for prediction errors and depurated natural frequencies.
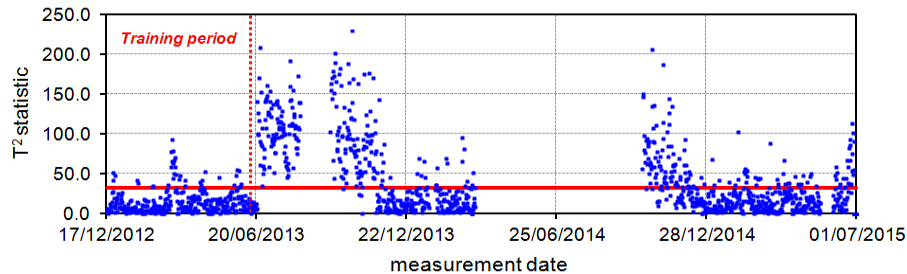
Figure 4.56 *Shewart T control chart obtained by using subgroups of data of 12 hours* (DR model)

Based on the trend exhibited by the T^2-*statistic*, the following comments can be drawn:

1. during the training period (i.e. 17/12/2012-16/06/2013), limited variations of the considered feature are observed and only few outliers exceeds the defined UCL, so that the absence of structural anomalies in the first six months of monitoring is once more confirmed;

2. corresponding to the seismic event of 21/06/2013, the T^2-*statistic* abruptly exceeds the defined control region, with relevant increases of the values and of the dispersion. In particular, the scattering of the reported points almost triples with respect to the training period (Figure 4.57a);

3. during the first following weeks, characterized by high temperatures, the T^2-*statistic* maintains the same large values and highly scattered trend (Figure 4.57a), in agreement with the results presented in terms of prediction error and depurated frequencies;

4. as expected, the values of the statistical feature progressively decrease moving on to Winter 2013/2014 and tend to get closer to the defined UCL (Figure 4.57b). Nonetheless, it should be noticed that the dispersion of the values remains larger than the one characterizing the training period, as confirmed by the detection of a larger number of points lying out of the control region. Therefore, notwithstanding the reduced prediction skills of
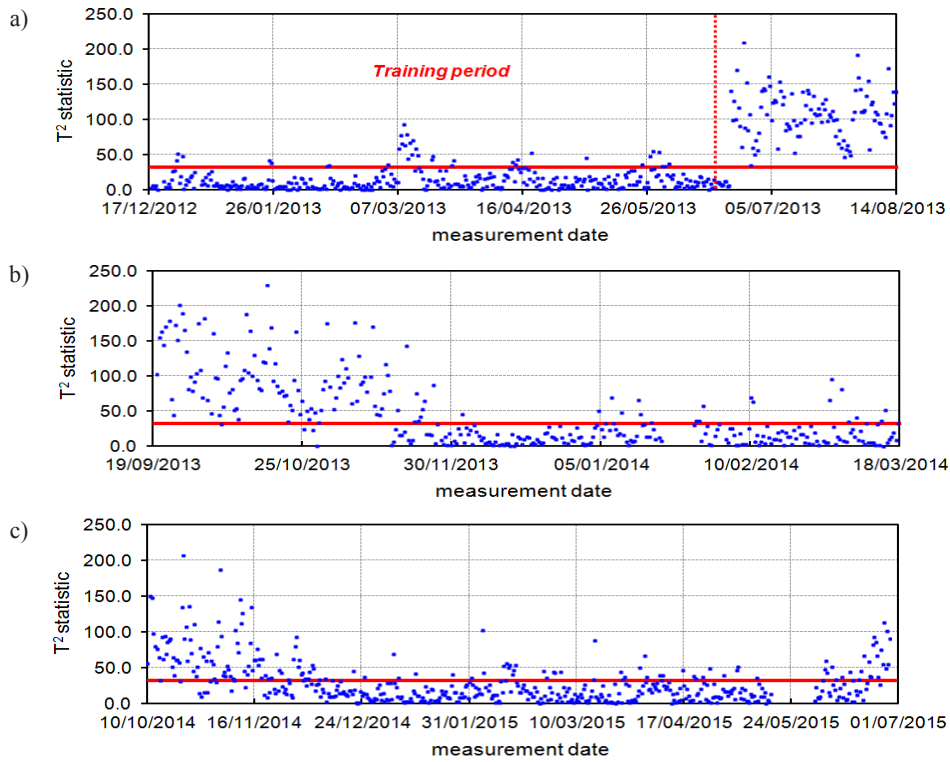
178

Figure 4.57 *Shewart T control chart (DR model) referred to the time intervals: a) 17/12/2012-13/08/2013; b) 19/09/2013-17/03/2014; c) 10/10/2014-30/06/2015*

the DR model during cold months, it is still possible to detect some differences with respect to the trend characterizing the reference period;

5. consistently with the improved performances of the DR model with an increased average temperature, the T^2-*statistics* again exceeds the UCL during the last weeks of Summer 2014, meanwhile exhibiting an increase in the dispersion of the points (Figure 4.57b). Just like the prediction error and the depurated frequencies, the detected values look comparable with those detected in the previous Summer. Therefore, it seems to be confirmed that no further structural changes occurred during the first post-earthquake year;

6. a group of few points characterized by larger values and standing out of the

defined trend can be observed between October and November 2014 (Figure 4.57c). Those occurrences are conceivably related to the temporary increase of the ambient excitation (strong wind) and the frequency decrease detected during the same days. When the level of ambient excitation lowers to usual values, the T^2-*statistic* returns to the previous trend, suggesting the reversibility of the structural changes experienced during this two-weeks' time-interval are not permanent;

7. in Winter 2014/2015, notwithstanding the expected lower values of the statistical feature associated with low average temperatures, a non-negligible number of points exceeds the UCL ((Figure 4.57c), as observed one year before in a similar temperature range. This result is consistent with the absence of new irreversible structural changes after 21/06/2013, all the while confirming the permanent character of the effects of the Garfagnana earthquake. It is worth noting that larger values of the outliers can be observed corresponding to the isolated spikes referred to transitory short periods of stronger ambient vibrations.

Concluding remarks

The application of a linear dynamic regression model to the experimental estimates obtained from the automated OMA process allowed to satisfyingly remove the effects of temperature from the natural frequencies of the *Gabbia* tower. In particular, the results presented in terms of residual errors, depurated natural frequencies and *Shewhart T* control chart reveal that the removal of the temperature effects by means of the linear dynamic regression model allows the clear detection of the structural change induced by the earthquake of 21/06/2013. Furthermore, the trend exhibited by the inspected temperature-independent features proves the damage to be irreversible, consistently with the results obtained in section 4.6.

In the next sub-section 4.7.2, the same methodology has been applied by using an ARX model, in an attempt to improve the quality of the frequency prediction with respect to the dynamic regression model.

4.7.2 *ARX model*

The implemented dynamic regression model, taking into account current and previous values of the input (i.e. external wall temperature), allowed to only partially model the thermal effects on the natural frequencies of the *Gabbia* tower. On one hand, the DR relationship proved effective in reproducing the fluctuations of the experimental frequencies due to the daily effect of temperature. On the other hand, the model could not as accurately predict the long-term oscillations due to the influence of the average temperature (conceivably combined with the effects of other unobserved factors).

In order to improve the prediction, an Auto-Regressive model with eXogenous input (ARX) has been implemented (see Chapter 1). ARX models assume the value f_k of the natural frequency at time k to be affected by outdoor temperatures at the same time k and at previous time instants, as well as by previous experimental estimates of the input. In particular, the use of past values of the output is expected to indirectly take into account the effects of those unmeasured factors that cannot be modeled otherwise (e.g. wind, humidity, etc.), leading in principle to more accurate predictions.

Single-Input Single-Output (SISO) ARX models have been implemented for the *Gabbia* tower, as only one input was available (i.e. the external wall temperature of the S-W front). Since several models can be fitted to the experimental data, depending on the amount of previous time instants considered for the input and the output, a comparative study of the performances has been carried out by using the *LF*, *FPE* and R^2 quality criteria (see Chapter 3). Eventually, a SISO ARX240 model has been selected,

characterized by n_a=2 previous estimates of the experimental frequency, n_b =4 past hourly values of the outdoor temperature and no delay between input and output (n_k=0).

Training period: 17/12/2012-16/06/2013

To calibrate the parameters of the SISO ARX240 model, the same training period defined for the DR relationship has been considered, i.e. between 17/12/2012 and 16/06/2013, in order to leave out the structural variation due to the earthquake of 21/06/2013.
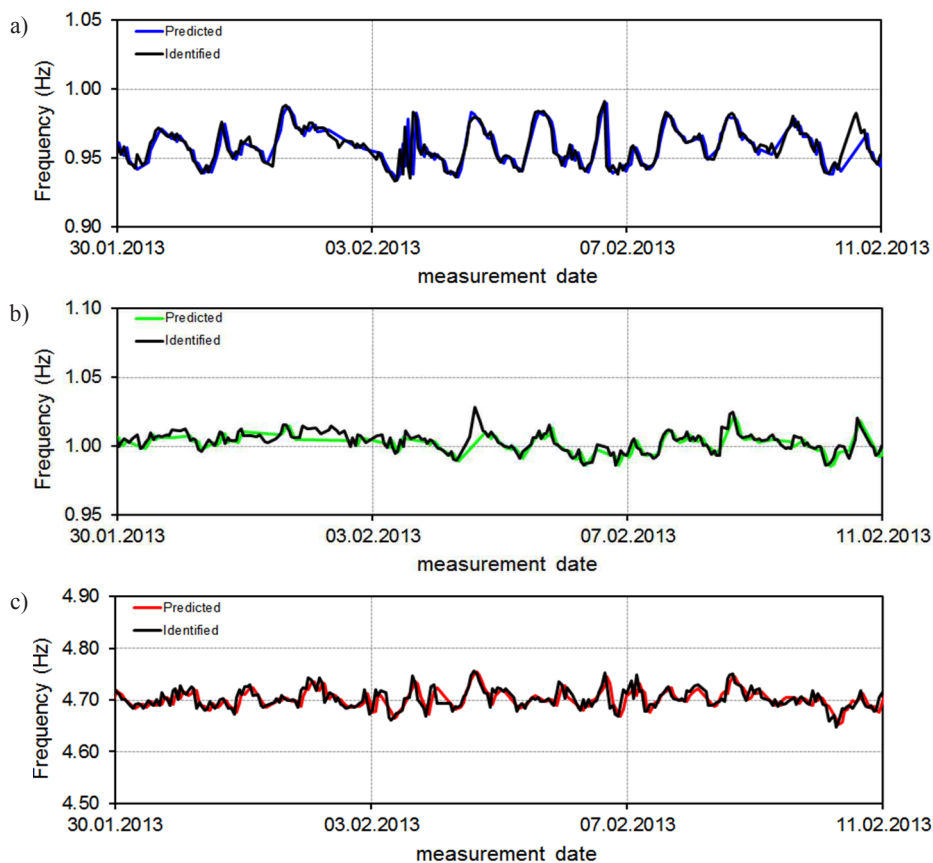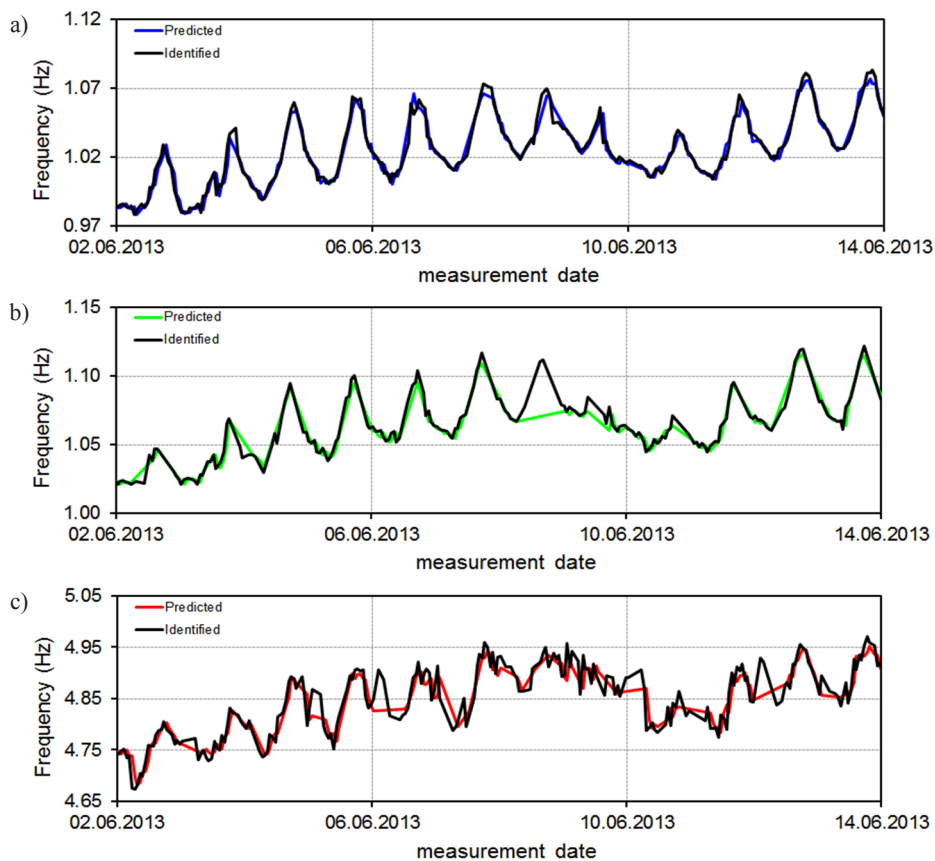

Figure 4.58 Predicted vs. Identified natural frequencies between 30/01/2013-10/02/2013 (ARX240 model): a) Mode B_1; b) Mode B_2; c) Mode T_1

The validation of the implemented ARX model has been performed by comparing experimental and numerical results for modes B_1, B_2 and T_1. At first, the time evolutions of identified and predicted natural frequencies have been plotted together, with reference to the same 12-day time intervals considered in paragraph 4.7.1 (Figure 4.58 for low temperatures and Figure 4.59 for high temperatures). The reported diagrams reveal an excellent accordance between predicted and experimental results, highlighting significant improvements with respect to the DR model.

Figure 4.59 Predicted vs. Identified natural frequencies between 02/06/2013-13/06/2013 (ARX240 model): a) Mode B_1; b) Mode B_2; c) Mode T_1

183

Indeed, for both time intervals the discordance in terms of amplitude is very limited and no delays can be detected between corresponding peaks. Conversely to the dynamic regression, where the different performance of the model between cold and warm periods was evident, only a minor worsening of the prediction can be detected for low temperatures as the difference of amplitude gets slightly larger (Figure 4.58). Nonetheless, the accuracy of the obtained results remains very high for both time intervals. This outcome conceivably suggests that the effects of the non-linear correlation between frequency and average temperature (detailed in paragraph 4.7.1) may be indirectly taken into account by the previous frequency values of the ARX model, leading to better predictions also when temperature is low.

The time evolution of the residual error is shown in Figure 4.60. The improved predictive skills of the ARX model, proved by the previous frequency comparison, are confirmed by the reported results. The investigation of Figure 4.60 reveals regular and straight diagrams for the three modes, characterized by weak scattering of the prediction error around the zero line.

In particular, the range of variation is more than halved with respect to the DR model (Figure 4.41), with fluctuations approximately between ±2% for the two bending modes (Figure 4.60 a, b) and between ±1% for mode T_1 (Figure 4.60c). The non-negligible dispersion of the values and the evident fluctuations characterizing the results of the dynamic regression are no longer observed, suggesting that the influence of environmental factors has been completely removed. The previous statement is confirmed by the time evolution of the corrected experimental frequency estimates (Figure 4.61-Figure 4.63). In particular, after the removal of the environmental effects, the range of variation of the frequencies of all modes has been significantly reduced and the trend looks completely straightened. Residual fluctuations are no longer detected and

184

the dispersion of the depurated values appears considerably small, consequently to the improved predictive skills. Hence, the application of the implemented ARX model to the experimental data leads to significant reductions of both the short term and the long term fluctuations of the frequency tracking (Figure 4.61b-Figure 4.63b), providing much better predictions than the DR relationship.
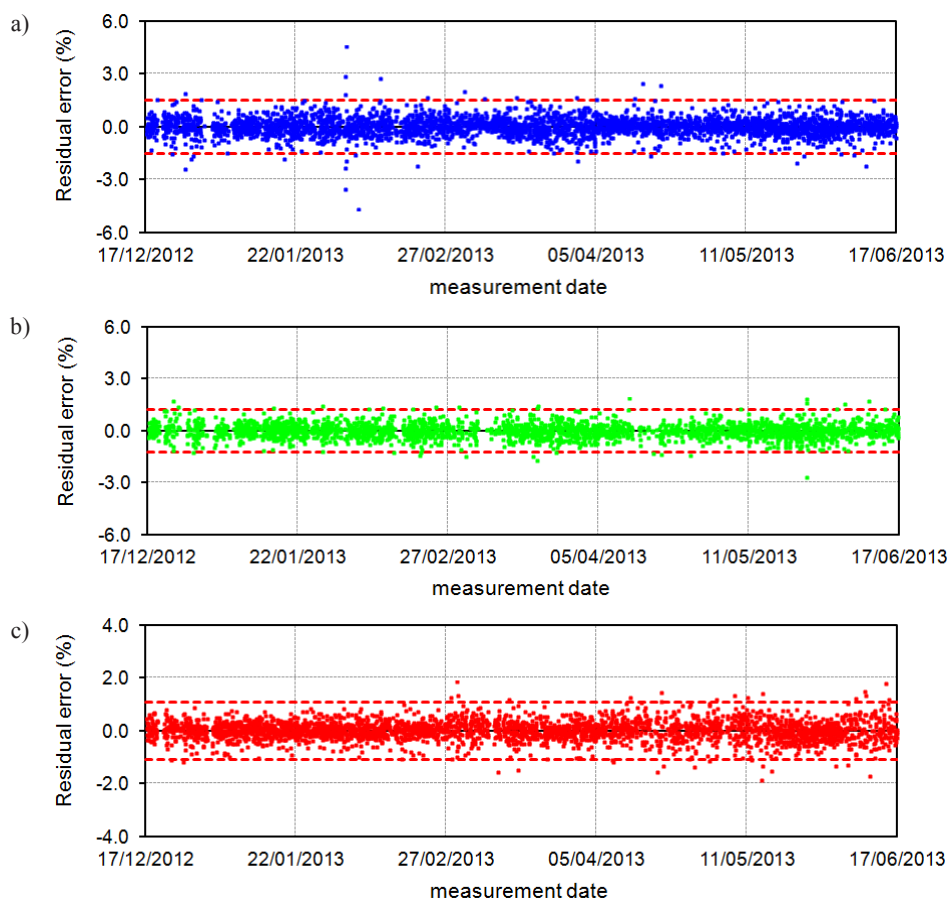

Figure 4.60 Time evolution of the residual error within the training period (ARX240 model): a) Mode B_1; b) Mode B_2; c) Mode T_1

In other words, the combined effects of average temperature and unobserved factors, not entirely modeled by the dynamic regression, are indirectly taken into account by the previous values of the experimental frequencies characterizing the ARX model. This explains the more accurate predictions and why, conversely to the dynamic regression, no residual correlation is detected for the obtained environment-free features.

The validation process of the SISO ARX240 model revealed an excellent accordance between experimental and predicted results for modes B_1, B_2 and T_1. Therefore, according to the SHM strategy presented in this Dissertation, the ARX240 model has been subsequently used to investigate the whole 30 months of monitoring, with the main purpose of identifying the structural anomaly detected on 21/06/2013.
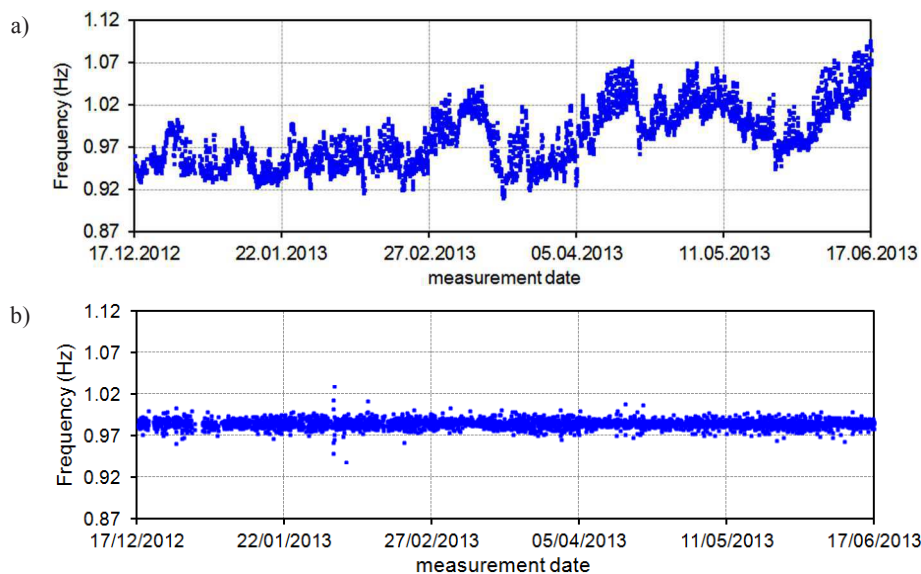
Figure 4.61 Time evolution, during the training period, of the natural frequency of Mode B_1 before (a) and after (b) the removal of the environmental effects (ARX240 model)
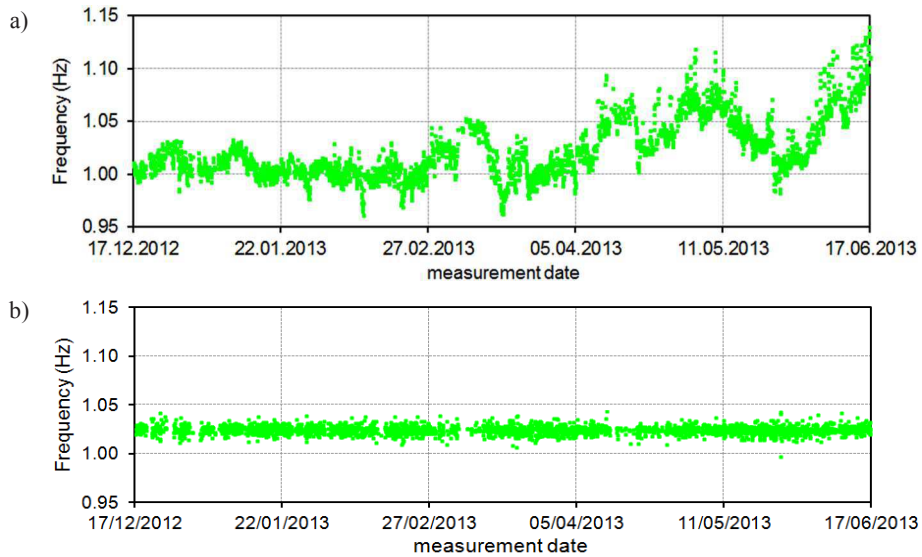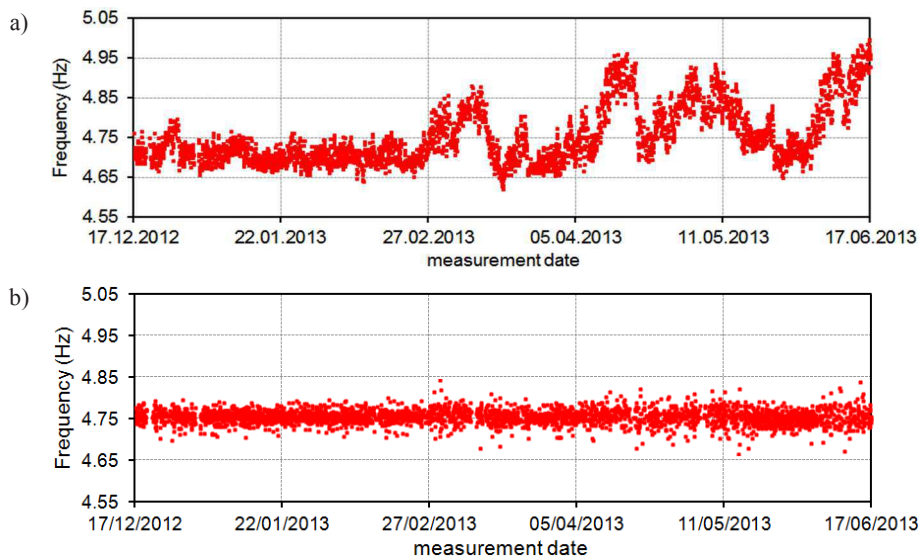
186

Figure 4.62 Time evolution, during the training period, of the natural frequency of Mode B_2 before (a) and after (b) the removal of the environmental effects (ARX240 model)

Figure 4.63 Time evolution, during the training period, of the natural frequency of Mode T_1 before (a) and after (b) the removal of the environmental effects (ARX240 model)
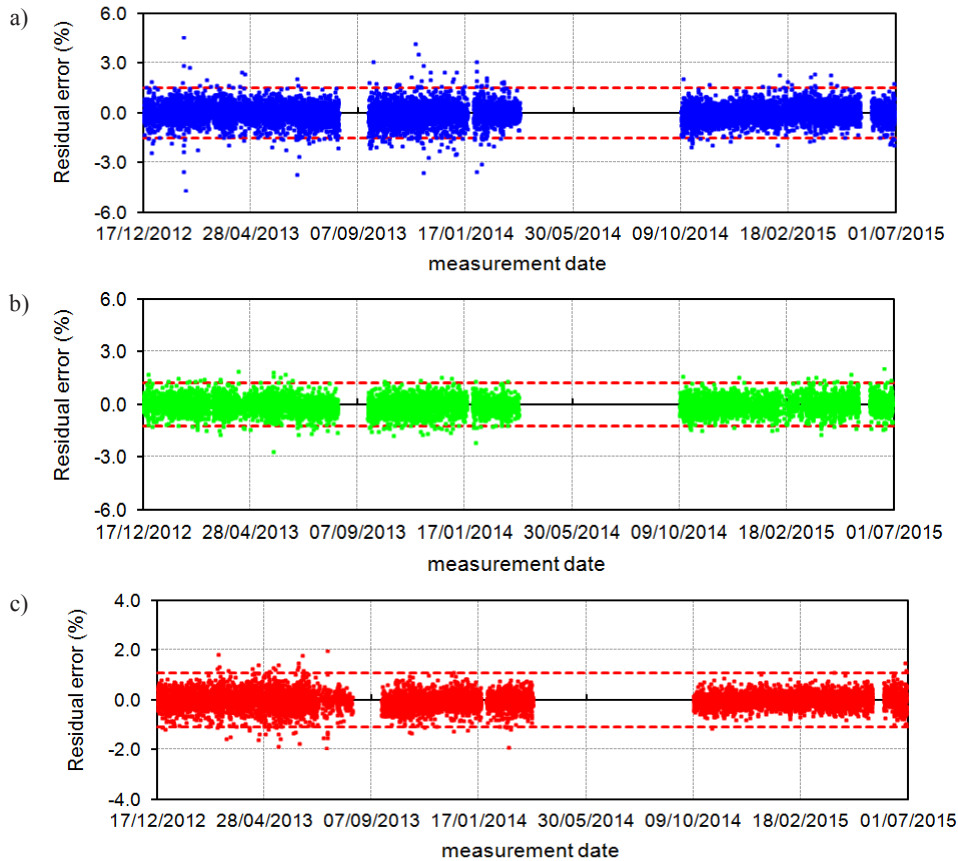
Entire monitoring period: 17/12/2012-30/06/2015

Figure 4.64 Residual errors during the entire monitored time period (ARX240 model):
a) Mode B_1; b) Mode B_2; c) Mode T_1

The time evolution of the residual errors over the whole monitoring period is presented in Figure 4.64 and suggests the following comments:

1. the first part of the plots (corresponding to the reference period) does not exhibit any relevant variation of the residual error. This result confirms that no evident structural change occurred within the first six months of monitoring, in accordance with the results of the DR model. The plotted values oscillate around 0% for all modes and are characterized by small

188

scattering;

2. after the training period, an unexpected result stands out form the reported diagrams: no sudden change of the residual error is detected corresponding to the seismic event of 21/06/2013. A zoom on the time interval between 17/12/2012 and 13/08/2013 (Figure 4.65) only allows to detect a slight downward shift of the values (especially for the two bending modes, Figure 4.65a-b), all the while keeping the same scattering of the reference period.
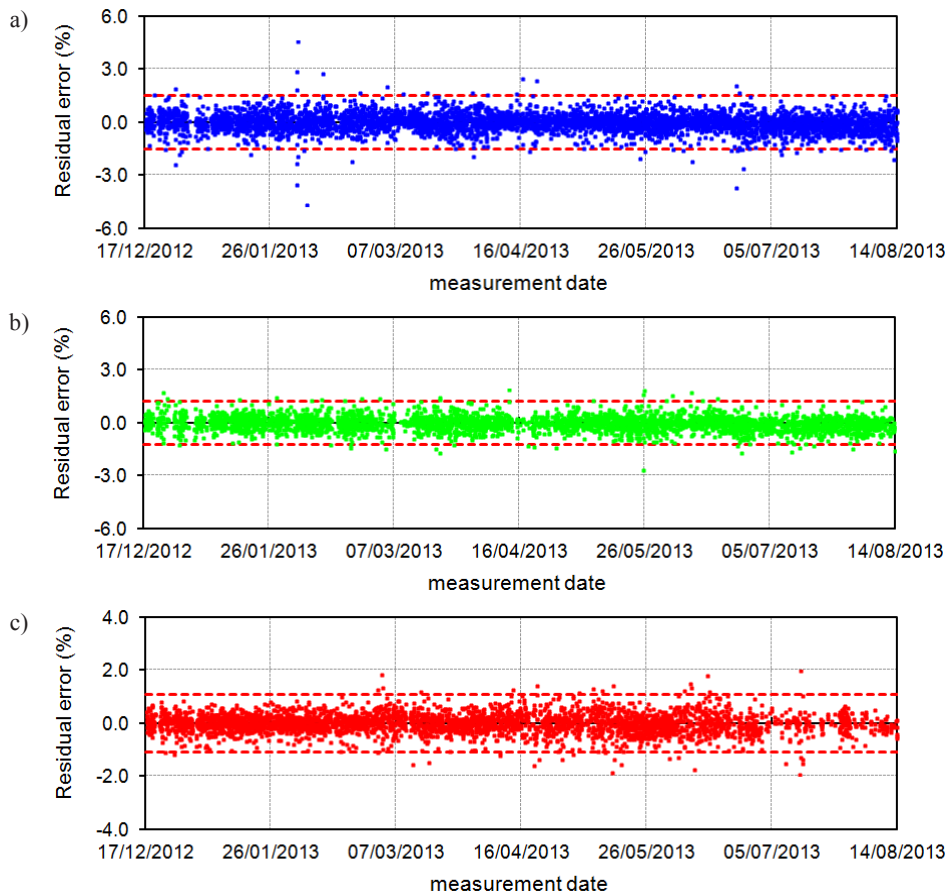

Figure 4.65 Residual error between 17/12/2012 and 13/08/2013 (ARX240 model): a) Mode B_1; b) Mode B_2; c) Mode T_1

These results are in clear discordance with the outcomes presented in the previous paragraphs, which revealed clear and sudden variations of the adopted indicators associated with the occurrence of irreversible effects of the seismic event. In the present case, had not been known that a significant earthquake occurred on 21/06/2013, the investigation of the obtained prediction error would not raise any alarm. This seems to suggest that the improved predictive skills of the ARX model are not paired by corresponding improvements of the damage detection ability;

3. in the following months of monitoring, the prediction error of the three global modes still ranges within the previously defined variation intervals and does not exhibit any sudden drop or increase of dispersion.

The inspection of the time evolution of the prediction error revealed the unexpected lack of any significant variation corresponding to the seismic event of 21/06/2013, as opposed to the results obtained from the previous regression analysis (static and dynamic). Such outcome is confirmed by the obtained trend of the natural frequencies after the removal of the temperature effects (Figure 4.66-Figure 4.68). As previously pointed out with respect to the reference period, the correction achieved with the ARX240 model leads to almost completely straight time evolutions, characterized by ranges of variations significantly smaller than those provided by the DR model. Nevertheless, just like the residual errors, none of the depurated frequencies exhibit any sudden variation after the Garfagnana earthquake.
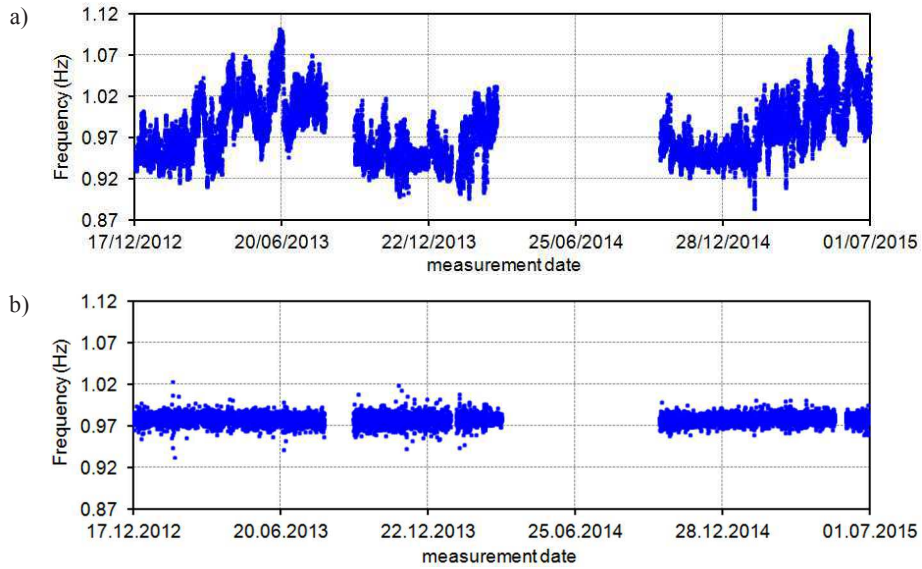
Figure 4.66 Time evolution of the natural frequency of Mode B_1: a) before and b) after the removal of the environmental effects (ARX240 model)
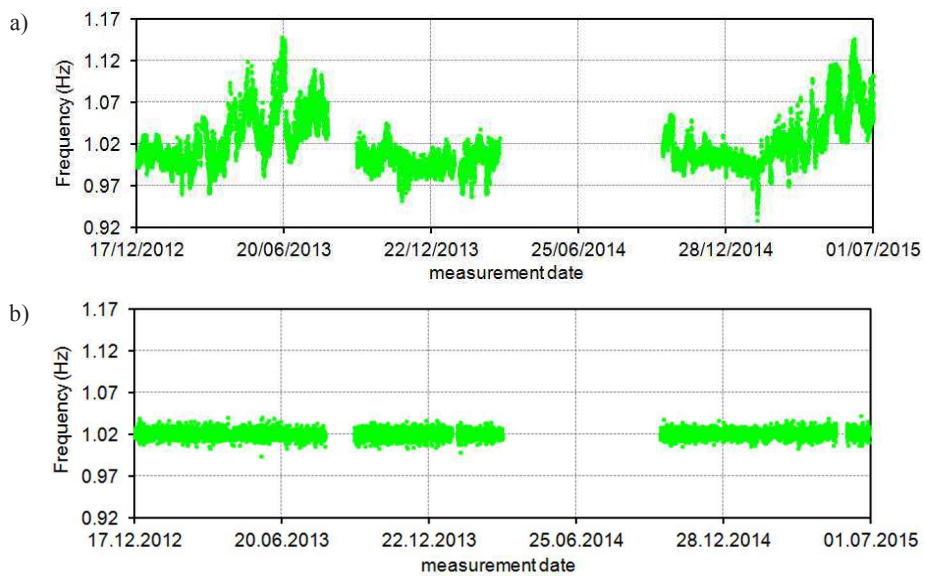

Figure 4.67 Time evolution of the natural frequency of Mode B_2: a) before and b) after the removal of the environmental effects (ARX240 model)
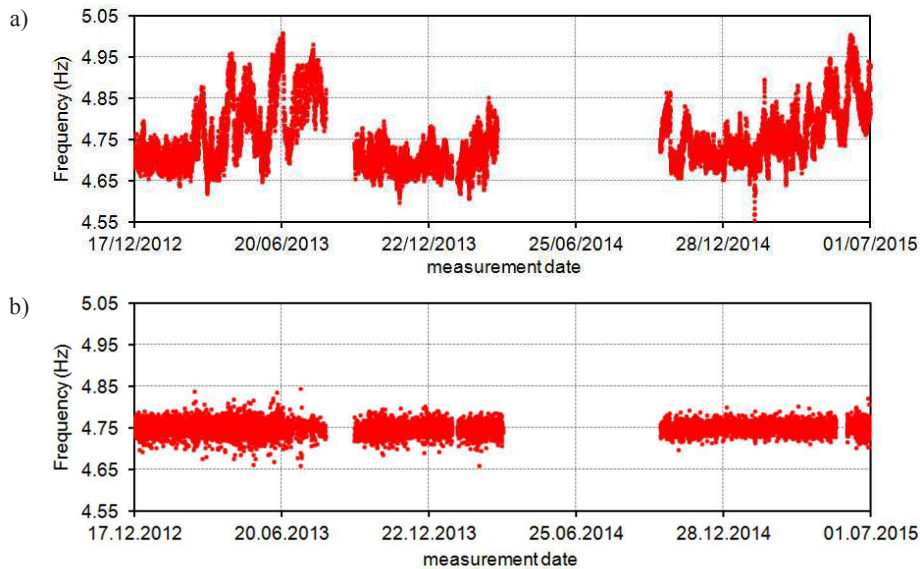
Figure 4.68 Time evolution of the natural frequency of Mode T_1: a) before and b) after the removal of the environmental effects (ARX240 model)

The results obtained by applying the ARX240 model to the experimental data are somehow surprising: conversely to the outcomes of the regression analysis, the effects due to the seismic event of 21/06/2013 could not be detected. Indeed, a very regular trend and a small dispersion of the values had to be expected, considering the improved predictive skills of the ARX model assessed during the validation process. Furthermore, the results referred to the reference period also made one expect a corresponding improvement of the damage detection skills, as a consequence of the significantly enhanced predictions. For this reason, the absence of an abrupt drop of the error on the day of the Garfagnana earthquake stands out as totally unforeseen, even more so as the occurrence of irreversible structural modifications has been confirmed by all the previously adopted methods (see previous paragraphs 4.6.1, 4.6.2 and 4.7.1). Such behavior suggests that the described improved predictive skills of the ARX models do not lead to enhancements in the detection of structural anomalies, where the static and dynamic regression analysis proved to be more

efficient. A possible explanation of the obtained results can be found by considering the one feature that characterizes ARX models: the use of previous values of the output. Indeed, the presence of past estimates of the frequency implicitly carries in information related to those factors (measured and unmeasured) that cause variations of the natural frequencies and that cannot be modeled by simply considering previous values of the input (as for the DR model). As observed from the time evolution of residual errors and corrected frequencies, this feature significantly improves the prediction skills and leads to much more accurate results. On the other hand, the obtained results are characterized by the lack of any significant variation after the Garfagnana earthquake. A possible explanation for such behavior could lie in the fact that the frequency drop caused by the seismic event has the same order of magnitude as the fluctuations induced by the temperature effects. Therefore, since the ARX model is able to follow the temperature-induced frequency variations with high accuracy, the sudden drop caused by the seismic event is reproduced as well. This, in turn, jeopardizes the possibility of detecting anomalous occurrences from environment-independent features.

Control charts

Enhancements in the damage detection process could be obtained by applying the multivariate *Shewhart T* control chart, as the plotted T^2-*statistic* takes into account the statistical properties of the obtained environment-independent residuals. In Figure 4.69, the *Shewhart T* control chart of the whole monitoring period has been reported, along with the defined UCL (i.e. the solid horizontal red line). In order to highlight the effects induced by the Garfagnana seismic event, subgroups of data of 24 hours have been considered.
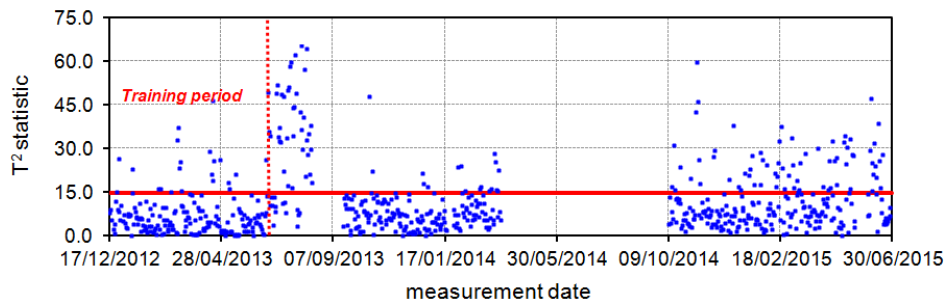
Figure 4.69 *Shewart T* control chart obtained by using subgroups of data of 24 hours (ARX240 model)

The reported trend appears significantly more articulated than the previously observed diagrams and the effects induced by the earthquake of 21/06/2013 are finally detectable. In particular, the time evolution of the T^2-*statistic* leads to the following considerations:

1. during the training period (i.e. 17/12/2012-16/06/2013), the plotted values range within the defined control region and only few outliers can be detected. This result is consistent with the outcomes of the DR model and confirms that no relevant structural variations took place in the first six months of monitoring;

2. on 21/06/2013, corresponding to the Garfagnana seismic event, a clear and sudden increase of the T^2-*statistic* is observed. As it can be observed from Figure 4.69, almost all values after the red-dashed line exceed the UCL. Simultaneously, the level of dispersion significantly increases too. In accordance with the results of the DR model, the plotted feature keeps the new trend during the first weeks after the earthquake;

3. during the interval between the two monitoring interruptions (i.e. from 19/09/2013 to 17/03/2014) the T^2-*statistic* is characterized by smaller values, almost entirely included within the control region. These results are only partially consistent with the outcomes of the dynamic regression: a gradual decrease of the T^2-*statistic* with a decreasing temperature could be observed

194

for the DR model, whereas no decreasing phase is detected in the reported diagrams. In particular, the T^2-*statistic* points are included in the UCL as soon as the monitoring is resumed (i.e. 19/09/2013). This behavior makes it harder to detect the irreversible effects induced by the seismic event, confirming the worse damage detection skills of the ARX model. With regards to the decrease of the statistic feature during cold periods, one should remember that ARX models are still linear relationships. Therefore, the described non-linearity of the frequency-average temperature correlation still affects the predictive skills of the model, changing the quality of the predictions between cold and warm periods. Even if this variation is significantly less marked than for the dynamic regression (as observed during the validation process), it appears to be enough to induce a decrease of the reported T^2-*statistic* when the temperature decreases;

4. low values of the T^2-*statistic* are detected during the last weeks of Summer 2014, as the daily and average temperatures decrease approaching Winter time. The detected values look comparable to those observed at the end of Summer 2013 in similar temperature conditions. Therefore, in accordance with the results provided by the DR model, the conclusion can be drawn that no further irreversible damage occurred during the first year after the earthquake;

5. after Winter 2014/2015, as the average temperature and the predictive skills of the ARX model increase, the number of points exceeding the UCL progressively increases too, making again visible the effects of the structural variations induced by the earthquake. Furthermore, in continuity with the conclusions of the previous, the similar values of the T^2-*statistic* in June 2013 and June 2015 provide proof that no permanent damage occurred over the last 9 months of monitoring either.

Concluding remarks

The implementation and application of an ARX model to the experimentally identified natural frequencies led to a complete removal of the environmental effects, with significant improvements of the predictive skills with respect to the dynamic regression relationship. Indeed, the use of previous values of the output allowed to indirectly take into account the effects of those factors that could not be entirely modeled by considering only past values of temperature. Nonetheless, this characteristic turned into a limitation when trying to detect anomalous occurrences, as the effects of structural modifications are also taken into account by the previous frequencies. This seems to be confirmed by the lack of sudden variations of the environment-independent indicators (i.e. prediction error and corrected frequencies) corresponding to the earthquake of 21/06/2013.

To conclude, the removal of the temperature effects by means of ARX model did not allow to directly detect the occurrence of the structural variation induced by the Garfagnana earthquake. Nevertheless, the effects of the seismic event could be observed by taking into account the statistical properties of the obtained features through the *Shewart T* control chart. The trend exhibited by the T^2-*statistics* is consistent with the irreversibility of the earthquake effects assessed in the previous paragraphs, but also confirms the worsened damage detection skills of the ARX model when compared to the regression analysis.

4.7.3 *Principal Component Analysis*

After the implementation of input-output models, the effects of temperature on the *Gabbia* tower have been modeled by performing a Principal Component Analysis of the experimental estimates. As PCA belongs in the category of output-only models (see Chapter 1), it only relies upon the identified natural frequencies while ignoring the measurements of any recorded input.

As described in Chapter 3, PCA needs the definition of a data set containing (at every hour) the frequency of each selected mode. Therefore, a preliminary step has consisted on removing the rows of the experimental data matrix, still referred to global modes B_1, B_2 and T_1, where not all the considered modes had been identified. Afterwards, the number of Principal Components (PCs) needed to reduce the dimension of the problem and remove the influence of temperature have been selected by analyzing the data collected over the training period.

Training period: 17/12/2012-16/06/2013

The PCA of the first six months of monitoring allowed to identify three singular values (SVs) of the data matrix, as only three modes have been considered to define the data set. Since the reference period has been selected by leaving out the effects of the earthquake of 21/06/2013, the obtained PCs will only be related to environmental factors. The obtained SVs are reported in Table 4-5 along with the correlation coefficients between the corresponding PCs, the natural frequencies of modes B_1, B_2 and T_1 and temperature.

Table 4-5 Statistics of the natural frequencies identified (SSI-Data) in the first AVT

SV	$\rho(B_1\text{-PCs})$	$\rho(B_2\text{-PCs})$	$\rho(T_1\text{-PCs})$	$\rho(T_h\text{-PCs})$	$\rho(T_{av72}\text{-PCs})$
2.888 (96%)	-0.979	-0.987	-0.975	-0.847	-0.838
0.075 (2.5%)	0.174	0.041	-0.217	0.199	0.041
0.037 (1.5%)	0.105	-0.158	0.054	-0.057	-0.004

B = bending mode; T = torsion mode

Table 4-5 shows that the first singular value of the data matrix explains the 96% of the frequency variation associated to the considered three modes. Furthermore:

1. the correlation coefficients referred to the three global modes reveal that, for all of them, the variation can be successfully explained by the first PC;

2. a significant correlation is detected between the first PC and the values of temperature averaged over one hour and 72 hours. This highlights that the first PC conceivably involves the combination of the two temperatures and confirms that both factors affect the variation of the natural frequencies, as previously demonstrated in this chapter.

Since the first SV alone can explain more than 90% of the fluctuations of the modes B_1, B_2 and T_1, the correction of the experimental natural frequencies has been performed by only considering the corresponding first PC.
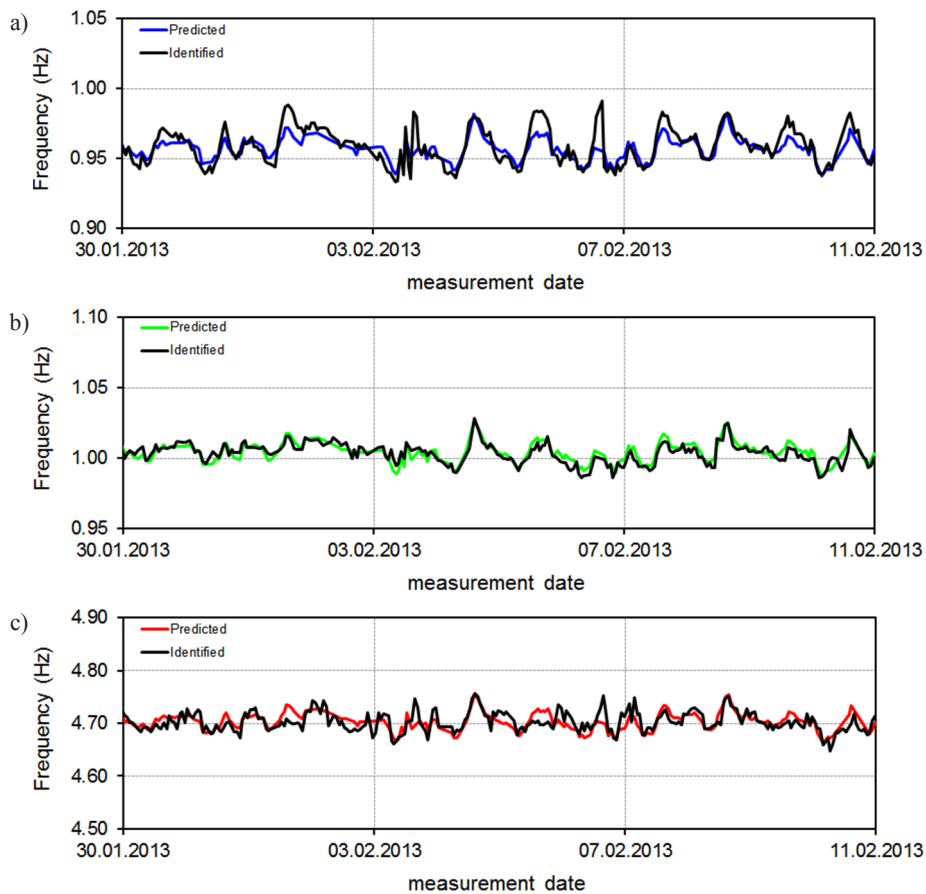
Figure 4.70 Predicted vs. Identified natural frequencies between 30/01/2013-10/02/2013 (PCA): a) Mode B_1; b) Mode B_2; c) Mode T_1

As for the input-output models, the results obtained over the training period have been compared to the experimental estimates for validation. Figure 4.70 and Figure 4.71 report the overlapped time evolutions of the natural frequencies, with reference to the previously defined cold (from 30/01/2013 to 10/02/2013) and warm (from 02/06/2013 to 13/06/2013) time intervals, respectively.
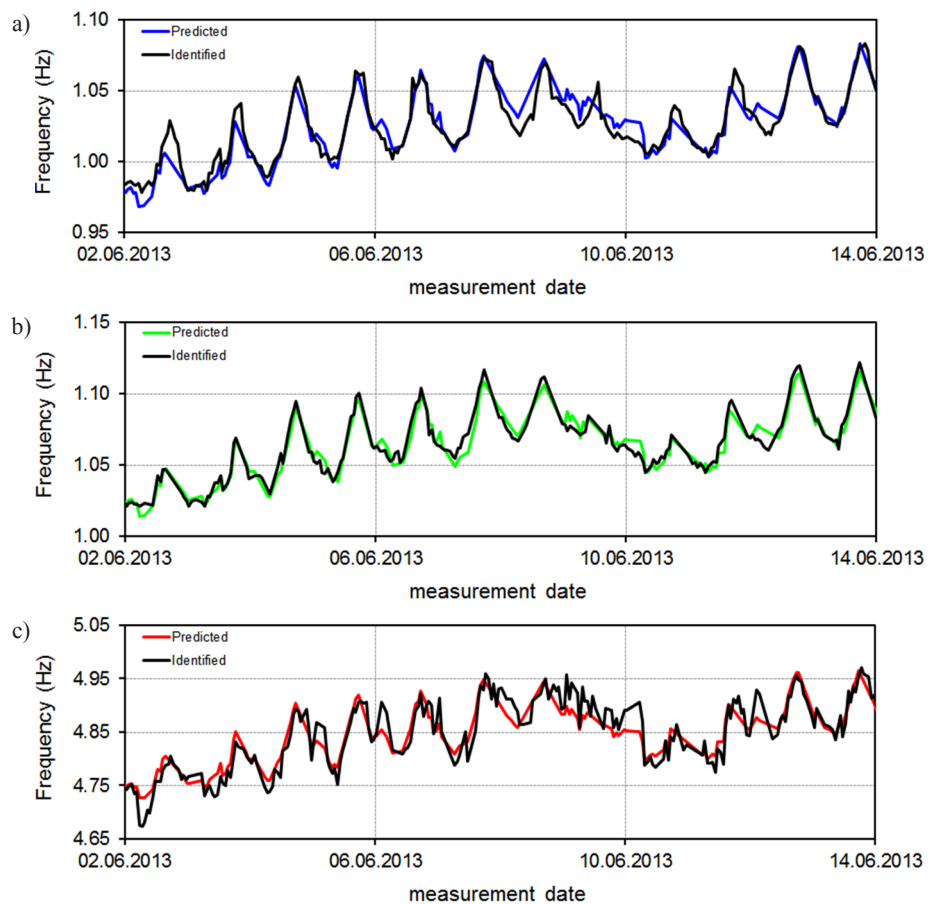

Figure 4.71 Predicted vs. Identified natural frequencies between 02/06/2013-13/06/2013 (PCA model): a) Mode B_1; b) Mode B_2; c) Mode T_1

The inspection of Figure 4.70 and Figure 4.71 reveals a very good agreement between identified and predicted results, confirming that the use of only the first PC is sufficient to accurately reproduce the experimental results. Indeed, the quality of the prediction has improved with respect to the DR relationship, even if it does not reach the accuracy obtained using the ARX model. Furthermore, the different predictive skills of the model between low and high temperature conditions can be detected also for the PCA, even if less relevant that it was observed for the dynamic regression. This suggests that the slight non-linearity observed in the dependence between frequency and average temperature still visibly affects the quality of the results, conversely to the ARX model where the difference between cold and warm periods was almost undetectable.

As the predictions provided by the PCA are more accurate than those of the DR model but not as good as the ones obtained using the ARX, it can be stated that, in terms of predictions, the PCA stands midway between the dynamic regression and the ARX models. This is especially confirmed by the prediction differences between cold and warm periods, not as evident as for the dynamic regression, but sensibly more marked than for the ARX model. Therefore, the same behavior is expected to be detected also for the results in terms of residual errors and cleaned observations.

The time evolution of the residual over the training period is reported in Figure 4.71 for modes B_1, B_2 and T_1. As it can be observed, for all modes the trend appears more regular than the one obtained for the dynamic regression. Unlike the results of the ARX model, some residual fluctuations can be still detected along with a slightly larger dispersion of the values. In particular, the variation intervals can be assumed approximately equal to: $\pm2.5\%$ for mode B_1 (Figure 4.71a), $\pm2\%$ for mode B_2 (Figure 4.71b) and $\pm1\%$ for mode T_1 (Figure 4.71c). The small scattering of the identified points and the minor remaining fluctuations, much less significant that those detected for the dynamic
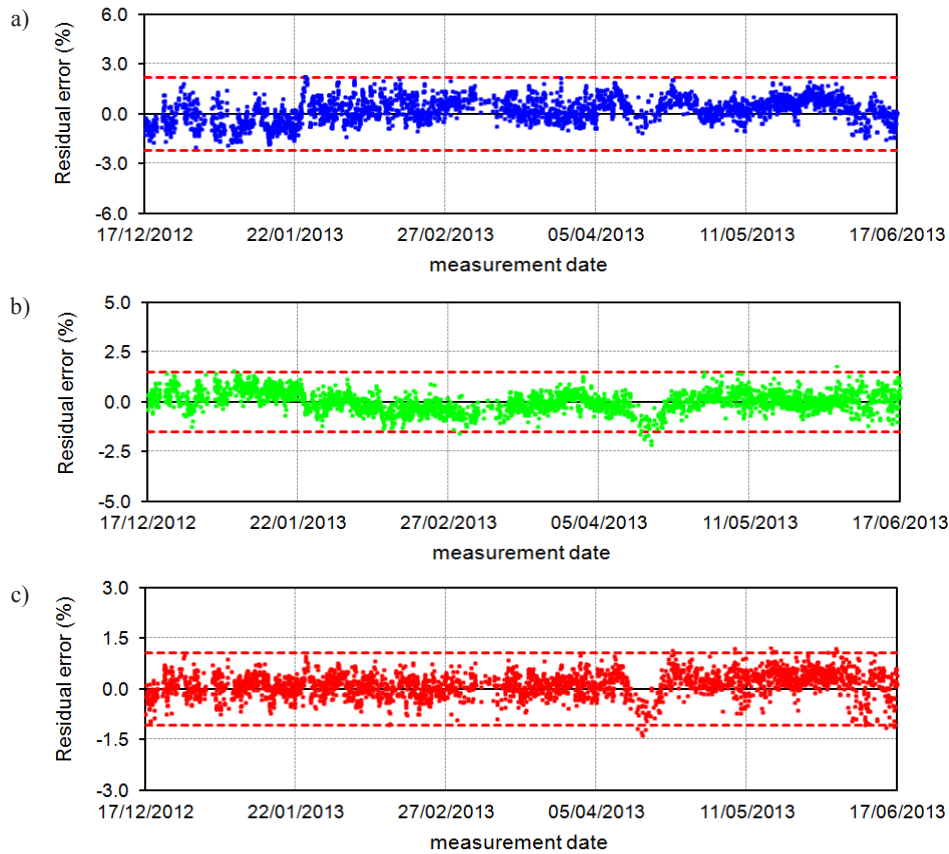
200

Figure 4.72 Time evolution of the residual error within the training period (PCA): a) Mode B_1; b) Mode B_2; c) Mode T_1

regression, suggest that the effects of the most relevant environmental factors (i.e. hourly and average temperature and, conceivably, other minor unobserved factors) has been correctly taken into account by considering only the first PC.

The results obtained in terms of depurated natural frequencies (Figure 4.73-Figure 4.75) are consistent with the previous comments and confirm the successful minimization of the temperature effects. After the application of the PCA, the depurated time evolutions exhibit very small scattering of the values and minor oscillations around the average frequency, with trend significantly straighter than those of the experimental estimates.

As expected, the investigation of prediction error and corrected frequencies revealed that the results of the PCA stand somewhere in between those of the DR and the ARX models: both the dispersion of the points and the residual fluctuations have been significantly reduced with respect to the dynamic regression. Nevertheless, the accuracy achieved by the ARX model could not yet be reached. Therefore, the use of the first PC allows to model the influence of temperature with more accuracy than using just previous measurements of the input (i.e. DR model); on the other hand, the ARX model could almost entirely remove the external factors (indirectly taken into account in the past values of the output), whereas the minor but non-negligible residual fluctuations of the reported time evolutions reveal that the supposedly environment-independent features are still slightly correlated with each other.
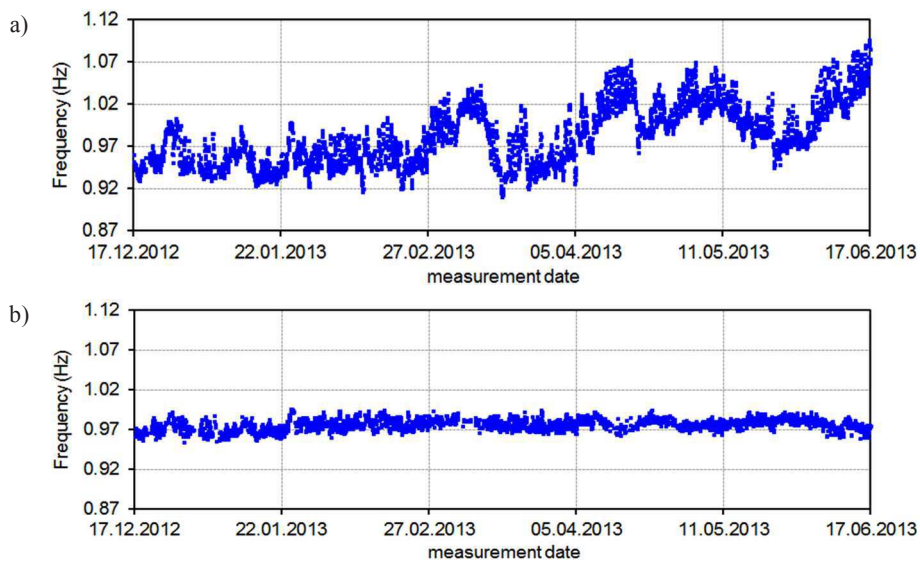

Figure 4.73 Time evolution, during the training period, of the natural frequency of Mode B_1 before (a) and after (b) the removal of the environmental effects (PCA)
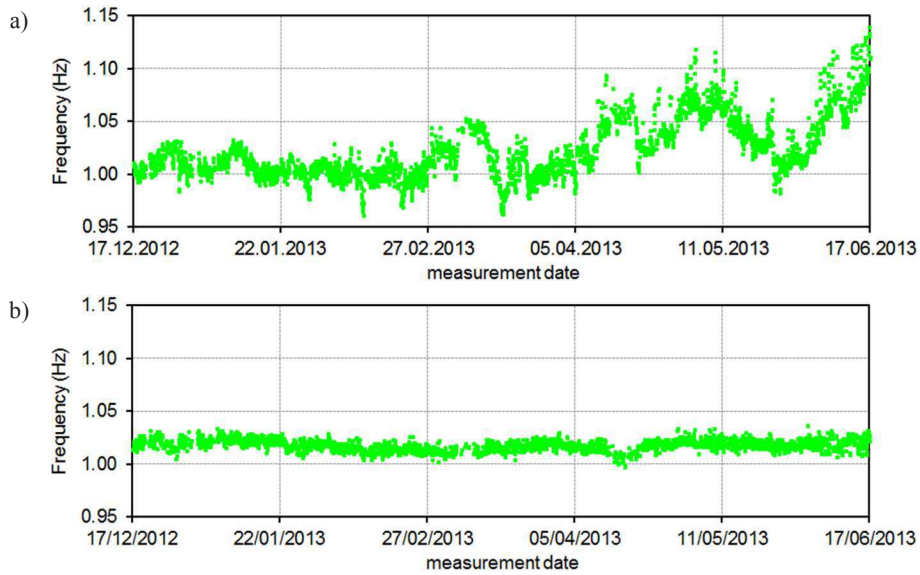
202

Figure 4.74 Time evolution, during the training period, of the natural frequency of Mode B_2 before (a) and after (b) the removal of the environmental effects (PCA)
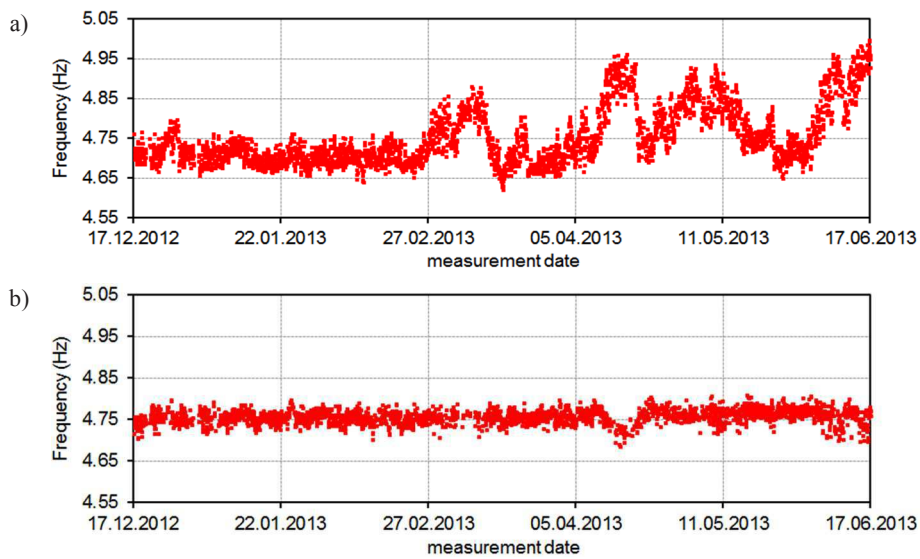

Figure 4.75 Time evolution, during the training period, of the natural frequency of Mode T_1 before (a) and after (b) the removal of the environmental effects (PCA)

This result is probably ascribable to the influence of other minor external factors not taken into account by the first PC, conceivably combined with some

residual effects of temperature.

The investigation of predicted frequencies, residual error and corrected frequencies allowed a sound validation of the PCA carried out over data collected during the training period. In the next section, the adopted output-only method has been applied to the whole monitoring period. In particular, considering the results obtained during the validation process, the damage detection skills of the PCA are again expected to fall midway between those exhibited by the two input-output methods.

Entire monitoring period: 17/12/2012-30/06/2015

The time evolution of the prediction error over the 30 months of monitoring is shown in Figure 4.76. As expected, the trends reported for modes B_1, B_2 and T_1 look more oscillating than those obtained from the ARX model.Nevertheless, the effects induced by the Garfagnana earthquake are not as clear and sudden as those detected by using the multiple regression analysis (static and dynamic). This seems to suggest that, notwithstanding the improved predictive skills of the PCA, the damage detection is still not comparable to that of the DR model.

The inspection of Figure 4.76 leads to the following comments:

1. in the initial months of monitoring the reported time evolutions do not exhibit any significant and sudden variation, again confirming that the behavior of the *Gabbia* tower during the training period (i.e. 17/12/2012-16/06/2013) was mainly affected by environmental factors;

2. a small but not negligible change in the distribution of the identified points can be observe corresponding to the seismic event of 21/06/2013. This variation is made more evident by focusing on the shorter time interval reported in Figure 4.77 (i.e. 17/12/2012-13/08/2013). After the occurrence of the earthquake (21/06/2013), the time evolutions of all modes shift downwards and settle themselves in the field of negative values. This drop is
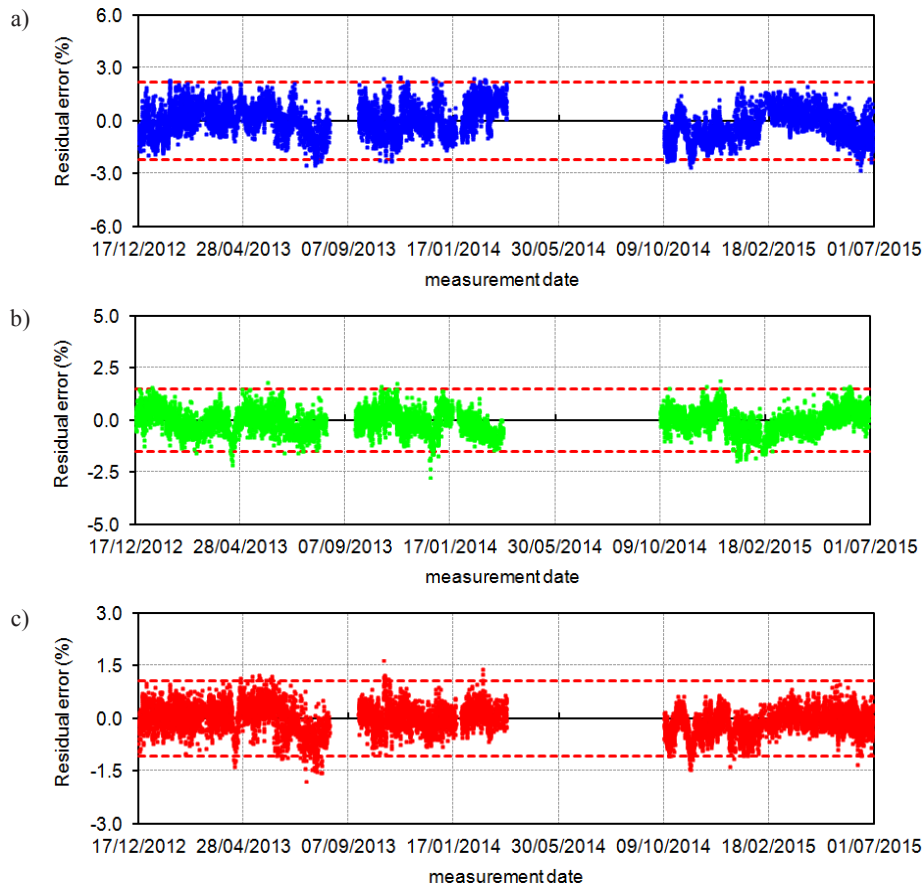
Figure 4.76 Residual errors during the entire monitored time period (PCA): a) Mode B_1; b) Mode B_2; c) Mode T_1

more sudden for modes B_2 (Figure 4.77b) and T_1 (Figure 4.77c), whereas a gradual decrease characterizes mode B_1 (Figure 4.77a). Even if the described shift is not as obvious as the one detected for the DR model, it reveals that the effects generated by the Garfagnana earthquake are still detectable after the application of the PCA. Indeed, clearer results are expected when more sensitive tools for damage detection (i.e. control charts) are adopted;
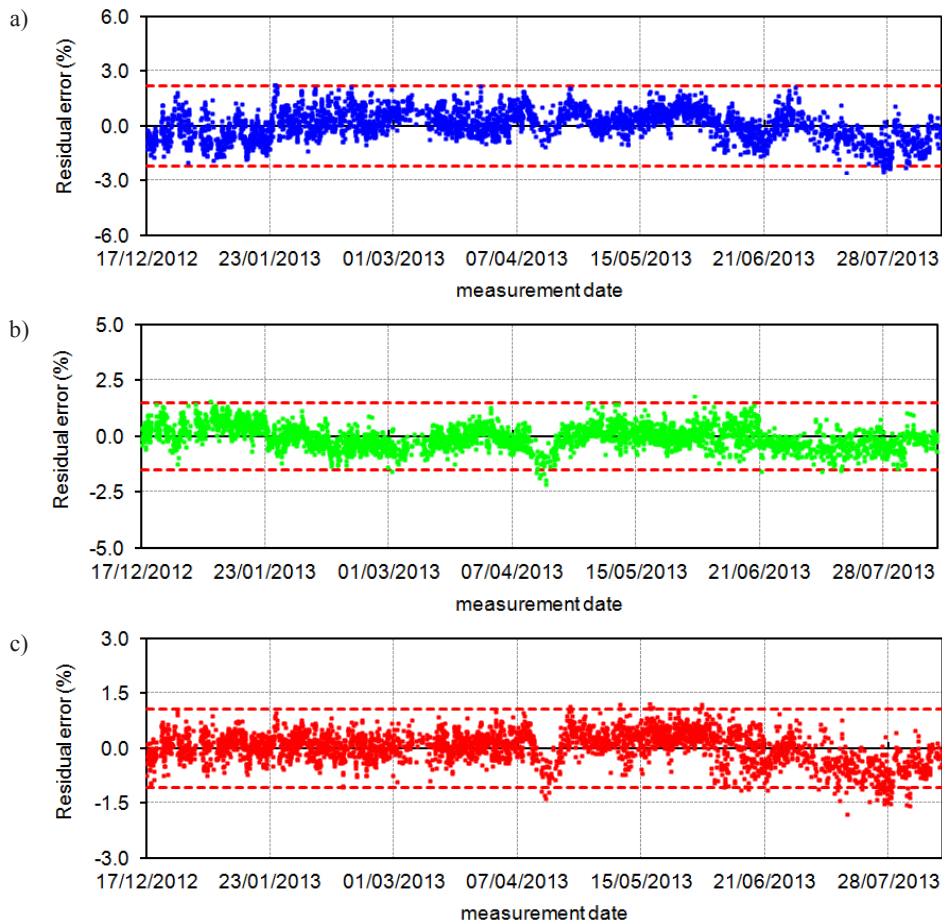
Figure 4.77 Residual error between 17/12/2012 and 13/08/2013 (PCA): a) Mode B_1; b) Mode B_2; c) Mode T_1

3. in the weeks from 21/06/2013 until the interruption of Summer 2013, the error maintains the new trend and oscillates in the field of negative values. In particular, the new ranges of variation can approximately be defined as: 0% ÷ -2.5% for mode B_1 (Figure 4.77a), 0% ÷ -1.5% for mode B_2 (Figure 4.77b) and 0% ÷ 1.5% for mode T_1 (Figure 4.77c);

4. the inspection of the time interval between September 2013 and March 2014 (Figure 4.78) still highlights a negative offset during the last weeks of Summer, even if smaller than the one detected during the warmer months of

June and July. After November 2013, the shift is no longer detected and the fluctuations of the error move back about the zero line. This behavior can be explained by recalling the difference in the predictive performances between warm and cold time periods, described during the previous validation process. Considering the both the investigations carried out in previous paragraph 4.6 and the results of the DR model proved the effects of the earthquake to be irreversible, the error is expected to drop again in the negative field as temperature increases.
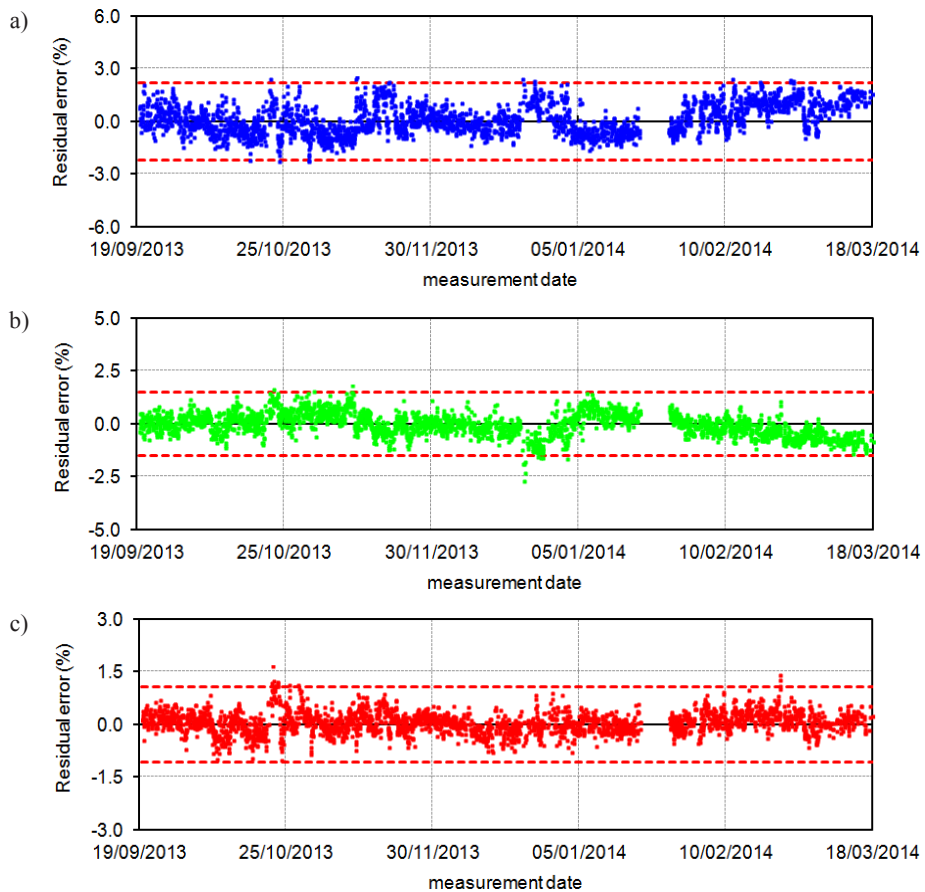

Figure 4.78 Residual error between 19/09/2013 and 17/03/2014 (PCA): a) Mode B_1; b) Mode B_2; c) Mode T_1

5. the lack of data during Summer 2014 does not allow to confirm the expected shift of the time evolutions during warmer months. Nonetheless, when the monitoring is resumed in October 2014, the residual error of all modes exhibits fluctuations in the field of negative values, with ranges of variation totally comparable to those identified after the earthquake (Figure 4.79, referred to the time interval 10/10/2014-30/06/2015). The fact that the values detected after the earthquake and at the end of Summer 2014 are characterized by similar magnitude reveals that no further irreversible changes occurred between 21/06/2013 and 10/10/2014. This assumption is consistent with the results of the previous investigations;

6. in accordance with the behavior detected in the previous year, the error resumes the original trend and fluctuates around zero in mid-November, corresponding to the arrival of Winter time (Figure 4.79). In this case, the continuous monitoring carried out over Spring and Summer 2014 allows to prove right the assumption made in previous point 4: as expected, when the predictive skills of the model increase with an increased temperature, the identified points progressively move downward and assume values comparable to those detected during the weeks after 21/06/2013 (Figure 4.76) and at the end of Summer 2013 (Figure 4.77). This result, along with the lack of further unexpected changes of the time evolutions, also confirms that no permanent structural variations occurred between 10/10/2014 and 30/06/2015;
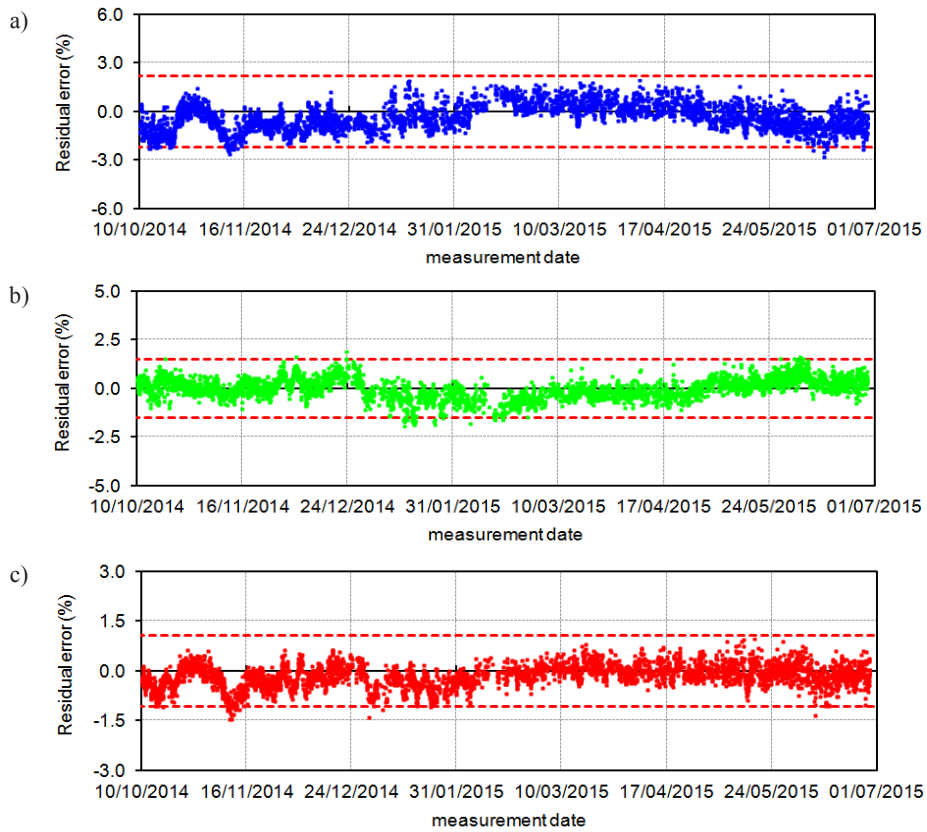
Figure 4.79 Residual error between 10/10/2014 and 30/06/2015 (PCA): a) Mode B_1; b) Mode B_2; c) Mode T_1

The results presented in terms of residual errors revealed a more meaningful behavior than the one obtained from the ARX model. The structural effects of the earthquake of 21/06/2013 can be detected during the whole monitoring period, even if the induced variations appear much less obvious than those highlighted by the results of the dynamic regression. This provides further proof that, in terms of both prediction and damage detection skills, the PCA falls in between the ARX and the DR models.
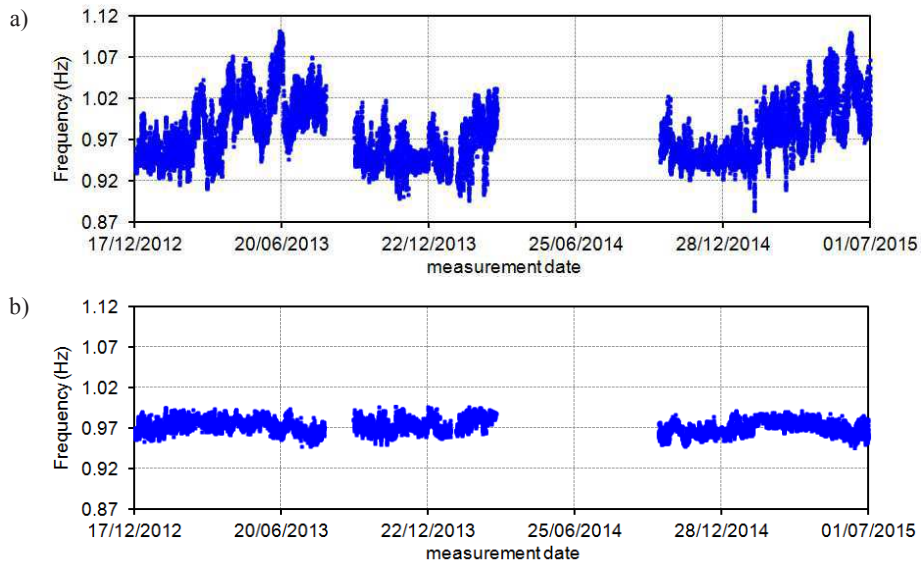
Figure 4.80 Time evolution of the natural frequency of Mode B_1: a) before and b) after the removal of the environmental effects (PCA)
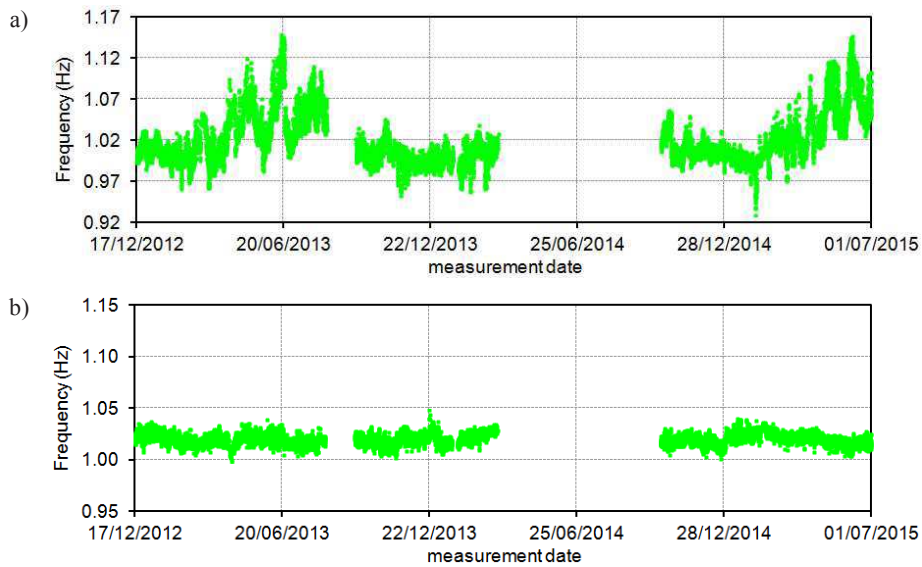

Figure 4.81 Time evolution of the natural frequency of Mode B_2: a) before and b) after the removal of the environmental effects (PCA)
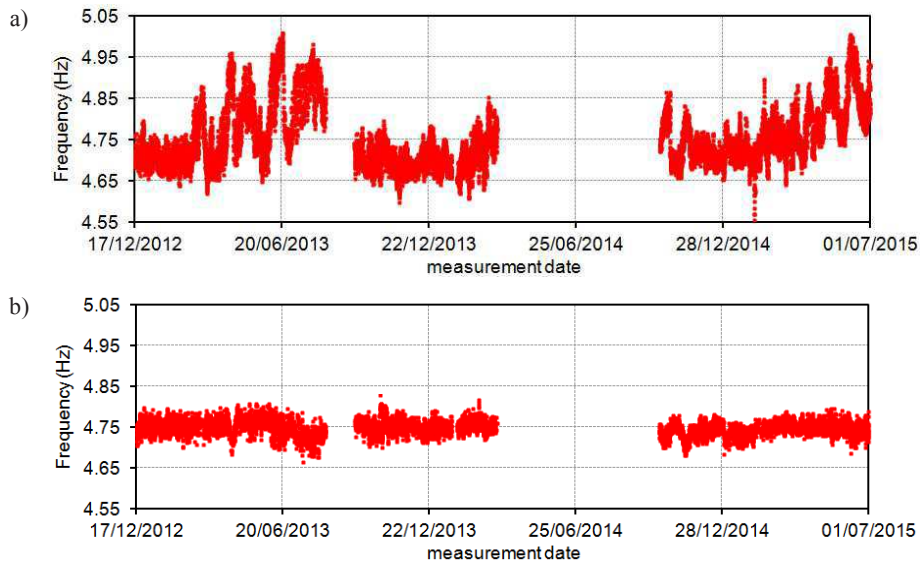
Figure 4.82 Time evolution of the natural frequency of Mode T_1: a) before and b) after the removal of the environmental effects (PCA)

Such outcome is consistent with the trend exhibited by the natural frequencies, after that the external effects carried in by the first PC have been removed (Figure 4.80b-Figure 4.82). As previously observed for the reference period, the correction achieved by adopting the PCA allowed to significantly reduce the fluctuations and the dispersion of the three frequencies, leading to better predictions with respect to the DR model. As expected on the base of the trend of the prediction error, a small drop of the frequencies is detected after the Garfagnana seismic event and all modes exhibit some residual fluctuations.

In particular, the following considerations can be made:

1. after the minimization of the environmental effects, the time evolutions of the three considered frequencies display small scattering and slight fluctuations around the average values. Once more, it should be noticed that the detected ranges of variation fall midway between those defined for DR and ARX models;

2. a small downward shift of the corrected frequencies can be detected on

21/06/2013 (Figure 4.80b-Figure 4.82b). No relevant variations of the dispersion are observed for the two bending modes, whereas mode T_1 displays a slight increase of the scattering. In the weeks between the seismic event and 13/08/2013 the corrected values hover around the new lower average frequencies;

3. as a consequence of the worsened prediction skills of the PCA with low temperature, the offset decreases moving towards November 2013, when all modes exhibit the original trend again;

4. the similar values assumed by the corrected frequencies during all warm periods reveal that: i) the structural effects of the Garfagnana earthquake are detected throughout the whole 30 months of monitoring; ii) the structural behavior of the Gabbia tower has not suffered further changes after 21/06/2013.

Control charts

After the investigation of residual error and depurated frequencies, the damage detection process has been performed by exploring the trend of the T^2-*statistic* feature in the *Shewhart T* control chart. On the base of the results obtained for DR and ARX models, an improvement in the detection of anomalous occurrences is expected for the PCA.
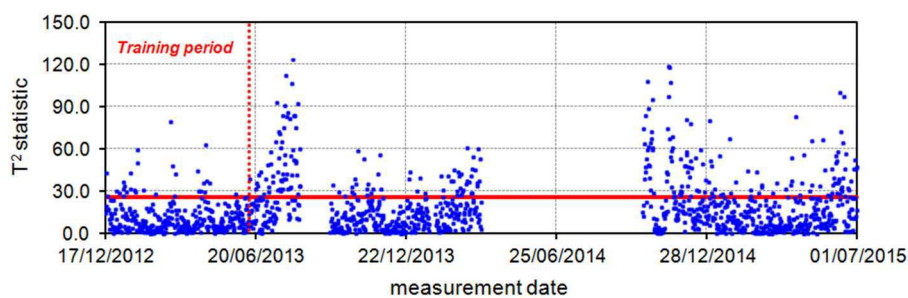

Figure 4.83 *Shewart T* control chart obtained by using subgroups of data of 12 hours (PCA)

212

The *Shewhart T* control chart covering the entire 30 months of monitoring is reported in Figure 4.83, along with the defined Upper Control Limit (UCL, i.e. the solid horizontal red line). Conversely to the ARX model, the effects of the earthquake of 21/06/2013 could already be detected from the environment-independent features obtained from the PCA. Therefore, subgroups of data of 12 hours were sufficient to adequately highlight the variation of the structural condition.
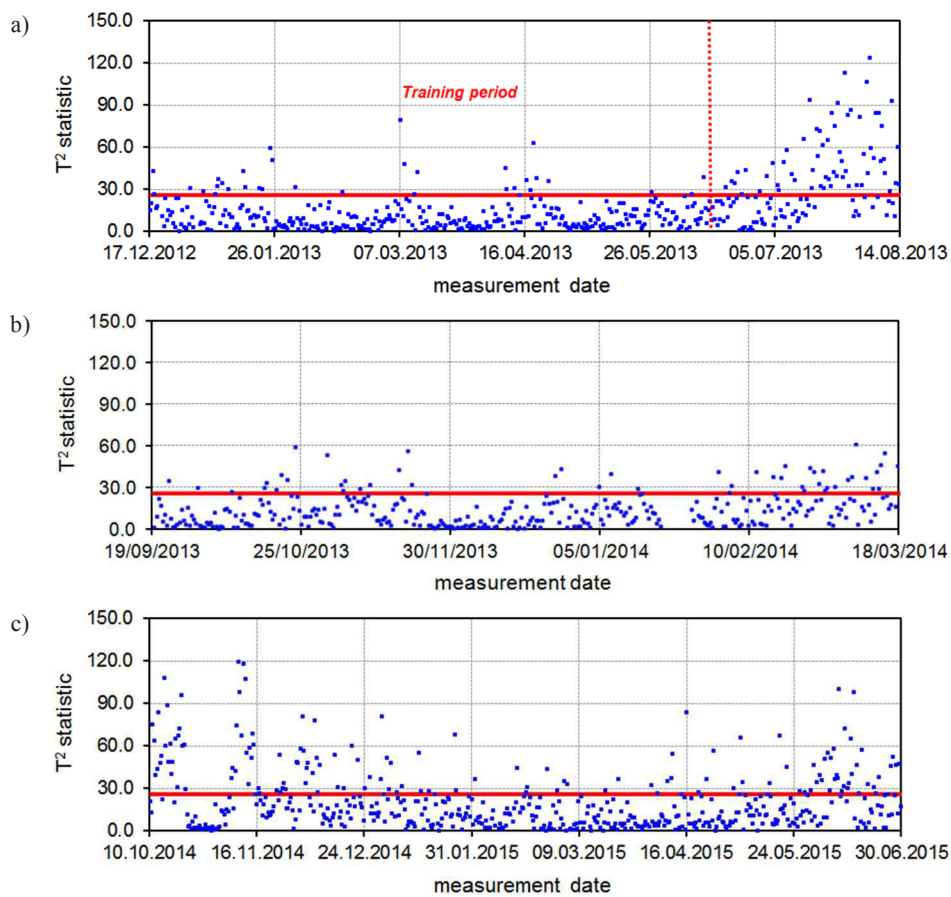

Figure 4.84 *Shewart T* control chart (PCA) referred to the time intervals: a) 17/12/2012-13/08/2013; b) 19/09/2013-17/03/2014; c) 10/10/2014-30/06/2015

The reported trend looks consistent with those obtained using the input-output methods, and once again place the damage detection skills of the PCA midway between the DR and the ARX models'. In particular, on the base of the time evolution of the T^2-*statistic*, the following considerations can be drawn:

1. during the reference period (i.e. 17/12/2012-16/06/2013), the diagram exhibits values below the red line, with only few points lying outside the control region;

2. after the six months of training, corresponding to the seismic event of 21/06/2013, the values of the T^2-*statistic* increase and exceed the UCL. Furthermore, the scattering significantly increases, too. Until the suspension of the monitoring in August 2013, the plotted points exceed the control region and display high dispersion (Figure 4.84a);

3. as expected, the obtained values decrease again getting closer to colder months (Figure 4.84b). Nonetheless, it should be noted that both the dispersion and the amount outliers are slightly larger than those observed during the reference period (Figure 4.84a). This outcome confirms that the effects induced by the earthquake are never entirely recovered, providing further proof of the occurrence of irreversible structural variations;

4. when the monitoring is resumed, on 10/10/2014, the trend of the T^2-*statistic* looks comparable to that observed after the earthquake, both in terms of scattering and value (Figure 4.84c). The fact that, after one year and in similar temperature conditions, the magnitude of the plotted feature did not change significantly is in accordance with the assumption of no permanent structural changes occurred during this time period;

5. as a consequence of the worsening of the prediction skills of the PCA, the dispersion and values of the T^2-*statistics* progressively decrease approaching Winter 2014/2015 (Figure 4.84c). The increased amount of outliers with respect to the reference period is even more evident in this case. This is

conceivably related to the presence of several episodes of stronger ambient excitation during the last 9 months of monitoring, as described in paragraph 4.7.1. Furthermore, moving towards Summer 2015, it is clear the tendency of the plotted feature to assume values comparable to those detected after 21/06/2013.

Concluding remarks

The implementation and application of the PCA to the estimates of the automated OMA revealed performances of the output-only method midway between those of the input-output models: in terms of prediction, PCA performed better than dynamic regression but could not match the accuracy of the ARX model; on the other hand, the damage detection skills of the multiple regression analysis allowed to better highlight the structural variations induced by the Garfagnana earthquake, whereas the same changes were not as obvious for the PCA. Indeed, had not been known that a significant earthquake occurred on 21/06/2013, the variations detected from the time evolution of residual error and depurated frequencies would not raise any alarm. Conversely, clear evidence of the occurrence of structural modifications was provided by the control charts.

To conclude, the results obtained by adopting the PCA confirmed the considerations made in the previous paragraphs. After the removal of the environmental effects, the control chart allows to clearly detect the drop of the natural frequencies occurred on 21/06/2013, revealing the occurrence of damage caused by the seismic event. Moreover, the time evolution of the investigated environment-independent features proves the damage to be irreversible and reveals that no further permanent structural modifications occurred during the 30 months of monitoring.

-Page intentionally left blank-

5 Structural Health Monitoring of the *San Vittore* bell tower in Arcisate, Italy

5.1 Introduction

The bell-tower of the *San Vittore* church in Arcisate (Varese, Northern Italy) has been studied by Politecnico di Milano since 2007. The past research [Binda et al. 2012, Gentile & Saisi 2013, Cabboi 2013, Gentile et al. 2015] involved: (a) historic and documentary studies; b) survey of the tower geometry and of the crack pattern; (c) non-destructive and slightly destructive tests of materials; (d) ambient vibration tests and modal identification; (d) FE modeling and vibration-based updating of the model; (e) continuous dynamic monitoring [Cabboi 2013] for several months (from June 2009 to February 2010).

It should be noticed that a static monitoring system [Binda et al. 2012], installed in the tower during the dynamic monitoring, indicated that no abnormal changes of the structural condition occurred and, at the same time, provided several temperature sensors to complement the dynamic monitoring and especially to evaluate if the availability of more temperature measurements improves the prediction of the environmental effects on modal frequencies.

This Chapter, after a brief description of the tower and the past research activity, focuses on the results of the continuous dynamic monitoring and on the application of the vibration-based SHM methodology outlined in the previous Chapter 3. As the tower was extensively studied in the past, the original contribution herein presented consists in the evaluation of the prediction skills of dynamic regression models when more temperature measurements are available.
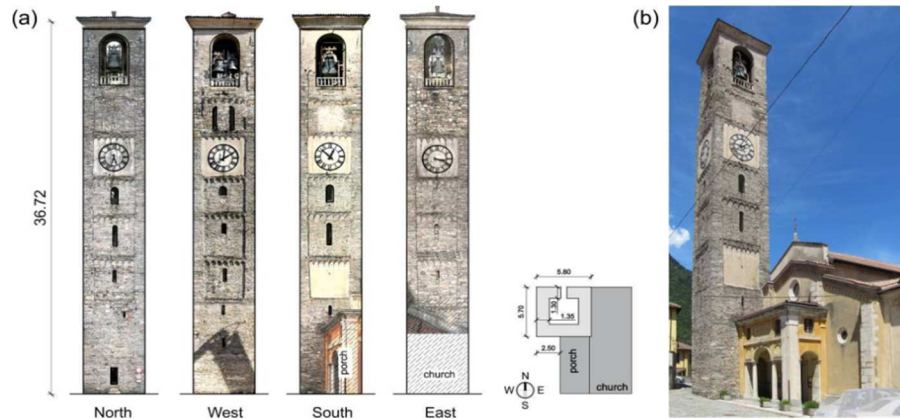
Figure 5.1 a) Fronts and b) general view of the *San Vittore* bell tower
[Gentile et al. 2015]

5.2   Description of the tower and historic background

Dedicated to St. Vittore, the church named *Chiesa Collegiata di San Vittore* in Arcisate (Varese, Northern Italy) was built in the XV century to replace the previously existent structure, erected in the IV century and modified six centuries later [Giampaolo 1960]. Connected to the church on the East side and partly on the South side is the bell tower (Figure 5.1), 37.0 m high and characterized by a 5.8 m square plan. The tower was built using stonework masonry and its foundations probably date back to the late Roman age, when the first church was constructed.

The first available historic document mentioning the tower dates back to the 1600s, and consists of a request submitted by St. Carlo Borromeo to modify the access to the building. Over the past centuries, the tower underwent several modifications and suffered significant damage, as reported in [Cazzani 1964]: in 1702 a lightning struck the top region of the building and caused severe damage, whereas the presence of meaningful cracks, concentrated in the masonry area between the porch and the tower, was reported at the beginning of the XX century.
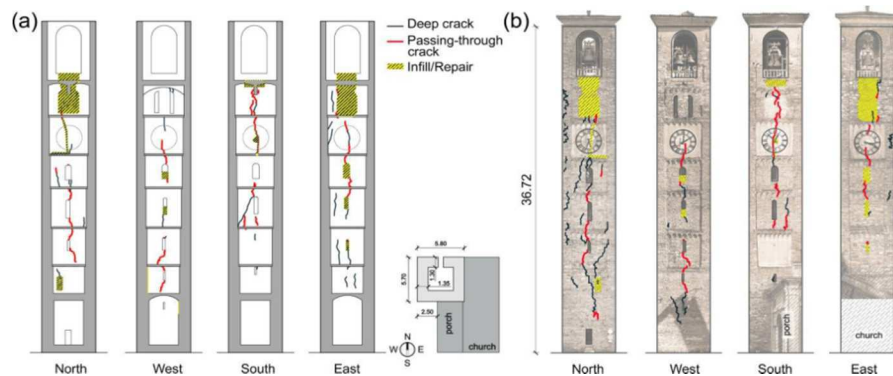
218

Figure 5.2 Crack patterns on: a) the vertical cross-sections and b) the fronts
[Gentile et al. 2015]

The structure is characterized by seven order of floors: the first five orders are detectable through masonry offsets at the corners and corresponding sequences of small hanging arches marking the floor level; the upper two levels were probably added in the XVIII century to host the bell trusses. The thickness of the masonry walls decreases progressively along the height, from 135 cm at the ground level down to 65 cm at the top floor [Binda et al. 2012].

The results obtained from non-destructive tests (i.e. sonic tests) and extensive on-site survey revealed a generally compact and well-realized stone masonry. Nevertheless, in several localized areas the masonry texture appears highly disordered and characterized by the presence of vertical joints. It is worth mentioning that the visual inspection was made especially difficult by the insufficient stone interlocking and erosion of mortar joints, leading to a difficult detection of the cracks. Hence, the crack pattern has also been investigated by means of an aerial platform, which allowed a closer inspection of the whole external wall surface and the detection of the flaw paths. As reported in Figure 5.2, the tower exhibits long vertical cracks on every side.

Most of the cracks, mainly observed between second and third floor order, even cross the entire wall thickness and pass through the keystones of the arch window openings. Aside from those major cracks, a diffused superficial pattern

219

was also detected on the tower's surface, particularly on the two fronts not connected to the church (i.e. North and West fronts, Figure 5.2).

The numerous superficial masonry discontinuities detected and the observed changes of the masonry texture, suggest the presence of past modifications. Such different construction phases, along with the realization of the floors, are unfortunately not datable.

Finally, it is to be noted that the visual inspection revealed the presence of widespread mortar erosion and infilled openings in the upper part of the tower, mainly on the East and North fronts (Figure 5.2). Furthermore, the infillings often appeared to be not properly linked to the surrounding load bearing masonry. Such results suggest that the area right beneath the belfry could conceivably be considered the most vulnerable part of the tower.

5.3   Preliminary ambient vibration tests

5.3.1   Testing procedures and modal identification

The modal characteristics of the bell tower have been identified by means of two ambient vibration tests (AVTs), performed in June 2007 and one year later, in June 2008. The acquisition system was very similar to the one used to investigate the dynamic behavior of the *Gabbia* tower and described in the previous chapter: a 16-channel data acquisition system, WR 731A piezoelectric accelerometers and WR P31 power unit/amplifier, connected to each sensor with a short cable (1.0 m) to power the accelerometer's internal amplifier, signal amplification and selective filtering. The response of the tower has been measured in 15 selected points, belonging to 5 different cross-sections identified along the height of the building. The sensors' layout adopted for the AVTs is reported in Figure 5.3, whereas Figure 5.4 shows the mounting of accelerometers 7-9 in the instrumented level at 22.78 m (Figure 5.3c).
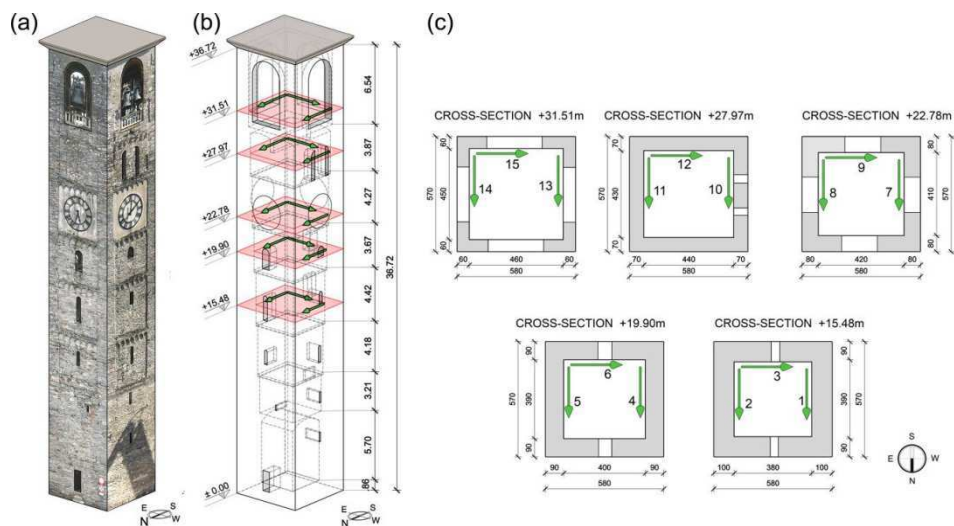
Figure 5.3 a) View of the tower; b) - c) Sensors' layout adopted in the dynamic tests and position of the accelerometers (dimensions in m) [Gentile et al. 2015]

Figure 5.4 Mounting of the accelerometers at test points 7 (a) and 8-9 (b)

Time windows of 3600 s have been adopted in both tests to acquire the acceleration time-histories induced by ambient excitation. This choice also allowed to comply with the mentioned recommendation for OMA techniques of a time windows' duration ranging between 1000 and 2000 times the fundamental period of the structure [e.g. Cantieni 2005]. It is worth mentioning that very low levels of ambient vibrations were experienced during both tests,

with the recorded acceleration never exceeding 0.4 cm/s^2.

A sampling frequency of 200 Hz has been adopted for the tests. As the significant frequency content of signals is below 6 Hz, low pass filtering and decimation have been applied to the recorded data before using the identification tools. This allowed to reduce the sampling frequency from 200 Hz to 20 Hz and obtain 72000 of samples per hour, with a time sampling of 0.05 s.

5.3.2   *Dynamic characteristics of the tower*

The extraction of the modal parameters from the recorded ambient vibration data has been carried out by using the SSI-Data method available in the commercial software ARTeMIS [SVS 2012]. The estimates of the natural frequencies have also been verified by inspecting the first Singular Value (SV) line of the spectral matrix, which is the mode indication function adopted in the FDD technique.

Notwithstanding the low level of ambient excitation experienced during both tests, the modal analysis performed by applying the SSI-Data technique to all of the collected data sets allowed to identify 5 vibration modes within the frequency range 0-6 Hz. The corresponding results are presented in Figure 5.5: the reported charts show the first SV line of the spectral matrix and the stabilization diagram obtained by applying the FDD and the SSI-Data algorithms, respectively, to each of the recorded datasets. The inspection Figure 5.5 reveals a clear accordance between SSI and FDD procedures: the alignments of stable poles identified by the SSI technique allow a clear identification of the vibration modes of the structure and correspond to well-defined local maxima of the first SV line of the FDD methods.

The natural frequencies and modal damping ratios identified via SSI-Data are summarized in Table 4-2. The inspection of Figure 5.5 and Table 4-2 reveals very close values of the modal frequencies estimated from the two tests.
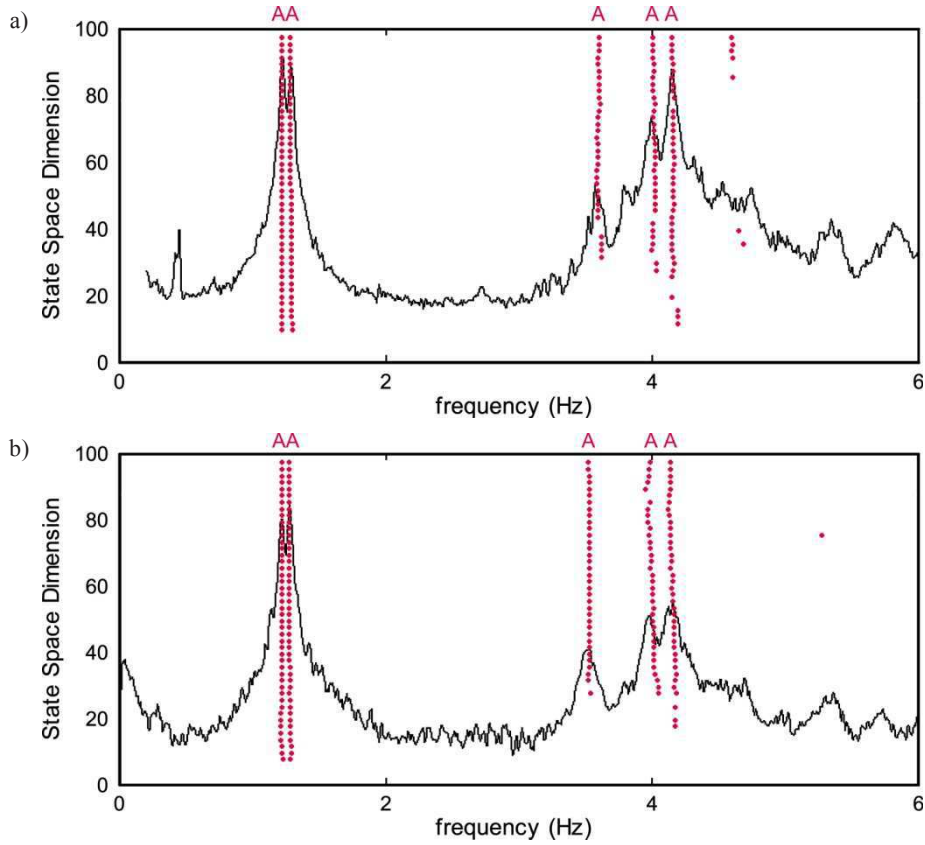
222

Figure 5.5 First Singular Value line (FDD), alignments of stable poles (SSI-Data) and automatic (A) identification of modal frequencies: a) June 2007; b); June 2008 [Gentile et al. 2015]

Table 5-1 Natural frequencies identified (SSI-Data) in the June 2007 and June 2008

Mode	f(Hz)		σ_f(Hz)		ξ (%)		σ_ξ (%)	
	2007	2008	2007	2008	2007	2008	2007	2008
B_1	1.216	1.207	0.001	0.004	1.16	1.15	0.210	0.270
B_2	1.283	1.272	0.003	0.002	0.91	0.88	0.290	0.270
T_1	3.598	3.545	0.010	0.016	1.49	1.55	0.17	0.56
B_3	4.009	3.979	0.006	0.009	1.62	1.34	0.16	0.45
B_4	4.156	4.157	0.005	0.012	1.17	1.78	0.19	0.48

B = bending mode; T = torsion mode

$f_{SSI} = 1.216$ Hz $f_{SSI} = 1.283$ Hz $f_{SSI} = 3.598$ Hz $f_{SSI} = 4.009$ Hz $f_{SSI} = 4.156$ Hz
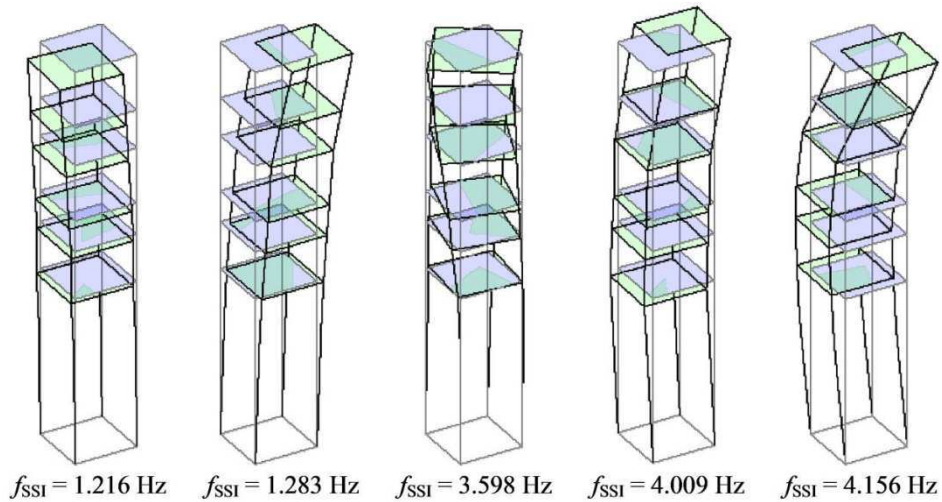
Figure 5.6 Vibration modes identified from ambient vibration data (SSI-Data, June 2007) [Gentile et al. 2015]

Furthermore, an excellent accordance is also observed in terms damping ratios, for the three lower modes.

Also the mode shapes identified in the two AVTs exhibit high accordance. Therefore, only the mode shapes estimated in June 2007 are shown in Figure 5.6. As expected from the structural scheme of the investigated structure, the detected modes can be classified as bending and torsion: four out of the five identified modes are dominant bending (B) (i.e. the first two, B_1-B_2, and the last two, B_3-B_4), whereas the remaining mode can be classified as torsion (T1). It is worth noting that the flexural displacements characterizing the dominant bending modes are mainly oriented along the diagonal directions.

5.4 Continuous dynamic monitoring: description of the system

In June 2009, a continuous dynamic monitoring system (Figure 5.7) was installed in the tower in order to better understand and investigate the time variance of the natural frequencies. The system acquired the tower's response to ambient excitation for eight months (from 25/06/2009 until 22/02/2010), although the monitoring had to be interrupted several times for maintenance reasons and to allow the installation of a new electrical system in the tower.
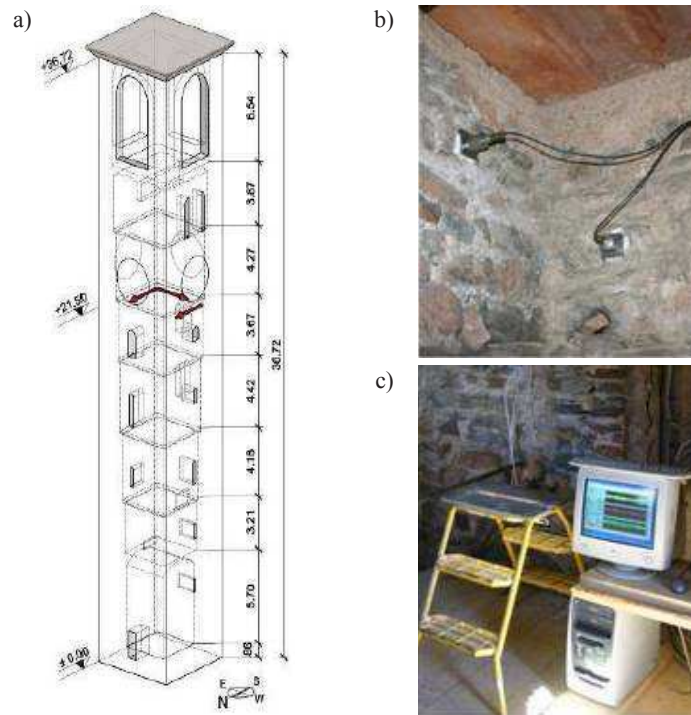

Figure 5.7 (a) Sensors layout (dimensions in m) adopted in the continuous dynamic monitoring of the *San Vittore* bell tower; (b) Accelerometers; (c) PC on site

The instrumentation installed inside the structure consisted of 3 uni-axial Dytran 3191A1 piezoelectric accelerometers (10 V/g, Figure 5.7b), a 4-channel data acquisition system (NI 9234) and one local PC to manage the continuous

acquisition and store the recorded (Figure 5.7c). Every hour, a new binary file containing the acceleration time series (sampled at 200 Hz) was created and stored in the local PC. The results obtained from the preliminary AVTs allowed to select the instrumented level so that all previously identified modes could still be detected: eventually, the three accelerometers were installed at 21.50 m from the ground level (Figure 5.7a).

The management of the acquired data was performed by applying the same LabVIEW toolkits used for the *Gabbia* tower, described in [Busatta 2012] and consisting of the automated execution of the following tasks:

1. creation of a database with the original data;
2. preliminary pre-processing (i.e. de-trending, automatic recognition and extraction of possible seismic events, creation of 1 dataset per hour);
3. evaluation of hourly-averaged acceleration amplitudes and temperature;
4. low-pass filtering and decimation of each dataset;
5. creation of a second database, with essential data records, to be used in the modal identification phase.

As previously mentioned, a static monitoring system installed few years earlier by the Politecnico di Milano [Binda et al. 2012] provided hourly average values of the wall temperatures. The static system was mainly aimed at monitoring the evolution of the crack pattern of the tower and consists of 15 extensometers and 8 temperature sensors, measuring internal and external wall temperature at different levels of the structure.

5.5 Continuous dynamic monitoring: general results

Consistently with the methodology adopted for the *Gabbia* tower, the modal parameters of the structure have been extracted from the measured acceleration data by using the automated procedure proposed in [Cabboi 2013] and based on the SSI-Cov algorithm. With regards to the calibration process, the model's

parameters and thresholds have been fixed by performing several manual analyses of the collected data-sets. Eventually, the following values have been selected:

1. the SSI-Cov time lag parameter i was set equal to 80;

2. data have been fitted using stochastic subspace models with order ranging between 30 and 120;

3. since the preliminary AVTs did not reveal the presence of complex modes, the automated cleaning and interpretation of the stabilization diagrams has been performed by using a threshold value of the MCF index equal to 0.2;

4. the tracking of the most meaningful modes has been carried out using a baseline list based on the results of the first AVT. Furthermore, threshold values have been set so that identified modes are kept when the variation is lower than 15% for frequency and higher than 0.85 for the MAC.

Figure 5.8 presents the time evolution of the indoor and outdoor temperatures recorded during the monitoring. Among the 8 available temperature measurements, only the data acquired on the inside of the East front (T-E1int) and on the outside of the North front (T-N3ext) have been used to investigate the correlation with the automatically identified natural frequencies. The choice was based on the correlation analysis performed in [Cabboi et al. 2013], which revealed those two temperatures to be the most representative of the internal and external thermal condition of the tower, respectively. The trends reported in Figure 5.8 exhibit fluctuations between -5°C and 30°C for both temperatures. Furthermore, it can be clearly observed that the external temperature is characterized by larger daily variations, observed especially during warm months (i.e. from June until October). Conversely, the inner temperature recorded on the East front exhibits a much smoother behavior. This difference between the two trends can be explained by considering the thermal inertia of the masonry walls, which provides an internal thermal environment

less susceptible to the large daily fluctuations of the outside temperature.

Figure 5.9 shows the evolution in time of the five identified natural frequencies during the monitoring period. From the inspection of the presented graph, the following observations are allowed:
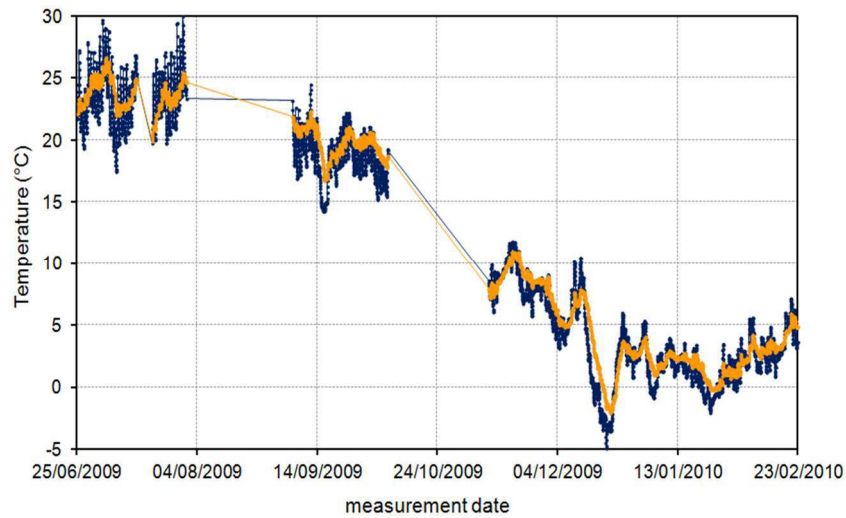

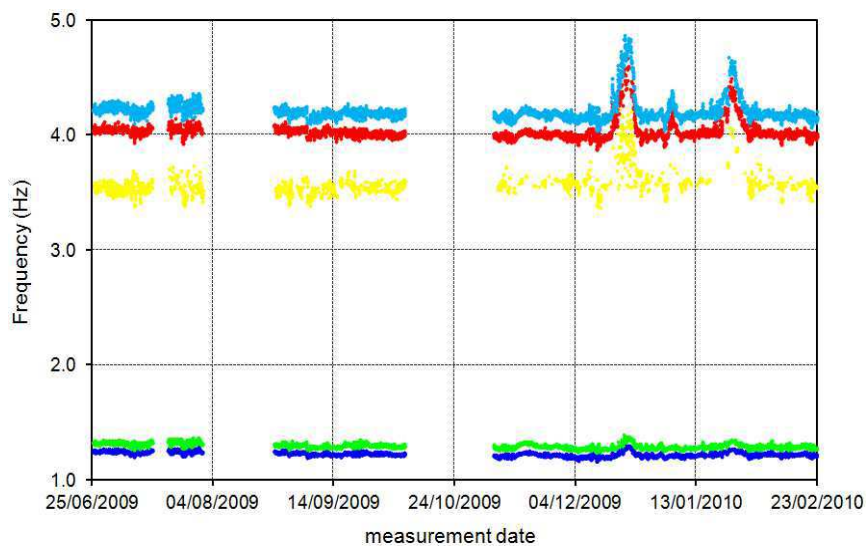**Figure 5.8** Temperature variation between 25/06/2009 and 22/02/2010

Figure 5.9 Variation of identified natural frequencies between 25/06/2009 and 22/02/2010

228

1. the frequencies of the bending modes exhibit a regular and lightly dispersed evolution, whereas a more scattered trend is detected for the torsion mode. Furthermore, the bending modes are characterized by a higher identification rate. This behavior is probably a consequence of the low level of ambient excitation that existed during the monitoring;

2. the modal frequencies often exhibit slight fluctuations over the monitoring period. Since only the response to micro-tremors and wind has been considered, these variations are likely related to temperature effects. Furthermore, the oscillations of the identified frequencies seem to be in phase with the temperature variations reported in Figure 5.8;

3. in December, January and February, three abrupt and significant increases of the natural frequencies can be observed, especially for the upper three modes. A thorough inspection of Figure 5.9 and the comparison with the temperature trends reported in Figure 5.8 reveal a correspondence between such variations and the occurrence of temperatures around 0°C. Therefore, this behavior can reasonably be related to the freezing of the structural system (including its foundation) and to the progressive development of ice, which causes a temporary stiffening of the structure by filling and closing minor and major cracks.

The statistics corresponding to the automatically identified frequencies are summarized in Table 5-2 through mean values, standard deviations and extreme values. The average values of the natural frequencies have also been compared to the correspondent quantities identified during the preliminary AVTs. It should be noted that the reported results have been obtained by omitting the three data intervals associated with low temperatures. As it can be observed, the torsion mode is characterized by a higher standard deviation than the bending modes, confirming the previously mentioned identification issues.

Table 5-2 Natural frequencies identified during the AVTs and statistics of the natural frequencies identified between 25/06/2009 and 22/02/2010 (SSI-Cov)

Mode	2007 f (Hz)	2008 f (Hz)	Monitoring f_{ave} (Hz)	σ_f (Hz)	f_{min} (Hz)	f_{max} (Hz)
B_1	1.211	1.211	1.228	0.019	1.162	1.290
B_2	1.289	1.270	1.297	0.021	1.240	1.367
T_1	3.564	3.525	3.553	0.057	3.371	3.774
B_3	3.984	3.984	4.023	0.034	3.880	4.184
B_4	4.141	4.141	4.196	0.042	4.043	4.372

B = bending mode; T = torsion mode

In order to better investigate the correlation with temperature, the automatically identified frequencies have been plotted versus indoor (Figure 5.10) and outdoor (Figure 5.11) temperature. Based on the temperature-frequency plots, the following comments can be made:

1. the effect of low temperatures and the consequent variation of the dynamic characteristics of the tower is clearly observed in both graphs. In particular, the modal frequencies rapidly increase and exhibit a higher dispersion for temperatures values around 0°C, with this behaviour being more evident for the three upper modes;

2. for temperatures out of the ice-risk interval, the diagrams of the four bending modes exhibit a positive slope. Conversely, a flat trend can be observed for mode T_1 both in Figure 5.10 and Figure 5.11. This behavior confirms the existence of a correlation between temperature and bending modes, but also suggests that temperature exerts a limited influence on the torsion mode;

3. two distinct populations of frequency-temperature points can be observed for each mode. In particular, a first group can approximately be detected for indoor temperatures below 11°C and external temperatures below 12°C. The second cluster is identified for internal temperatures over 17°C and external temperatures over 14°C. The two clouds exhibit dissimilar slopes, revealing

a variation in the frequency-temperature correlation within the investigated temperature range. This difference can be better detected by studying the diagrams reported in Figure 5.12 and Figure 5.13 (referred to the four bending modes), where the effects of low temperatures have been omitted;
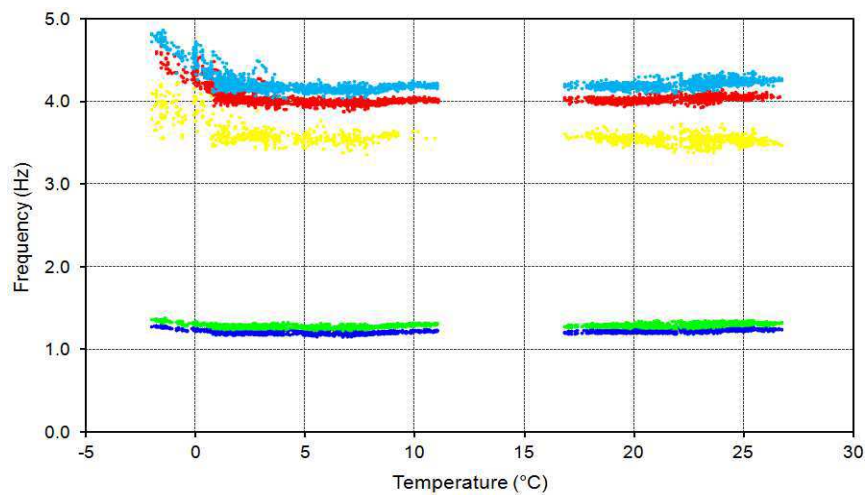

Figure 5.10 Frequency (SSI-Cov) variation vs measured indoor temperature T-E1int between 25/06/2009 and 22/02/2010 (including low temperature periods)
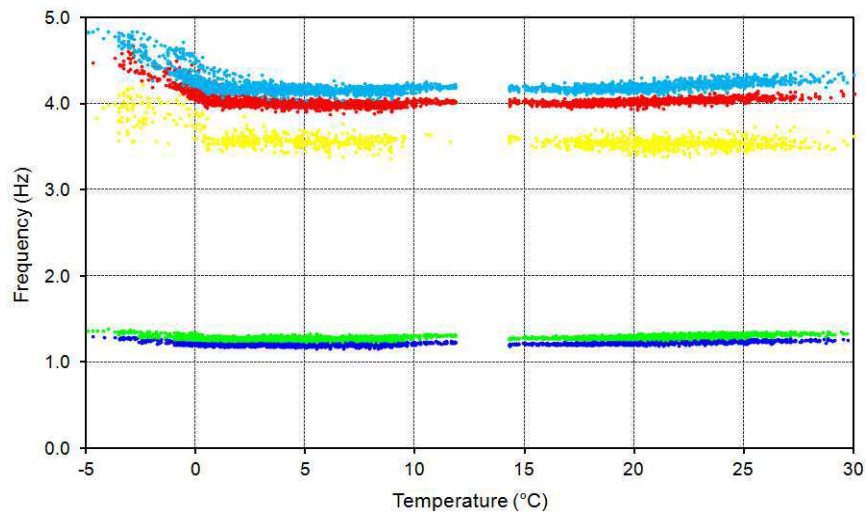

Figure 5.11 Frequency (SSI-Cov) variation vs measured outdoor temperature T-N1ext between 25/06/2009 and 22/02/2010 (including low temperature periods)
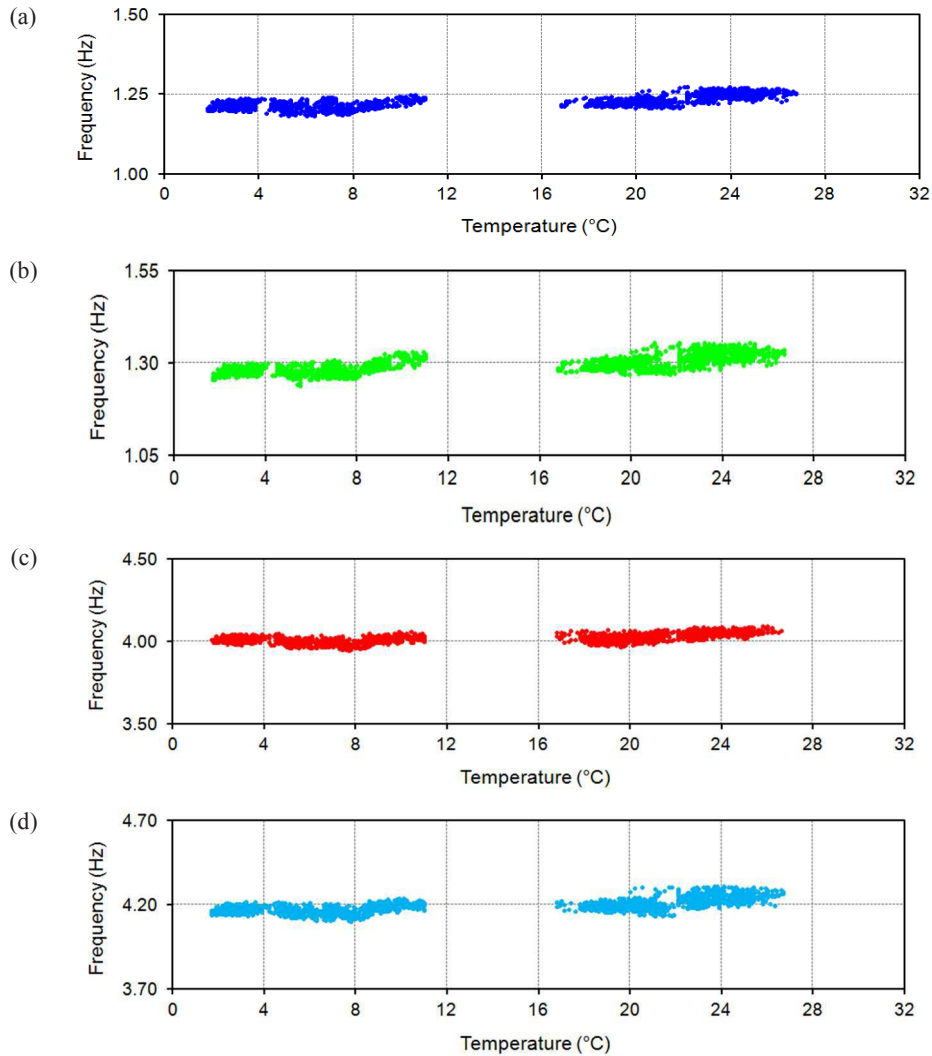
231

(a)

(b)

(c)

(d)

Figure 5.12 Frequency (SSI-Cov) variation vs. measured indoor temperature T-E1int (low temperature periods removed): (a) mode B_1, (b) mode B_2, (c) mode B_3, (d) mode B_4

4. for the cluster characterized by higher temperatures, all diagrams show a clear tendency of the bending frequencies to increase with an increased temperature. This trend is consistent with the one observed for the *Gabbia* tower and can be explained by the temporary increase of stiffness and modal frequencies due to the thermal expansion of materials, which determines the

temporary closure of superficial cracks, minor masonry discontinuities or mortar gaps. Such correlation can be observed for both internal and external temperatures, even though a higher scattering is observed in the former case. This outcome is related to the high thermal inertia of the masonry walls that determines an almost constant internal thermal condition of the tower;
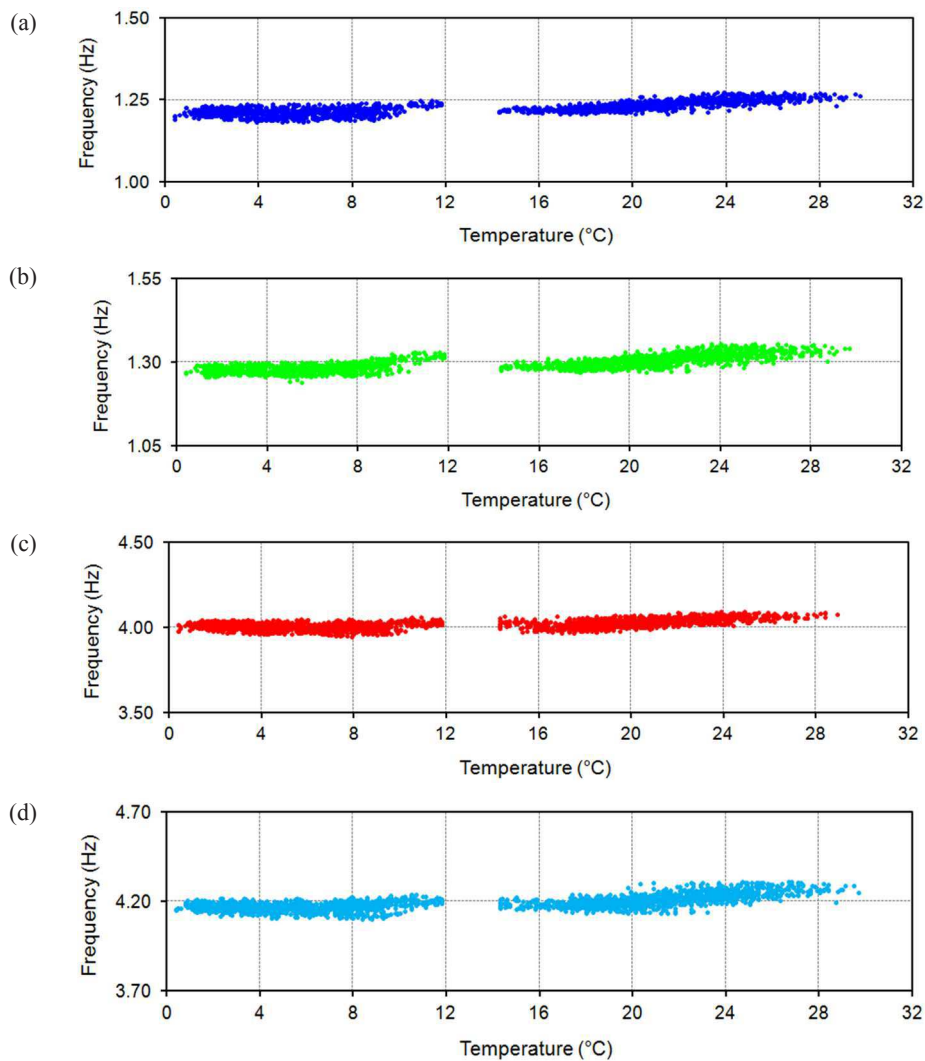

Figure 5.13 Frequency (SSI-Cov) variation vs. measured outdoor temperature T-N1ext (low temperature periods removed): (a) mode B_1, (b) mode B_2, (c) mode B_3, (d) mode B_4

5. when temperatures assume values in the lower of the two detected ranges, the reported correlation weakens. In particular, the slopes of the frequency-temperature clouds decrease, becoming almost null for modes B_3 and B_4. Therefore, even if temperatures around 0°C are omitted, the described behavior defines a slightly bi-linear correlation between bending frequencies and temperature (both internal and external). Indeed, this non-linear dependence is expected to produce some effects in the results of the linear models adopted to remove the effects of environmental factors, as it will be described in the following section 5.6.

5.6   Modeling and removal of temperature effects

The correlations diagrams showed in Figure 5.10-Figure 5.13 revealed the non-negligible influence of temperature on the dynamic behavior of the *San Vittore* bell tower. Therefore, the same strategy described in Chapter 3 and applied to the *Gabbia* tower (see Chapter 4), has been herein adopted to mitigate the effects of temperature on the experimental natural frequencies. The obtained features, insensitive to the environmental effects, have subsequently been used to investigate the structural condition of the bell tower. In particular, the detection of structural anomalies has again been performed by exploring the time evolution of prediction errors and experimental frequencies depurated from the temperature effects. Furthermore, the damage detection process has been completed by applying the *Shewhart T* control chart.

Before moving on to the description of the results, it is necessary to point out a major difference with respect to the case of the *Gabbia* tower. In the previous case study, the monitoring system was characterized by a single temperature sensor installed on the outside of the S-W front. Therefore, in the process of removing the environmental effects, the measurements collected by such sensor were the only quantities available as input of the adopted input-output models

234

(i.e. dynamic regression and ARX). In the present case, the inputs have been chosen among the 8 different temperatures collected by the existing static monitoring system. This allowed to establish input-output relationships characterized by more than a single input. In particular, as previously mentioned, correlation studies [Cabboi et al. 2013] revealed the wall-temperatures recorded by sensors E1int (inside of the East front) and N3ext (outside of the North front) to be the most representative of the internal and external thermal condition of the tower, respectively. Therefore, those quantities have been adopted as inputs for the following analyses. Indeed, the availability of internal and external temperature sensors should allow a more comprehensive evaluation of the thermal effects on the natural frequencies. Therefore, non-negligible enhancements of the predictions are expected with respect to the previous case study.

The effects of temperature have been minimized by applying a dynamic regression model implemented in Matlab. In particular, the model has firstly been implemented by taking into account only the outdoor temperature. Afterwards, the measurements collected by the internal sensor have been considered too. This double passage allowed to better highlight the expected improvements of the model's performances when a larger number of inputs is available. It is also worth reminding that, due to the identification issues experienced for mode T_1 over the whole monitoring period, the decision has been made to neglect the torsion mode in the following analyses. Therefore, only the results referred to bending modes B_1-B_4 will be presented in the following.

5.6.1   Single Input Dynamic Regression model: external temperature

Consistently with the study of the *Gabbia* tower, a dynamic linear regression model (see Chapter 1) has been established between the value f_k of the natural

frequencies at time k and the temperatures recorded by the external sensor N3ext at the same time k as well as at previous time instants. For simplicity, in the following the model will be referred to as SIDR (Single Input Dynamic Regression).

Since the quality of the obtained predictions is determined by the amount of past values of the input, the performances of the SIDR model have been assessed using three quality criteria (see Chapters 3 and 4): *Loss Function* (LF), *Aikake's Final Prediction Error* (FPE) and *coefficient of determination R^2* [Ljung 1999, Johnson & Wichern 1992]. Based on those criteria, 16 values of the external temperature were selected: one at the current time and 15 referred to previous hourly time intervals.

The calibration of the parameters of the model has been performed by considering a training period of 7 months (i.e. between 25/06/2009 and 15/01/2010). As it can be observed in previous Figure 5.8, the selected reference interval takes into account the whole range of variation exhibited by the external temperature during the monitoring activity, therefore leading to a more accurate understanding of the thermal condition of the tower. It should also be noted that the time frames characterized by very low temperatures have been taken out of the training period, for the corresponding experimental frequencies are not representative of the common operational conditions but descend from an anomalous behavior of the structure.

To validate the implemented regression model, experimental and numerical results have been compared over the reference period. It should be reminded that, in the case of the *Gabbia* tower, the slight non-linear dependence of frequency on temperature led to changing performances of the model for high and low temperatures (see Chapter 4). Hence, a particular attention has been firstly devoted to the comparison between identified and predicted natural frequencies during warm and cold periods. The comparison is exemplified by

referring to two 12-day time frames (i.e. 26/06/2009-07/07/2009 and 26/11/2009-07/12/2009), as shown in Figure 4.40 and Figure 4.39, respectively. The inspection of Figure 4.40 and Figure 4.39 reveals a degree of accordance comparable to the one obtained for the *Gabbia* tower with the same model.
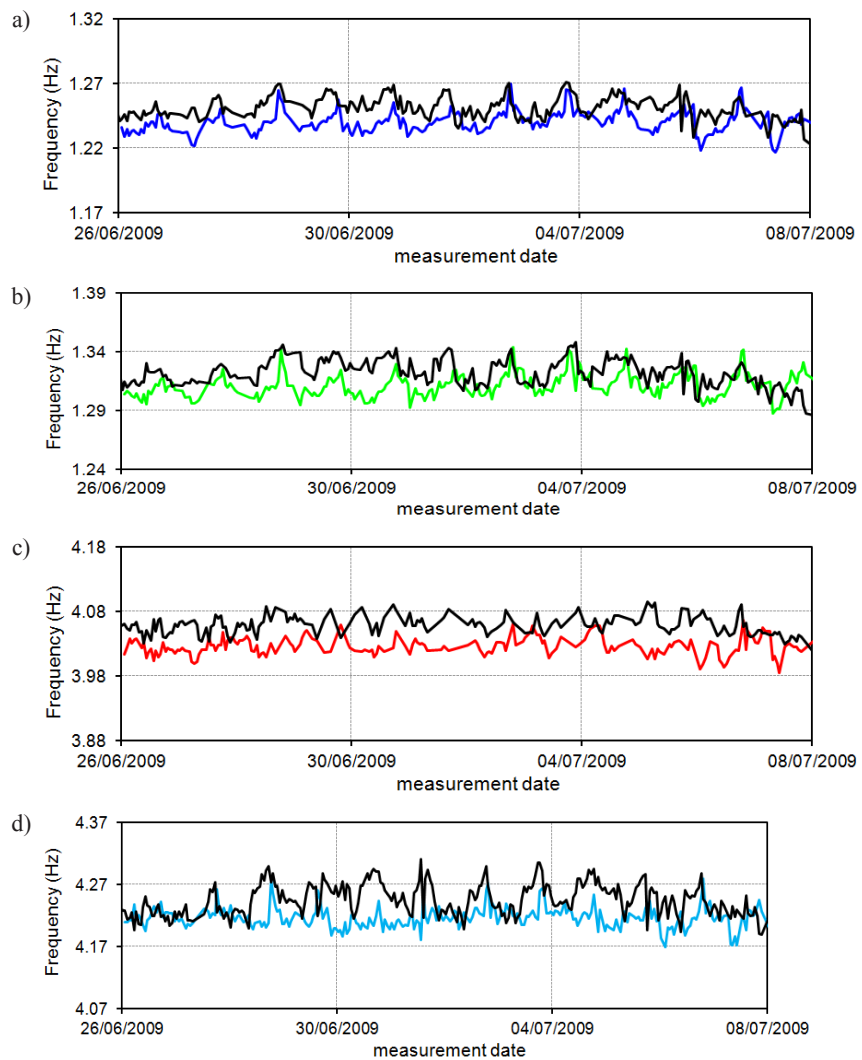

Figure 5.14 Predicted vs. Identified natural frequencies between 26/06/2009-07/07/2009 (SIDR model): a) Mode B1; b) Mode B2; c) Mode B3; d) Mode B4
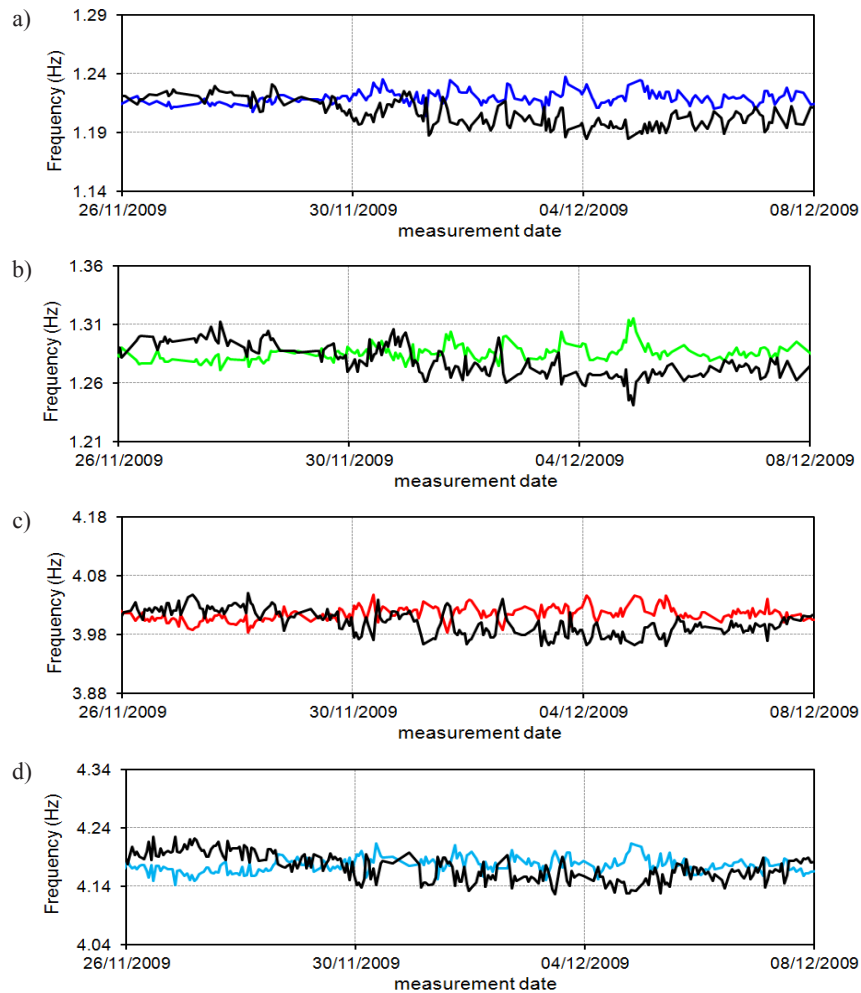
237

Figure 5.15 Predicted vs. Identified natural frequencies between 26/11/2009-07/12/2009 (SIDR model): a) Mode B_1; b) Mode B_2; c) Mode B_3; d) Mode B_4

Considering the similarity of the two case studies and of the implemented dynamic regression models, the consistency of the results seems to outline a threshold level for the accuracy achievable by using just the measurement of one external temperature. Furthermore, as for the previous case study, the check reveals a better quality of the predictions for higher temperatures (Figure 4.40), whereas the accordance worsen significantly during cold periods (Figure 4.39).

As it can be observed, discrepancies in terms of amplitude can also be detected between 26/06/2009 and 07/07/2009 (Figure 4.40), but for all four modes the predicted frequencies seem to follow the general trend of the experimental estimates. On the other hand, when a cold time interval is considered (Figure 4.39), a major discordance between the two time evolutions can be observed. Therefore, as expected from the results of the *Gabbia* tower, the described non-linearity of the frequency-temperature correlation has a non-negligible influence on the performances of the SIDR model, which is based on the assumption of linear correlation between input and output. In particular, the prediction skills of the model are not constant over the whole investigated temperature range but worsen as the temperature decreases.

After the validation process, the SIDR model has been applied to the whole monitoring period by considering the remaining five weeks (i.e. from 16/01/2010 to 22/02/2010). The obtained results have been investigated in terms of residual error and frequencies depurated from the temperature effects.

In Figure 5.16, the evolution of the residual error of the four bending modes has been reported. It should be reminded that the reported values are normalized with respect to the average value of the training period. As it can be observed, the ranges of variation obtained from the application of the SIDR model are totally comparable to those provided by the DR model for the *Gabbia* tower. As previously mentioned, this consistency seems to suggest that, for masonry towers, a better accuracy of the results could be hardly obtained when measurements of only one external temperature are adopted to establish a dynamic regression. In particular, the inspection of Figure 5.16 allows to observe that:

1. both in the training period (i.e. 25/06/2009-15/01/2010) and after the training period (i.e. the last 5 weeks of monitoring), no sudden decreases of the residual errors can be observed: the residuals still range within the defined
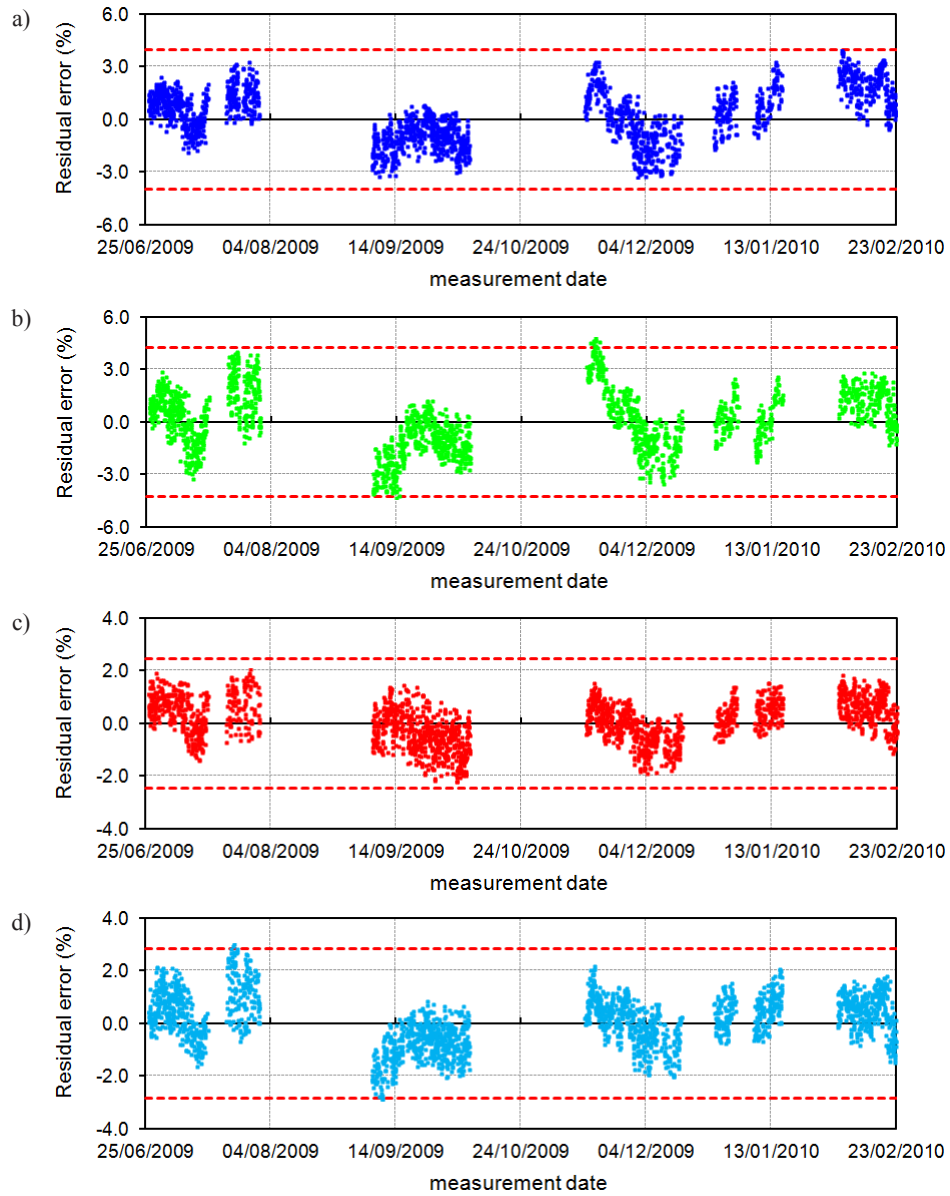
Figure 5.16 Residual error during the entire monitored time period (SIDR model): a) Mode B_1; b) Mode B_2; c) Mode B_3; d) Mode B_4

variation limits. This suggests that the structure did not suffer any remarkable modification during the investigated period and is in full agreement with the results obtained through the static monitoring system

240

[Binda et al. 2012]. which highlighted the absence of anomalous structural behaviors within the considered nine months;

2. evident long-term residual fluctuations and large dispersion of the values are revealed for all fours modes. These results are in accordance with the outcomes obtained for the *Gabbia* tower when the DR model has been applied. In particular, they seem to confirm the assumption that, when only measurements of one external temperature are available, dynamic regressions can satisfyingly reproduce the daily effects of temperature but cannot as accurately model the influence of the average temperature (see Chapter 4).

The previous conclusions are confirmed by the results obtained in terms of natural frequencies depurated from the environmental effects. Figure 5.17 reports the time evolution of the experimental estimates before and after the removal of the effects of external temperature. The time evolution of the four corrected frequencies (Figure 5.17) still reveals some non-negligible long term fluctuations. This result is consistent with the trends exhibited by the prediction error and provides further evidence that the influence of the average temperature on the natural frequencies (probably combined with the non-modeled effect of other unobserved factors) has not been successfully removed.

The application of a dynamic regression model established by using measurements of only one external temperature sensor, provided results similar to those obtained by applying the same model to the *Gabbia* tower. More specifically:

1. after the application of analogous models, the results obtained for the two case studies range within similar variation intervals. This outcome suggests that a higher accuracy is conceivably difficult to achieve when DR models are used to predict the natural frequencies of masonry towers starting from measurements of just one external temperature;
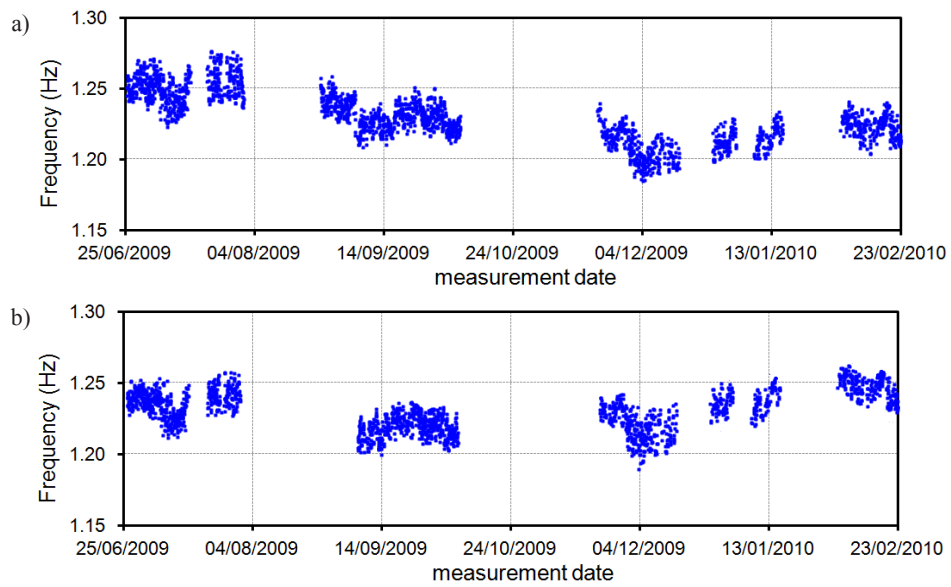
241

Figure 5.17 Mode B$_1$: time evolution of the natural frequency before (a) and after (b) the removal of the environmental effects (SIDR model)

Figure 5.17 Mode B$_2$: time evolution of the natural frequency before (c) and after (d) the removal of the environmental effects (SIDR model)

Figure 5.17 Mode B₃: time evolution of the natural frequency before (e) and after (f) the removal of the environmental effects (SIDR model)
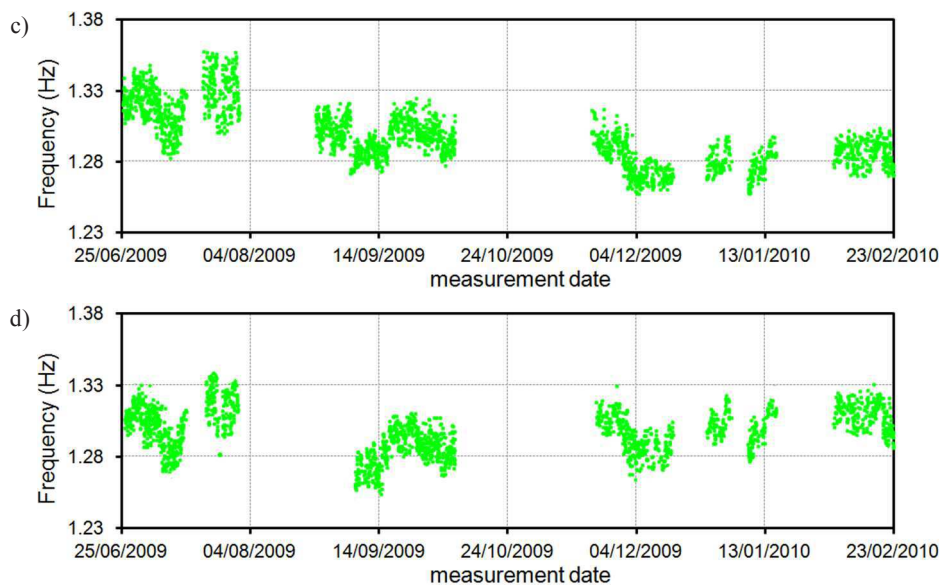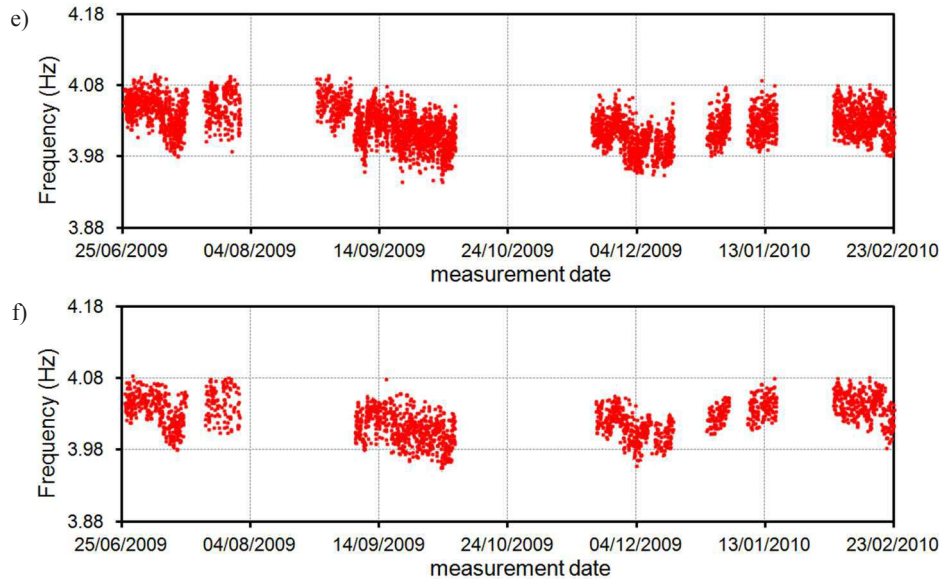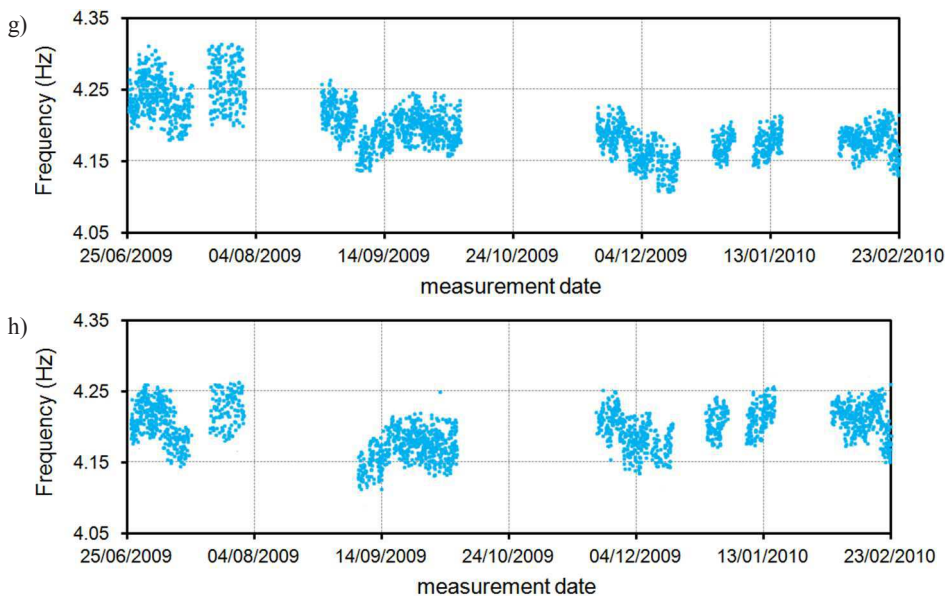

Figure 5.17 Mode B₄: time evolution of the natural frequency before (g) and after (h) the removal of the environmental effects (SIDR model)

2. the residual long-term fluctuations detected also for the present case study

confirm the assumptions made in the previous chapter: the use of previous values of one external temperature allows a significant mitigation of the daily thermal effects, but the influence of the average temperature cannot be entirely modeled. Indeed, the use of a second temperature sensor installed on the inside front of the walls might allow to indirectly take into account the effect of the average temperature. The results achieved by moving from a SIDR model to a MIDR (Multiple Input Dynamic Regression) model are discussed in detail in the next sub-section 5.6.2.

5.6.2 *Multiple input dynamic linear regression model: external and internal temperature*

In order to enhance the predictive skills of the SIDR model and remove the residual fluctuations of the corrected frequencies, a new dynamic regression model has been established by accounting for also the temperature measured on the inside of the tower. The additional input is characterized by variations over longer time periods, since the daily fluctuations of temperature significantly decrease moving from the outdoor front to the indoor. Therefore, the newly considered values are expected to indirectly take into account the effects of the average temperature and improve the quality of the predictions.

The use of *LF*, *FPE* and R^2 [Ljung 1999, Johnson & Wichern 1992] quality criteria allowed to compare the different performances obtained by varying the number of past temperatures taken into account. Eventually, a model characterized by 14 values of the inputs has been selected: 3 for the internal temperature (current time and 2 previous hourly intervals) and 11 for the external temperature (current time and 10 previous hourly intervals).

The parameters of the model have been calibrated by considering the same 7-month training period used for the SIDR relationship and defined between 25/06/2009 and 15/01/2010. Subsequently, the implemented model has been

validated by comparing experimental and numerical results. Figure 5.18 and Figure 5.19 report the overlapped time evolution of predicted and experimental frequencies over the same 12-day time frames defined in the previous paragraph and referred to warm and cold periods, respectively.
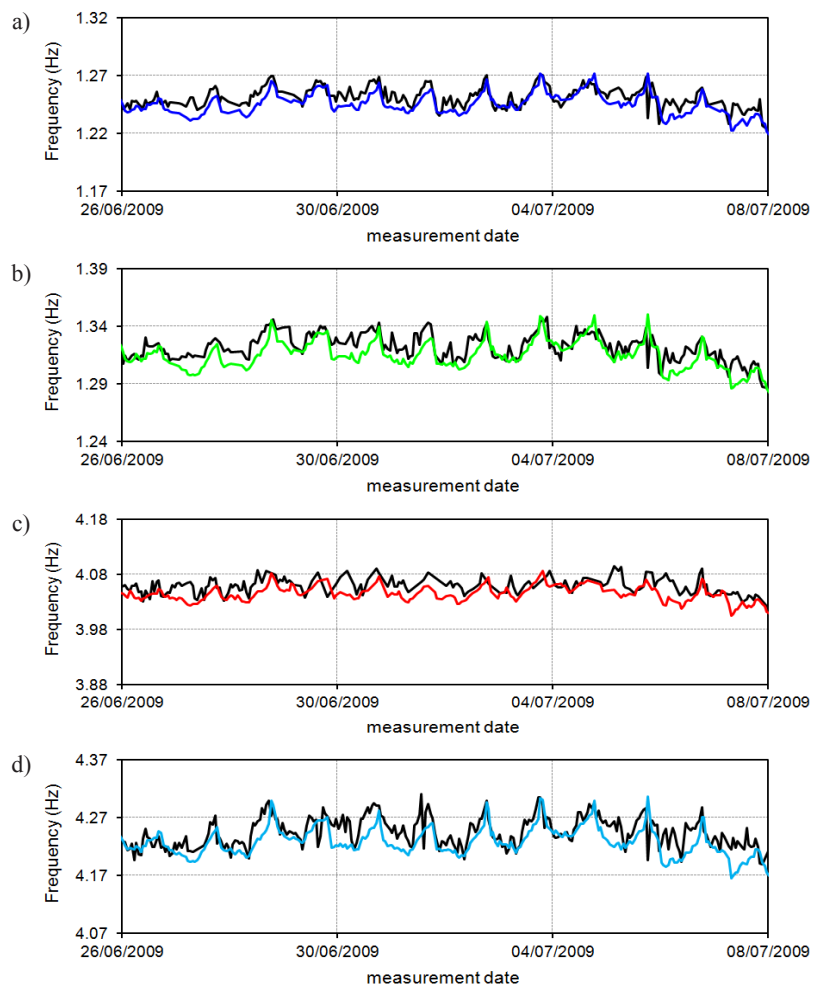

Figure 5.18 Predicted vs. Identified natural frequencies between 26/06/2009-08/07/2009 (MIDR model): a) Mode B_1; b) Mode B_2; c) Mode B_3; d) Mode B_4

245
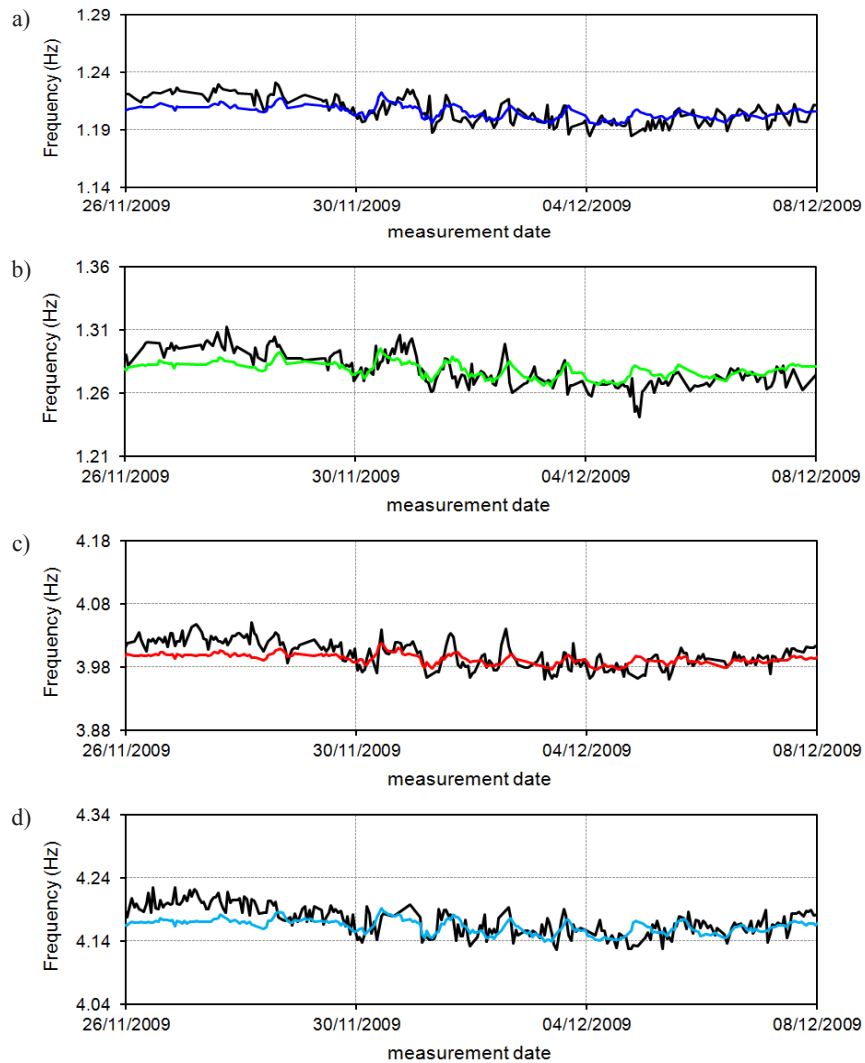
Figure 5.19 Predicted vs. Identified natural frequencies between 26/11/2009-07/12/2009 (MIDR model): a) Mode B_1; b) Mode B_2; c) Mode B_3; d) Mode B_4

With regards to the single input model (Figure 4.40 and Figure 4.39), a clear improvement in the prediction skills can be observed. In the present case, the predicted frequencies follow more accurately the daily variations of the natural frequencies and also the difference in terms of magnitude has significantly decreased. Nonetheless, a different quality of the predictions between warm and

cold time frames can still be detected: the accordance between the two trends decreases with a decreased temperature, along with an increase of the difference in terms of amplitude (Figure 5.19). This result suggests that, even by taking into account more than one input, the effects of the bi-linear frequency-temperature correlation on the prediction skills of the model cannot be completely removed.

The previous comparison seems to confirm the expectations on the additional use of temperatures recorded on the inside of the masonry fronts: previous values of the internal temperature, less oscillating than the external one and characterized by long seasonal fluctuations, allow to improve the predictive skills of the dynamic regression and lead to more accurate predictions both in warm and cold time periods.

To provide further evidence of the previous outcome and to verify the absence of relevant modifications of the structural behavior, the time evolution of the residual error of the four bending frequencies is shown in Figure 5.20. The comparison between the presented plots and those referred to a single input model (Figure 5.16) reveals that the combined use of external and internal measurements of temperature allows a relevant enhancement of the prediction skills. In particular, the following considerations can be made:

1. the fluctuations of the residuals have been sensibly reduced for all modes. The new ranges of variation can be approximately defined as: ±2.5% for modes B_1 and B_2 (Figure 5.20 a, b), ±1.5% for modes B_3 (Figure 5.20 c) and ±2% for the fourth bending mode (Figure 5.20 d). Furthermore, the reported values appear significantly less scattered, leading to more compact trends;

2. the previously detected long term fluctuations have been considerably reduced. This achievement, along with the results of point 1, confirms that the availability of internal and external temperature measurements allows a more comprehensive characterization of the thermal effects on the natural

247

frequencies. Therefore, not only the daily fluctuations, but also the effects of the average temperature can be better modeled;
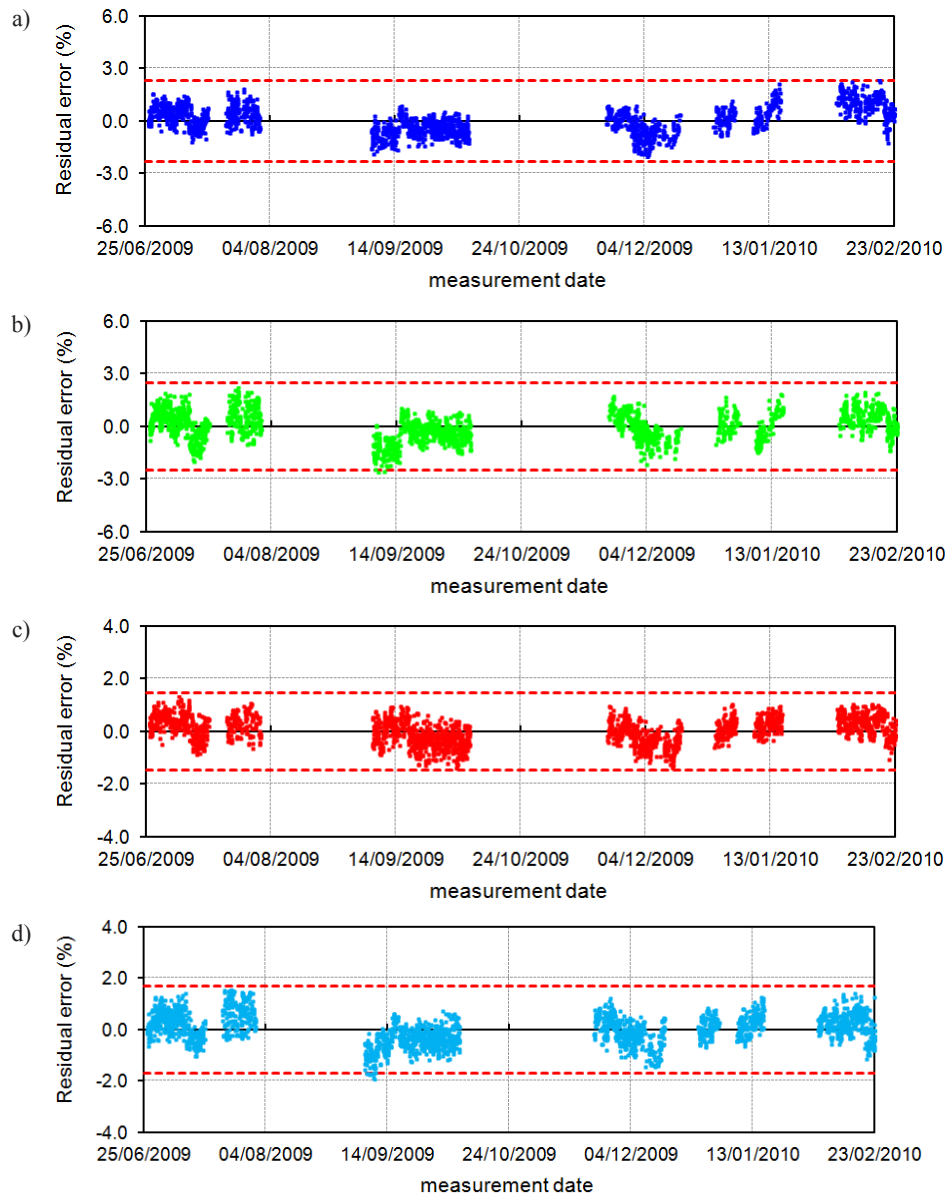

Figure 5.20 Residual error during the entire monitored time period (MIDR model): a) Mode B_1; b) Mode B_2; c) Mode B_3; d) Mode B_4

3. as no significant structural changes were documented during the static monitoring and consistently with the SIDR model, no abrupt variation of the residual errors can be observed during the dynamic monitoring period, confirming once more that the structure exhibited a regular behavior over the whole investigated period.

Of course, the enhanced prediction skills of the MIDR model are confirmed by the time evolution of the depurated frequencies reported in Figure 5.21. The comparison with the diagrams referred to the SIDR model (Figure 5.17) reveals a more successful mitigation of the temperature effects, with frequencies oscillating around the average value within a sensibly smaller range of variation. Furthermore, as for the residual error, the use of measurements of the internal temperature also led to a relevant reduction of the scattering. In particular, the following considerations are allowed:

1. after the application of the MIDR model, the time evolution of the depurated frequencies exhibit smaller fluctuations than those obtained for the SIDR. This results in straighter and less scattered trends. In particular, the new variation intervals can be defined as: 1.22-1.25 Hz for mode B_1 (Figure 5.21b), 1.28-1.32 Hz for mode B_2 (Figure 5.21d), 3.98-4.06 Hz for mode B_3 (Figure 5.21f') and 4.15-4.25 for mode B_4 (Figure 5.21h);

2. the residual long term fluctuations previously detected in Figure 5.17have been considerably reduced, confirming once more that the availability of an inner temperature sensor allows to more accurately model the effects of average temperature;

3. during the entire monitoring, the reported time evolutions are characterized by a regular trend with no sudden variations. This outcome provides further proof of the absence of relevant structural variations within the investigated time period.

a)

b)

Figure 5.21 Mode B_1: time evolution of the natural frequency before (a) and after (b) the removal of the environmental effects (MIDR model)

c)

d)

Figure 5.21 Mode B_2: time evolution of the natural frequency before (c) and after (d) the removal of the environmental effects (MIDR model)

250

e)

f)

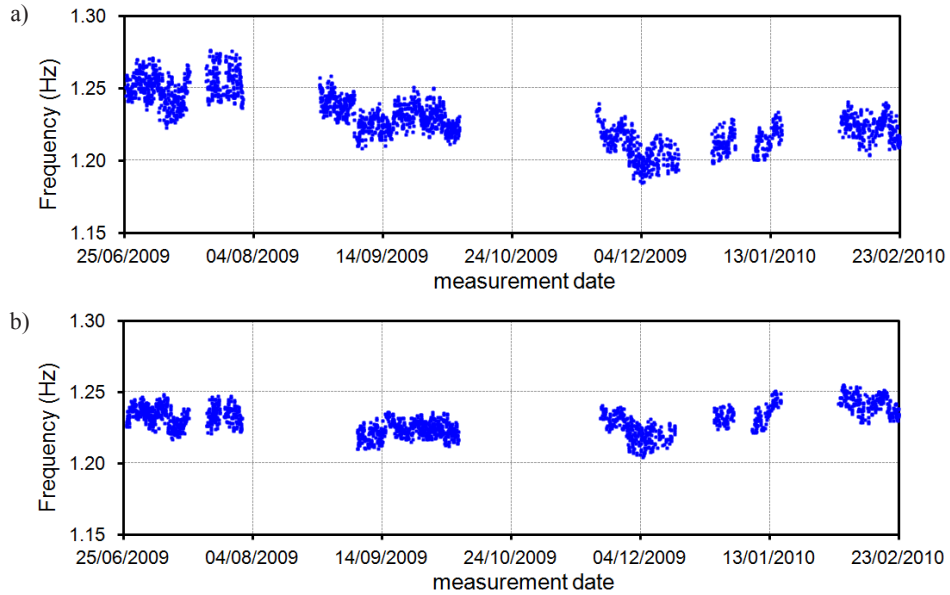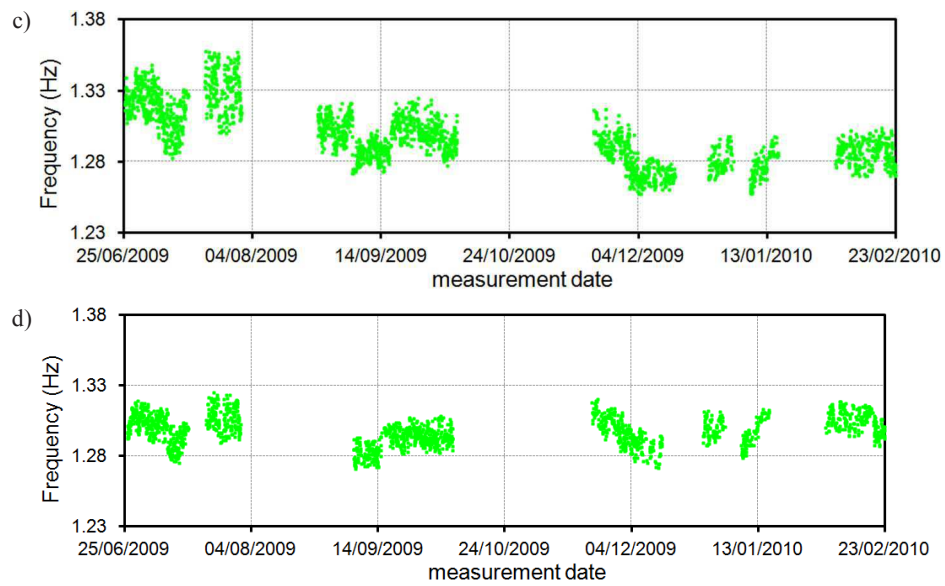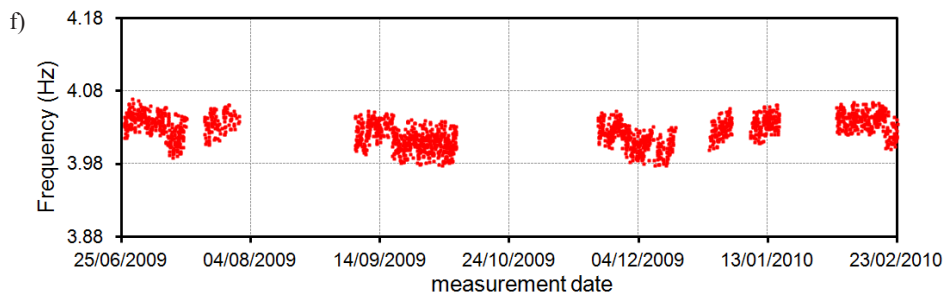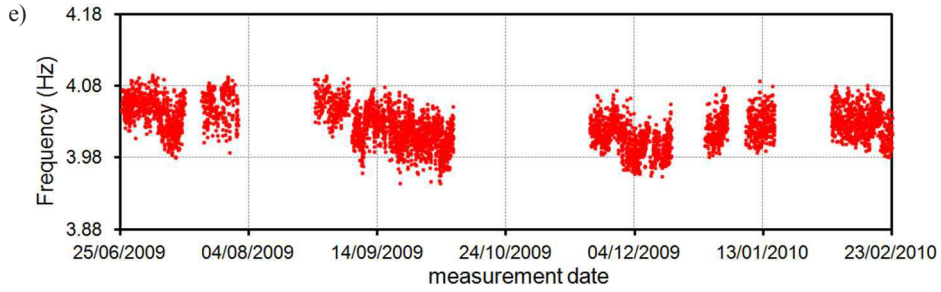**Figure 5.21** Mode B$_3$: time evolution of the natural frequency before (e) and after (f) the removal of the environmental effects (MIDR model)
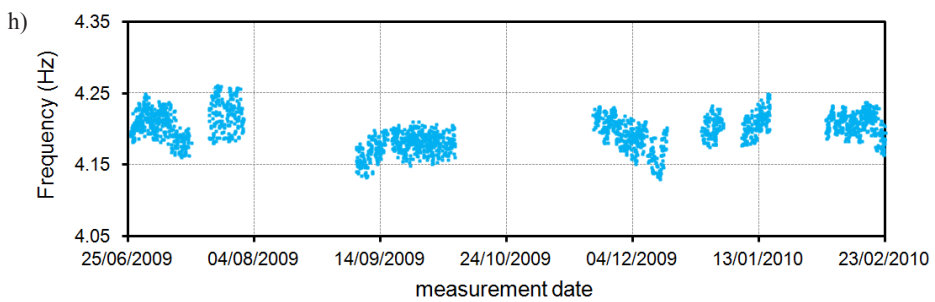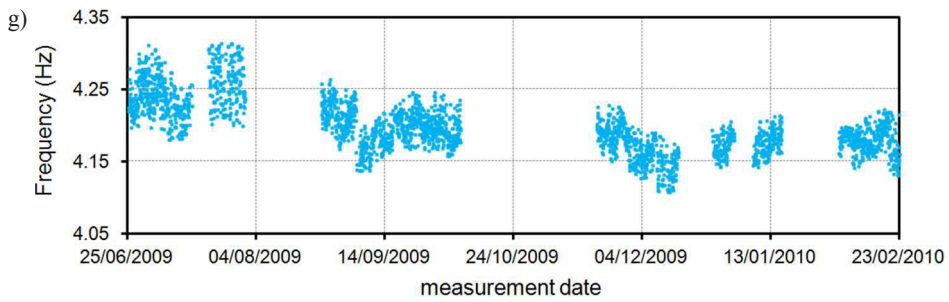
g)

h)

Figure 5.21 Mode B$_4$: time evolution of the natural frequency before (g) and after (h) the removal of the environmental effects (MIDR model)

The results obtained from the application of the MIDR model proved the

251

expectations on the improvement of the prediction skills to be well founded. The possibility to establish a dynamic regression relationship by using previous values of both external and internal temperatures allowed to better characterize the thermal condition of the masonry tower and led to the achievement of a double goal:

1. the variation intervals and the scattering of the considered temperature independent features (i.e. residual errors and depurated frequencies) have been significantly reduced, resulting in more accurate predictions;

2. after the application of the SIDR model, long term fluctuations of prediction error and of the corrected frequencies could be observed for both the investigated towers, due to the impossibility of completely modeling the effects of the average temperature. The results obtained from the MIDR model revealed much smaller residual variations, suggesting that the availability of inputs recorded on the inside of the masonry walls can take into account also the influence of the average temperature, as less exposed to the large daily temperature range characterizing the outer fronts.

Finally, to provide further evidence of the absence of anomalous occurrences not observed during the training periods, the multivariate *Shewhart T* control chart [Montgomery 1997] has been applied to the results of the MIDR model. Considering that both the static monitoring system and the two dynamic regression models confirmed that the tower exhibited a regular behavior over the whole nine months of dynamic monitoring, the plotted T^2-*statistic* feature is expected to not exceed the Upper Control Limit (UCL), defined from the experimental samples collected during the training period.

The resulting control chart is shown in Figure 5.22 and, as expected, the trend of the T^2-*statistic* is consistent with the results obtained in terms of residual errors and corrected frequencies. It is worth mentioning that subgroups of data of 12 hours have been considered in order to obtain the control chart of

Figure 5.22. The figure shows that:

1. during the training period (i.e. 25/06/2009-15/01/2010), the considered feature ranges far below the UCL (i.e. the solid horizontal red line), and only few points are characterized by values close to the defined limit (that, anyway, is never exceeded);

2. during the last five weeks of monitoring (i.e. after 15/01/2010), the T^2-*statistic* does not reveal any variation of the trend or the scattering, confirming the no anomalous occurrences took place during the dynamic monitoring of the bell tower of the *Chiesa Colleggiata di San Vittore*.
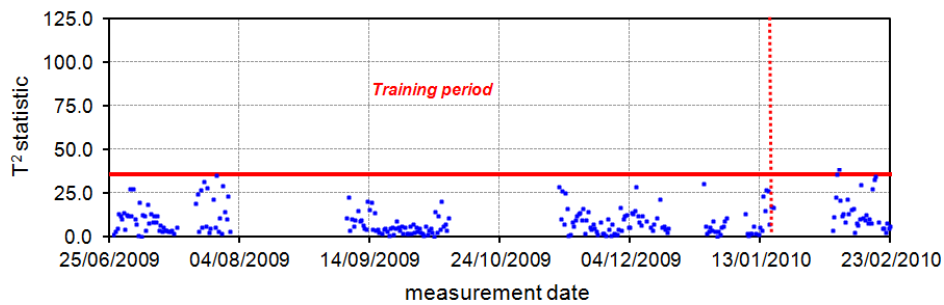

Figure 5.22 *Shewart T* control chart obtained by using subgroups of data of 12 hours (MIDR model)

-Page intentionally left blank-

Conclusions

A vibration-based Structural Health Monitoring strategy for historic masonry towers has been proposed in the present Dissertation. The approach is based on the preliminary availability of the results of a traditional data collection phase (i.e. historic and documentary research, on-site and topographic survey, visual inspection, non-destructive and minor-destructive tests of materials on site), aimed at reaching an appropriate level of knowledge of the structure, and consists of the following tasks:

a) preliminary AVTs, meant to provide useful indications for the subsequent long-term monitoring (i.e. accurate estimates of the dynamic characteristics, positions to be permanently instrumented, influence of the environmental factors). For this purpose, the number of sensors (i.e. accelerometers and temperature sensors) and the duration of the tests have to be properly selected;

b) installation of a continuous dynamic monitoring system, as simple as 3 accelerometers and few environmental sensors, combined with the use of an automated SSI-Cov based technique to continuously identify the modal parameters from the recorded response;

c) preliminary analysis of the time evolution of the natural frequencies, used as damage-sensitive features, in order to highlight the correlation with changing environmental factors (e.g. temperature);

d) mitigation of the environmental effects on the natural frequencies by means of Dynamic Regression models, ARX models and Principal Component Analysis (PCA)-based tools;

e) detection of abnormal structural changes and damage, by studying the time evolution of the residual errors and depurated frequencies or by means of the statistical tool referred to as *Shewhart T* control chart. For residual error and control chart, control limits have been computed from the experimental

255

samples collected during an appropriate reference period. This allows associating any observation laying outside of the defined limits to the presence of unusual sources of variability (e.g. the occurrence of damage).

The proposed methodology has been at first exemplified on the case study of the *Gabbia* tower in Mantua. The procedure has been applied to the response data collected over about 30 months by a simple monitoring system consisting of 3 highly sensitive accelerometers and 1 temperature sensor. In June 2013, after about six months from the beginning of the monitoring, a seismic episode occurred in the neighboring Garfagnana region and induced accelerations on top of the tower which exceeded by 40-50 times the response generally observed in operational conditions. The results, obtained from time-frequency analysis, inspection of the frequency tracking of the global modes and correlation between global frequencies and external temperature, indicate the occurrence of abnormal and irreversible structural changes induced by the earthquake. Hence, this case study was seen as a challenging opportunity to validate the proposed methodology by identifying the occurrence of abnormal structural changes or damage under changing environmental conditions.

The results obtained for the case study of the *Gabbia* tower lead to the following conclusions:

1. as a consequence of the cantilever-like structural behavior of historic masonry towers, a simple monitoring system consisting of three accelerometers and one temperature sensor installed in the upper region of the structure are sufficient to provide meaningful information for preventive conservation and/or SHM purposes;

2. the application of state-of-the-art tools for automated operational modal analysis allows accurately tracking the natural frequencies of the structure. After the removal/minimization of the effect of environmental factors, these

modal parameters can be successfully used as indicators of the structural condition in the following damage detection phase;

3. the use of a temperature sensor allows successfully estimating the dominant effect of temperature on the natural frequencies. In particular, the analysis of the frequency-temperature correlation revealed that the natural frequency of the global modes tends to increase with an increased temperature as a consequence of the thermal expansion of the materials. This phenomenon, inducing the closing of the minor gaps and cracks of the masonry, leads to a transitory "compacting" and therefore to a temporary increase of modal stiffness and frequency. Furthermore, a two-fold effect of the temperature could be detected: on one side, daily variations of the external temperature lead to the short-spaced oscillations of the natural frequencies, whereas, on the other hand, slow fluctuations of the experimental frequencies over long time periods are related to the effect of average temperature;

4. the effects of temperature on the natural frequencies of the *Gabbia* tower were at first accounted for and removed by applying a linear dynamic regression model to the experimental estimates obtained from the automated OMA process. The obtained results revealed that the prediction skills of the linear dynamic regression model are not constant during the whole monitoring period but improve for warm months. This is a consequence of the slightly non-linear correlation between the average temperature and the experimental frequencies, which appears to be more significant at higher temperatures. Furthermore, the application of the linear dynamic regression allows clearly detecting the occurrence of earthquake-induced structural anomalies by investigating the time evolution of residual errors, depurated natural frequencies and *Shewhart T* control chart. The trend exhibited by the inspected temperature-independent features also proves the damage to be irreversible;

257

5. the effects of environmental factors were subsequently minimized by applying an ARX model to the identified natural frequencies. This led to a complete removal of the external effects, with significant improvements of the predictive skills with respect to the dynamic regression relationship. The use of previous values of the output allowed indirectly taking into account the effects of those factors that could not be entirely modeled by the dynamic regression, which only considers past values of temperature. Nevertheless, the excellent predictive skills of the ARX model turned into a limitation in the damage detection process, as the effects of structural modifications were also reproduced due to the order of magnitude of the seismic event, which is the same as the fluctuations induced by the temperature effects. Therefore, the lack of sudden variations of prediction error and corrected frequencies did not allow to directly detect the occurrence of the damage induced by the Garfagnana earthquake, proving the worsened damage detection skills of the ARX model when compared to the regression analysis. On the other hand, the damage induced by the seismic event could be detected through the *Shewart T* control chart, which also confirmed the irreversibility of the earthquake effects;

6. finally, the PCA was applied to the estimates of the automated OMA in order to remove the environmental effects. The results revealed performances midway between those of the previous input-output models: in terms of prediction, PCA performed better than dynamic regression but could not match the accuracy of the ARX model; on the other hand, the damage detection skills of the multiple regression analysis better highlighted the structural variations induced by the Garfagnana earthquake, whereas the same changes were not as obvious for the PCA. Indeed, had not been known that a significant earthquake occurred on 21/06/2013, the variations detected from the time evolution of residual error and depurated frequencies would

258

not raise any alarm. Conversely, clear evidence of the occurrence of structural modifications was provided by the *Shewhart T* control chart;

7. the results of the second preliminary AVT highlighted the presence of a local mode involving torsion of the upper levels of the tower. The behavior of this mode looks very different than the one exhibited by the global modes. The automated OMA revealed a highly changing natural frequency, characterized by significant fluctuations over the considered 30 months. Conversely to the behavior exhibited by the global mode, the maximum and minimum values of the natural frequency are identified in the cold and in the hot seasons, respectively. The inspection of the frequency-temperature diagrams and of the frequency tracking highlighted the possible progress of a damage mechanism involving the upper part of the tower, conceivably triggered by the thrust exerted by the wooden covering on the surrounding walls. Such assumption seems to be confirmed by the frequency losses detected for the local mode over the monitoring period.

To further investigate some tasks of the adopted SHM methodology, the bell tower of the *Chiesa Collegiata di San Vittore* in Arcisate has been subsequently examined. The tower was extensively studied in the past by the Politecnico di Milano, which installed a continuous static monitoring system to monitor the evolution of the crack pattern. The proposed SHM methodology has been applied to data sets collected between June 2009 and February 2012 by a continuous dynamic monitoring system consisting, once more, of 3 accelerometers. In this case temperature measurements were available from 8 internal and external sensors, previously installed in the tower as part of the static monitoring system. Since the previous research activities did not detect the presence of any structural change over the considered 9 month interval, the main goal in this phase was the evaluation of the different performances of the dynamic regression model in removing/minimizing the environmental effects

on modal frequencies, when both indoor and outdoor temperature sensors are available.

In order to properly compare the results with those of the first case study, and to better highlight the expected improvements of the prediction skills when inputs are recorded by a larger number of sensors, the dynamic regression model has been firstly implemented by taking into account only the values of one outdoor temperature. The removal/minimization of the temperature effects provided results totally comparable to those of the *Gabbia* tower. Considering the similarity of the two case studies and of the implemented dynamic regression models, the consistency of the results seems to outline a threshold level for the accuracy achievable by using just the measurements of one external temperature.

Afterwards, the temperatures collected by one internal sensor have also been considered in the implementation of the dynamic regression model. The results obtained in terms of residual error, depurated frequencies and control chart revealed that the combined use of external and internal measurements of temperature leads to a relevant enhancement of the prediction skills of the model. Indeed, the availability of previous values of the internal temperature, less oscillating than the external one and characterized by long seasonal fluctuations, allows a more comprehensive characterization of the thermal effects on the natural frequencies. Therefore, not only the daily fluctuations, but also the effects of the average temperature can be better modeled.

To conclude, the results obtained for both case studies, and especially the detection of structural damage under changing environmental conditions for the *Gabbia* tower, prove that a possible key role can be played by the combined use of continuous dynamic monitoring and proposed SHM methodology in the preventive conservation of historic masonry towers.

260

References

❖ Allemang R. J.; Brown D. L. (1982) *A Correlation Coefficient for Modal Vector Analysis*, In: Proc. of International Modal Analysis Conference (IMAC I), Orlando, Florida, USA.

❖ Allemang R.J., Brown D.L., Philips A.W. (2010) *Survey of modal techniques applicable to autonomous/semi-autonomous parameter identification*, In: P. Sas, B. Bergen (Eds), Proc. of ISMA2010 International Conference on Noise and Vibration Engineering, Leuven, Belgium, 3331-3372.

❖ Andersen P., Brincker R., Goursat M., Mevel L. (2007) *Automated modal parameter estimation for operational modal analysis of large systems*, In: Proc. of Second International Operational Modal Analysis Conference (IOMAC 2007), Copenhagen, Denmark, vol. 1: 299-308.

❖ Aras F., Krstevska L., Altay G., Tashkov L. (2011) *Experimental and numerical modal analysis of a historical masonry palace*, Construction and Building Materials **25** (1): 81-91.

❖ Bayraktar A., Türker T., Sevım B., Altunişik A.C., Yildirim F. (2009) *Modal parameter identification of Hagia Sofia bell-tower via ambient vibration test*, Journal of Nondestructive Evaluation, 28: 37-47.

❖ Bendat J.S., Piersol A.G. (1986) *Random Data, Analysis and Measurement Procedure*s, John Wiley & Sons, New York, USA.

❖ Bendat J.S., Piersol A.G. (1993) *Engineering Applications of Correlation and Spectral Analysis*, Second Edition, John Wiley & Sons, New York, USA.

❖ Bennati S., Nardini L., Salvatore W. (2005) *Dynamic behavior of a medieval masonry bell tower. II: measurement and modeling of the tower motion*, Journal of Structural Engineering ASCE **131**(11): 1656-1664.

❖ Bertazzolo G. (1628) *Urbis Mantuae Descriptio*.

❖ Binda, L., Condoleo, P., Tiraboschi, C., Rigamonti, P. (2012) *On site investigation and crack monitoring of an ancient bell-tower,* In: Proc. of SFR 2012 (1-10), July 3-5, Edinburgh, Scotland.

❖ Bonato P., Ceravolo R., De Stefano A., Molinari F. (2000) *Cross-time frequency techniques for the identification of masonry buildings*, Mechanical Systems and Signal Processing, **14**(1): 91-109.

❖ Bongiovanni G., Clemente P., Buffarini G. (2000) *Analysis of the seismic response of a damaged masonry bell tower*, In: Proc. of 12th World Conference on Earthquake Engineering (12WCEE).

❖ Box G., Wilson K. (1951) *On the experimental attainment of optimum conditions*, J. R. Stat. Soc. Ser. B (Methodol.) **13**(1): 1-45.

❖ Box G., Draper N. (1986) *Empirical Model-building and Response Surface*, John Wiley & Sons, New York, USA.

❖ Brincker R., Zhang L.M., Andersen P. (2000) *Modal identification from ambient responses using Frequency Domain Decomposition*, In: Proc. 18th Int. Modal Analysis Conference (IMAC-XVIII), San Antonio, Texas, USA, 625-630.

❖ Brincker R., Ventura C.E., Andersen P. (2001) *Damping estimation by Frequency Domain Decomposition*, In: Proc. 19th Int. Modal Analysis Conference (IMAC-XIX), Orlando, FL, USA, 698-703.

❖ Brincker R., Andersen P., Jacobsen N.J. (2007) *Automated frequency domain decomposition for operational modal analysis*, In: Proc. 25th Int. Modal Analysis Conference (IMAC-XXV), Orlando,FL, USA.

❖ Brownjohn J.M.W., Magalhães F., Caetano E., Cunha A. (2010) *Ambient vibration re-testing and operational modal analysis of the Humber Bridge*, Engineering Structures **32**: 2003-2018.

❖ Busatta F. (2012) *Dynamic monitoring and automated modal analysis of large structures: methodological aspects and application to a historic*

iron bridge, Ph.D. Thesis, Politecnico di Milano.

❖ Cabboi A., Gentile C., Saisi A. (2013) *Frequency tracking and FE model identification of a masonry tower*, In: Proc. of the 5th International Operational Modal Analysis Conference, IOMAC'13, Guimaraes, Portugal.

❖ Cabboi A. (2013) *Automatic operational modal analysis: challenges and application to historic structures and infrastructures*, Ph.D. Thesis, Università di Cagliari.

❖ Cabboi A., Gentile C., Saisi A. (2015) *Automated modal and structural identification of a stone masonry bell-tower for SHM*, In: Proc. of 6th World Conference of Structural Control and Monitoring, Barcelona.

❖ Cantieni R. (2014) *One-year monitoring of a historic bell tower*, In: Proc. of the 9th International Conference on Structural Dynamics (EURODYN 2014), Porto, Portugal, 1493-1500.

❖ Casarin F., Modena C. (2008) *Seismic assessment of complex historical buildings: application to Reggio Emilia Cathedral, Italy*, International Journal of Architectural Heritage, **2** (3): 304-27.

❖ Casarin F., Modena C., Bello E., Da Porto F., Girardello P., Lorenzoni F (2012) *Structural Health Monitoring of the Roman Arena of Verona*, In: Proc. of 8th International Conference on Structural Analysis of Historical Constructions (SAHC 2012), Wroclow, Poland.

❖ Carden J.P., Brownjohn J.M.W. (2008) *Fuzzy clustering of stability diagrams for vibration-based structural health monitoring*, Comput. Aided Civ. Infrastructure Eng., 23(5): 360-372.

❖ Cattari S., Degli Abbati S., Ferretti D., Lagomarsino S., Ottonelli D., Tralli A. (2014) *Damage assessment of fortresses after the 2012 Emilia earthquake (Italy)*, Bull. Earthquake Eng. **12**: 2333-2365.

❖ Cazzani E. (1964) *Arcisate nella storia e nell'arte*, Ceresio.

❖ Chauhan S., Tcherniak D. (2009) *Clustering approaches to automatic modal parameter estimation*, In: Proc. of the 27th International Modal Analysis Conference (IMAC XXVII), Orlando, FL, USA.

❖ Clough R. W.; Penzien J. (1993) *Dynamics of Structures*, 2nd edition, McGraw-Hill, New York, USA.

❖ Cross E.J., Koo K.Y., Brownjohn J.M.W., Worden K. (2013) *Long-term monitoring and data analysis of the Tamar Bridge*, Mechanical Systems and Signal Processing **25**: 16-34.

❖ D'Ambrisi A., Mariani V., Mezzi M. (2012) *Seismic assessment of a historical masonry tower with nonlinear static and dynamic analyses tuned on ambient vibration tests*, Engineering Structures, **36**: 210-219.

❖ Deraemaeker A., Reynders E., De Roeck G., Kullaa J. (2008) *Vibration-based structural health monitoring using output-only measurements under changing environment*, Mechanical Systems and Signal Processing **22**(1): 38-56.

❖ Doebling S.W., Farrar C.R., Prime M.B., Shevitz D. (1996) *Damage identification and health monitoring of structural and mechanical systems from changes in their vibration characteristics: a literature review*, Los Alamos National Laboratory, New Mexico, NM.

❖ Farrar C.R., Doebling S.W., Cornwell P.J., Straser E.G. (1997) *Variability of modal parameters measured on the Alamosa Canyon Bridge*, In: Proc. of IMAC 15, Orlando, FL, USA, 257-263.

❖ Gentile C., Saisi A. (2007) *Ambient vibration testing of historic masonry towers for structural identification and damage assessment,* Construction and Building Materials **21** (6): 1311-1321.

❖ Gentile C., Saisi A. (2011) *Ambient vibration testing and condition assessment of the Paderno iron arch bridge (1889)*, Construction and

Building Materials, **25**: 3709-20.

❖ Gentile C., Saisi A., Cabboi A. (2012) *Dynamic monitoring of a masonry tower*, In: Proc. of the International Conference on Structural Analysis of Historical Construction (SAHC 2012), Wroclaw, Poland.

❖ Gentile C., Saisi A. (2013) *Operational modal testing of historic structures at different levels of excitation*, Construction and Building Materials, **48**: 1273-85.

❖ Gentile C., Saisi A., Cabboi A. (2015) Structural identification of a masonry tower based on operational modal analysis, International Journal of Architectural Heritage; **9**(2): 98-110.

❖ Giampaolo L. (1960) *La topografia della Pieve di Arcisate di Nicolò Sormani 1728*, Società Storica Varesina.

❖ Goethals I., Vanluyten B., De Moor B. (2004) *Reliable spurious mode rejection using self learning algorithms*, In: P. Sas, M. De Munck (Eds), Proc. of ISMA 2004 International Conference on Noise and Vibration Engineering, Leuven, Belgium, 991-1004.

❖ Hair J., Anderson R., Tatham R., Black W. (1998) *Multivariate Data Analysis*, Prentice Hall.

❖ Harris C.M. (1995) *Harris' Shock and Vibration Handbook*, Fourth Edition, McGraw-Hill, New York, USA.

❖ Hu W.H., Moutinho C., Magalhães F., Caetano E., Cunha Á. (2009) *Analysis and Extraction of Temperature Effects on Natural Frequencies of a Footbridge based on Continuous Dynamic Monitoring*, In: Proc. of IOMAC International Operational Modal Analysis Conference, Portonovo, Italy.

❖ Hu W.H., Said S., Rohrmann R.G., Rücker W., Cunha A., Rogge A. (2015) *Vibration-based structural health monitoring of a highway bridge based on continuous dynamic measurements over 14 years*, In: Proc. of

SHMII7 7th International Conference on Structural Health Monitoring of Intelligent Infrastructures, Turin, Italy.

❖ Ivorra S., Pallarés F.J. (2006) *Dynamic investigation on a masonry bell tower*, Engineering Structures, **25**(5): 660-67.

❖ Ivorra S., Pallarés F.J., Adam J.M. (2008) *Experimental and numerical studies on the bell tower of Santa Justa y Rufina (Orihuela-Spain)*, In: Proc. of Structural Analysis of Historic Construction (SAHC) 2008, 349-355.

❖ Jacobsen N.J., Andersen P., Brincker R. (2006) *Using Enhanced Frequency Domain Decomposition as a robust technique to harmonic excitation in Operational Modal Analysis*, In: Proc. of ISMA2006, Leuven, Belgium.

❖ Jaishi B., Ren W.X., Zong Z.H., Maskey P.N. (2003) *Dynamic and seismic performance of old multi-tiered temples in Nepal*, Engineering Structures, **25**(14): 1827-39.

❖ Johnson R. A., Wichern D. W. (1992) *Applied Multivariate Statistical Analysis*, Prentice Hall, Englewood Cliffs, NJ, USA.

❖ Juang J.N. (1994) *Applied system identification*, Prentice Hall, Englewood Cliffs, NJ, USA.

❖ Júlio E., Rebelo C., Dias-da-Costa D. (2008) *Structural assessment of the tower of the University of Coimbra by modal identification*, Engineering Structure, **30**: 3468-3477.

❖ Kullaa J. (2003) *Damage detection of the Z24 bridge using control charts*, Mechanical Systems and Signal Processing **17**(1): 163-170.

❖ Kullaa J. (2004) *Structural Health Monitoring of a Crane in Variable Configurations*, In: Proc. of ISMA International Conference on Noise and Vibration Engineering, Leuven, Belgium.

❖ Ljung L. (1999) *System Identification: Theory for the User*, Prentice Hall,

Englewood Cliffs, NJ, USA.

❖ Luzi L., Pacor F., Ameri G., Puglia R., Burrato P., Massa M., Augliera P., Franceschina G., Lovati S., Castro R. (2013) *Overview on the strong-motion data recorded during the May-June 2012 Emilia seismic sequence*, Seismol. Res. Lett*., **84**: 629-644.

❖ Magalhães F., Cunha A., Caetano E. (2008) *Dynamic monitoring of a long span arch bridge*, Engineering Structures **30**: 3034-3044.

❖ Magalhães F., Cunha A., Caetano E. (2009) *Online automatic identification of the modal parameters of a long span arch bridge*, Mechanical System and Signal Processing, **23**(2): 316-329.

❖ Magalhães F., Cunha A. (2011) *Explaining operational modal analysis with data from an arch bridge,* Mechanical Systems and Signal Processing, **25**(5): 1431-50.

❖ Magalhães F., Cunha A., Caetano E. (2012) *Vibration based structural health monitoring of an arch bridge: From automated OMA to damage detection*, Mechanical Systems and Signal Processing **28**: 212-228;

❖ Moser P., Moaveni B. (2011) *Environmental effects on the identified natural frequencies of the Dowling Hall Footbridge*, Mechanical Systems and Signal Processing **25**: 2336-2357.

❖ Montgomery D. (1997) *Introduction to Statistical Quality Control – Third Edition*, Wiley, New York, USA.

❖ Newland D.E. (1993) *An introduction to random vibrations, spectral and wavelet analysis – Third Edition*, Longman Scientific & Technical, Harlow, Essex, Engalnd.

❖ Oliveira C.S., Çakti E., Stengel D., Branco M. (2012) *Minaret behavior under earthquake loading: the case of historical Istanbul*, Earthquake Engineering & Structural Dynamics, **41**: 19-39.

❖ Peppa R.S., Elliott K.B., Schenk A. (1992) *A consistent-mode indicator*

for the eigensystem realization algorithm, Report NASA TM-107607, National Aeronautics and Space Administration.

❖ Peppa R.S., James III G.H., Zimmerman D.C (1997), *Autonomous modal identification of the Space Shuttle tail rudder*, Report NASA TM-112866, National Aeronautics and Space Administration.

❖ Pau A., Vestroni F. (2008) *Vibration analysis and dynamic characterization of the Colosseum*, Structural Control and Health Monitoring, **15**(8): 1105-21.

❖ Peeters B., De Roeck G. (1999) *Reference based stochastic subspace identification for output only modal analysis*, Mechanical Systems and Signal Processing, **13** (6): 855–878.

❖ Peeters B. (2000) *System identification and damage detection in civil engineering*, Ph.D. Thesis, Katholieke Universiteit Leuven.

❖ Peeters B., De Roeck G. (2001) *One year monitoring of the Z24-Bridge: environmental effects versus damage events*, Earthquake Engineering and Structural Dynamics, **30**(2):149-171.

❖ Peeters B., Van der Auweraer H., Guillaume P., Leuridan J. (2004) *The PolyMAX frequency domain method: a new standard for modal parameter estimation?*, Shock and Vibration, **11**(3-4): 395-409.

❖ Peña F., Lourenço P.B., Mendes N., Oliveira D.V. (2010) *Numerical models for the seismic assessment of an old masonry tower*, Engineering Structures, **32**(5): 1466-78.

❖ Prevosto M. (1982) *Algorithmes d'Identification des Caractéristiques Vibratoires de Structures Mécaniques Complexes*, PhD thesis, Université de Rennes I, France.

❖ Rainieri C., Fabbrocino G. (2010) *Automated output-only dynamic identification of civil engineering structures*, Mechanical System and Signal Processing, **24**: 678-695.

❖ Ramos L.F., Casarin F., Algeri C., Lourenço P.B., Modena C. (2006) *Investigation techniques carried out on the Qutb Minar, New Delhi, India*, In: Proc. of SAHC Structural Analysis of Historical Constructions, New Delhi, India.

❖ Ramos L.F., Marques L., Lourenço P.B., De Roeck G., Campos-Costa A., Roque J. (2010) *Monitoring historical masonry structures with operational modal analysis: two case studies*, Mechanical System and Signal Processing **24**: 1291-1305.

❖ Ramos L.F., Aguilar R., Lourenço P.B., Moreira S. (2013) *Dynamic structural health monitoring of Saint Torcato church*, Mechanical Systems and Signal Processing **35**: 1-15.

❖ Reynders E, Houbrechts J, De Roeck G. (2012) *Fully automated (operational) modal analysis,* Mechanical System and Signal Processing, **29**: 228-250.

❖ Robert G.P., Pearson A.J. (1998) *Health monitoring of structures – towards a stethoscope for bridges*, In: Proc. of ISMA 23, the International Conference on Noise and Vibration Engineering, Leuven, Belgium.

❖ Saisi A., Gentile C. (2015) *Post-earthquake diagnostic investigation of a historic masonry tower*, Journal of Cultural Heritage, 16(4): 602-609.

❖ Scionti M., Lanslots J., Goethals L., Vecchio A., Van der Auweraer H., Peeters B., De Moor B. (2003) *Tools to improve detection of structural changes from in-flight flutter data*, In: Proc. of the 8th International Conference on Recent Advances in Structural Dynamics (ISVR), Southampton, UK.

❖ Scionti M., Lanslots J. (2004) *Stabilization diagrams: pole identification using fuzzy clustering techniques*, Advanced Engineering Software, **36**(11-12): 768-779.

❖ Shih C.Y., Tsuei Y.G., Allemang R.J., Brown D.L. (1988) *Complex mode indication function and its application to spatial domain parameter estimation*, Mechanical Systems and Signal Processing, **2**(4): 367-377.

❖ Sohn. H., Worden K., Farrar C.R. (2003) *Statistical damage classification under changing environmental and operational conditions*, Journal of Intelligent Material Systems and Structures, **13**(9): 561-574.

❖ Sohn H. (2007) *Effects of environmental and operational variability on structural health monitoring*, Philos. Trans. R. Soc. A: Math. Phys. Eng. Sci. **365** (1851) 539.

❖ Sorrentino L., Liberatore L., Decanini L., Liberatore D. (2014) *The performance of churches in the 2012 Emilia earthquake*, Bull. Earthquake Eng., **12**: 2299-2331.

❖ SVS, *ARTeMIS Extractor 2011*, http://www.svibs.com/, 2012.

❖ Ubertini F., Gentile C., Materazzi A.L. (2013) *Automated modal identification in operational conditions and its application to bridges*, Engineering Structures, **46**: 264–278.

❖ Ubertini F., Gentile C., Materazzi A.L. (2013) *Time-frequency analysis of dispersive phenomena in bridges*, In: Proc. IOMAC'13, 5th International Operational Modal Analysis Conference, Guimaraes, Portugal

❖ Van Overschee P., De Moor B. (1996) *Subspace identification for linear systems: theory, implementation, applications*, Kluwer Academic Publishers.

❖ Vanlanduit S., Verboven P., Guillame P., Schoukens J. (2003) *An automatic frequency domain modal parameter estimation algorithm*, Journal of Sound and Vibrations, 265(3): 647-661.

❖ Vanlanduit S., Parloo E., Cauberghe B., Guillaume P., Verboven P. (2005) *A Robust Singular Value Decomposition for Damage Detection under Changing Operational Conditions and Structural Uncertainties*,

Journal of Sound and Vibration **284**(3-5): 1033-1050.

❖ Verboven P., Parloo E., Guillaume P., Van Overmeire M. (2002) *Autonomous structural health monitoring - part I: modal parameter estimation and tracking*, Mechanical System and Signal Processing **16**: 637-357.

❖ Verboven P., Cauberghe B., Parloo E., Vanlanduit S., Guillaume P. (2004) *User-assisting tools for a fast frequency-domain modal parameter estimation method*, Mechanical System and Signal Processing, **18**(4): 759–780.

❖ Welch P.D. (1967) *The use of Fast Fourier Transform for the Estimation of Power Spectra: a Method based on Time Averaging over short Modified Periodograms*, IEEE Transaction on Audio and Electro-Acoustics, AU-15(2).

❖ Worden K., Manson G. (2000) *Damage identification using multivariate statistics: Kernel discriminant analysis*, Inverse Problems in Engineering **8**(1): 25-46.

❖ Yan A.M., Kerschen G., De Boe P., Golinval J.C. (2005a) *Structural damage diagnosis under varying environmental conditions – Part I: A linear analysis*, Mechanical Systems and Signal Processing **19**(4): 847-864.

❖ Yan A.M., Kerschen G., De Boe P., Golinval J.C. (2005b) *Structural damage diagnosis under varying environmental conditions – Part II: local PCA for non-linear cases*, Mechanical Systems and Signal Processing **19**(4): 865-880.

❖ Xu M. (2013) *Dynamic monitoring and structure assessment of "Gabbia Tower"*, M.Sc. Thesis, Politecnico di Milano.

❖ Zuccoli N. (1988) *Historic research on the Gabbia Tower (in Italian)*, Municipality of Mantua Internal Report.